Linking The Cortical Microstructure To Oscillatory Dynamics Through In Vivo Imaging

Laura Bloomfield

Supervisors : Krish D. Singh and Derek K. Jones

A thesis submitted to Cardiff University for the degree of Doctor of Philosophy

January 2021

Thesis Summary

Uncovering the intricate relationship between the brain's structure and function remains a fundamental goal of the neuroscience field. Significantly, recent advancesin the neuroimaging field are now allowing for the investigation of this relationship at the microstructural level, opening up a wealth of new research possibilities. Of particular interest, is the ability to probe the myelin content of the cortex non- invasively and with high resolution.

Notably a close relationship is known to exist between the cyto and myelo architecture of the brain and converging lines of evidence point to the potential existence of a relationship between myelination of the cortical grey matter and electrophysiological responses. Of particular interest in this regard are neural oscillations, which have been widely implicated in a variety of cognitive processes and clinical conditions. Thus, this thesis seeks to explore the possibility of investigating the relationship between a key aspect of the cortical microstructure, namely its myelin content and oscillatory dynamics in-vivo, through the use of highresolution 7T MRI in combination with MEG. Ultimately, the novel insights gained through this approach could have important implications for the understanding of brain structure-function relationships in both health and disease.

Acknowledgements

Firstly, I would like to thank my supervisors Krish Singh and Derek Jones for theircontinued help, support and guidance throughout the completion of this thesis.

I would also like to offer thanks to numerous individuals at CUBRIC for their invaluable assistance during the completion of this project. Special thanks must go toSlawomir Kusima and John Evans for all their help and expertise with the 7T side of the project and Gavin Perry for his assistance in the MEG.

I would also like to thank all the participants who took part in this study for their participation and the Cardiff University School of Psychology for funding my PhD.

Lastly, I would like to thank my friends and family for their enduring support, andthe other PhD students I shared this journey with, for helping me along the way.

Data Collection

All data collection and analysis for this thesis was performed by me.

The exception to this is the data for the larger comparison cohort included in chapter6 which was collected by a number of other researchers as part of a larger cohort study.

List of Acronyms

The following Acronyms and Abbreviations are utilised throughout the main text of this thesis:

3T 3 Tesla

7T 7 Tesla

AAL Automated Anatomical Labelling

DCM Dynamic Causal Modelling

GABA Gamma-aminobutyric acid

GRE Gradient recalled echo

MRI Magnetic resonance imaging

MEG Magnetoencephalography

ROI Region of interest

qMT Quantative Magnetisation Transfer

Contents

Chapter 1

General Introduction

1.1 Rationale

Recent advances in neuroimaging are enabling the investigation of brain structure and function on a much finer scale than ever before. Importantly, such investigations have the potential to advance our understanding of structure-function relationships by allowing for the estimation of direct correlations between brain microstructure and function in vivo. Correspondingly, there has been a renewal of interest in using high resolution quantitative MRI techniques in order to probe the microstructure of the brain and in particular its myelin content.

The cortical grey matter contains numerous myelinated fibres, the spatial organization of which varies across the cortex. Significantly, a close relationship is also thought to exist between the cytoarchitecture and myeloarchitecture of the brain. For example, the horizontal myelinated fibres of the cortex have been suggested to correspond to the axon collaterals of pyramidal cells (the primary generators of the MEG/EEG signal). Building on this close association, a recent study by Helbling et al. (2015) demonstrated that estimates of cortical myelin content can predict the magnitude of electrophysiological responses derived using MEG, thus demonstrating the feasibility of using MRI derived myelin estimates to investigate structure-function relationships at the microstructural level.

Neural oscillations are thought to enable the coordinated activity of neuronal populations during normal brain functioning and aberrant oscillatory dynamics have been extensively implicated in a wide range of clinical conditions. However numerous questions remain regarding the generation of these signals and their relation to the underlying neuroanatomy. Thus, the objective of the current research is to investigate the relationship between the microstructure of the brain and neuronal oscillations at both the local and network level, with a view to gaining new insights into the nature of these signals and their relation to the underlying neuroanatomy.Ultimately, given the purported role of oscillations in cognition, such an investigation could provide new insights into the nature

of structure-function relationships and their relevance for cognition and pave the way for a greater understanding of the pathophysiology of clinical conditions.

The aim of this introductory chapter is to provide important contextual information regarding the themes of this thesis as well as a detailed overview of the concepts discussed in the experimental chapters of this thesis.

1.2 Structure-function relationships in the brain

It remains a fundamental tenet of the neuroscience field that the structure of the brain and its function are closely interrelated. Consequently, the understanding of behaviour, in health and disease, is dependent upon knowledge of both these crucial facets of the brain. Yet, despite having been the subject of intense research, there remain many unanswered questions regarding the complex interplay between brain structure and function. Indeed, although significant inroads have undoubtedly been made into the understanding of the brain's neurophysiology, the precise question of how the distinctive structural architecture of a given cortical area shapes its function has remained somewhat elusive and is thus the subject of ongoing investigation (Weiskopf, Mohammadi, Lutti, & Callaghan, 2015).

However, in recent years there has been growing recognition of the fact that multimodal imaging studies, combining both structural and functional neuroimaging data, could help to revolutionise our understanding of structure-function relationships (Calhoun & Sui, 2016). Such investigations can provide a more in-depth understanding of brain functioning and its relevance for cognition by informing our understanding of how the structure of the brain shapes its function and providing insight into which aspects of brain physiology (both structural and functional) could be important for shaping behaviour and cognition (Calhoun & Sui, 2016).

A key challenge facing investigations of structure-function relationships in the human brain is that the cortical neuroanatomy can be understood at many different levels, from the microscopic to the macroscopic (Devlin & Poldrack, 2007). In the context of the neuroimaging field, given the technical limitations inherent in the available methods, the predominant focus with regards to mapping structure to function has necessarily been at the macrostructural level. However, from histological investigations the microstructure of the cortical grey matter is known to be exceedingly complex. Indeed, rather than existing as a uniform entity, the human neocortex exhibits a highly intricate organised structure, typically defined by a six-layer architecture, though some regional differences are

apparent (Molyneaux, Arlotta, Menezes, & Macklis, 2007). Within each of these layers, distinct populations of neurons can be found, each with their own unique morphological characteristics (Molyneaux et al., 2007).

In total, the human cortex is thought to constitute approximately 100 billion neurons (Herculano-Houzel, 2009). Two major classes of neurons account for these figures. The first and most abundant of these are pyramidal cells, located in all cortical layers (except layer 1), which constitute roughly 70-85% of the total population of neurons in the brain (DeFelipe & Farinas, 1992). A characteristic feature of these cells is their long axons. The second predominant class of neurons in the cortex are interneurons which possess short axons. These interneurons can also be differentiated into multiple morphological types, depending on the cortical area and layer in which they are situated (DeFelipe & Farinas, 1992).

Historically, cortical layers have been distinguished by the predominant types, sizes and packing density of cells (Palomero-Gallagher & Zilles, 2019). However, the existence of myelinated cortical fibres has been known for centuries and examination of the density of such fibres has also proven instrumental to the analysis of cortical layering patterns. Indeed, a further key component of the brain's microstructure is its myelin content. Myelin is a fatty substance composed of lipid bilayers that wrap tightly around axons forming a coating that provides a source of insulation (Pirko & Noseworthy, 2007). In the central nervous system myelin is produced by glial cells known as oligodendrocytes. Interestingly, although most prominent in the white matter of the brain, the cortical grey matter also contains numerous myelinated fibres, the spatial organization of which varies across the cortex (Nieuwenhuys, 2013). On the basis of the density of these myelinated fibres, cortical layers have been distinguished. Of note, the borders of cyto and myeloarchitecturally defined layers have also been shown to be comparable (Palomero-Gallagher & Zilles, 2019).

Significantly, recent advances in neuroimaging that enable the quantification of brain structure and function on a much finer scale than ever before (Weiskopf et al., 2015) make it possible to measure microstructural properties of human brain tissue, such as the myelin content, non-invasively and with high resolution. Such advancements have raised the exciting prospect of being able to estimate direct correlations between the microstructure and function of the cortex in vivo (Weiskopf et al., 2015). Correspondingly, cortical myelin has garnered increasing attention over the past few years. .

1.3 A Brief History of the Cortical Myeloarchitecture

The term myeloarchitecture, first introduced by Vogt in 1903, can be defined as the pattern and distribution of myelinated fibres in the cortex (Nieuwenhuys, 2013). The investigation of this particular facet of the cortical microstructure began in in the 18th century with Italian neuroanatomist Gennaris' 1782 discovery of a white stripe in the occipital lobe of ex-vivo human brain tissue, now commonly referred to as the Stria of Gennari. However, it was not until a number of years later, at the turn of the 20th century, that a systematic research program dedicated to elucidating the nature of the cortical myeloarchitecture truly came to fruition, thanks to the efforts of Cécile and Oskar Vogt and their numerous collaborators (Palomero-Gallagher & Zilles 2019).

Throughout the history of neuroscience, the structure of the cortex and its delineation into cortical areas, to which particular functions can be ascribed, has been the subject of intense investigation (Geyer, Weiss, Reimann, Lohmann, & Turner, 2011). In order to provide a precise mapping of structure and function in the brain, the early 20th century witnessed the evolution of two principle neuroanatomical disciplines (Amunts, & Zilles, 2015). The first of these consisted of histological studies of the cortical cytoarchitecture pioneered by Brodmann, who focused on the spatial distribution of cell bodies (Geyer et al., 2011). Using this approach Brodmann produced a parcellation of the cortex on the basis of its cytoarchitecture, commonly referred to as the Brodmann maps, which were first published in 1908 (Brodmann,1908). These iconic maps became a staple of the neuroscience field and are still in use today.

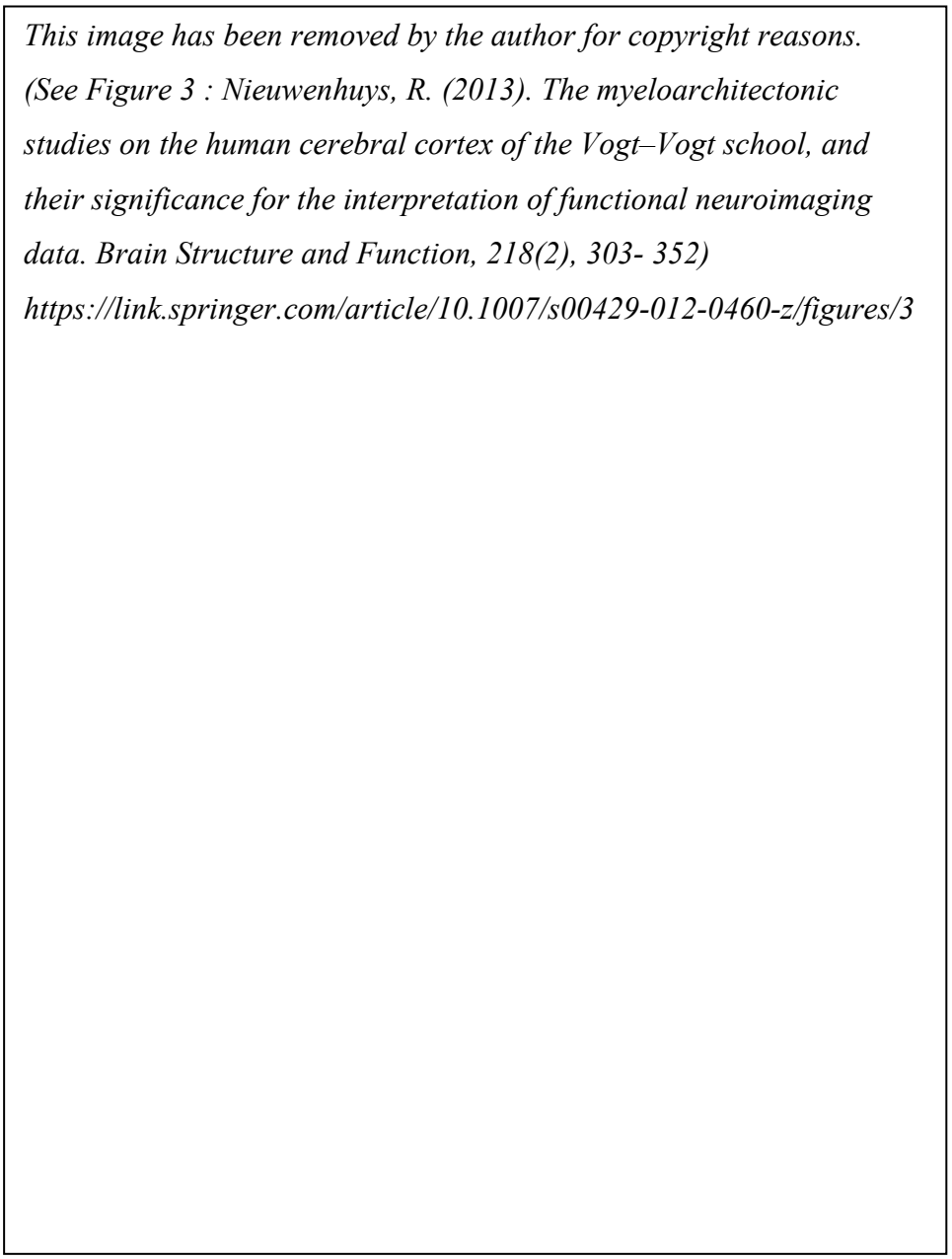

Figure 1.1: *Diagram of the cytoarchitectonic and myeloarchitectonic layers of the cortex produced by Vogt (1903), taken from Nieuwenhuys, R. (2013). The myeloarchitectonic studies on the human cerebral cortex of the Vogt–Vogt school, and their significance for the interpretation of functional neuroimaging data. Brain Structure and Function, 218(2), 303- 352.*

However, less commonly known, is that around the same time, Cécile and Oskar Vogt were focusing on the study of the myeloarchitecture of the brain. Significantly, akin to the cells of the cerebral cortex, the spatial organisation of the myelinated tangential and radial fibres that constitute its myeloarchitecture vary across the cortex. On the basis of local differences in the morphology of such fibres, it is possible to identify and delineate unique cortical areas. This endeavour constitutes the primary aim of the neuroanatomical subdiscipline referred to as myeloarchitectonics (Nieuwenhuys, 2013).

The radial myelinated fibres observed in the cortex typically form bundles and were distinguished by the Vogts into three types, namely euradiate (radial fibres that do not extend beyond layer 3), supraradiate (radial fibre bundles that transverse almost the entire depth of the cortex) and infraradiate (characterised by short radii that terminate at layer 5) (Nieuwenhuys, 2013). In contrast, the tangential myelinated fibres run parallel to the cortical surface, characteristically forming layers. Noteworthy examples of these layers of tangentially oriented fibres include the inner and outer bands (or stripes) of Baillarger (Zilles, Palomero-Gallagher, & Amunts, 2015).

With regards to the patterns of transverse fibres observed in the cortex, the Vogts also distinguished four prominent types: specifically, bistriate, unistriate, unitostriate and astriate. The bistriate type, for example, is characterised by the presence of two distinct bands of Baillarger whilst the key feature of the unistriate type is that only the external stripe of Baillarger can be distinguished. Although present, the inner band of Baillarger cannot be discerned in this type due to a high density of fibres in layer 6 (Nieuwenhuys, 2013). Examples of each of these different types are illustrated in Figure 1.2.

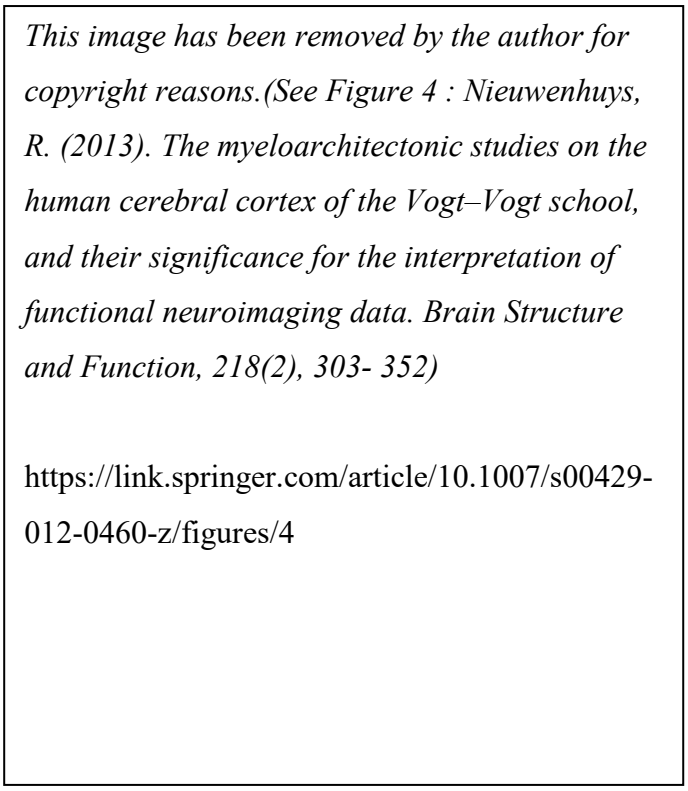

Figure 1.2: *Diagram showing the 4 principal classifications of tangential myelinated fibres that define myeloarchitectonic areas, according to Vogt.* ***a*** *refers to the bistriate type,* ***b*** *to the unistriate type* ***, c*** *to the unitostriate type and* ***d*** *to the astriate type****.*** *Produced by Vogt (1910) and taken from Nieuwenhuys, R. (2013). The myeloarchitectonic studies on the human cerebral cortex of the Vogt–Vogt school, and their significance for the interpretationof functional neuroimaging data. Brain Structure and Function, 218(2), 303-352.*

Between 1910 and 1970 the Vogts and a number of other collaborators and pioneers of the field published extensive studies on the myeloarchitecture of the cortex (Nieuwenhuys, & Broere, 2017). On the basis of these efforts the cortex has been suggested to contain roughly 185 cortical areas (Nieuwenhuys, 2013).

Despite the existence of this rich body of research, and in contrast to studies of the cortical cytoarchitecture, the myeloarchitecture of the brain has been largely neglected over the past hundred years (Nieuwenhuys, 2013). However, in recent years the study of cortical myelination has received new impetus (see Figure 1.3). This is largely due to the advent of more advanced MRI techniques, sensitive to myelin, that have spurred a corresponding renewal of interest in examining the myeloarchitecture of the brain in vivo.

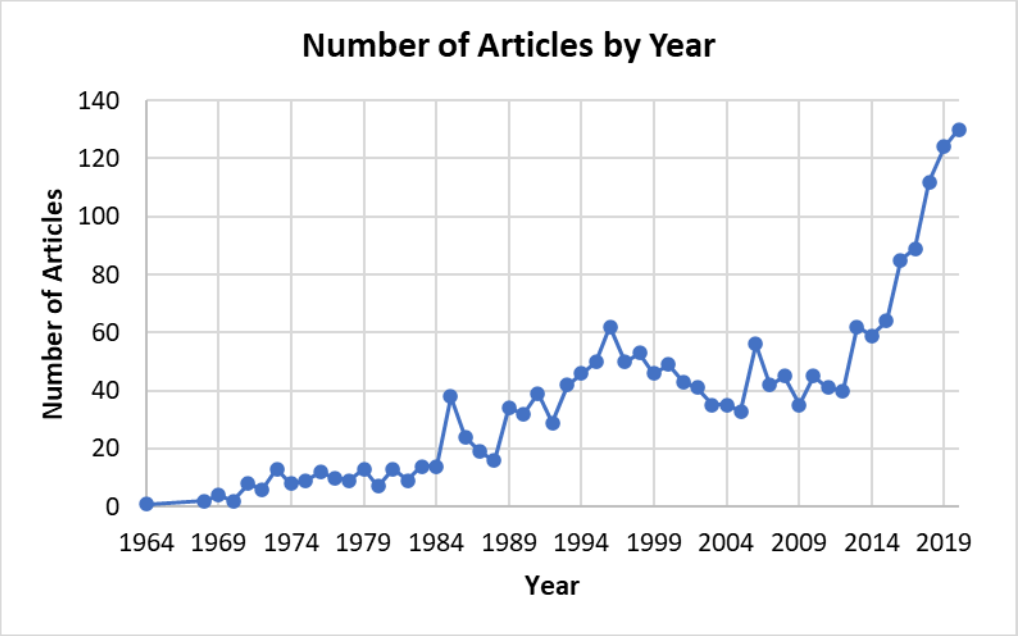

Figure 1.3: *Analysis of Scopus database search for terms "cortical myelin" and "myeloarchitecture" for the years 1964-2020. Scopus is the largest abstract and citation database of peer-reviewed literature and indexes abstracts and references from thousands of scientific journals.*

1.4 Myelin Mapping

Significantly, myelin possesses several important properties that make it MR visible, including its high lipid content. To date, in-vivo investigations of the cortical myeloarchitecture have employed a range of different imaging approaches in order to investigate myelin content (e.g., T1-weighted images, T2-weighted images, T1/T2w ratio images) (Waehnert et al., 2016). There has been particular interest in using T1 (the longitudinal relaxation time) as a biomarker for cortical myelination (Tardif, Gauthier, Steele, Bazin, Schäfer, 2016) as, in healthy subjects, T1 is mostly thought to reflect variations in myelin content (Lutti, Dick, Sereno, & Weiskopf, 2014). Indeed, a recent histological study concluded that myelin is the dominant source of contrast in T1 maps (Stüber, Morawski, Schäfer, Labadie, Wähnert, 2014). Thus far, a number of studies have demonstrated the efficacy of using T1 (or R1 = 1/T1) as a biomarker for myelin concentration, having

demonstrated robust differences in T1 linked to myelin density differences both between brain areas and across volunteers (Waehnert et al., 2016). Furthermore, in line with histology, such studies have also consistently demonstrated a pattern of a decrease in myelin content from primary sensory to transmodal areas (Huntenburg, et al., 2017).

In vivo analyses of the cortical myeloarchitecture based on T1 have employed a variety of quantitative MRI techniques in order to produce T1 or R1 maps of the cortex (Lutti et al., 2014). Quantitative MRI can be seen to confer a number of advantages over traditional weighted images in this regard as the parameters produced using such an approach are more directly related to the underlying biology than conventional weighed images (Weiskopf et al., 2015). This is owing to the fact that they are less susceptible to experimental biases such as inhomogeneties in the magnetic field (Waehnert et al, 2016). As such, quantitative MRI has the potential to provide measures of specific MR parameters (e.g. T1) that can be used as biomarkers of microstructural tissue properties such as myelin (Weiskopf et al. 2015). Significantly, thanks to recent developments in the field of MRI, the application of quantitative MRI has now become feasible at high resolution within reasonable scan times (Tardif et al. 2016). Consequently, investigations of the cortical myeloarchitecture are also increasingly taking advantage of the higher resolution afforded by imaging at 7T in order to achieve submillimetre isotropic resolutions; thus allowing for the visualisation of a higher level of intracortical detail than ever before (Waehnert et al, 2016).

There are a variety of different imaging approaches that can be applied in order to derive quantitative T1 maps of the cortex, with the gold standard technique being the use of an inversion recovery sequence (Tardif et al, 2016). However, the scan times required for such experiments at high field can be prohibitively long (Lutti 2014). Other faster approaches have been proposed, including the use of variable flip angle methods; though again, a potentially prohibitive factor is that such techniques are especially susceptible to biases in the B_1^+ field, particularly at field strengths greater than 3T (Tardif et al, 2016).

Obtaining high resolution images can be viewed as being of particular importance in the context of myelin imaging, given the thinness of the myelinated layers of the cortex. For example, this consideration can be seen to be of particular importance in the context of investigating myelination of the visual cortex, given that the myelinated layers within the primary visual cortex (V1) are only 1.1mm in thickness and the structure of V1 is also highly

convoluted. Hence partial volume effects can result in poor definition between the grey and white matter boundary in this region (Bock et al., 2013).

1.5 Laminar MRI

Traditionally, the laminar structure of the cortex has predominantly been observable through the use of invasive histology-based methods, making it a challenging investigative target. However, in recent years there has been growing interest in the visualisation of the cortical laminae in-vivo. To this end, methodological advances inthe field of MRI have been harnessed in order to explore the laminar structure of the cortex non-invasively. Early proof of concept studies naturally focused on the highly myelinated stria of Gennari, a hallmark feature of the primary visual cortex (e.g. Barbier et al., 2002, Turner et al., 2008). However, successful visualisation of the layered structure of the cortex and in particular the inner band of Balliarger, has also been achieved in areas outside of the primary visual cortex (Trampel, Bazin, Pine & Weiskopf, 2019).

Within the cortex, myelin density is also known to vary across the cortical laminae. For example, myelination is higher in deeper cortical layers compared to those occurring more superficially. Significantly, a number of studies have recently demonstrated the feasibility of conducting MRI investigations of the cortical laminae and in particular, intra-cortical myelination patterns, using quantitative MRI techniques. For example, Sereno, Lutti, Weiskopf & Dick (2013) used quantitative R1 mapping in order to measure local myelination patterns within visual areas of the cortex. Significantly, akin to findings from ex-vivo post-mortem investigations, they were able to observe a decrease in R1 values when moving from deeper to more superficial layers, with a notable plateauing in the middle layers. A further study of the auditory cortex by Dick et al. (2012), again using quantitative R1, also found a similar pattern of a decrease in R1 from the grey/white matter border to superficial depths of the cortex, with a notable plateau once again evident at middle cortical depths. Such findings evidently correspond with the known patterns and distribution of intracortical myelin, thus pointing to the utility of quantitative MRI techniques in the investigation of depth-specific patterns of cortical myelination.

Although the aforementioned studies have typically focused on a particular cortical area, more recent investigations have employed 7T MRI in order to investigate depth-specific patterns of intra-cortical myelination on a whole brain level. For example, Sprooten et al. (2019) acquired high resolution T1 maps at 0.5mm isotropic and extracted T1 values sampled at 20 cortical depths in 148 different cortical areas. Significantly, in line with previous investigations, they were also able to show a decrease in T1, which is inversely related to myelin (and R1), from the pial surface to the boundary of the grey and white matter. Once again, a slight levelling was also observed, in this instance between 50% and 75% of the cortical depth. Furthermore, evidence of regional differences including higher myelination of sensory cortices was also apparent.

Intriguingly, recent studies have also highlighted evidence of depth specific changes in intracortical myelination during adolescence (Whitaker et al., 2016; Lebenberg et al., 2019; Grydeland et al., 2019). Such results are in line with evidence suggesting that cortical areas show differing developmental trajectories with regards to their myelination patterns and furthermore that changes in intracortical myelination with maturation are also in evidence at the level of cortical layers (Glasser & Van Essen, 2011; Lebenberg et al., 2019; Grydeland et al., 2019)

In recent years, an alternative approach to T1 Mapping, one with reduced sensitivity to RF inhomogeneities, has been developed based on the commonly used Magnetization Prepared Rapid Gradient Echo (MPRAGE) sequence (Lutti, 2014). This sequence was designed as a means of obtaining bias free T1-w images in combination with the estimation of quantitative T1 maps at high field (Marques & Grutter, 2013). A particular advantage of the Magnetization Prepared 2 Rapid Acquisition Gradient Echoes (MP2RAGE) sequence is thus its suitability for use at high field. Furthermore, the sequence also allows T1 to be disentangled from the contribution of other factors such as T2* and proton density that are present in standard T1-weighted images, thus allowing for quantitative comparisons between subjects and scanners (Huntenburg et al., 2017).

To date a number of publications have demonstrated the utility of the MP2RAGE sequence at 7T in providing high resolution quantitative T1 maps suitable for studying the myeloarchitecture of the brain (Marques, Khabipova, & Gruetter, 2017). Though alternative approaches to deriving estimates of myelin, such as Magnetization Transfer (MT) imaging, may offer greater specificity for myelin, such techniques provide lower resolution and can be

challenging to implement at 7T (Huntenburg et al., 2017). Furthermore, a recent study utilising the MP2RAGE sequence at 7T found evidence to suggest that the R1 maps derived using this technique provided both higher reliability and reproducibility than other parameters (e.g. T1 and T2* images, both weighted and quantitative) (Haast, Ivanov, Formisano,& Uludağ, 2016).

However, despite optimisation of the MP2RAGE sequence for use at high field, the resulting T1 maps can show some residual transmit field biases. That said, it has been shown that such residual sensitivities to B_1^+ inhomogeneities can be removed using information derived from a B_1^+ map (Marques & Grutter, 2013). In particular, a number of studies have demonstrated the feasibility of using the Saturation Prepared with 2 Rapid Gradient Echoes (SA2RAGE) (Eggenschwiler, Kober, Magill, Gruetter & Marques, 2012) B_1^+ mapping sequence in order to provide a map of the B_1^+ field that can be used to correct the T1 maps obtained from the MP2RAGE sequence for inhomogeneties in the B_1^+ field (Marques & Grutter, 2013). Thus, in the current thesis we proposed to investigate the utility of using the MP2RAGE sequence, in combination with a map of the B_1^+ field (acquired using SA2RAGE), in order to derive high-resolution, bias free, quantitative T1 maps of the cortex that can be used as an in vivo marker of cortical myelination.

1.6 Cyto and myeloarchitecture

The aforementioned myeloarchitectonic descriptions of the cortex produced by the Vogts were derived using preparations of brain tissue stained with the Weigert method, which has the ability to detect myelinated nerve fibres. While this approach undoubtedly led to the production of beautifully detailed depictions of the cortical myeloarchitecture (Nieuwenhuys, 2013), other researchers, such as Braitenberg (1962) sought to develop a more objective, quantitative approach to the appraisal of myeloarchitectonics. This was achieved through the use of optical measurements of sections of brain tissue, again stained using the Weigert method. Using this novel approach, estimates of fibre density could be extracted, based on the assumption that light absorption is exponentially related to the number of fibres per volume of the cortex (Braitenberg, 1962).

Interestingly, in addition to documenting the fibre density in 14 different cortical areas using this approach, Braintenberg also made a number of observations regarding the relationships between the myeloarchitecture of the cortex and its functional microcircuitry. Of particular interest, in the context of the current thesis, is Braitenberg's observation that "Most of the horizontal fibres in the strias are, according to Cajal, collaterals of the descending axons of pyramidal cells" (Braitenburg, 1962). Braitenburg further remarks that these horizontal axon collaterals leave the descending axons approximately 200-300 μ below the pyramidal cell body. Given that pyramidal cells are known to be predominantly located in layers 3 and 5 of the cortex, this would consequently produce two main maxima of horizontal fibres in layers 4 and 6 (when shifted downwards by the aforementioned distance with respect to the location of the pyramidal cell bodies). Significantly, these locations correspond to that of two stria, also known as the inner and outer bands of Balliager, which constitute a major feature of the cortical myeloarchitecture. Figure 1.4 taken from Braitenberg (1962) illustrates this principle and shows the estimated contribution of pyramidal cells to the population of myelinated fibres in the cortex.

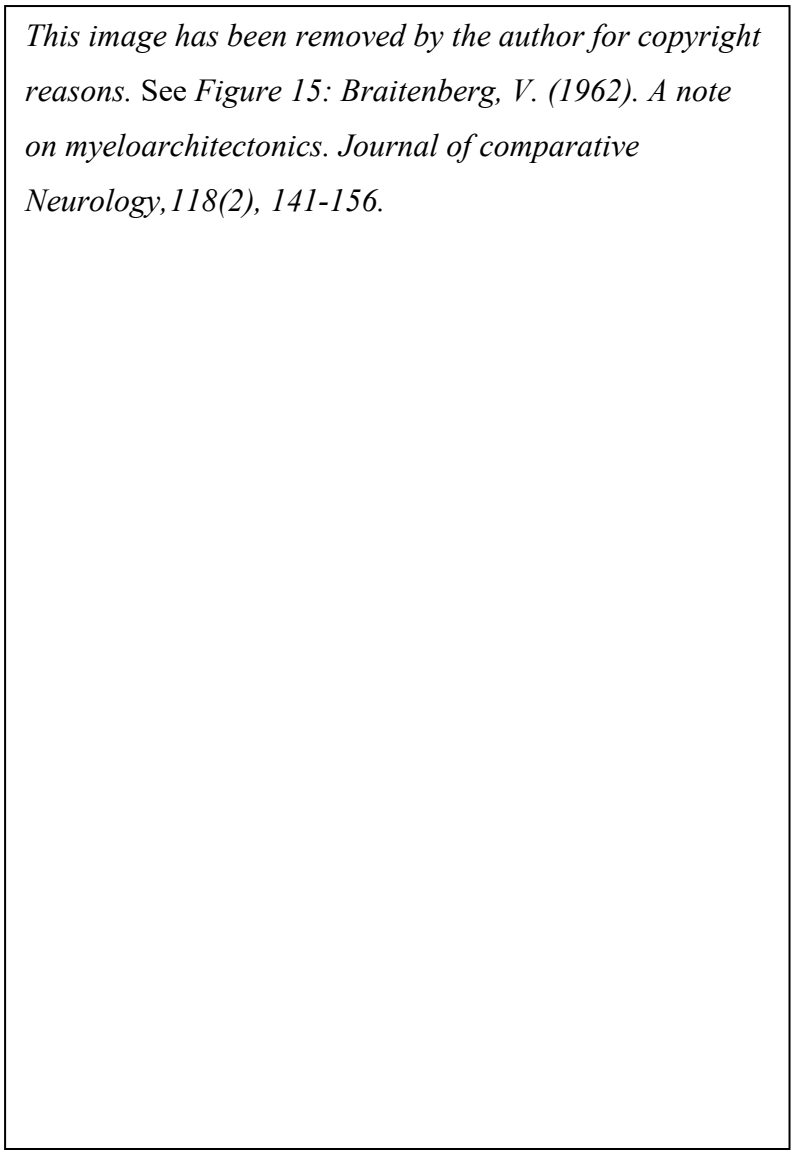

Figure 1.4: *Graphic representation of the results of Braitenberg's analysis showing the contribution of pyramidal cells and their afferents to the population of myelinated fibres inthe cortex. The numbers on the x axis corresponds to the 6 layers of the cortex (given here in roman numerals). For clarity, the original Figure caption is included. Taken from Braitenberg, V. (1962). A note on myeloarchitectonics. Journal of comparative Neurology,118(2), 141-156.*

Throughout much of history, studies have tended to focus on explorations of either the cytoarchitecture or myeloarchitecture of the cortex, with a much greater emphasis on the former evident in the literature. However, the aforementioned observations by Braitenberg (1962) point to an important yet often overlooked fact, namely that a close relationship exists between these two facets of the cortical neurophysiology and furthermore that they are likely inextricably linked.

Indeed, from classical histological investigations, it is evident that the myeloarchitecture and cytoarchitecture of the brain are essentially two aspects of the same anatomical reality and both reflect the cortical microarchitecture (Nieuwenhuys, 2013). In support of this a further study by Hellwig (1993) demonstrated how information derived from the cytoarchitecture could be used to estimate myelin density in 14 different cortical areas. Adapting Hellwig's approach, a recent study has demonstrated that in-vivo quantitative maps of T1-contrast, related to myelin, can also be predicted on the basis of cytoarchitectural a-priori information (Dinse, Härtwich,Waehnert, Tardif, Schäfer, 2015). Furthermore, it is suggested that this modelling approach could also be used to make inferences about the brain's cytoarchitecture by using quantitative T1 maps to make estimates regarding patterns of cytoarchitecture (Dinse et al., 2015).

Grey matter myelin is thought to predominantly occur in the local connections between neurons connecting neighbouring layers of the cortex (Allen, et al., 2017). However, in recent years, emerging evidence has also suggested that another key feature of the cortical microcircuitry, namely inhibitory interneurons, might also be myelinated. Advances in neuroanatomy methods have also allowed for important new insights into cortical myelin, by allowing for its direct visualisation on the axonal arbours of neurons (Micheva et al., 2016). For example, hitherto, the distribution of myelinated swathes along the length of axons had been assumed to be uniform. However, using electron microscopy to produce 3-D reconstructions of the axons of individual pyramidal cells, derived from mouse neocortex, Tomassy et al. (2014) were able to show evidence of heterogenous profiles of myelination of pyramidal cells. Furthermore, myelination patterns were also found to vary in different cortical layers, with the superficial layers of the cortex exhibiting the most diverse profiles.

Using recently developed methods to study myelination in the mouse neocortex, Micheva et al. (2016) also found that a significant portion of cortical myelin can be found on the axons of parvalbumin-positive basket cells, a type of inhibitory interneurons. Significantly, this finding seemingly stands in direct contradiction to the aforementioned assertion of earlier authors such as Braitenberg (1962) that the horizontal myelinated fibres of the cortex correspond to the axons of pyramidal cells (Turner, 2019).

A further study by Micheva et al. (2018) using neurosurgically excised tissue obtained during surgery for epilepsy treatment also investigated, for the first time, the relative abundance of inhibitory myelinated axons in the cortex of the human brain. Significantly, this study also found evidence of myelinated parvalbumin interneurons in all layers of the human cortex.

However, it is interesting to note that the proportion of myelinated interneurons found in this study was far less than that documented in the authors' earlier study of the mouse cortex. For example, based on their experimental findings, Micheva et al. (2018) estimated the highest percentage of inhibitory GABA myelinated axons in the human cortex to be localised to layer 3, where they account for roughly 10%. Conversely, in mice, GABA myelinated axons were found to constitute roughly 48% of the axons in layers 2/3 of the mouse cortex.

However, it should be noted that the human samples utilised in this study were taken from the temporal cortex, whereas those from the mouse model were obtained from the visual and somatosensory cortices. Regardless of the obvious challenges arising from inter-species comparisons, given that the latter brain regions are known to be more heavily myelinated than the temporal cortex, it is therefore rather unsurprising that significant differences in the proportion of myelinated GABA axons were found. Notably, the visual cortex is also the region of the human brain that has the highest GABA receptor density (Zilles & Palomero-Gallagher, 2017). That said, it is interesting to note that the density of non-GABA myelinated axons was not found to differ significantly between the human and mouse cortical samples, except in the superficial layers of the cortex (layers 1, 2 and 3), where the humans' cortex was found to possess a greater density of non-GABA myelinated axons. Ultimately, further research in a more diverse array of brain areas is required in order to disentangle these findings. Given that deficits in both pyramidal cells and inhibitory interneuron functioning have been implicated in a wide array of psychiatric disorders, such investigations could ultimately be of great clinical significance.

Significantly, pyramidal cells and inhibitory interneurons have been implicated in the generation of neural oscillations which represent a key facet of neural activity thought to be involved in a wide range of sensory and cognitive processes.

1.7 Neural oscillations

As mentioned above, mapping the myeloarchitecture of the brain in-vivo has the potential to significantly enhance our understanding of structure-function relationships by allowing for the estimation of direct correlations between microstructure and function in vivo. Thus far, a number of studies have already employed high resolution fMRI in combination with

structural MRI in order to probe the relationship between brain structure and function (e.g. Dick et al., 2012). However, although fMRI is capable of providing excellent spatial resolution, given the somewhat convoluted dependence of the BOLD signal on both haemodynamic and neurovascular coupling parameters, it cannot be interpreted as a quantitative index of neural activity and is thus only able to provide an indirect view (Hall, Robson, Morris, & Brookes, 2014, Singh, 2012).

Electrophysiological techniques, such as MEG on the other hand, whilst offering poorer spatial resolution in comparison to fMRI, possess excellent temporal resolution (millisecond precision) and are able to provide a direct measure of cortical current flow (Helbling et al., 2015). The origin of the MEG signal observed at the scalp is thought to derive from the coordinated activity of networks of pyramidal cells and it is estimated that a minimum of 10,000 to 50,000 pyramidal cells are required in order to produce a signal detectable with MEG (Baillet, 2017).

A key strength of more direct neurophysiological imaging techniques, such as MEG is its ability to investigate a rich variety of neural activity, including neural oscillations. Such oscillations are a prominent feature of neuronal activity and can be measured using invasive local field potential (LFP) recordings, where they are believed to reflect the summed post-synaptic potentials of neurons located in close proximity (within a millimetre) of the recording electrode (Singh, 2012). However, these signals can also be measured non-invasively using MEG/EEG. At this macroscopic level these signals are thought to represent the synchronous activity of a much larger area of the cortex (Singh, 2012). Significantly, the synchronization of oscillatory activity has been touted as a fundamental mechanism sub-serving neuronal communication (Schnitzler, & Gross, 2005). Indeed, converging evidence suggests that neural oscillations represent a central process enabling the coordinated activity of neuronal populations during normal brain functioning (Uhlhaas & Singer, 2010).

Notably, neuronal oscillations are typically categorized into five frequency bands, namely delta, theta, alpha, beta and gamma - and there exists ongoing debate within the neuroscience community regarding the functional roles of these different frequencies and whether they have distinct physiological roles (Engel, & Fries, 2010).

Oscillations in the gamma range in particular have garnered much research interest and constitute the main focus of Chapters 3, 4 and 5 of this thesis. Though the exact genesis of these oscillations remains the subject of continued investigation, gamma oscillations are

thought to be produced by networks of reciprocally connected excitatory pyramidal cells and inhibitory interneurons and are thus believed to emerge from the coordinated interaction of excitation and inhibition (Buzsaki and Wang, 2012). These oscillations have been attributed a wide range of functions and implicated in a variety of cognitive and behavioural processes, including memory (Sederberg et al., 2007) and attention (Bauer, Stenner, Friston, & Dolan, 2014). Furthermore, they have been suggested to play a role in both local and large-scale cortical processing (Uhlhaas & Singer, 2010).

Recent evidence has also suggested that synchronisation in the gamma band is strongest in the superficial layers of the cortex, from which feedforward projections typically originate, indicating that gamma oscillations may also subserve feedforward processing in the brain (Michalareas et al., 2016). Aberrant oscillatory dynamics in the gamma range have also been implicated in a wide range of clinicalconditions including schizophrenia (Uhlhaas & Singer, 2010; Shaw, et al. 2019), Alzheimer's disease (Başar et al., 2017) and autism (Simon & Wallace, 2016; Seymour et al., 2019). However, in addition to their mechanisms of generation, the functional and clinical significance of gamma band oscillations remains the subject of intense debate.

As aforementioned, mapping the myeloarchitecture of the brain in-vivo has the potential to significantly enhance our understanding of structure-function relationships by allowing for the estimation of direct correlations between microstructure and function in vivo.

1.8 Myelin – functional significance

As outlined above, a growing body of research has considered the spatial distribution of myelin in the brain and its implications for both the accurate delineation of cortical areas and the investigation of structure-function relationships. However, discoveries of regional and indeed laminar differences in the distribution of cortical myelin revealed by such work naturally raises the intriguing question of what the functional significance of these patterns of cortical myelination might be.

In this regard, it is important to consider that myelin itself has also been implicated in subserving brain communication, through its ability to help speed nerve conduction, at least in the case of the subcortical white matter (Fields, 2014).

According to Turner (2019), however, in comparison to their white matter counterparts the myelinated radial fibres found in the cortex are considerably smaller, being typically less than 2mm in length. Thus, explaining the myelination ofthese axons in terms of its necessity in facilitating high conduction velocities is somewhat unconvincing. Thus, it is likely that other functional considerations might also be at play.

Of note, the timing and synchrony of action potentials is essential for the optimal functioning of neuronal networks and intra-cortical myelin has been suggested to play a key role in optimization of these parameters (Tardif et al. 2015). To date the majority of studies have focused on the importance of white matter myelination and its role in neuronal synchronisation. For example, a relationship between white matter myelination and the amplitude of electrophysiological responses has previously been demonstrated (Westlye, Walhovd, Bjørnerud, Due-Tønnessen & Fjell, 2008). In contrast to the more global, large-scale integration effects of WM myelin, it is possible that intracortical myelin might also influence synchronization occurring within more local neuronal networks, which could in turn be reflected in the magnitude of signals recorded using MEG/EEG (Grydeland, Westlye, Walhovd & Fjell, 2015). In line with this suggestion, a recent multimodal MRI-EEG study found that the amplitude of the ERN response, a putative marker of error and processing and cortical control, was positively associated with levels of myelin in the posterior cingulate cortex (Grydeland et al., 2015). The authors of this study interpret this finding as suggesting that the degree of cortical myelination may play a role in error monitoring through its relationship with ERN, possibly by assisting local neural synchronisation. Thus, this study can be seen to provide evidence to suggest that synchronous activity reflecting error processing is related to inter-individual variability in intracortical myelin.

Myelin has also been proposed to have an important role to play in shaping neural activity, for example, by adaptively influencing the establishment of precise temporal relations in the brain (Pajevic, Basser & Fields, 2014). In support of this, there is evidence, largely from animal models, of a relationship between myelin and electrophysiology.For example, Gibson et al. (2014) demonstrated that optogenetic stimulation of the premotor cortex in mice promoted oligodendrogenesis, and thus increases in myelination, specifically within the deep layers of the premotor cortex and subcortical white matter. Similarly, in a study by Mitew et al. (2018) stimulation of somatosensory axons in the mouse brain increased both the proliferation and differentiation of oligodendrocyte progenitor cells (OPCs) in the underlying white matter. Stimulated axons were also found to display an increased probability of being

myelinated compared to neighbouring non-stimulated axons, in addition to being ensheathed with thicker myelin. Conversely, attenuating neuronal firing was found to reduce axonal myelination in a selective activity-dependent manner, providing compelling evidence for the role of neural activity in shaping myelination.

Intriguingly it has also been observed that more plastic regions of the cortex, such as those located in frontal regions, possess more complex cortical circuitry whilst also exhibiting less myelin, compared to, for example, primary sensory areas. Furthermore, there is evidence to suggest that myelin-associated factors inhibit both the growth of new axons and synapse formation (e.g. Kapfhammer & Schwab, 1994). This in turn might therefore act to reduce the plasticity of highly myelinated regions of the cortex (Glasser et al., 2014). Consequently, myelin in the cortical grey matter has also been proposed to have a role to play in inhibiting the plasticity of cortical microcircuits (Glasser et al., 2014, Turner, 2019).

Ultimately, a number of intriguing roles have been attributed to myelin in the cortical grey matter and much additional research encompassing a broad array of neuroscientific techniques will be required in order to further explore these possibilities. Furthermore, moving beyond the functioning of particular brain areas it is important to consider how the patterns of myelination observed in the cortex might also influence and indeed be shaped by cortical connectivity.

1.9 Network Perspective

In recent years there has been growing recognition of the fact that inter-areal connectivity and network formation is likely of critical importance for brain functioning (Brookes et al., 2016). Traditionally, brain-behaviour relationships have been studied on the basis of a univariate, regional approach, in line with the view that cognitive functions can be attributed to the isolated operations of particular brain areas (Mišić & Sporns, 2016). In contrast, recent years have witnessed a relative paradigm shift within the neuroimaging field in line with increasing recognition of the importance of dynamic interactions between distributed neuronal populations and brain regions in brain functioning and cognition (Bressler & Menon, 2010). Consequently, there has been growing interest in approaching the brain from a network perspective. Such an approach has been aided by technical advances within the neuroimaging

field that have opened a wealth of new possibilities for studying the structure and function of the human brain at the network level (Sporns, 2013).

A considerable body of research has focused on the role of neural oscillations at the network level, and it is thought that these signals may play an important role in global as well as local brain communication. Indeed, converging evidence suggests that neural oscillations represent a fundamental process enabling the coordinated activity of neuronal populations during normal brain functioning (Uhlhaas & Singer,2010). Measures of association between neuronal oscillations can be investigated through the use of both the correlation of their relative phase or amplitude and there is a growing evidence indicative of the fact that such correlations of frequency-specific oscillations in diffuse cortical networks index the neural interactions underlying cognitive processes (Siegel, Donner, & Engel, 2012).

Inter-regional connectivity has also been consistently found even when the brain is ostensibly at rest, and recent years have correspondingly witnessed a rapid growth in the number of resting-state MEG investigations; with such studies having pointed to the role of oscillations in the formation of such intrinsic networks (Brookes et al., 2016). Electrophysiological investigations of resting state connectivity represent a valuable tool for investigating the nature of intrinsic brain activity, owing to their rich temporal resolution and ability to disentangle the oscillatory frequency-specific origins of resting state networks (Colclough et al., 2016).

Building on this idea, a recent study by Hunt et al. (2016) probed the relationship between myelination of the cortex and resting state oscillatory networks and found evidence suggestive of a relationship between the microstructure of the brain and its function at the network level. This study was based on the idea that, given evidence from animal models of electrical-activity dependent myelination, if functional networks are indeed representative of pathways of electrophysiological communication in the brain, then these pathways might therefore shape myeloarchitecture. Hence, a relationship between functional connectivity and the myeloarchitecture of the brain might be discernible. In the investigation by Hunt et al., (2016) structural covariance of myelination was used in order to derive a structural network. The structure of cortical regions is known to show marked inter-individual differences and there is also increasing recognition of the fact that inter-individual differences in the structure of a brain region often co-varies with inter-individual differences in other brain regions (Alexander-Bloch, Giedd, & Bullmore,2013). This phenomenon is known as structural

covariance and shows that inter-individual differences in regional structure are coordinated within communities of brain regions that fluctuate together in size across the population (Alexander-Bloch,Giedd, & Bullmore, 2013).

Significantly, Hunt et al. (2016) found that functional networks in the beta and gamma bands significantly predicted the spatial pattern of structural covariance, given that brain areas that were found to be highly functionally connected also exhibited cross-subject covariation in myeloarchitecture. This raises the intriguing possibility that, given the role of myelin in speeding neuronal conduction, cortical myelination may be shaped to support functional networks as this could maximise the efficiency of their formation. This study can therefore be seen to provide compelling evidence of a relation between the microstructure of the brain and oscillatory networks, thus demonstrating the feasibility of investigating the relationship between the microstructure of the brain and its function in the context of cortical networks.

A considerable body of research in monkeys has also suggested that an intricate relationship likely exists between the microstructure of the brain and connectivity (Huntenberg et al., 2017). For example, long range connections have been preferentially found between brain regions that demonstrate similar microstructural properties. As such it has been suggested that microstructural features of the cortex, such as its myelin content, may also be related to functional connectivity patterns. In line with this suggestion, a multi-modal MRI–fMRI study by Huntenberg et al. (2017) has documented evidence of a relationship between intercortical myelin and functional connectivity. Indeed, this investigation found that regions that exhibit similar myelin content show higher functional connectivity than regions that differ in their myelin content. Significantly, this study also controlled for variations of cortical thickness and found that intracortical T1 captures variance in functional connectivity beyond what is explained by cortical thickness. Hence, this pattern of findings can also be taken to suggest that the microstructure of the brain may have an important role to play in shaping connectivity in the brain and may be representative of a general wiring rule of the cerebral cortex (Huntenburg et al., 2017).

Thesis objectives and outline of experimental chapters

Taken together, the converging lines of evidence outlined above suggest that an investigation of the relationship between inter-individual variability in intra-cortical myelin and MEG signals could provide fascinating new insights into the nature of structure-function relationships in the brain and their relevance for cognition. Thus, the principle aim of the current project is to determine whether the relationship between the microstructure of the brain and its oscillatory dynamics can be explored in vivo. The study will correspondingly adopt a multimodal neuroimaging approach utilising high resolution quantitative MRI, in combination with MEG, in order to investigate the relationship between cortical myelin and MEG signals. More specifically, we propose to investigate the relationship between the cortical myeloarchitecture and a key feature of neural activity, known to be of great cognitive and clinical relevance: namely, cortical oscillatory dynamics. In sum, the primary aims of the current thesis are as follows:

1) To develop a robust and reliable imaging pipeline that allows for the acquisition of high resolution quantitative T1 maps that can be used to relate indices of cortical myelination to in vivo markers of electrophysiology.

2) To replicate findings of an association between MEG signal strength and myelin density in relevant cortical regions.

3) To explore the relationship between myelination of the cortex and neural oscillations at both the local and network level.

In accordance with these aims we conducted a multi-modal investigation, combining7T MRI and MEG, in which participants completed a number of experimental paradigms designed to probe oscillatory dynamics at the local and network levels. The next chapter of this thesis (Chapter 2) explores in more detail the methodologies employed in the present investigation and in particular the development of our pipeline for deriving high resolution estimates of cortical myelin content at 7T.

In Chapter 3 of this thesis, which constitutes the first experimental chapter proper, the relationship between visual gamma oscillations, as measured using MEG, and myelination of the primary visual cortex is explored. Significant correlations, between induced peak gamma

oscillatory dynamics and myelin, were not found after correcting for multiple comparisons. However, further exploratory analyses of the whole frequency spectra did point to an intriguing potential relationship between 40 Hz gamma activity and superficial myelin content.

In the second experimental chapter of this thesis (Chapter 4) we exploit the greater specificity of computational modelling approaches, and in particular dynamic causal modelling (DCM), in order to investigate the potential existence of relationships between the cortical microcircuitry and myelin content in the visual cortex.

Ultimately, we did not find evidence of a significant relationship between the DCM model parameters and our cortical myelin estimates. However, methodological limitations may have contributed to this null finding. Future avenues of research potentially better suited to elucidating the relationship between the cortical myeloarchitecture and the neurophysiology of visual gamma are discussed.

Moving beyond the visual cortex Chapter 5 of this thesis details a novel investigation of the relationship between inter-individual variability in gamma band auditory steady state responses (ASSRs) and myelination across the cortical depth. In this study a trend indicative of a positive correlation between the amplitude of the ASSR and cortical myelination, particularly at lower cortical depths, was observed. However, further research is required in order to test the validity and significance of the trend observed.

The final experimental chapter of this thesis (Chapter 6) adopts a network level approach in order to explore the relationship between depth-specific estimates of intra-cortical myelin and MEG derived functional connectivity. Notably, here, for the first time, we show evidence of a cortical depth-dependent relationship between cortical myelin and frequency-specific resting-state MEG networks.

Lastly, the final chapter of this thesis (Chapter 7) provides a general discussion of the main findings of the present thesis and their interpretation in light of the pre-existing literature. Important avenues of future research are also discussed.

Chapter 2

Methods

2.1 Abstract

This chapter provides an overview of the neuroimaging methodologies employed in this thesis. A more detailed description of the analysis procedures and pipelines utilised is provided in the relevant experimental chapters. The first neuroimaging technique described in this chapter is Magnetoencephalography (MEG) which was used to in order to derive our measures of oscillatory dynamics. The remainder of this chapter is dedicated to the second neuroimaging technique employed in this thesis, namely magnetic resonance imaging (MRI). Finally, the development of the pipeline for acquiring high resolution estimates of cortical myelin content at 7T relevant for all the experimental chapters of this thesis is described.

2.2 MEG – Basic principles

The first key neuroimaging technique employed in this thesis is Magnetoencephalography (MEG), a non-invasive functional imaging method which provides a direct window onto neural activity in the brain. The use of MEG as a neuroimaging technique was first demonstrated by Cohen (1968) who showed that it was possible to detect the magnetic fields outside the human head produced by alpha-rhythm currents. This pioneering study was based on the use of a single sensor. However, today MEG recordings are typically performed using multichannel systems that provide whole head coverage.

The basic principles of MEG rely on the fact that all electrical currents are accompanied by a corresponding electromagnetic field perpendicular to the direction of the current (in accordance with Ampere's right hand grip rule). This principle is as true for a current carrying wire as it is for the electrical currents produced by neural activity in the brain.

Crucially, the strength of the magnetic field produced is dependent on a number of factors including the strength, distance, and geometry of the electrical current distribution from which it arises (Hari, Parkkonen, & Nangini, 2010).

Significantly, MEG is a neuroimaging technique that is able to measure the resultant neuromagnetic fields generated by neural activity in the brain. A key advantage of MEG in contrast to EEG is that these neuromagnetic fields are thought to be relatively unaffected by the presence of the skull, although significant attenuation occurs for deeper sources (Okada, Lahteenmäki, & Xu, 1999). That said, the measurement of these magnetic signals is far from trivial, especially when consideration is given to the fact that neuromagnetic fields are exceedingly weak, being in the region of 10–100 fT (Hari & Salmelin, 2012), especially in contrast to the magnetic fields generated by noise factors in the environment.
Thus, the ability to detect these signals relies on the use of an innovation known as a super-conducting quantum interference device (SQUID) (Zimmerman, Thiene & Harding, 1970). These devices are extremely sensitive detectors of magnetic fields, possessing enough sensitivity to measure the weak neuromagnetic fields produced by neural activity in the brain. Once detected, SQUIDs have the ability to convert magnetic flux into an electric voltage, which is recorded (Hari, Parkkonen, & Nangini, 2010). However, whilst SQUIDS undoubtedly exhibit high sensitivity to magnetic fields their configuration is not optimal for the detection of those produced by the brain (Vrba and Robinsons, 2001). Consequently, they are typically used in conjunction with larger pickup coils, known as gradiometers, the geometry of which is optimised to ensure that external magnetic disturbances, such as those more distant from the brain, are reduced (Hämäläinen, Hari, Ilmoniemi, Knuutila & Lounasmaa, 1993). Of note, a diverse array of configurations of these pickup coils exists though there are four main types, namely Magnetometers, 1st and 2nd order axial gradiometers, and planar gradiometers, each if which detects a different field pattern (Vrba and Robinsons, 2001).

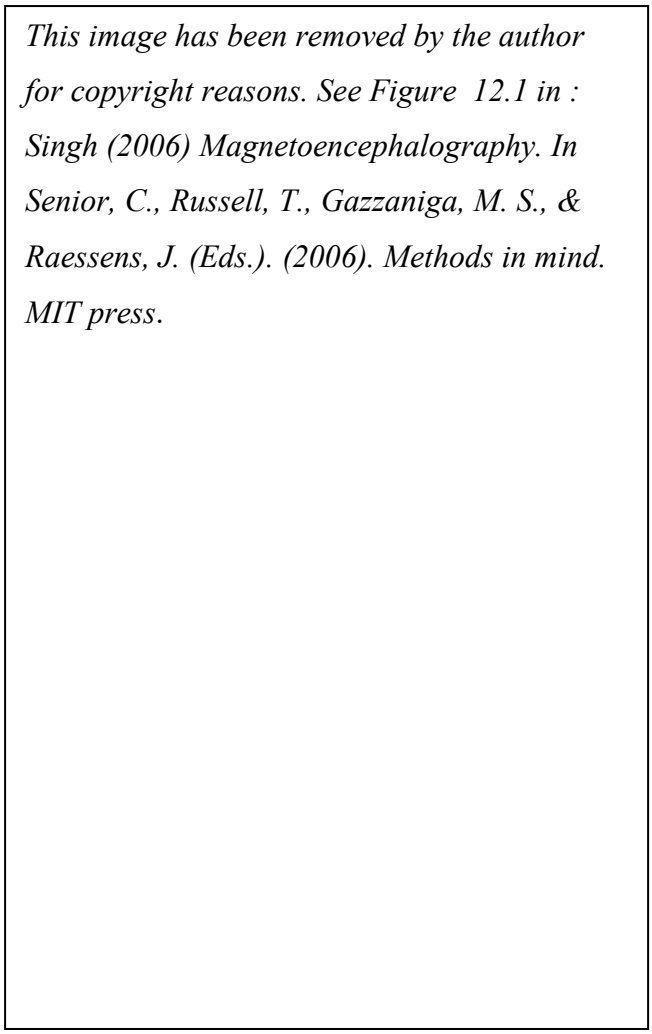

Figure 2.1 *: **A)** Overview of the generation of a measurable MEG signal (magnetic field) from populations of synchronously firing pyramidal cells. **B)** This part of the figure represents the source configurations generated in the MEG sensors by different dipole (single focal neuronal source) orientations. In this figure red delineates magnetic fields entering the head, whist blue indicates field lines exiting the head. For the radial source orientation, no field is measured. Figure taken from Singh (2006) Magnetoencephalography. In Senior, C., Russell, T., Gazzaniga, M. S., & Raessens, J. (Eds.). (2006). Methods in mind. MIT press.*

The main generators of the MEG signal observed at the scalp are thought to be the synchronous postsynaptic currents produced by pyramidal neurons (Hämäläinen and Hari, 2002). This is largely owing to the fact that they typically last longer than action potentials whose occurrence is much more rapid (Baillet, 2001). It is estimated that a minimum of 10,000 to 50,000 pyramidal cells are required in order to produce a signal detectable with MEG (Baillet, 2017). A further requirement is that the dendritic processes of these cells are spatially aligned in order to allow for the measurement of a detectable signal. The apical dendrites of pyramidal cells possess a similar orientation and are arranged parallel to one another and perpendicular to the cortical surface. They are thus said to have an 'open field' configuration as the electrical fields from such cells can extend over long distances and can thus be detected at a distance from their neuronal source (Murakami, & Okada, 2006, da Silva, 2013).

Two key factors determine both the amplitude of neuromagnetic fields and the extent to which localisation of the underlying currents is possible. The first of these is the Bio-savart law, according to which a magnetic field will get weaker with distance from the current source. Furthermore, radially oriented current dipoles will not produce a magnetic field outside of a spherically symmetric homogeneous volume conductor (Sarvas, 1987). On the basis of these principles, MEG has been argued to be insensitive to both deep and radially oriented sources (i.e the cortical gyri). However, there is reason to be optimistic, at least with regards to the latter point. More specifically, Hillebrand & Barnes (2002) found that radial sources form less than 5% of the whole cortical area, and thus source orientation does not constitute a significant limitation of the sensitivity of MEG.

A key strength of MEG as a neuroimaging approach lies in its ability to not only measure neural activity with millisecond precision, but also to localise the sources of this activity in the brain. However, in this regard, a particular challenge in the context of MEG research lies in the ill-posed nature of the MEG inverse problem. The MEG inverse problem seeks to estimate neural current sources underlying an observed distribution of the magnetic field measured using MEG sensors (Baillet, Mosher, & Leahy, 2001). However, this inverse problem is said to be ill posed due to non uniqueness. More specifically, the MEG inverse problem is known to have no unique solution as there are an infinite number of neuronal current distributions that could give rise to the same observed data (Hämäläinen et al., 1993, Dassios & Fokas, 2013).

Consequently, it is impossible to derive a solution to the MEG inverse problem on the basis of the measured data alone. However, providing that appropriate assumptions about the source of interest are made, the solution to the MEG inverse problem can be rendered unique (Hämäläinen et al., 1993). A vast array of methods exist for solving the MEG inverse problem, each of which possesses its own unique set of advantages and limitations. Once such method, applied in the current thesis, that has proven popular in the literature, is the beamforming approach. Put simply, beamformers act as a spatial filter in order to discriminate between signals originating from locations of interest in the brain and those that derive from elsewhere (Baillet, Mosher, & Leahy, 2001). The key principle behind the beamformer approach is that for any given location in the brain it is possible to calculate an optimal set of weights, such that the weighted sum of the MEG sensors is able to provide an estimate of the neural current at that particular location (Barnes & Hillebrand, 2003). There are a number of advantages associated with beamforming approaches to source localisation, including the fact that it is ideally suited to the study of oscillatory activity (Singh, 2006).

However, a significant limitation of beamformer approaches arises due to the assumption of this method that the time series of sources in the brain are not correlated. In such a case, where sources are perfectly correlated in a linear fashion, the beamformer will recover little to no power (Hillebrand et al., 2005). Consequently, beamformer approaches are not optimal for the study of auditory responses such as the auditory steady state responses (ASSR) which are known to give rise to temporally correlated bilateral activation of the auditory cortices.

Thus, a further commonly used source localisation approach, known as minimum norm estimation, was also used in Chapter 5 of this thesis, in order to localise ASSRs. The minimum norm approach uses a distributed source model, in which the amplitude of a large number of dipoles is kept fixed (Hämäläinen, Lin & Mosher, 2010). On the basis of the measured MEG data the amplitude of these dipoles can then be determined. However, this requires additional a priori constraints on the nature of the current density being measured (Hämäläinen, Lin & Mosher, 2010). A key advantage of the minimum norm approach is that unlike in beamformer implementations, correlated sources will not suffer cancellation. Yet a key challenge with this approach is that it can lead to more diffuse solutions that favour superficial sources (Singh, 2006).

2.3 MRI - Basic Principles

Magnetic resonance imaging (MRI) is a non-invasive neuroimaging technique widely used to investigate both the structure and function of the brain. Since the advent of the first MRI scan of a human participant in 1977 (Mansfield & Maudsley, 1977), the technique has seen significant growth, both in terms of its methodology and its popularity within research and clinical settings. MRI can be broadly categorised into two subtypes, namely structural and functional MRI, however the main focus of this thesis will be on the former.

Structural MRI relies on the mapping of the distribution of hydrogen nuclei, which are abundant in the human body. Hydrogen nuclei consist of a single proton and consequently possess the quantum mechanical property known as spin. As a hydrogen nucleus spins around on its own axis, a magnetic moment or field is induced around it. In this way these hydrogen nuclei essentially act as small magnets and have a north and a south magnetic pole. Under normal circumstances the magnetic moments of these nuclei are randomly oriented and thus produce no overall magnetic effect (the net magnetization is zero). However, in the presence of a strong external magnetic field (B0), on aggregate the magnetic moments of these hydrogen nuclei align themselves with the direction of the B0 field either in parallel (spin-up) or anti-parallel (spin-down). Consequently, the orientation of the magnetic moments become non-random creating a net magnetization that is measurable. More specifically, at any given moment in time there are always slightly more nuclei aligned in parallel with the main magnetic field, producing a net magnetisation vector parallel to the magnetic field (Abragam, 1961).

The B0 field also has another important impact on hydrogen protons, affecting how fast they precess. The application of the B0 field produces an additional secondary precession of the nuclei around the main magnetic field. The speed at which these nuclei precess is often referred to as the Larmor frequency and is determined by the Larmor equation, $\omega = \gamma B$, where ω is the Larmor frequency (MHz), γ is the gyromagnetic ratio (MHz/tesla) and B is the strength of the external magnetic field (B0). The precession frequency is therefore directly proportional to the strength of the magnetic field (B0). A typical MRI scan involves the perturbation of the alignment of the hydrogen protons with the B0 field , through the use of a radio frequency (RF) pulse, applied perpendicular to the B0 field,

which produces an oscillating magnetic field known as the B_1^+ field. The purpose of the RF field is to cause the hydrogen protons to fall out of alignment with B0 and occurs due to the transfer of energy from the RF pulse to the protons. Importantly, the frequency of the RF field must be the same as the precessional frequency of the hydrogen protons, in order to ensure that energy transfer can occur. This phenomenon is referred to as resonance.

There are two main impacts on the hydrogen protons associated with the application of the RF field. Firstly, the application of an RF pulse gives energy to the hydrogen nuclei and causes the aggregate effect of a net increase in the number of high energy spin-down nuclei. Concurrently, the application of the RF pulse causes the hydrogen protons to precess in phase. In this context, phase refers to the position of a magnetic moment on its precessional path at any given moment in time. Thus, when hydrogen protons precess in phase, their magnetic moments are at the same place on the precessional path at a given moment in time. As a result of these effects the net magnetization is flipped towards the transverse plane. After the application of the RF pulse the hydrogen nuclei seek to return to their former low-energy state and their magnetic moments de-phase through the process known as relaxation. It is during this process of relaxation that RF waves are emitted from the body, which can be measured by receiver coils. It is from this signal that MRI images are generated.

The process of relaxation has two key consequences, namely the recovery of longitudinal magnetisation (T1 recovery) and the loss of coherent magnetisation in the transverse plane (T2 decay). Both of these represent important sources of contrast in MRI images, however here we focus on the concept of T1. The process of T1 recovery occurs when hydrogen nuclei give up their energy to their surrounding environment and return to equilibrium. According to the classical physics explanation, the proportion of spin up and spin down nuclei changes allowing the net magnetization vector to realign to the longitudinal plane. However, the quantum physics explanation posits that the number of high energy spins decreases, whilst the number of low energy spins increases as the high energy spins lose energy during the relaxation process.

In 1946 Bloch modelled the process of T1 relaxation as a simple exponential process with the time constant T1 (time taken for the net magnetization to reach 63% of its maximum value). The process of T1 relaxation is known to occur at different rates for different

tissues according to their unique properties. For example, the T1 (longitudinal relaxation time) of water is 2500ms, whereas for the brain's white matter this has been shown to be considerably shorter at 500ms (Westbrook & Talbot, 2018; Steen et al., 1994; Wansapura et al., 1999). Notably, given that T1 varies between tissues, it provides an important source of contrast in MRI images. Thus, in the case of T1-weighted images, contrast is predominantly determined by the T1 properties of the tissues being imaged. Hence, the T1 contrast between tissues is typically accentuated in order to produce detailed depictions of the cortical anatomy.

Spatial encoding is achieved in MRI through the use of specially designed gradient coils. The idea that utilising a magnetic field gradient in addition to the main magnetic field could be used for signal localisation purposes, given that signals along the gradient will have different frequencies, was proposed by Lauterbur in 1973. Thus, in order to gain spatial information, gradient coils are used in order to apply an additional magnetic field that distorts the main magnetic field in a predictable way, with the precessional frequency of protons varying as a function of their position along the direction of the gradient. Typically, 3 gradient coils are used in MRI – the X,Y Z gradient coils, each of which acts along a different axis.

2.4 T1 and Myelin

Of particular interest in the context of the present study is the fact that the longitudinal relaxation time (T1) is sensitive to the myelin content of the brain (Lutti et al., 2014). More specifically, T1 has been suggested to be sensitive to factors including myelin bound cholesterol (Koenig,1991). To date, a number of studies combining quantitative MRI methods and histology have demonstrated evidence of a high correlation between the brain's myelin content and T1 relaxationtimes, with this relationship having been reported to be as high as r =0.89 in post-mortem samples (Schmierer et al., 2008). Of note, such studies have focused on examining this relationship in the brain's heavily myelinated white matter. However, as argued by Lutti et al. (2014) there is no theoretical reason to suspect that this relationship will differ in the case of the myelin contained in the cortical grey matter.

Although, the relative contribution of particular compounds to MR parameters such as T1 remains the subject of ongoing investigation, myelin has been suggested to be the

dominant source of contrast in T1 images. For example, Stuber et al., (2014) used a novel technique, proton induced X-ray emission (PIXE), in order to investigate the relative contributions of iron and myelin as sources of contrast in MP2RAGE derived T1 maps in both the grey and white matter of the brain.

Significantly Stuber et al. (2014) found that, on average, myelin had a contribution of 64% to R1 (1/T1) contrast in the grey matter of the brain and 90% in the white matter. Iron was also found to contribute to R1 contrast, although to a lesser extent,with an average contribution of 36% on grey matter and 10% in white matter. Thus, these results pointed to myelin as being the dominant source of contrast in T1 (and R1) maps.

2.5 MP2RAGE

In the present study we chose to utilise the MP2RAGE sequence in order to derive our high resolution R1 maps. The decision to use this method was guided by the suitability of this technique for use at 7T, its ability to acquire high-resolution T1 maps in a relatively short acquisition time, and previous studies demonstrating the utility of the method.

The MP2RAGE sequence (see Figure 2.2) was specifically designed as a means of obtaining bias free T1-weighted images in combination with the estimation of quantitative T1 maps at high field (Marques & Grutter, 2013). The MP2RAGE is an extension of the standard MPRAGE sequence which is frequently used to obtain T1-weighted images of the brain. In the MP2RAGE sequence, there are two inversions, and two volumes are acquired after each inversion. By acquiring two gradient echo images at different inversion times (GRE_{TI1} and GRE_{TI2}), whilst keeping other sequence parameters constant, both images will be equally affected by the B_1^+ field, proton density and T2* effects. Combining these images, by means of a ratio method (see Eq1.) , will therefore result in a synthetic image independent of these aforementioned effects. Thus, theMP2RAGE can be seen as a method of quickly measuring T1. Given its reduced susceptibility to inhomogeneities in the B_1^+ field, the MP2RAGE sequence is also an attractive option for T1 imaging at high field (>3T).

Eq1:

$$\text{MP2RAGE} = \frac{GRE_{TI1}\, GRE_{TI2}}{GRE^2_{TI1} + GRE^2_{TI2}}$$

Given the acquisition of two inversion times, the MP2RAGE also provides a quick method of calculating T1 maps. In order to calculate these maps, the sequence parameters and inversion efficiency of the adiabatic inversion pulse are taken into account (Marques et al., 2010). Using Bloch simulations of these parameters based on the original equations defined in (Marques et al., 2010) the T1 value of each pixel in the image can be calculated through linear interpolation. These simulations and the subsequent estimation of the T1 maps are also integrated into the scanner workflow and thus T1 maps are readily accessible following the scan acquisition (Marques et al., 2010).

This image has been removed by the author for copyright reasons. See Figure 1: Marques, J. P., Kober, T.,Krueger, G., van der Zwaag, W., Van de Moortele, P. F., & Gruetter, R. (2010). MP2RAGE, a self bias-field corrected sequence for improved segmentation and T1-mapping at high field. Neuroimage, 49(2), 1271-1281.

Fig 2.2: *Diagram of the MP2RAGE sequence taken from Marques, J. P., Kober, T.,Krueger, G., van der Zwaag, W., Van de Moortele, P. F., & Gruetter, R. (2010). MP2RAGE, a self bias-field corrected sequence for improved segmentation and T1-mapping at high field. Neuroimage, 49(2), 1271-1281. The two inversion times (TI_1 and TI_2) are defined as the time from the middle of the inversion pulse to the excitation corresponding to the center k-space line in the phase encoding in the slab selection direction. $MP2RAGE_{TR}$ refers to the time between two successive inversion pulses. TR is the time between successive excitation pulses in the GRE kernel, which is composed of n excitations.*

2.6 B_1^+ Mapping

7T MRI allows for the visualisation of the human brain in an unprecedented level of detail, owning to its higher contrast and SNR. However, as the popular saying goes, 'there's no such thing as a free lunch' and these gains come at the expense of the need to grapple with a number of technical challenges associated with imaging at higher field strengths (>3T). One of the most challenging problems to navigate, in the context of high field imaging, is the issue of inhomogeneity in the B_1^+ (RF) field (Balchandani, & Naidich, 2015). These variations in the B_1^+ field are the result of the shorter RF wavelength at 7T, in comparison to lower field strengths, which are more similar to the dimensions of the human head. Significantly, this can result in a reduction of the strength of the B_1^+ field in the brain's periphery in comparison with the centre of the head. Ultimately, this can lead to a number of undesirable effects including changes in image contrast and even signal drop out (Balchandani, & Naidich, 2015).

Unfortunately, these inhomogeneities in the B_1^+ field have been shown to affect the majority of quantitative MRI methods, including T1 mapping (Lutti et al., 2012). Indeed, despite optimisation of the MP2RAGE sequence for use at high field, the resulting T1 maps can show some residual transmit field biases. Thus, it is imperative to derive an accurate measure of the distribution of the B_1^+ field such that an appropriate correction strategy can be employed. Consequently, in the context of quantitative imaging at 7T, the use of a robust B_1^+ mapping technique is vital (Lutti et al., 2012).

A variety of different methods exist for mapping the B_1^+ field, including the relatively straightforward double-angle method (Stollberger, & Wach, 1996) and phase-based approaches such as the Bloch-Siegert method (Sacolick et al., 2010). However, of particular interest in the context of the present thesis, is that studies have already demonstrated the feasibility of using a B_1^+ mapping sequence, known as the SA2RAGE, in order to provide a map of the B_1^+ field that can be used to correct the T1 maps, obtained from the MP2RAGE sequence, for B_1^+ inhomogeneties (Marques & Grutter, 2013).

The recently developed SA2RAGE sequence (Eggenschwiler et al., 2012) allows for a 3D acquisition of the B_1^+ field in a short acquisition time and has been shown to possess a high degree of accuracy over a wide range of B_1^+ values, whilst maintaining a low specific absorption rate (SAR). Furthermore, it is possible to acquire relatively high resolution B_1^+ maps using this method (i.e. 2mm isotropic). This is a particular advantage in the context of the present study as acquiring a higher resolution B_1^+ map will reduce

the likelihood of B_1^+ errors bleeding from the estimations in the skull or fat tissues into relevant cortical areas when the B_1^+ maps are interpolated to the same resolution at the MP2RAGE images. Full details of theSA2RAGE sequence are shown in Figure 2.3.

Hence, for the current project, we investigated the utility of using the MP2RAGE sequence in combination with a map of the B_1^+ field (acquired using SA2RAGE) in order to derive high-resolution, bias free, quantitative T1 maps of the cortex that can be used as an in vivo marker of cortical myelination.

This image has been removed by the author for copyright reasons. See Figure 1: Eggenschwiler, F., Kober, T., Magill, A. W., Gruetter, R., & Marques, J. P. (2012). SA2RAGE: A new sequence for fast $B1^+$ *mapping. Magnetic Resonance in Medicine, 67(6), 1609-1619.*

Figure 2.3 *: Schematic of the SA2RAGE sequence. Taken from Eggenschwiler, F., Kober, T., Magill, A. W., Gruetter, R., & Marques, J. P. (2012). SA2RAGE: A new sequence for fast* $B1^+$ *mapping. Magnetic Resonance in Medicine, 67(6), 1609-1619. The SA2RAGE consists of a 90° RF saturation pulse followed by two gradient echo blocks. The excitation pulses of the two (low) flip angles* α_1 *and* α_2 *within the gradient recalled echo (GRE) blocks are separated by a short repetition time* TR_{flash}*. TD1= the first delay time, whilst TD2= the second delay time.* $TR_{SA2RAGE}$ *= repetition time. First phase encoding direction = PE1, PE2 = second phase encoding direction.*

.

B_1^+ Correction Procedure

In the current thesis SA2RAGE derived maps of the B_1^+ field were used to correct the T1 maps produced by the MP2RAGE sequence for residual transmit field biases in order to

produce bias free high-resolution T1 maps. An overview of the steps involved in this correction procedure are outlined below.

Each participant's SA2RAGE derived B_1^+ map was first registered and interpolated to the same resolution as the MP2RAGE volumes using FSL's FLIRT registration algorithm. This registration is performed using the second inversion contrast image from both the SA2RAGE and the MP2RAGE given that these feature high signal intensity and lower contrast than the combined images. The spatial transformations derived from this registration were then applied to the SA2RAGE B_1^+ maps and the MP2RAGE UNI image. The UNI image is a T1-weighted image, referred to as a uniform (UNI) image.

Subsequently, these registered and interpolated B_1^+ maps were then used to correct the high resolution MP2RAGE Uniform images and T1 maps for residual RF transmit field biases using the methodology outlined in Marques & Gruetter (2013). The code for this B_1^+ correction procedure was kindly supplied by JP Marques and is summarised below.

Firstly, 2D lookup tables (see Figure 2.4) detailing the T1 values associated with particular values of The MP2RAGE signal and B_1^+ are calculated. Similarly, a further 2D lookup Table containing the B_1^+ values associated with particular values of the SA2RAGE signal and T1 were calculated. Examples of these lookup tables are shown in Figure 2.4.

Using these two lookup tables a 2-D interpolation was then iteratively performed for each pixel in the images. In the first instance, the B_1^+ was calculated by assuming a constant value of T1 throughout the brain (1.5 seconds). The B_1^+ values derived using this approach were then used to estimate the T1 values, again this was achieved through the 2D interpolation of the MP2RAGE lookup table (Figure 2.4 a). This process is then repeated using the new T1 estimates for each of the image voxels. Three repetitions of this process are conducted after which, variations in both T1 values and B_1^+ have been found to be less than 10^{-3} on the third and final iteration (Marques & Grutter, 2013). As a result of this process corrected B_1^+ and T1 maps are produced. Figure 2.5 shows an example of the effect of the B_1^+ correction procedure on the T1 maps.

This image has been removed by the author for copyright reasons. See Figure 3: Marques, J. P., & Gruetter (2013). New Developments and Applications of the MP2RAGE Sequence-Focusing theContrast and High Spatial Resolution R 1 Mapping. PloS one, 8(7), e69294

***Figure 2.4**: This Figure depicts an example of the Lookup tables used to compute: (a) the R1 (1/T1) maps for the MP2RAGE sequence and (b) the* B_1^+ *maps for the Sa2RAGE in the original work by Marques et al.,(2013). Figure taken from Marques, J. P., & Gruetter (2013). New Developments and Applications of the MP2RAGE Sequence-Focusing theContrast and High Spatial Resolution R 1 Mapping. PloS one, 8(7), e69294*

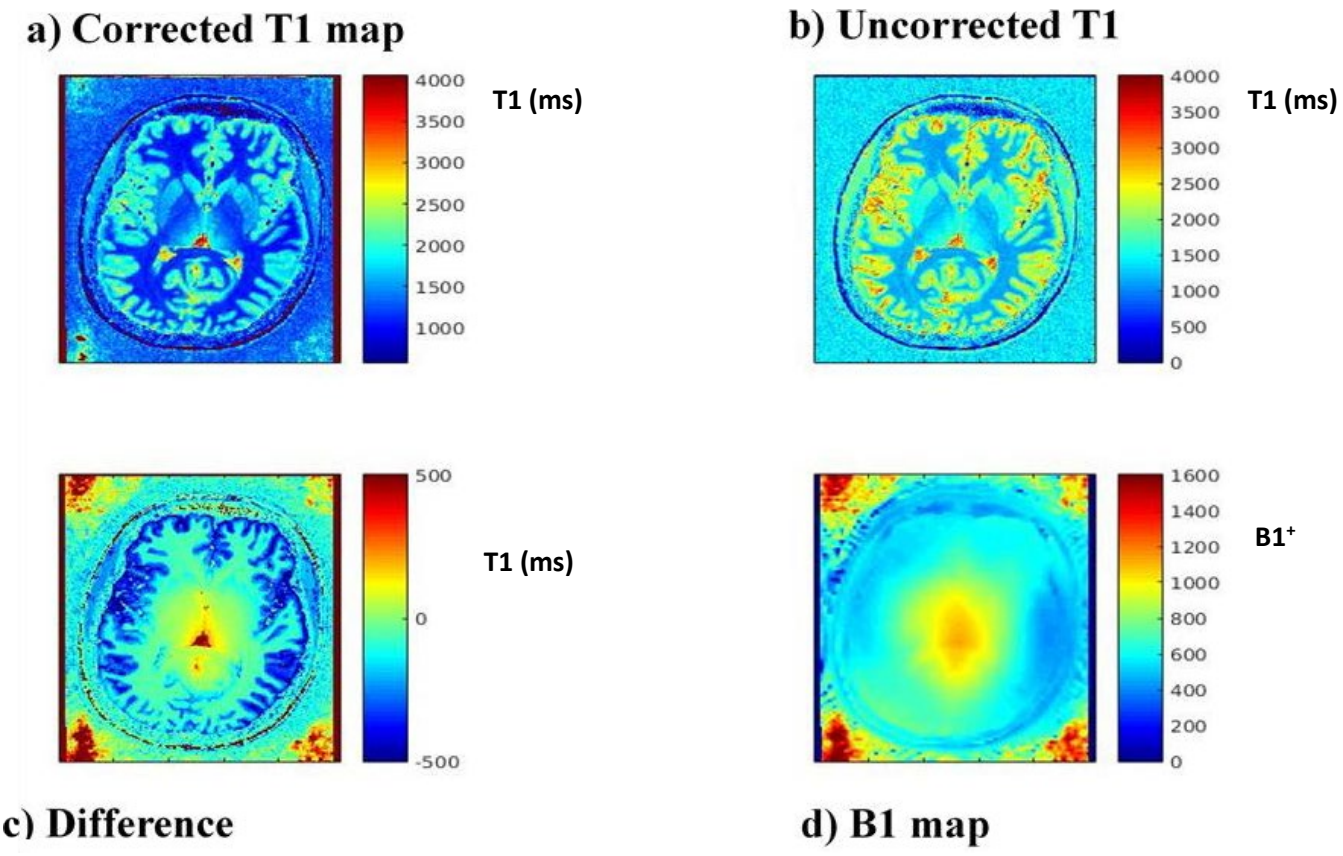

***Figure 2.5:** axial images from a representative subject depicting (a) corrected and (b) uncorrected T1 maps (c) T1 difference map (corrected T1 map – uncorrected T1map) – note the different colour scale values in (c) compared to (a) and (b). (d)* B_1^+ *map*

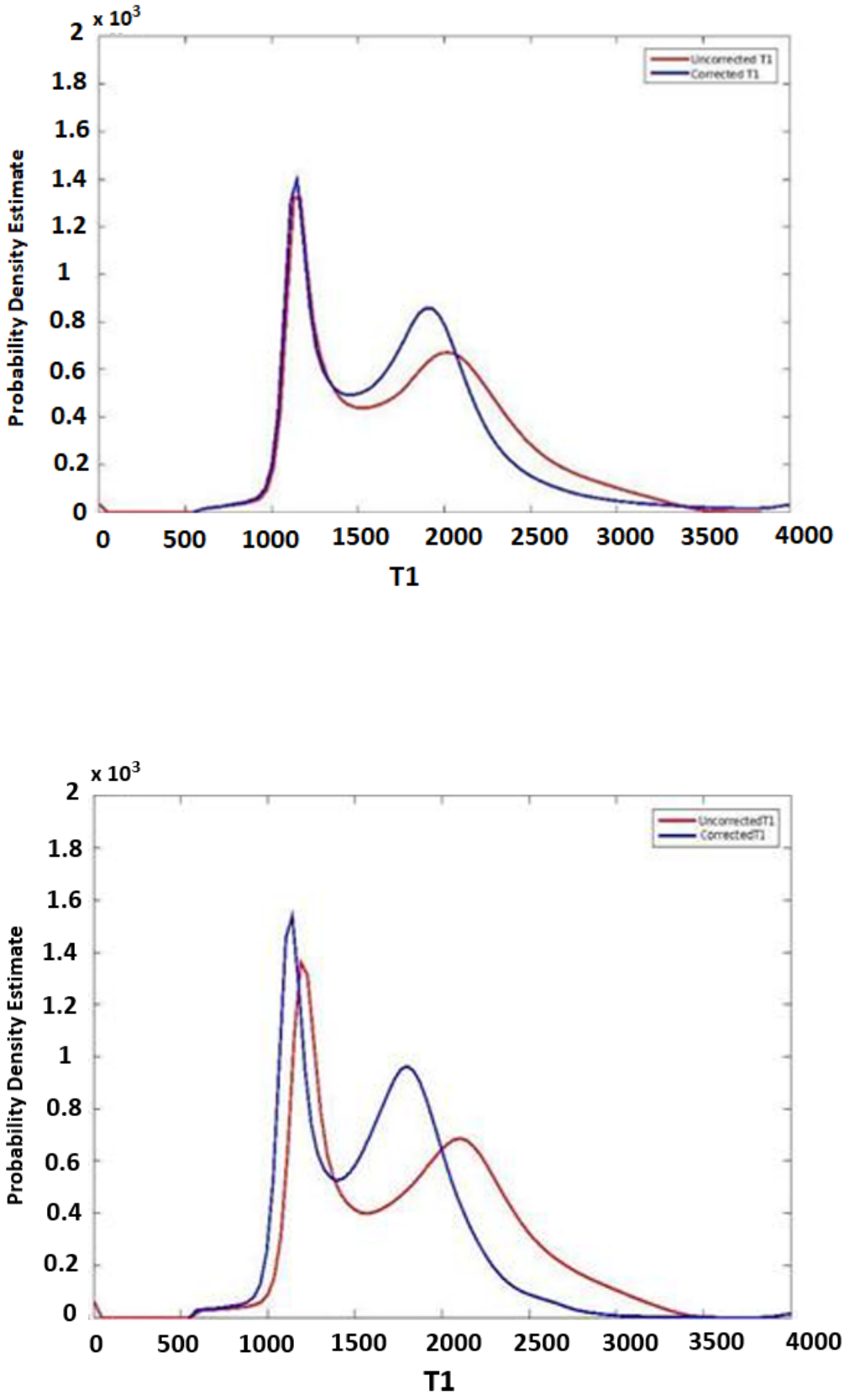

Figure 2.6*: Histogram of corrected (BLUE) and uncorrected (RED) T1 values from2 example subjects*.

Figure 2.6 depicts the T1 values from two example subjects' skull-stripped T1 maps both before and after the implementation of the B_1^+ correction procedure. As shown here the implementation of the B_1^+ correction procedure led to changes in cortical T1 values. In particular, decreases in cortical T1 values were predominant. From Figure 2.6 it is also apparent that following the application of the B_1^+ correction procedure the corrected T1 maps appear to have a narrower distribution.

2.7 Reliability analysis

Prior to the main experimental studies included in this thesis, we sought to determine the reliability of the T1 estimates derived using the methods outlined above. Thus, a small reliability study was conducted to investigate the reproducibility of the T1 values derived from the corrected MP2RAGE T1 maps.

Participants

4 participants took part in this investigation. All participants were aged between 18-30 years and had no history of psychological or neurological disorders. Ethical approval was obtained from the Cardiff University School of Psychology Ethics Committee and all participants provided written informed consent prior to their participation.

Each participant was scanned on two separate occasions with an interval of 7 days between each scan session.

MRI Data Collection

The imaging acquisition protocol was the same for both the initial and repeat scan session.

Quantitative T1 maps and T1-weighted images were acquired for each participant on a 7T MR system (Magnetom, Siemens Healthcare) at submillimetre resolution using the MP2RAGE sequence (MP2RAGE acquisition parameters: TR =6s, TD1/TD2=0.8/2.7s, $\alpha1/\alpha2$=7/5 degrees, TRGRE=6.4 ms, iPAT=3 and 6/8 partial Fourier sampling was used

in the phase-encoding direction and 6/8 partial Fourier in the slice-encoding direction. Resolution = 0.65mm isotropic. TA = 10 min 44s).

A tailored adiabatic inversion pulse was also used for inversion (Hurley et al. 2010). This sequence outputs 4 different imaging volumes: First Inversion image (INV1), Second Inversion image (INV2), a T1-weighted image (UNI image) and finally a quantitative T1 map. Note the sequence parameters chosen for the MP2RAGE acquisition were based on those outlined in Marques et al. (2013) for 'Protocol A - high CNR'.

The B_1^+ field was also measured separately using the SA2RAGE sequence(SA2RAGE acquisition parameters: TR =2.4s, TD1/TD2=0.042/1.8 s, α1/α2=4/11 degrees, TRGRE= 2.1 ms, iPAT=2 and 6/8 partial Fourier sampling was used in the phase encoding direction and 6/8 partial Fourier in slice encoding direction. Resolution = 2x2x2.5 mm. TA = 2 min 16 s).

The SA2RAGE derived maps of the B_1^+ field were used to correct the T1 maps produced by the MP2RAGE sequence for residual transmit field biases, in order to produce bias free high-resolution T1 maps as outlined in Section 2.6.

Quantitative T1 Reproducibility Analysis

For both the initial and repeat scan sessions, each subject's skull-stripped T1 map was segmented into three different tissue types (Grey Matter, White Matter, CSF) using FSL's FAST segmentation algorithm.

In order to evaluate T1 values in the cortex, the grey matter partial volume maps produced using the FAST segmentation algorithm were then thresholded at a probability level of 0.9 in order to obtain a grey matter mask for each participant. Each participant's thresholded binary grey matter mask was then used to mask their corrected T1 Maps.

Mean grey matter T1 values were then extracted from the masked T1 maps, for each participant, for both the initial and repeat scan sessions. An ICC analysis was then conducted in order to evaluate the reliability of the observed cortical grey matter T1 values.

Results

T1 reproducibility

Subject	Scan 1 Corrected T1	Scan 2 Corrected T1
P1	2034.9	2020.1
P2	1954.7	1950.9
P3	1960.3	1946.5
P4	2002.1	1997.3

Table 2.1 : *Mean Grey matter T1 values for each subject and scan session*

The results of the reproducibility analysis revealed that the corrected quantitative T1maps showed good reproducibility (see Table 2.1). Indeed, corrected cortical Grey matter T1 values were found to have a strong ICC (single measures ICC= 0.96; average measures ICC=0.98) (see Figure 2.7) .

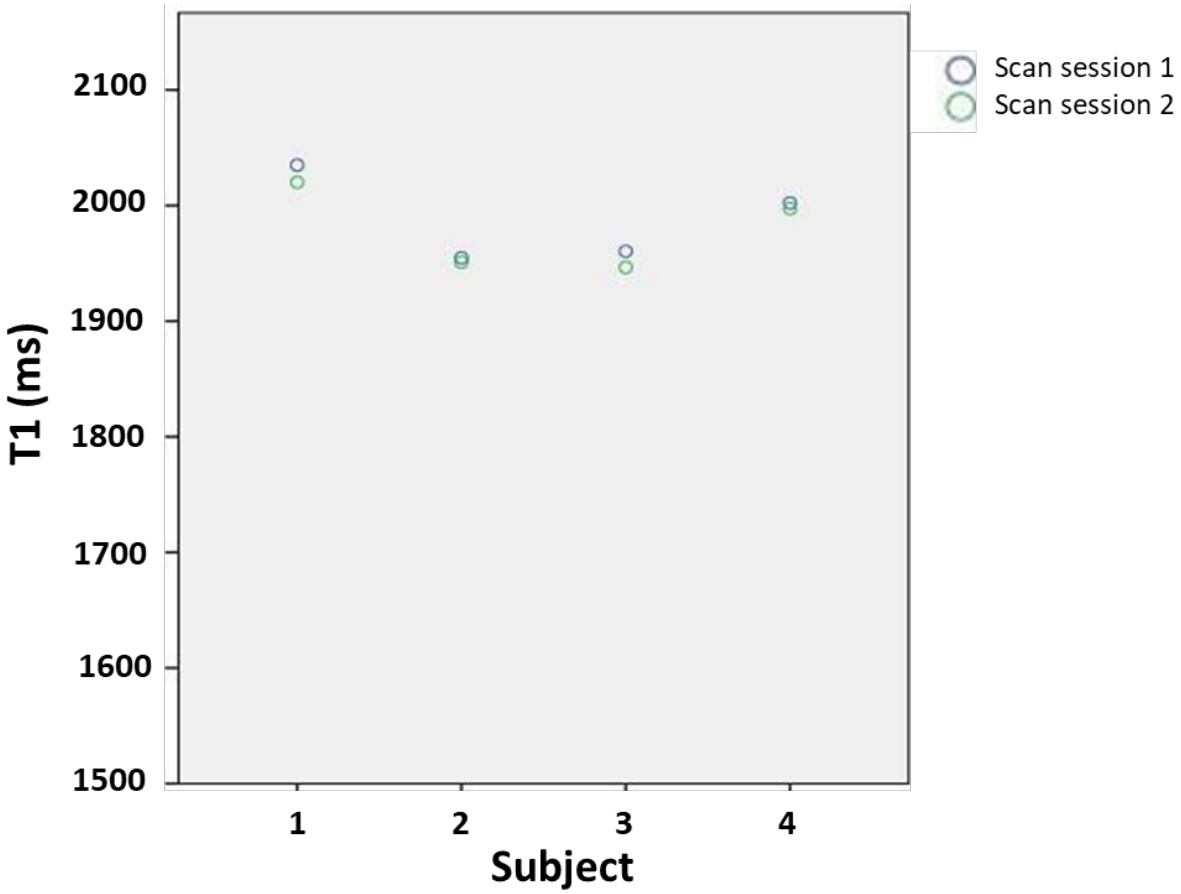

Figure 2.7: *ICC plot for repeated scan sessions for the 4 subjects included in* the reproducibility *study. The T1 values here are given in seconds.*

Interestingly, as illustrated by Figure 2.8 the B_1^+ maps also appeared to show a similar distribution of B_1^+ values across participants. Furthermore, the distribution of B_1^+ values also appeared to show scan/re-scan reproducibility within participants.

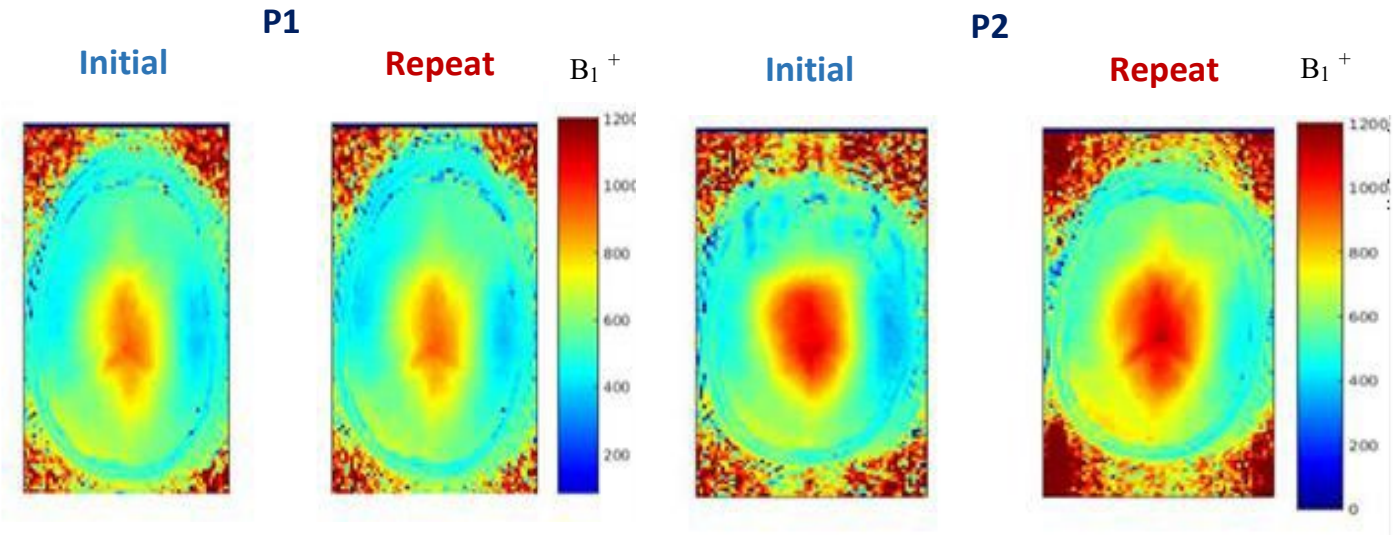

Figure 2.8 : *Axial* B_1^+ *maps for 2 participants for initial and repeat scan sessions.*

2.8 Development of pre-processing pipeline

A significant challenge associated with imaging at 7T concerns the processing of the large high-resolution datasets this generates. While significant strides have been made in recent years with regards to the development of suitable pre-processing pipelines, the processing of high-resolution datasets remains challenging. MP2RAGE images in particular are known to present significant problems for commonly used automatic image processing pipelines (e.g. Freesurfer), given that such software tools are typically optimised for use with images obtained at lower field strengths (Bazin et al., 2014).

During the production of this thesis, substantial challenges were encountered with regards to attempts to process our high-resolution MP2RAGE data using standard pipelines. In particular, skull stripping errors and suboptimal segmentation of the brain's grey and white matter are common issues encountered.

Consequently, a significant proportion of time was dedicated to designing an optimal pipeline for the analysis of these high-resolution datasets, as shown in Figure 2.9.
The following section thus provides an overview of the approach and rationale used in order to derive our depth-specific R1 estimates.

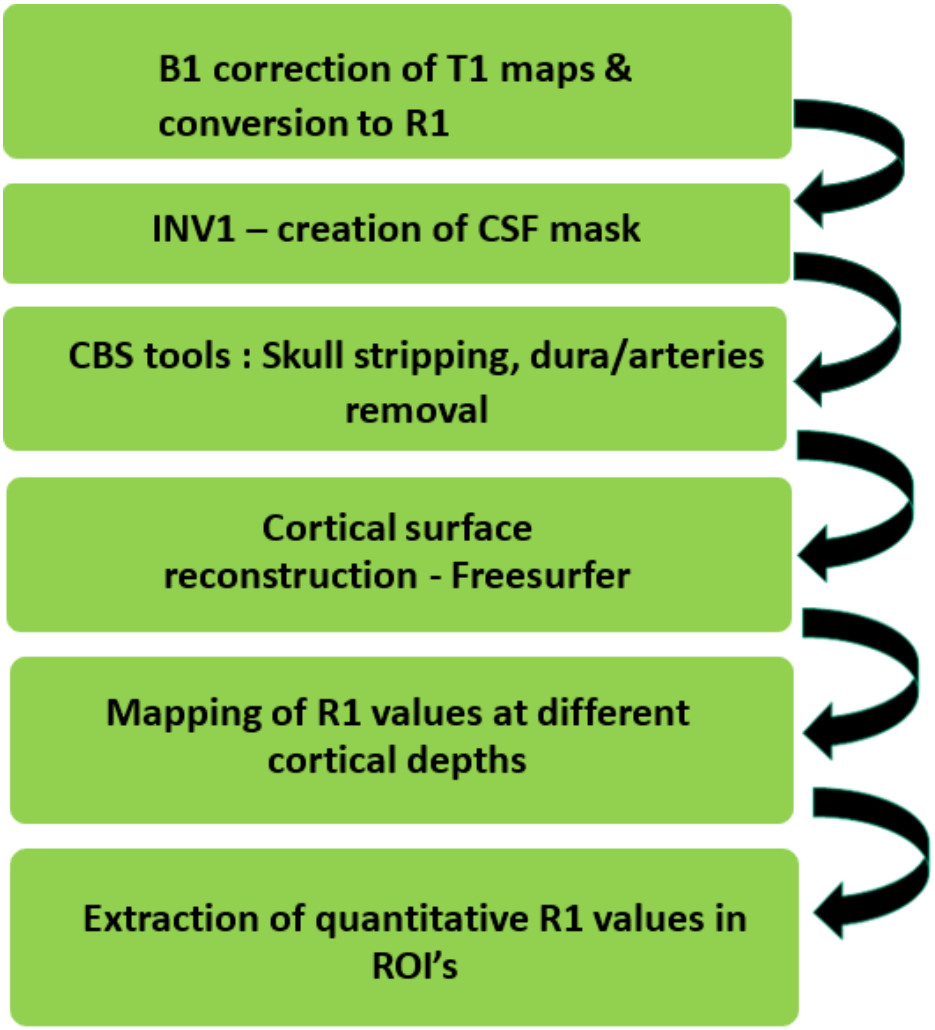

Figure 2.9 : *Schematic Overview of the Analysis Pipeline*

As shown in Figure 2.10 the application of the B_1^+ correction procedure results in a clear improvement in the delineation of the grey matter border following Freesurfer (Fischl, 2012) processing.

However, in order to improve segmentation outcomes further a number of pre- processing steps, including a selection of those recommend by Haast et al. (2018), were performed on the different volumes produced by the MP2RAGE sequence (e.g.INV2, UNI).

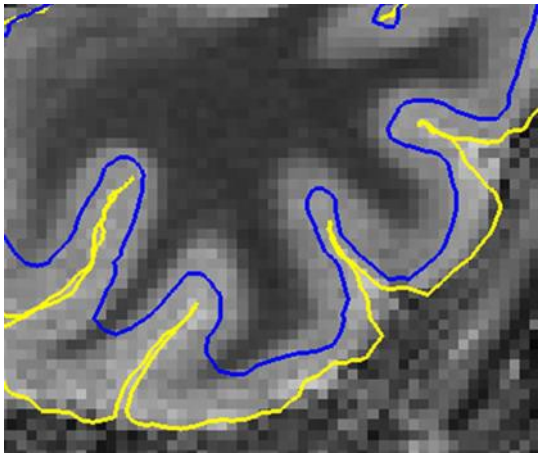

Figure 2.10 *: example section of Freesurfer output showing the Freesurfer pial surface reconstructions produced using the corrected T1-weighted images (yellow line) and the uncorrected T1-weighted images (blue line) in this temporalregion. Here the surfaces have been overlaid on the subject's original T1 map.*

In order to improve skull stripping outcomes, we first bias-corrected each participant's second inversion volume (INV2) from the MP2RAGE using the N4 algorithm, as implemented in the ANTS toolbox (Tustison et al., 2010). The N4 bias field correction algorithm is a method of correcting intensity non-uniformities (known as a bias field) in MRI data that is commonly used during the analysis of such images. The decision to utilise the second inversion image in order to derive the brain mask was driven by the fact that this image provides the best contrast between tissues located inside and outside of the brain. The bias corrected INV2 volume was subsequently skull stripped using FSL's BET routine in order to produce a brain mask.

One of the key benefits of imaging at 7T is the ability to visualise the cortex in an incredible level of detail. However, with this detail comes a number of further challenges, especially given that the majority of image processing software were trained on data collected at 1mm in which such a level of detail is not present. For example, on the high resolution MP2RAGE images collected for this thesis, the cerebral vasculature can be seen in rich detail. As argued by Waehnert et al. (2016) these blood vessels should ideally be masked out as they can lead to segmentation errors. Hence, we chose to mask out the arteries from our datasets using the CBS tools software (CBS High-Res Brain Processing tools, Max Planck Institute for Human Cognitive and Brain Sciences, Leipzig, Germany, https://www.cbs.mpg.de/institute/software/cbs-tools).

A further key issue relates to the brain's dura matter, another aspect of its fine structural detail that becomes noticeably apparent at higher resolutions. Unfortunately, the dura

matter, a thin membrane like structure that surrounds the brain, presents a significant challenge for image segmentation algorithms in the context of high resolution 7T datasets as its intensity is similar to that of the cortical grey matter (Bazin et al., 2014). For example, in the case of Freesurfer reconstructions, this can lead to the erroneous inclusion of the dura matter in the pial surface. In order to circumvent this issue, we again chose to remove the dura matter from our datasets. This was achieved by masking out the dura matter using the techniques provided in the CBS tools software. Finally, a further common issue encountered during the processing of our high resolution 7T data sets was the misclassification of CSF as grey matter in some brain regions. Thus, a CSF mask was created using the first inversion image (INV1), as this image provides good contrast between the CSF and GM of the brain. This mask was subsequently applied to the B_1^+ corrected T1-weighted image.

Surface reconstruction

Following pre-processing of the MP2RAGE T1-weighted images a surface-based analysis was conducted. Surface based approaches represent an attractive option for the study of the cortex given that many characteristic features of cortical areas, such as their columnar and laminar organization, are best understood in the context of the morphology and geometry of the cortical surface (Dale, Fischl, & Sereno, 1999).

Whilst a number of different tools are available for surface-based reconstruction, here we utilised the popular Freesurfer software, which provides an automatic set of tools for the reconstruction of the cortical surface (Dale, Fischl, & Sereno, 1999, Fischl, 2012). Examples of the Freesurfer surface reconstructions are shown in Figure 2.11.

A)

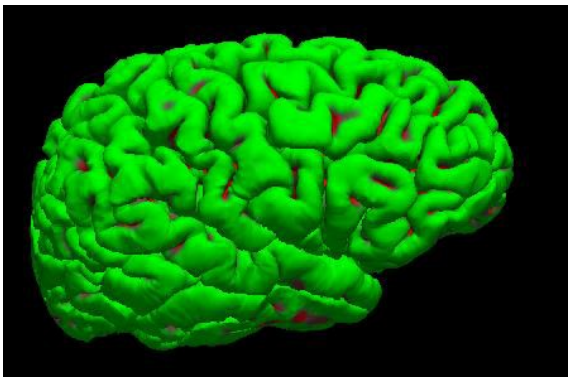

B)

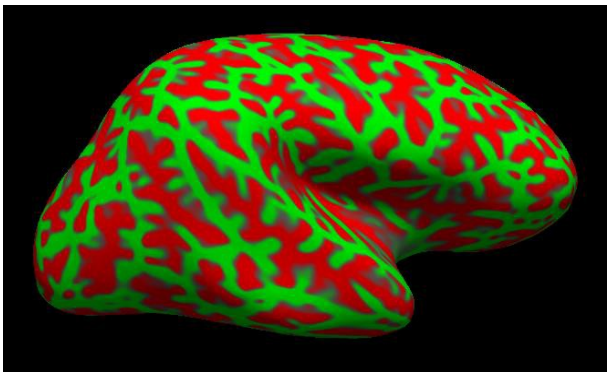

Figure 2.11: *Example A) Right Pial surface and B) Right Inflated surface* reconstructions produced *using the Freesurfer v7 recon- all pipeline. In these surface representations* red indicates *a cortical sulcus and green indicates the presence of a cortical gyrus.*

Equi-volume layering

Until recently, the predominant method of modelling the cortical laminae has been through the use of equi-distant approaches in which the cortical surfaces (layers) are constructed in such a way that a constant distance is kept between these surfaces and the boundaries of the cortex. However, this ignores the fact that a high degree of folding is exhibited by the cerebral cortex. Furthermore, intracortical surfaces constructed in an equi-distant manner have been found to diverge from the anatomical layers observed using high resolution post-mortem MRI scans, calling into question the anatomical accuracy of this approach (Waehnert et al., 2014).

Significantly, Bok (1929) observed that the thickness of cortical layers actually varies across the cortex and is related to cortical curvature (see Figure 2.12). Based upon his observations in this regard, he argued that layer thickness changes occur in order to compensate for cortical folding patterns, thus allowing cortical segments to preserve their volume. Inspired by these findings, Waehnert et al. (2014) developed a novel method for modelling the cortical laminae that, akin to Bok's observation of the cortical anatomy, allows for the preservation of volume and changes in layer thickness in order to compensate for cortical folding in the gyri and sulci of the cortex.

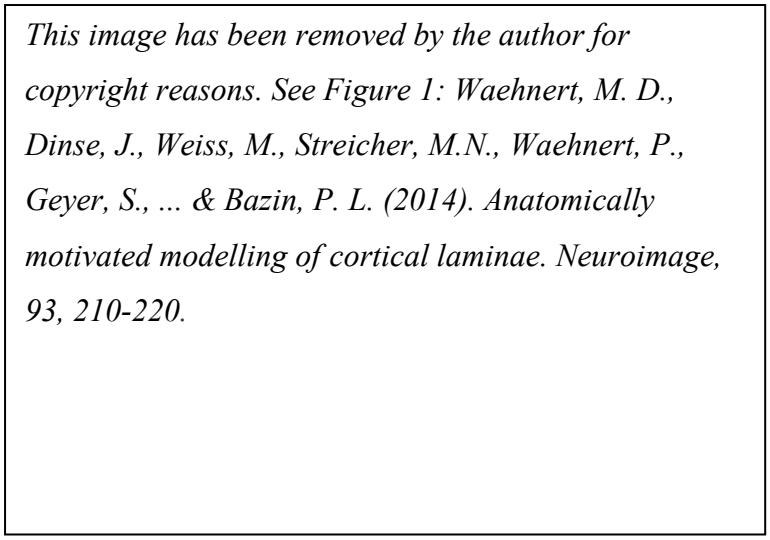

Figure 2.12 : *Sketch from Bok 1929 of a cortical cross section depicting the six cytoarchitectonic layers of the cortex. Notable in this diagram is the fact that at locations* of *high curvature a layer is relatively thick, whereas at locations of low curvature layers are comparatively thin. Figure taken from Waehnert, M. D., Dinse, J., Weiss, M., Streicher, M.N., Waehnert, P., Geyer, S., ... & Bazin, P. L. (2014). Anatomically motivated modelling of cortical laminae. Neuroimage, 93, 210-220.*

Significantly, this method has been found to perform better than equi-distant approaches when applied to ultra-high resolution post-mortem MRI data and even in-vivo MRI data acquired at 0.7 mm isotropic resolution (Waehnert et al., 2014). Thus, in order to derive depth-specific R1 estimates in the cortex, we employed an equi-volume layering approach. This was implemented using the code provided in the following GitHub toolbox : https://github.com/kwagstyl/surface_tools. The equations for generating the surfaces in this toolbox are derived from the original work by Waehnert et al. (2014).

More specifically, we generated 11 equi-volumetric cortical surfaces within the cortex. However, to reduce the risk of partial voluming between the different tissue types present in the cortex (e.g. grey matter, white matter, CSF) the 2 surfaces closest to the pial and white matter borders were excluded. Hence only 7 of these surfaces are examined in the experimental chapters of this thesis. R1 values were subsequently systematically sampled along these 7 surfaces by mapping the R1 maps onto these surfaces using the Freesurfer mri_vol2surf function, which assigns the values from a given volume to each surface vertex.

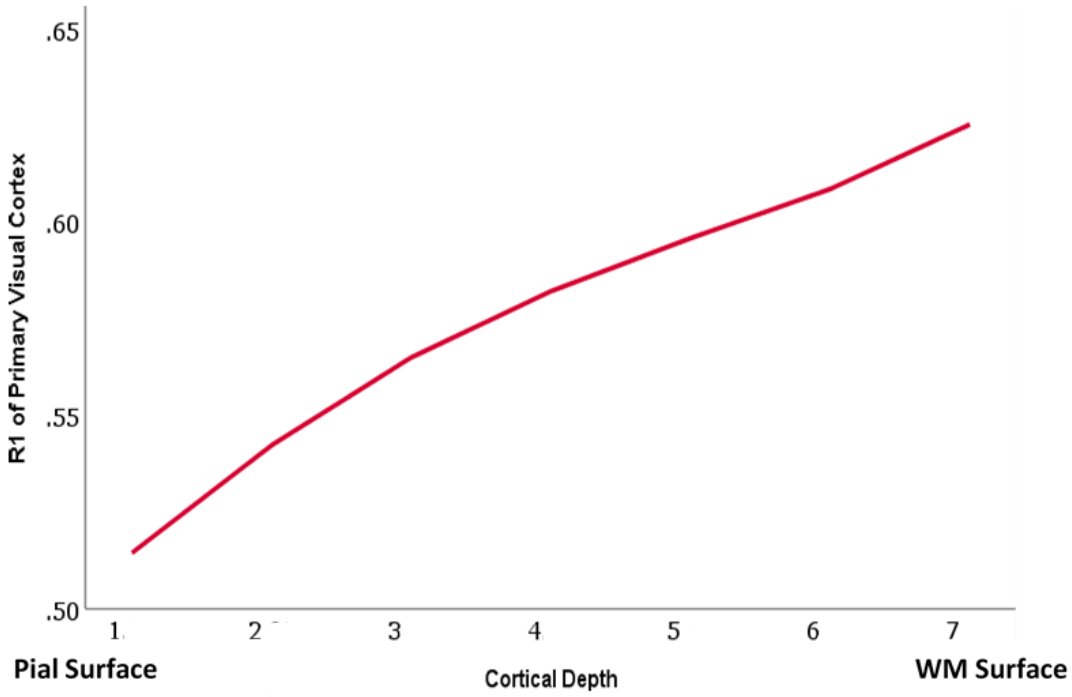

Figure 2.13 : *Average R1 Values sampled in the primary visual cortex for each of 7 cortical depths.*

The final stage of our MRI analysis pipeline involved the extraction of R1 values across the cortical depth in Freesurfer-defined regions of interest. In Figure 2.13, R1 values in the primary visual cortex (averaged over 35 subjects), obtained using our analysis pipeline and sampled at 7 different cortical depths using the aforementioned equi-volume layering approach, are shown. Notably, in line with the known myeloarchitecture of the cortex there is a clear increase in R1 (myelin) when sampling from the pial surface to the white matter border, thus validating our approach outlined in this chapter.

Chapter 3

Investigating the Relationship Between Cortical Myelination and Visual Oscillatory Dynamics InVivo

3.1 Abstract

A close relationship exists between the cyto and myeloarchitecture of the cortex. In support of this, Helbling et al. (2015) demonstrated that MRI derived estimates of cortical myelin were positively correlated with the strength of MEG auditory Evoked Response Fields (ERF). Myelin has also been suggested to aid oscillatory synchrony,which has been widely implicated in cognition and an array of clinical disorders. However, the precise neural underpinnings of oscillatory activity remains the subject of intense research. The present study combined high-resolution 7T MRI of R1, a myelin-sensitive MRI metric, with MEG to test the hypothesis that visual gamma oscillatory dynamics are related to myelination of the primary visual cortex (V1). We also investigated whether such a relationship might be specific to a particular cortical depth. The results of this investigation did not reveal evidence of a significant correlation between either the peak amplitude of the initial evoked gamma spike, or the later sustained gamma response, and R1 estimates in primary visual cortex. Similarly, no relationship was found between cortical myelin and peak frequency estimates. However, further exploratory analyses of the whole frequency spectra did point to a potential relationship between 40 Hz gamma activity and superficial myelin which requires further investigation.

3.2 Introduction

The structure of the brain and its function are known to be closely intertwined. Yet, despite having been the subject of decades of research, many unanswered questions remain regarding the complex interplay between brain structure and function. To date our knowledge of the brain's microstructure has largely been informed by ex-vivo post-mortem histological studies and by extrapolating from animal models (Edwards, Kirilina, Mohammadi, & Weiskopf, 2018). However, recent developments in the field of MRI are now enabling the quantification of brain structure and function on a much finer scale than ever before. Indeed, it is now possible to non-invasively measure microstructural properties of human brain tissue, such as the myelin content, with high resolution (Weiskopf, Mohammadi, Lutti, & Callaghan, 2015). Such investigations can be seen to provide a unique opportunity to move beyond classical approaches by allowing for the investigation of the brain's microstructure in vivo (Weiskopf et al., 2015).

In recent years there has been a corresponding renewal of interest in using high resolution quantitative MRI techniques in order to probe the microstructure of the brain and in particular its myelin content (Waehnert, Dinse, Schäfer, Geyer, Bazin,2016). Significantly, although most prominent in the white matter of the brain, the cortical grey matter also contains numerous myelinated fibres, the spatial organization of which varies across the cortex (Nieuwenhuys, 2013).

As is evident from previous histological investigations, a close relationship exists between the cytoarchitecture and myeloarchitecture of the brain, (Nieuwenhuys, 2013). Of note, the horizontal myelinated fibres of the cortex have been proposed to correspond to the axon collaterals of pyramidal cells (the primary generators of the MEG/EEG signal). These pyramidal cells are most prominent in layers III and V of the cortex, producing two maxima of horizontal fibres thought to be consistent with the inner and outer bands of Baillarger, two major myeloarchitectural features of the cortex (Dinse et al., 2015).

Building on the close relationship between the cyto and myeloarchitecture of the brain, Helbling et al., (2015) demonstrated that MRI derived estimates of cortical myelin could be used to both refine MEG source location estimates and predict the magnitude of electrophysiological signals. This study was based on the assumption that given the close relationship between the cyto and myeloarchitecture of the brain, local myelin density is expected to be positively correlated with the density of pyramidal cells. Utilising a combination of MEG and structural MRI measures, Helbling et al. (2015) reported

evidence of a positive correlation between the magnitude of MEG signals derived from an auditory pitch perception paradigm and myelin estimates in relevant auditory cortical regions. Whilst a number of MRI metrics were employed to probe the cortical myeloarchitecture, R1 was also found to be the best predictor of MEG dipole strength.

In the above study auditory Evoked Response Fields (ERF's) and dipole moment strength were utilised as an index of neural activity. However, a key advantage of a more direct neuroimaging technique such as MEG lies in its ability to explore the rich assortment of neural activity, including neural oscillations (Singh, 2012). Such oscillations are a prominent feature of neuronal activity and the synchronization of oscillatory activity has been proposed as a fundamental mechanism sub-serving neuronal communication (Schnitzler, & Gross, 2005). Indeed, converging lines of evidence suggest that neural oscillations may act to enable the coordinated activity of neuronal populations during normal brain functioning (Uhlhaas & Singer, 2010). Notably, neuronal oscillations are typically categorized into five frequency bands, namely delta, theta, alpha, beta and gamma. Oscillations in the gamma range in particular have been the subject of intense research and will be the focus of this chapter.

The exact genesis of visual gamma oscillations remains the subject of continued investigation and debate. However, one widely regarded hypothesis (PING model) contends that these signals are produced by networks of reciprocally connected excitatory pyramidal cells and inhibitory interneurons. They are thus believed to emerge from the coordinated interaction of excitation and inhibition (Buzsaki and Wang, 2012).

Gamma oscillations have been attributed a wide range of functions and implicated in a variety of sensory, cognitive and behavioural processes, including memory (Sederberg et al., 2007) and attention (Bauer, Stenner, Friston, & Dolan, 2014). Furthermore, they have been suggested to play a role in both local and large-scale cortical processing (Uhlhaas & Singer, 2010). Aberrant oscillatory dynamics in the gamma range have also been extensively implicated in a wide range of clinical conditions including schizophrenia (Uhlhaas & Singer, 2010), Alzheimers disease (Başar et al., 2017) and autism (Simon & Wallace, 2016). However, in addition to their mechanisms of generation, the functional and clinical significance of gamma band oscillations remains the subject of considerable debate.

Gamma oscillations are observed in many brain regions during both wake and sleep (Buzsaki and Wang, 2012). However, the visual cortex has been particularly well characterised (Gilbert,1983, Tong, 2003) making it an ideal substrate for investigating

structure-function relationships in the brain. Gamma oscillations can be reliably induced in the visual cortex using high contrast square wave grating stimuli. In response to such stimuli the visual cortex produces two characteristic responses, namely an initial evoked response and a later induced narrow band response. The evoked gamma response is also commonly referred to as the gamma spike or broadband gamma given the broad range of its frequency content (~30 - 100+ Hz). This transient response occurs ~ 0 - 300ms after stimulus onset. The later, narrow band oscillations, which are usually lower in frequency, are also commonly referred to as sustained gamma. This response typically lasts for the duration of the stimulus (Swettenham, Muthukumaraswamy & Singh, 2009).

Significantly, these two variants of gamma activity are commonly conflated in the literature (Ray & Maunsell, 2011). However, recent work by Bartoli et al. (2019) has highlighted the different response properties of these oscillatory signals, pointing to the potential importance of considering these two types of gamma activity as separate phenomena. For example, in their study, whilst both broad and narrow band gamma oscillations demonstrated an increase in amplitude with increasing stimulus contrast, only the narrow band oscillations demonstrated a characteristic change in peak frequency dependent on stimulus contrast. Interestingly, this study also found that narrowband oscillations occurred most reliably in response to grating stimuli and reddish hues, in addition to natural images in which these features are present . Conversely, broadband gamma oscillations were found reliably for all stimulus types under investigation.

Notably, controversy also surrounds the origins of the high frequency broadband gamma responses observed in the visual cortex. For example, utilising recording in anaesthetised cats Castelo-Branco, Neuenschwander & Singer (1998) found that high frequency gamma activity (60 -120 Hz) is generated in the retina, before propagating to the LGN and visual cortex, by means of feedforward synchronisation. In contrast, their results pointed to lower frequency gamma oscillations (30-60 Hz) as being generated solely by cortical mechanisms. However, other investigations, such as that by Heinrich & Bach (2004), conducted in humans, contend that oscillations in the gamma range in the retina and visual cortex are in fact distinct phenomena. Thus, much controversy surrounds both the existence of different types of gamma oscillations in the visual cortex, the potentially distinct functions of these signals and indeed their origins.

Furthermore, evidence such as that outlined above can be seen to raise a number of intriguing questions regarding the way in which gamma oscillations are currently

conceptualised. Thus, in light of recent work highlighting the importance of considering narrow and broadband gamma oscillations as both spectrally and functionally distinct responses, in this work we consider both the initial narrowband gamma spike in addition to the broadband gamma response.

Despite the many unanswered questions regarding gamma frequency oscillations in the visual cortex, two key characteristics of these phenomena, namely their amplitude and frequency, have been found to be highly reliable within participants (Tan, Gross & Uhlhaas, 2016; Muthukumaraswamy et al., 2010). Intriguingly, the amplitude and frequency of these signals is also known to show considerable inter- individual variability, the mechanistic basis of which remains the subject of ongoing investigation (Perry et al., 2013). However, a likely candidate source of such inter- individual differences could be the underlying structure and physiology of the visual cortex itself (Shaw et al., 2017; Shaw et al., 2019). Furthermore, variability in peak gamma frequency has been shown to be genetically determined (van Pelt, Boomsma,& Fries, 2012).

To date, a number of studies have attempted to explore the structural correlates of visual gamma oscillations. However, thus far, such efforts have yielded somewhat mixed results that are far from conclusive. For example, although Schwarzkopf et al. (2012) and Gregory et al. (2016) reported evidence of a positive correlation between gamma peak frequency and the size of primary visual cortex (V1), further studies such as that by Perry et al. (2013) have failed to replicate this association. More recently, a study by Van Pelt, Shumskaya and Fries (2018), that employed a considerably larger sample of participants than the aforementioned studies (158 subjects), actually reported a negative correlation between gamma peak frequency and the size of V1 in addition to a positive correlation with cortical thickness. A similarly confusing picture emerges when considering purported relationships between gamma frequency and concentrations of the inhibitory neurotransmitter GABA in the visual cortex, with studies again reporting contradictory findings (e.g. Muthukumaraswamy et al. 2009; Cousijn et al., 2014). However, owing to the aforementioned advances in the field of MRI there is now the potential to harness the greater specificity of microstructural imaging methods to investigate direct correlations between important microstructural properties of the brain, such as its myelin content and gamma oscillatory dynamics.

Interestingly, myelin itself has also been implicated in subserving brain communication through its ability to increase the speed of nerve conduction (Fields, 2014). Indeed, intra-cortical myelin is thought to play a key role in optimizing the timing and synchrony of

action potentials, a necessity for the optimal functioning of neuronal networks (Tardif et al., 2016). To date, the majority of studies have focused on the importance of white matter myelination and its role in neuronal synchronisation. However, it is possible that intracortical myelin might also influence synchronization occurring within more local neuronal networks, which could in turn be reflected in the magnitude of signals recorded using MEG/EEG (Grydeland, Westlye, Walhovd & Fjell, 2015). In line with this suggestion, a recent multimodal MRI-EEG study found that an increase in amplitude of an electrophysiological marker (ERN response) of error and processing and cortical control, was associated with higher levels of myelin in the posterior cingulate cortex(Grydeland et al., 2015). Such a finding can be taken to suggest synchronous activity reflecting error processing is related to inter-individual variability in intercortical myelin. Barratt et al. (2017) also found evidence of a diminished gamma band response in the visual cortex of a cohort of MS patients compared to controls and suggested that one potential interpretation of this finding is that the widespread cortical demyelination observed in MS may provide explanation for the reduced visual gamma amplitude observed in this population (Barratt et al., 2017).

A growing body of evidence has also suggested that synchronisation in the gamma band is strongest in the superficial layers of the cortex, from which feedforward projections typically originate, indicating that gamma oscillations may also subserve feedforward processing in the brain (Michalareas et al., 2016). To date much of the evidence in support of this theory has come from animal studies, with direct evidence in humans remaining sparse, though recent MEG studies have attempted to investigate the laminar hypothesis non-invasively by utilising modelling approaches in combination with improvements in the SNR of MEG data (Bonaiuto et al., 2018). Notably this study by Bonaiuto et al. (2018) demonstrated the feasibility of distinguishing between activity arising from the deep and superficial layers of the cortex. Still, direct evidence of the layer-specific origins of gamma oscillations in human participants remains lacking.

Investigations of cortical myelination are also increasingly taking advantage of the benefits conferred by imaging at high field. Imaging at 7T allows for the acquisition of datasets at submillimetre isotropic resolution with increased contrast to noise ratio conferring a number of important advantages from the perspective of myelin imaging (Waehnert et al., 2016). In particular, such high-resolution images have the potential to allow exploration of the laminar structure of the cortex, which would be of great relevance to attempts to relate the cortical microstructure to oscillatory dynamics.

In sum, the precise neurobiological underpinnings of gamma oscillations, their mechanisms of generation and indeed their functional significance, remain the subject of ongoing debate. Yet, given the wide-ranging functions attributed to these signals, gaining a greater understanding of the nature of gamma oscillations and their relation to the cortical microstructure could provide valuable new insights into their functional roles in both health and disease. Thus, here we focus on gamma oscillations and aim to extend the approach adopted by Helbing et al. (2015) to further explore the relationship between the microstructure of the cortex and gamma oscillatory dynamics, with a view to gaining new insights into the nature of these signals and their relation to the underlying neuroanatomy. More specifically, given that gamma oscillations are suggested to be generated by superficial pyramidal cells within the cortical columns of V1, we hypothesised that gamma oscillatory dynamics should depend on the density of pyramidal cells, whose axons are myelinated. Hence, we hypothesised, akin to Helbling et al. (2015), that a relationship might therefore exist between myelin in V1 and visual gamma oscillations.

In addition, the study also aims to acquire higher resolution images than previous investigations in order to assess myelination at different cortical depths and its relation to gamma oscillatory dynamics. The present study will therefore adopt a multimodal neuroimaging approach utilising high resolution quantitative MRI in combination with MEG in order to investigate the relationship between depth-specific cortical myelin estimates and gamma oscillatory dynamics. In this study visual gamma oscillations are elicited using a visual grating paradigm, given that such stimuli are known to induce strong gamma band responses in participants' visual cortex (Muthukumaraswamy & Singh, 2009).

It is hypothesised that the magnitude of visual gamma oscillatory signals will be positively correlated with the concentration of myelin in the primary visual cortex and furthermore that a relationship might also exist between other aspects of oscillatory morphology such as peak frequency estimates and the cortical myeloarchitecture.

3.3 Methods

Participants

38 healthy participants took part in this study. All participants were aged between18-30 years and had normal or corrected to normal vision, normal hearing, and no history of psychological or neurological disorders. Ethical approval was obtained from the Cardiff University School of Psychology Ethics Committee and all participants provided informed consent prior to their participation.

MEG Methods

Visual Motor Experiment Design

Stimuli consisted of stationary, black/white, square-wave vertical gratings (spatial frequency = 3 c.p.d, size = 8° x 8° of visual angle) presented at maximum contrast on a grey background. Stimuli were presented to the lower left visual field with a small red fixation square located at the top right-hand edge of the stimulus. Each stimulus appeared on the screen for a jittered duration of 1.5-2s. This was followed by an inter-trial interval of 4s seconds during which only the red dot was present. Participants were instructed to maintain fixation on the red dot throughout the experiment and to make an abduction of their right index finger when the grating disappeared from the screen. The experiment consisted of a total of 100 trials (approx. 10mins).

The Stimulus presentations were implemented in MATLAB (The Mathworks, Inc.: Natick, MA, USA) and displayed using a ProPixx projector system (VPixx Technologies) with a refresh rate set to 100 Hz.

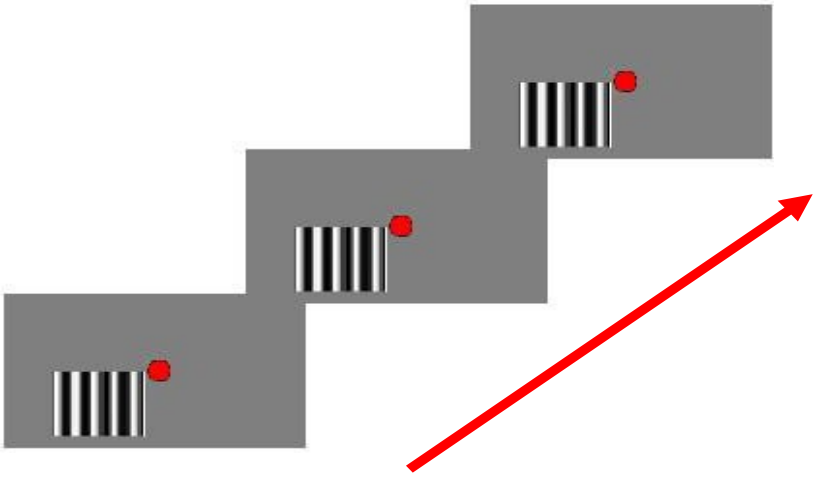

Figure 3.1: *Illustration of visual grating paradigm*

MEG Data Acquisition

Whole head MEG recordings were acquired using a 275 channel CTF axial gradiometer system at a sampling rate of 1200 Hz. For the purpose of noise rejection, an additional 29 reference channels were recorded and the primary sensors were analysed as synthetic third-order gradiometers (Vrba and Robinson, 2001). Participants were seated in an upright position during the recording sessions. Prior to the MEG recording, participants were fitted with three electromagnetic head coils located at a fixed distance from the nasion and the two pre-auricular points, the location of which was recorded continuously for MRI co-registration purposes. The location of these markers was verified afterwards using high resolution digital photographs.

Co-registration – co-registration was performed using the T1-weighted UNI image from the MP2RAGE sequence. Each subject's UNI image was first downsampled to 1mm isotropic resolution and co-registered to the MEG data by marking the points on the MR image corresponding to the position of the fiducial coils. These fiducial coils are head localisation coils. They are placed at key anatomical landmarks referred to as the fiducial points, namely the left and right pre-auricular points and the nasion.

MEG Data Processing

The MEG analyses presented in this chapter were performed using the Fieldtrip toolbox (Oostenveld, Fries, Maris, & Schoffelen, 2011) and custom Matlab scripts.

Pre-processing- Each participant's data set was epoched from 2 seconds before stimulus onset to 2 seconds after stimulus onset. Artefact rejection was then performed manually. Specifically, each participant's data was visually inspected to identify eye, muscle, and head movement artefacts. Each dataset was subsequently band-pass-filtered between 30-80 Hz.

Source Reconstruction

Each participant's co-registered MRI was segmented into the following tissue types: brain, skull and scalp. A volume conduction model of the head was then created based on the subjects segmented MRI using the 'single-shell' method (single-shell volume conduction model (Nolte, 2003). This head model was chosen for this analysis as it is the method recommended by Fieldtrip for most MEG analyses.

The source model was then constructed using a high-resolution 1mm grid in order to improve SNR. In this step an inverse warping procedure was also utilised in order to allow for the creation of source grids that are consistent across participants. In brief, a template grid based on a template MRI in Montreal Neurological Institute (MNI) space available in SPM12 (Ashburner et al., 2014) was used. Each participant's MRI was warped to this template MRI. The inverse transformation matrix was then applied to the template grid. As a consequence of this procedure, it is possible to create source grids that are consistent across subjects thus allowing for equitable comparisons. The leadfield matrix was then constructed for each grid point taking into account the previously computed head model and channel positions.

Beamforming - An LCMV Beamformer analysis was then performed for source localisation purposes. In this procedure the signals at each source location are reconstructed by weighting the signals at each sensor by a set of beamformer weights. In this way these beamformer weights essentially act as a spatial filter. This method allows

for the estimation of activity at any given brain location. The calculation of these beamformer weights depends on two key factors, namely the leadfield matrix and the data covariance. Here we chose to use an LCMV beamformer which relies on source estimates calculated in the time domain.

In order to ensure that any difference between the stimulus and baseline conditions were not simply due to differences in the beamformer weights, the source estimates were calculated for the stimulus and baseline epochs using common filters (i.e. the same set of beamformer weights were used). These 'common weights' were derived by calculating the covariance matrix using both the baseline and stimulus epochs.

After projecting the gamma power through the common beamformer weights separately for both the stimulus (0.3s to 1.5s) and baseline (-1.5s to -0.3s) epochs the contrast between these two conditions was then calculated. More specifically, the percentage change between the stimulus and baseline conditions for each voxel location was estimated. The peak voxel showing the greatest increase in gamma power (30-80 Hz) in the occipital cortex, measured as percentage change from baseline, was then identified for each subject.

Virtual sensors - Finally, virtual sensor time series data were reconstructed at these locations of peak gamma activity by multiplying the data by the corresponding beamformer weights. This resulted in the construction of an activity time-series for each trial at this peak location. Time frequency analyses were then performed using the Hilbert transform in order to explore the characteristics of both the initial evoked gamma spike (0-0.3s) and the later sustained gamma response (0.3-1.5s). The resulting time frequency plots were visually inspected for quality control purposes. Three subjects did not show an identifiable visual gamma response and thus their data was excluded from the subsequent analyses, leaving a final MEG data sample size of 35.

The peak amplitude (percentage change from baseline) and frequency of the sustained gamma response (30-80 Hz) was calculated for each participant. The peak amplitude (percentage change from baseline) and frequency of the earlier (0 - 0.3s), evoked gamma response (30-160 Hz) was also estimated.

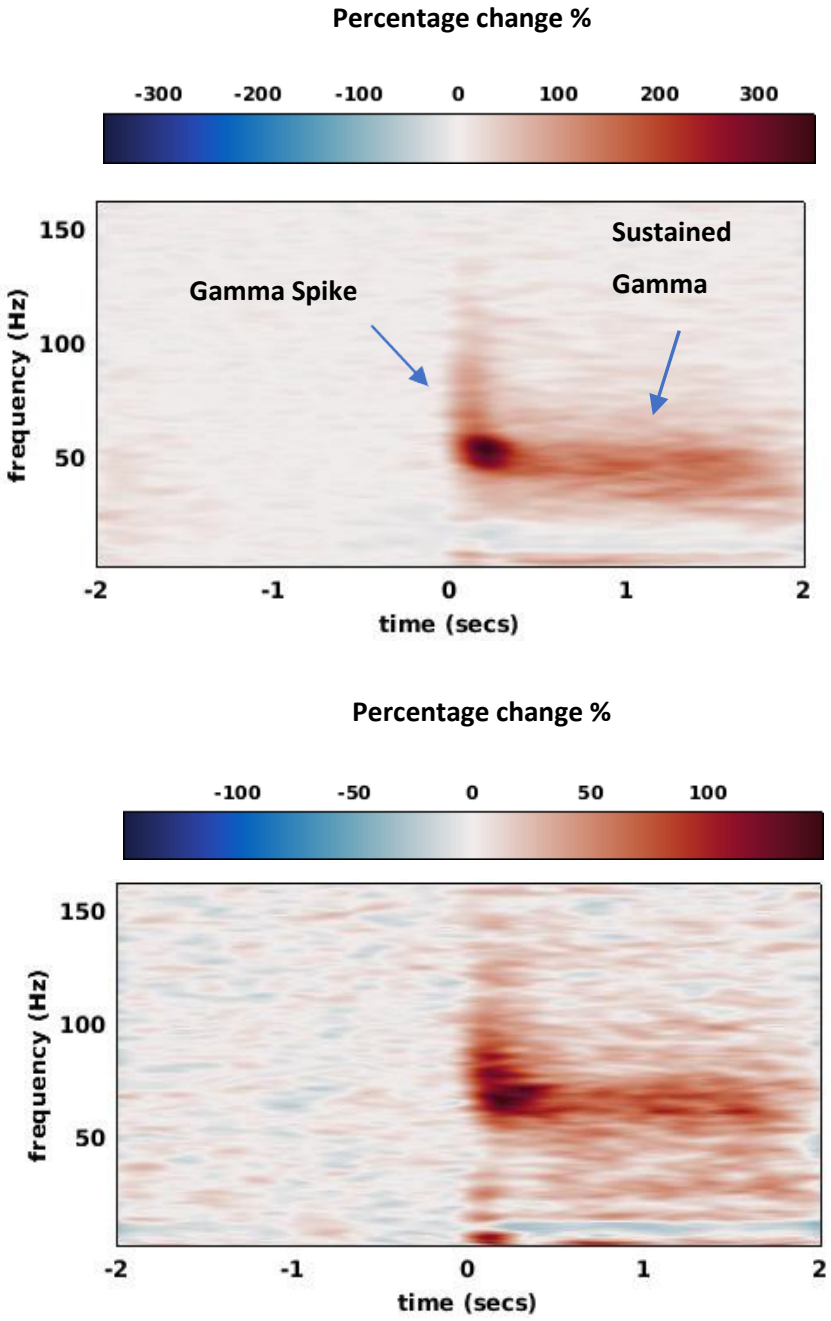

Figure 3.2: *Example visual gamma spectrograms from two representative subjects depicting both the initial gamma spike and later sustained gamma response.*

MRI Data Collection

Quantitative T1 maps and T1-weighted images were acquired for each participant on a 7T MR system (Magnetom, Siemens healthineers, Erlangen, Germany.) at submillimetre resolution using the MP2RAGE sequence (MP2RAGE acquisition parameters: TR =6s, TD1/TD2=0.8/2.7s, α1/α2=7/5 degrees, TRGRE=6.4 ms, iPAT=3 and 6/8 partial). Fourier sampling was used in the phase encoding direction and 6/8 partial Fourier in the slice encoding direction. Resolution = 0.65mm isotropic. TA = 10 min 44s. A tailored adiabatic inversion pulse was also used for inversion (Hurley et al. 2010).
This sequence outputs 4 different imaging volumes (1st inversion image INV1, second inversion image INV2, a T1-weighted image (UNI image) and finally a quantiative T1 MAP). Given that the T1 maps derived from the MP2RAGE sequence can show some residual sensitivity to inhomogeneities in the B_1^+ field, the B_1^+ field was also measured separately using the SA2RAGE sequence (SA2RAGE acquisition parameters: TR = 2.4s,TD1/TD2 = 0.042/1.8 s, α1/α2 = 4/11 degrees, TRGRE= 2.1 ms, iPAT= 2 and 6/8 partial Fourier sampling was used in the phase encoding direction and 6/8 partial Fourier in the slice encoding direction. Resolution = 2x2x2.5mm.TA = 2 min 16 s.

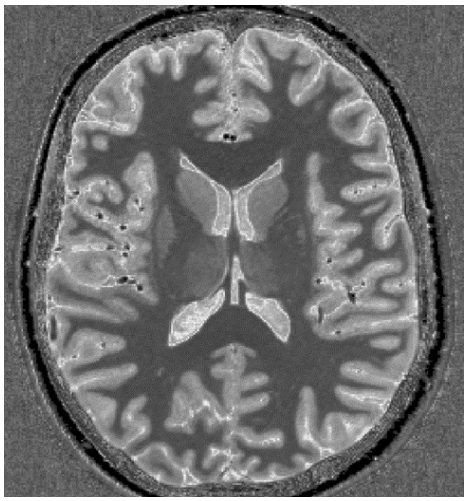

Figure 3.3: *Example T1 map at 0.65mm isotropic resolution.*

Calculation of R1 maps and B_1^+ correction procedure

The SA2RAGE derived maps of the B_1^+ field were used to correct the T1 maps produced by the MP2RAGE sequence for residual transmit field biases, in order to produce bias free high resolution T1 maps. Each participant's SA2RAGE derived B_1^+ map was first registered and interpolated to the same resolution as the MP2RAGE volumes using FSL's FLIRT registration algorithm. Subsequently these registered and interpolated B_1^+ maps were utilised to correct the high resolution MP2RAGE Uniform images and T1 maps for residual RF transmit field biases using the methodology outlined in Marques & Gruetter (2013).

Following this correction procedure each participant's corrected T1 map was converted to an R1 map (R1=1/T1) for ease of interpretation given the positive correlation between R1 and myelin.

MRI Pre-processing and Analysis

In order to improve segmentation outcomes a number of pre-processing steps, including a selection of those recommend by Haast et al. (2018), were performed on the different volumes produced by the MP2RAGE sequence (e.g. INV2,UNI). In brief, each participant's second inversion volume (INV2) was first bias corrected using the N4 algorithm. This volume was subsequently skull stripped using FSL's BET routine in order to produce a brain mask. Finally, the CBS tools software package was also used to remove additional non-brain tissue (arteries and dura) from the corrected T1-weighted image (UNI image). A common issue encountered during the processing of these images is the misclassification of CSF as grey matter in some brain regions. Thus, a CSF mask was also created using the first inversion image (INV1) and applied to the corrected T1-weighted image.

Each participant's pre-processed B_1^+ corrected T1-weighted image was then processed at native 0.65 mm resolution using the Freesurfer 7 'recon all' pipeline, which performs all of the Freesurfer cortical surface reconstruction steps, in order to construct a representation of the cortical surface. The resultant surfaces were visually inspected for quality control purposes and manual corrections were performed where necessary.

Following Freesurfer processing, participants' individual quantitative R1 volumes were then mapped onto the cortical surfaces. Initially, each subject's quantitative R1 map was sampled on their cortical surface using the Freesurfer mri_vol2surf function by averaging between 20-80% of the cortical depth to reduce the risk of partial voluming.

Cortical depth analysis - A cortical depth analysis was also performed by projecting the R1 maps onto the cortical surface using an equi-volume layering approach (Waehnert, et al., 2014). This involved the creation of 11 different surfaces. R1 values were then systematically sampled along these surfaces. Again, to reduce the risk of partial voluming only 7 of these surfaces were included in the subsequent analyses (the 2 surfaces closest to the pial and white matter surfaces were excluded from the subsequent analysis). Thus, we chose to only use equi-volume surfaces at the following fractional cortical depths (projecting from the pial surface): 0.2, 0.3, 0.4, 0.5, 0.6, 0.7, 0.8. Accordingly, estimates of myelin content at 7 cortical depths were derived. In the remainder of this chapter the following naming convention will be used to refer to the different cortical depths investigated depth: 1, 2, 3, 4, 5, 6, 7. Depth 1 is closest to the pial surface whereas depth 7 is the closest to the GM/WM border.

Extraction of V1 myelin content - For each participant we first extracted the mean R1 value (sampling at 20-80 % of the cortical depth, from the white matter surface) in the Freesurfer-defined pericalcarine label to give an estimate of the myelination of each subject's primary visual cortex .We then repeated this process for each of the equi-volume surfaces. In this way a mean R1 for the Freesurfer defined pericalcarine label was derived for each subject at each of the 7 cortical depths. Following quality assessment of participants' MRI scans and Freesurfer surfaces 3 scans were found to be unusable and were excluded from the ensuing analysis. Thus, data from only 32 participants was included in the multi-modal analysis (6 datasets were removed in total following the quality assessment of participants' visual gamma responses and MRI data).

Multimodal analysis

R1 and visual gamma amplitude - In order to investigate the relationship between R1 values in the primary visual cortex and participants' visual gamma responses a correlation analysis was conducted. This was done for R1 values in each layer and, additionally for the mean R1 averaged across 20%-80% of the cortical depth. Correlations between these R1 values and gamma amplitudes were performed for two visual responses: the initial evoked gamma spike and the sustained induced gamma response. It was hypothesised that there would be a positive correlation between the amplitude of these MEG responses and R1 in the primary visual cortex.

We first calculated the correlation between participants' R1 values in the primary visual cortex averaged across 20-80% of the cortical depth and the amplitude of the initial evoked gamma spike. Given the non-normal distribution of the amplitude data (Shapiro-Wilk Test sig. = < 0.05), the Spearman's correlation coefficient was used for this analysis. Similarly, we also investigated the correlation between participants' R1 values in primary visual cortex averaged across 20-80% of the cortical depth and the amplitude of the sustained gamma response. Again, the Spearman's correlation coefficient was used, given the non-normal distribution of the amplitude data (Shapiro-Wilk Test sig. = < 0.05).

In order to investigate the depth specificity of any relationship between cortical myelin (R1) and visual gamma amplitude, the correlation between the amplitude of both the gamma spike and sustained gamma responses was investigated in relation to the R1 values at each of the 7 cortical depths. Again, it was hypothesised that any relationship between depth specific R1 values and the amplitude of the visual gamma responses would be positive.

R1 and visual gamma peak frequency – An exploratory analysis was also conducted to investigate a possible relationship between myelination of the primary visual cortex and the peak frequency of participants' visual gamma responses. We first calculated the Spearman's correlation between participants' R1 values in primary visual cortex averaged across 20-80% of the cortical depth and the peak frequency of the evoked gamma spike. The Spearman's correlation coefficient was used in this instance given the non-normal distribution of the data (Shapiro-Wilk Test sig. = < 0.05). The Pearson's correlation between participants' R1 values in primary visual cortex averaged across 20-80% of the

cortical depth and the peak frequency of the sustained gamma response was also calculated.

In order to investigate the depth specificity of any relationship between cortical myelin (R1) and visual gamma peak frequency the Spearman's correlation between R1 values at each of the 7 cortical depths and the peak frequency of the evoked gamma spike was estimated. Finally, the Pearson's correlation between the peak frequency of the sustained gamma response and R1 values at each of the 7 cortical depths was calculated.

Whole spectra analysis – In addition to assessing correlations between the peak amplitude and frequency of the visual gamma response and R1, the relationship between depth-resolved R1 values and the full frequency spectra was also investigated. For this analysis, the baseline (-1.2s – 0s) and stimulus (0.3s - 1.5s) periods of participants' virtual sensor time courses were extracted. A spectral analysis was then performed on each of these epochs using a multi-taper frequency transformation (mtmfft) and discrete prolate spheroidal sequence (dpss) filter. The frequency range was set as 0-100 Hz. Following this analysis, the percentage change in power between the stimulus and baseline conditions was calculated in order to derive a third condition consisting of the difference spectra.

In order to investigate the relationship between power across the frequency spectra and R1 a correlation analysis was then conducted for each of the three conditions. Specifically, the Pearson's correlation across subjects was calculated between R1 values at each depth and power at each frequency. In this way correlation coefficients were derived describing the relationship between R1 at each of the 7 cortical depths and each frequency point for each condition. Plots were then produced to provide a visual representation of these correlations between R1 and the spectra for each condition.

3.4 Results

Gamma spike amplitude and R1 – A non-significant relationship was found between R1 values in primary visual cortex averaged across 20-80% of the cortical depth and the amplitude of the initial gamma spike (r =0.037, p = 0.420). As shown in Table 3.1, the correlations between the gamma spike amplitude and R1 values sampled at different cortical depths were also non-significant.

Cortical Depth	R-val	P-val
20-80	0.037	0.420
1	0.031	0.433
2	-0.009	0.481
3	0.047	0.400
4	0.109	0.276
5	0.060	0.371
6	0.104	0.285
7	0.050	0.393

Table 3.1: *Table showing the correlations (R-values) and corresponding p-values for the relationship between R1 values in primary visual cortex at each cortical depth and the amplitude of the initial gamma spike.*

Sustained gamma amplitude and R1 – A non-significant relationship was found between R1 values in primary visual cortex averaged across 20-80% of the cortical depth and the amplitude of the sustained gamma response (r = 0.077, p = 0.337). As shown in Table 3.2 the correlations between the gamma spike amplitude and R1 values sampled at different cortical depths were also non-significant. However, all correlations were found to be positive.

Cortical Depth	R-val	P-val
20-80	0.077	0.337
1	0.101	0.292
2	0.119	0.259
3	0.085	0.321
4	0.110	0.275
5	0.091	0.310
6	0.148	0.209
7	0.104	0.286

Table 3.2: *Table showing the correlations (R-values) and corresponding p-values for the relationship between R1 values in primary visual cortex at each cortical depth and the amplitude of the sustained gamma response.*

Gamma spike peak frequency and R1 - A non-significant negative relationship was found between R1 values in primary visual cortex averaged across 20-80% of the cortical depth and peak frequency of the gamma spike (r = -0.006, p =0.974). As shown in Table 3.3 the correlations between the gamma spike peak frequency and R1 were also not significant.

Cortical Depth	R-val	P-val
20-80	-0.006	0.974
1	-0.077	0.674
2	-0.006	0.973
3	0.014	0.938
4	0.064	0.728
5	0.058	0.753
6	0.099	0.589
7	0.087	0.638

Table 3.3*: Table showing the correlations (R-values) and corresponding p-values for the relationship between R1 values in primary visual cortex at each cortical depth and the peak frequency of the gamma spike.*

Sustained gamma peak frequency and R1 - A non-significant negative relationship was also found between R1 values in primary visual cortex averaged across 20-80% of the cortical depth and the sustained gamma peak frequency (r =-0.091, p =0.621). As shown in Table 3.4 the correlations between the sustained gamma peak frequency and R1 values sampled at different cortical depths were also all negative. However, once more, these relationships did not meet the threshold for statistical significance.

Cortical Depth	R-val	P-val
20-80	-0.091	0.621
1	-0.119	0.517
2	-0.088	0.631
3	-0.062	0.734
4	-0.042	0.819
5	-0.033	0.857
6	-0.035	0.850
7	-0.071	0.698

Table 3.4: *Table showing the correlations (R-values) and corresponding p-values for the relationship between R1 values in primary visual cortex at each cortical depth and the peak frequency of the sustained gamma response.*

Whole spectra analysis – For the baseline spectra the strongest correlations were observed between lower frequencies (~15-20 Hz) and myelin values sampled deep in the cortex (depth 7) (see Table 3.5).

Frequency (Hz)	R-val	P-val	Depth
14	0.39	0.028	**7**
14	0.38	0.032	**7**
15	0.36	0.044	**7**

Table 3.5: *Table showing the frequencies and corresponding cortical depths at which significant correlations were found between R1 values in primary visual cortex and MEG amplitude in the baseline spectra.*

In the case of the spectra derived for the stimulation period, the strongest correlations are observed between myelin values at more superficial depths of the cortex (depth 2) and ~ 40 Hz (see Table 3.6).

Frequency (Hz)	R-val	P-val	Depth
38	0.36	0.043	**2**
39	0.36	0.043	**2**
39	0.36	0.045	**2**
40	0.37	0.037	**2**
41	0.36	0.041	**2**
43	0.36	0.042	**2**
44	0.36	0.043	**2**

Table 3.6: *Table showing the frequencies and corresponding cortical depths at which significant correlations were found between R1 values in primary visual cortex and MEG amplitude in the spectra for the stimulation period.*

Finally, for the difference spectra, the strongest correlations were again found between R1 values sampled at superficial-mid regions of the cortex (depths 2-4) and ~ 40 Hz (see Table 3.7).

Frequency (Hz)	R-val	P-val	Depth
38	0.35	0.049	3
40	0.35	0.047	2
40	0.36	0.0441	3
40	0.35	0.049	4

Table 3.7: *Table showing the frequencies and corresponding cortical depths at which significant correlations were found between R1 values in primary visual cortex and MEG amplitude in the difference spectra.*

As detailed in Tables 3.5-3.7 this analysis revealed evidence of significant positive correlations between the amplitude of participants' responses in the beta and low gamma bands and R1 values sampled at particular cortical depths. However, it should be noted that these results would not survive multiple comparisons correction. Multiple comparisons correction refers to the process of adjusting the significance level (p-value) in order to reduce the risk of false positives when performing multiple statistical tests.

The pattern of results from the full spectra analysis can be clearly observed in Figures 3.4-3.6 which depict visual representations of the correlations (and corresponding p- values) between MEG activity at each frequency and R1 sampled at the 7 cortical depths investigated in this study. As shown in Figure 3.4, which represents these relations in the baseline period, the strongest correlations are observed between R1 at lower cortical depths and activity at approximately 15-20 Hz.

A)

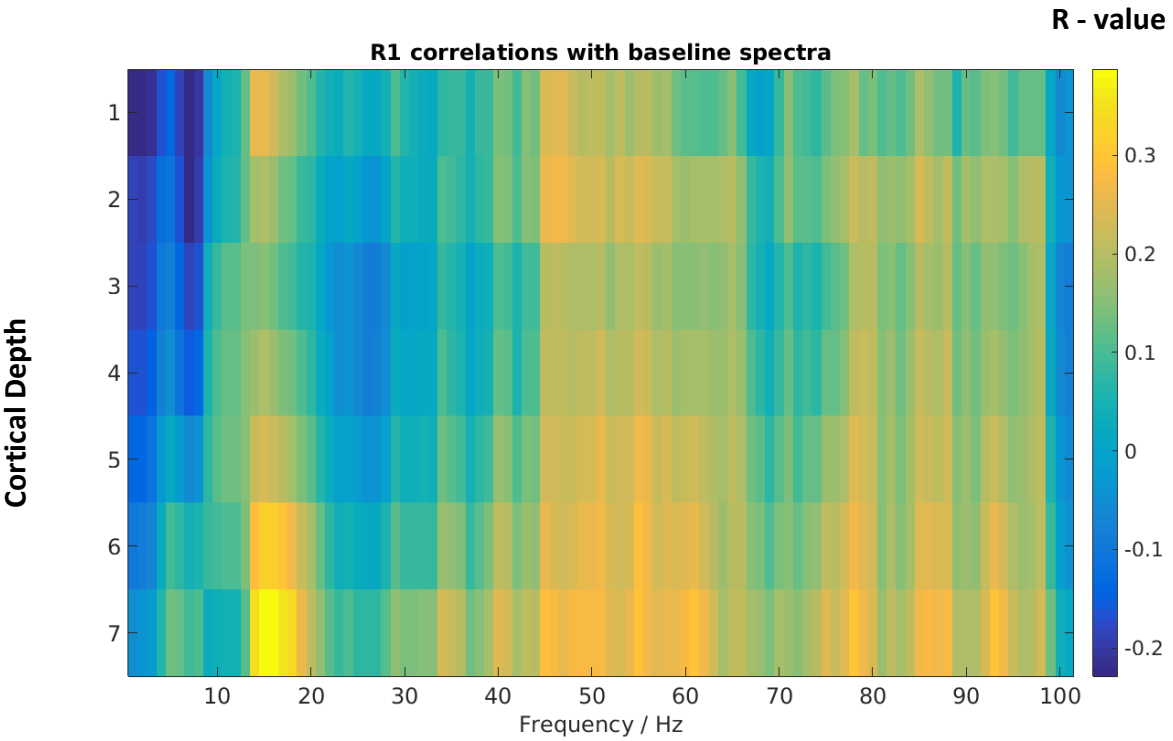

B)

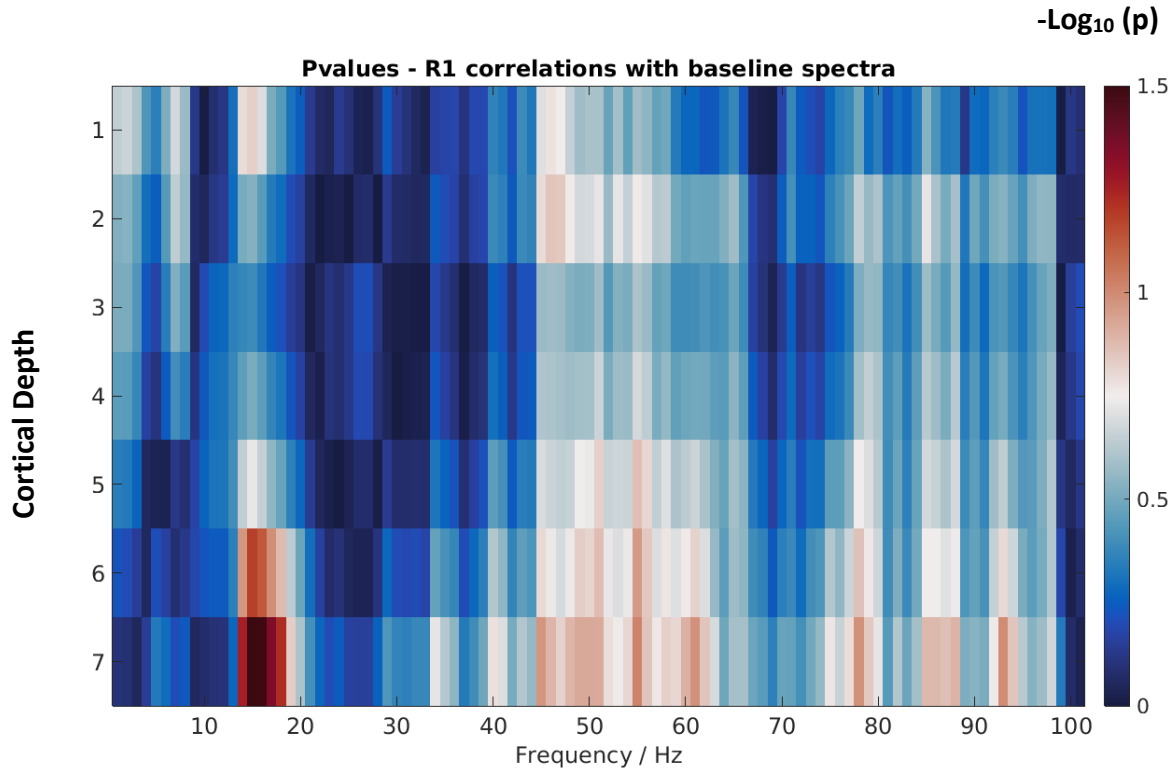

Figure 3.4: *Visual representations of **A)** the correlations between MEG activity at each frequency during the baseline period and R1 values at the 7 cortical depths and **B)** the corresponding p-values, plotted here as -log$_{10}$.*

In Figure 3.5, which shows the relationship between MEG activity in the stimulation period and R1, the strongest correlations can be observed between R1 at more superficial cortical depths (depth 2) and activity at approximately 40 Hz. There is also a hint of a relationship between activity in the alpha and beta ranges and R1sampled deep in the cortex (depth 7).

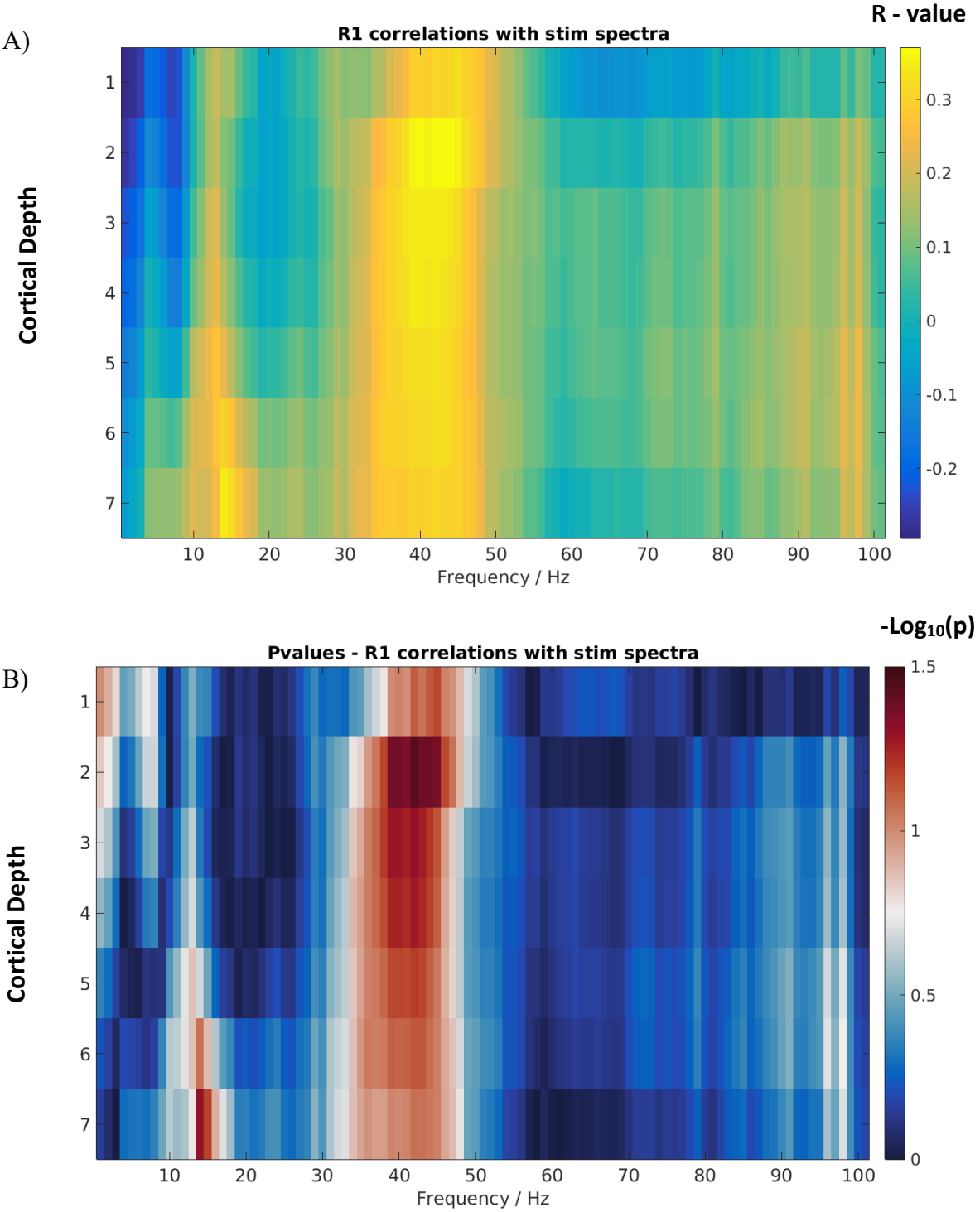

Figure 3.5: *Visual representation of* ***A)*** *the correlations between MEG activity at each frequency during the stimulation period and R1 values at the 7 cortical depths and R1 values at the 7 cortical depths and* ***B)*** *the corresponding p-values, plotted here as -log*$_{10}$.

Finally in Figure 3.6, which shows the relationship between the difference spectra and R1, the strongest correlations can again be observed between R1 at more superficial cortical depths (depths 2-4) and activity at approximately 40 Hz.

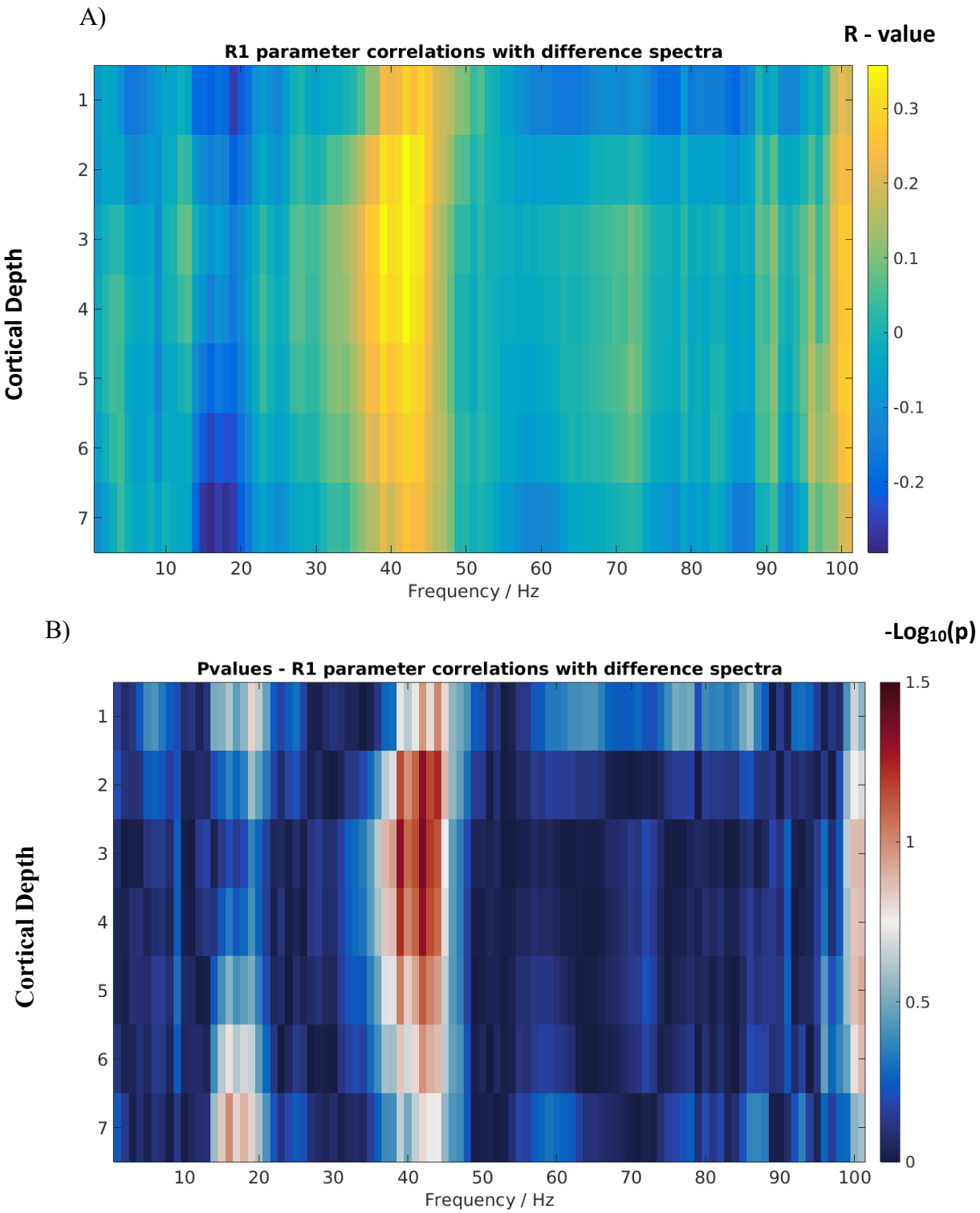

Figure 3.6: *Visual representation of **A)** the correlations between MEG activity at each frequency in the difference spectra and R1 values at the 7 cortical depths and **B)** the corresponding p-values, plotted here as -log*$_{10}$.

3.5 Discussion

The present study investigated the relationship between the microstructure of the cortex and visual gamma oscillatory dynamics. It was hypothesised that, given the close relationship between the myeloarchitecture of the cortex and its cytoarchitecture, a positive association might therefore exist between the amplitude of visual gamma oscillations and MRI derived estimates of cortical myelin content in primary visual cortex. Furthermore, the relationship between R1 estimates and another key oscillatory parameter, namely peak frequency, was also explored. The results of this investigation did not reveal evidence of a significant correlation between the peak amplitude of the initial evoked gamma spike or the later sustained gamma response and R1 estimates in primary visual cortex. Similarly, non-significant relationships were found between R1 in primary visual cortex and the peak frequency of either the initial evoked gamma spike or the sustained gamma response. Thus, in sum, this investigation did not find evidence of a relationship between either the peak amplitude or frequency of visual gamma oscillations and myelin estimates (R1) in primary visual cortex.

The results of the present study did not, therefore, replicate the findings of Helbling et al. (2015) of an association between R1 and the amplitude of MEG derived responses. However, our inability to replicate the findings of Helbling et al. (2015) could potentially be related to distinct differences in the methodologies employed by each study, including the choice of neural activity to be investigated. While the present study investigated the relationship between oscillatory dynamics and R1, ERP's were employed in the study by Helbling et al., (2015). Inherent differences in these two distinct types of neural activity, and in particular their mechanisms of generation, might therefore go some way towards explaining the discrepant findings. Furthermore, the present study focused on the visual cortex, whereas the auditory cortex was the substrate investigated by Helbling et al. (2015). Although these sensory cortices undoubtedly share some common features, for example with regards to their organisation, microstructure and neural mechanisms (Rauschecker, 2015), it is possible that a different interplay of factors may determine the characteristics of gamma oscillatory activity in visual cortex compared to the auditory cortex. Hence, it could be the case that the relationship documented by Helbling et al. (2015) is not generalisable to the visual cortex.

It should also be noted that a number of other factors may have precluded our ability to detect a relationship between R1 and visual gamma oscillatory dynamics. For example, by

averaging our R1 estimates over the whole of the V1 label we may have inadvertently diluted any potential relationship between cortical myelin and visual gamma metrics. This issue also speaks to the broader challenge of reconciling the differing spatial resolutions of MEG and MRI data (particularly 7T MRI data). Furthermore, visual gamma oscillations are known to possess a large degree of individual variability and a wide range of factors have been proposed as potential sources of such variability (Muthukumaraswamy et al., 2010; van Pelt, Shumskaya & Fries, 2018). Thus, it is possible that other sources of variance may have led to larger individual differences in our oscillatory measures, weakening our ability to detect a relationship between the cortical microstructure and oscillatory dynamics. For this reason, it would be beneficial for future investigations to adopt a larger sample size than was possible in this study in order to offset this high degree of variability. On a related point it should also be considered that healthy adult subjects, from a restricted age range, were utilised in the present study. In such a population, individual differences in cortical myelin are likely to be subtle. Therefore, it may be of benefit for future investigations to investigate the relationship between the cortical myeloarchitectural and oscillatory dynamics in populations in which a larger degree of individual variability in cortical myelin might be expected, such as in the case of demyelinating disorders or differing age groups.

To date a number of studies have employed dynamic causal modelling approaches as a means to investigate the precise neurobiological mechanisms underlying individual differences in visual gamma oscillations. For example, Pinotsis et al. (2016) demonstrated that variability in visual gamma responses was related to changes in the balance of excitation and inhibition and furthermore that such variability is likely explained by inter-individual differences in the intrinsic connections involving interneurons in PING (pyramidal-interneuron) networks. Furthermore, a study by Shaw et al., (2016) showed that inter-individual differences in intrinsic connections between superficial pyramidal cells and inhibitory interneurons were the primary determinants of variation in visually induced gamma responses. Conversely, connections between interneurons and pyramidal cells in deeper layers of the cortex were found to mediate variations in beta responses. A key advantage of adopting a modelling approach such as this lies in its ability to afford greater mechanistic insights compared to more traditional analyses of such physiological signals. Such models have thus been suggested to have the potential to provide greater insights into the mechanisms underlying variability (Shaw et al, 2016). Such an approach also confers the advantage of being able to model a number of other key factors thought to be involved in the genesis and morphology of gamma oscillations (e.g.

cortical excitation inhibition balance). Thus, it may be of benefit to harness the greater specificity of such models for application to the current dataset. Consequently, such an approach will be adopted in a later chapter of this thesis.

Whilst the initial part of this investigation focused on assessing the relationship between the peak amplitude of visual gamma oscillations and cortical myelin content, the relationship between R1 and the full frequency spectra was also explored. Interestingly, the results of this whole spectra analysis pointed to the existence of a relationship between superficial myelin content and induced gamma oscillations occurring at a frequency of approximately 40 Hz. Furthermore, with regards to the baseline spectra, the strongest correlations were observed between lower frequencies (~15-20 Hz) and R1 values sampled deep in the cortex. This relationship is also evident, though to a lesser extent, in the spectra for the stimulation period. Alpha and beta peaks are often suppressed during stimulation; hence it is not surprising that a stronger relationship is observed with these lower frequency oscillations in the baseline period. It should be noted that these correlations would not survive the threshold for multiple comparisons testing. Nevertheless, this pattern of results is certainly intriguing and further investigation and replication in a larger sample would be of benefit.

Significantly, the findings of the whole spectra analysis are in accordance with the large body of literature, principally derived from animal models, that has implicated the superficial layers of the cortex as being the likely origin of gamma oscillations. Indeed Figure 3.6, which depicts the correlation between R1 values sampled across the cortical depth and the difference spectra, bears a striking resemblance to results derived from animal models regarding the layer specificity of gamma oscillations. For example, Figure 3.7 is taken from a study examining LFP oscillatory activity in the macaque monkey and shows gamma activity at approximately 40 Hz in both the mid and superficial cortical layers. Similar work derived from animal models and indirect approaches (e.g. modelling and simulations) has also pointed to the deeper cortical layers as being the likely source of lower frequency oscillatory activity occurring in the alpha and beta ranges.

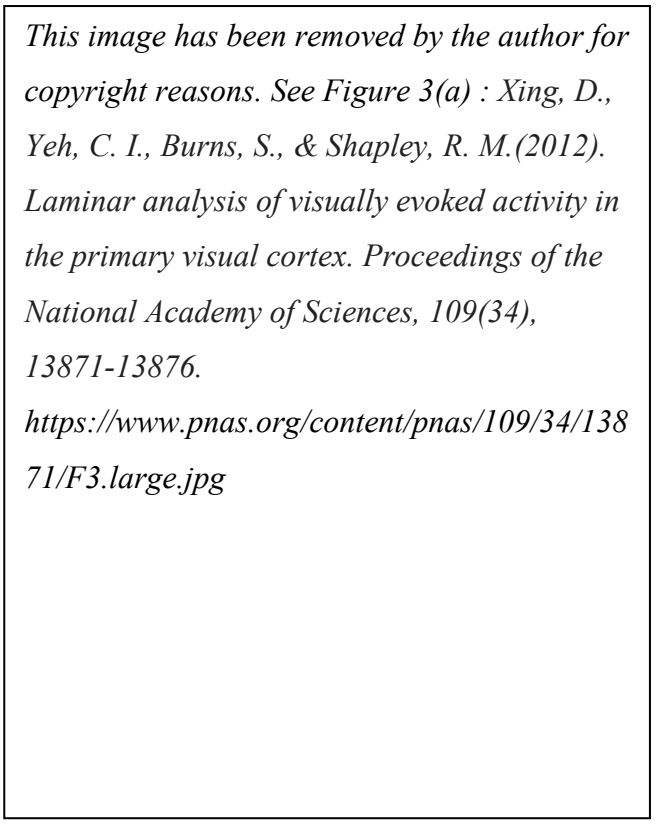

Figure 3.7 : *Taken from - Xing, D., Yeh, C. I., Burns, S., & Shapley, R. M.(2012). Laminar analysis of visually evoked activity in the primary visual cortex. Proceedings of the National Academy of Sciences, 109(34), 13871-13876. This Figure depicts the power spectrum of the local field potential (LFP) plotted as a function of cortical depth. Here the Power spectrum represents the averaged relative power in the period of 0.3s to 2s after stimulus onset).*

To date much of the evidence suggesting that higher frequency oscillations originate superficially in the cortex in the supragranular layers, whereas lower frequency activity originates in the deeper infragranular layers has come from animal studies, with direct evidence in humans remaining sparse. However, recent MEG studies have attempted to investigate the laminar hypothesis non-invasively by utilising modelling approaches in combination with improvements in the SNR of MEG data gained through the use of a novel head-cast technology (Bonaiuto et al., 2018). The results of the present study can be seen to provide further compelling evidence in humans of the laminar specific hypothesis. Significantly, such a finding has important implications for the understanding of brain function and its relationship to the underlying microstructure.

The localisation of the relationship between visual gamma and myelin density to activity occurring at approximately 40 Hz also poses a number of intriguing questions with regards to the significance of this particular frequency. Whilst 40 Hz activity is commonly seen in

the auditory cortex and has been proposed as its resonant or 'working' frequency, very little concurrent evidence exists with regards to visual cortex. However, of note, there is a real sparsity of studies investigating the presence of a resonant frequency in visual cortex. The limited literature that does exist on this subject has also reported rather mixed findings, though there is somewhat of a consensus that the peak response in visual cortex is found in the lower frequency alpha and beta ranges.

Despite the relative dearth of studies examining 40 Hz frequency responses in the human visual cortex, in recent years activity at this frequency has been garnering increasing attention for its proposed therapeutic benefits. Intriguingly, studies utilising mouse models of Alzheimer's disease have demonstrated that visual stimulation and entrainment at 40 Hz, but not at other frequencies, lead to a reduction in amyloid levels and stimulated the activity of microglia (Iaccarino et al., 2016). Such findings have led to the suggestion that 40 Hz gamma entrainment might provide neuroprotective effects in the case of neurodegenerative disease (Adaikkan & Tsai 2020). Although the focus of these studies has been on evoked gamma activity, our finding of a relationship between induced gamma activity at 40 Hz and myelin in visual cortex might also be seen to have implications for such studies, especially given that myelin abnormalities have also been widely implicated in neurodegenerative disorders such as Alzheimer's disease. Future studies examining 40 Hz visual gamma activity, its functional correlates and relations to the underlying cortical microstructure might therefore represent a valuable avenue for future research.

One potential explanation for our finding that participants' peak gamma amplitudes did not correlate with cortical myelin content, unlike 40 Hz activity, is that these may reflect distinct sub-types of gamma activity. For example, it could be speculated that in addition to the commonly investigated gamma spike and later sustained gamma responses, individuals also exhibit a further gamma response at approximately 40 Hz. Significantly, these distinct types of gamma activity might originate from different neural populations and have differing mechanisms of generation, with 40 Hz activity being more closely related to populations of myelinated neurons in the cortex.

In conclusion, the present study did not find evidence of a statistically significant relationship between the peak amplitude and frequency of visual gamma oscillations and R1 estimates in relevant cortical regions. A number of factors, including methodological limitations of this study, may have contributed to this finding. Thus, without further investigation it is not possible to state that these results provide evidence against the notion of a relationship between myelination of visual cortex and gamma oscillatory

dynamics. Intriguingly, the results of the whole spectra analysis did however point to the potential existence of a relationship between superficial cortical myelin and 40 Hz gamma activity. This finding warrants further investigation and replication in a larger sample of subjects before definitive conclusions can be drawn.

Chapter 4

Microcircuits and Microstructure: An Investigation of the Relationship Between Neurophysiologically-Informed Modelling of Oscillatory Responses and Cortical Myelination

4.1 Abstract

In-vivo investigation of the underlying cortical microcircuitry responsible for generating neural responses remains a key aim of the neuroimaging field. Of particular interest is the understanding of the neurophysiological mechanisms underpinning gamma oscillations, given their purported role in cognition and increasing association with a wide array of neuropsychiatric disorders. Computational modelling approaches, such as dynamic causal modelling (DCM) of oscillatory dynamics, represent an attractive method for investigating the cortical microcircuits responsible for the generation of these signals. However, often neglected, is that in addition to its cytoarchitecure, the cortical myeloarchitecture also represents a key component of the cortical microstructure. Furthermore, there is increasing recognition that these two facets are likely inextricably linked. Thus, here we extended the body of work outlined in Chapter 3 of this thesis by combining DCM modelling of visual gamma oscillatory responses with high-resolution MRI estimates of cortical R1 (myelin), in order to investigate whether a relationship might exist between specific parameters of the DCM model and depth-specific cortical myelin estimates. Ultimately, we did not find evidence of a significant relationship between the DCM model parameters and our cortical myelin estimates. However, methodological limitations associated with this study may have contributed to this null finding. Thus, future avenues of research are discussed that might be better suited to elucidating the relationship between the cortical

myeloarchitecture, and the neurophysiology of visual gamma oscillations, using computational modelling approaches.

4.2 Introduction

The synchronization of oscillatory activity has been touted as a fundamental mechanism sub-serving neuronal communication (Schnitzler, & Gross, 2005). Indeed, converging lines of evidence suggest that neural oscillations represent a central process enabling the coordinated activity of neuronal populations during normal brain functioning (Uhlhaas & Singer, 2010). Notably, in addition to the growing body of literature highlighting their cognitive and clinical significance, there is also compelling evidence to suggest that frequency-specific oscillations are generated in distinct neuronal circuits through the interactions of particular neuronal cell types (Buzsáki & Wang, 2012; Shaw et al., 2017) making them an attractive target for investigation.

Oscillations in the gamma range have been the subject of much attention for numerous reasons outlined below and are observed in many brain regions during both wake and sleep (Buzsaki and Wang, 2012). Though the exact genesis of these oscillations remains the subject of continued investigation, they are thought to be produced by networks of reciprocally connected excitatory pyramidal cells and inhibitory interneurons and are thus believed to emerge from the coordinated interaction of excitation and inhibition (Buzsaki and Wang, 2012). Evidence from animal studies and modelling approaches have also suggested that synchronisation in the gamma band is strongest in the superficial layers of the cortex, from which feedforward projections typically originate (Michalareas et al., 2016). Of particular interest, is that gamma oscillations have been suggested to play a key role in a number of facets of cognition, from early sensory processing to higher-order cognitive functions (Mathalon & Sohal, 2015). Gamma oscillations are also of great relevance to the study of clinical populations. Indeed, aberrant gamma oscillatory dynamics have been extensively and increasingly implicated in the pathophysiology of a wide range of clinical conditions (Mathalon & Sohal, 2015). Thus, further exploration of these potentially crucial neural signals can be seen to have great import for the understanding of brain function and cognition in both health and disease.

The previous chapter of this thesis explored the relationship between visual gamma oscillatory dynamics and myelination of the primary visual cortex. This study was based

on the hypothesis that given the close relationship between the cyto and myeloarchitecture of the cortex (Nieuwenhuys, 2013; Helbling et al., 2015; Dinse et al., 2015), and the potential role of cortical myelination in facilitating oscillatory synchrony (Tardif et al., 2016), a relationship might therefore exist between cortical myelin measured using MRI and oscillatory dynamics derived using MEG. In this investigation no significant relationship was found between visual gamma peak frequency or amplitude, and myelin estimates in the primary visual cortex.

However, it is notable that multiple factors are thought to influence visual gamma oscillatory dynamics, including those intrinsic to the cortex. Hence, it is possible that a lack of specificity with regards to the precise microcircuitry involved in the generation of gamma oscillations might have precluded our ability to detect the existence of a potential relationship between cortical myelin and oscillatory dynamics. Consequently, it might therefore be of benefit to extend our previous investigation by harnessing the greater specificity afforded by computational modelling approaches in order to probe the relationship between particular facets of the cortical microcircuitry and grey matter myelination.

One of the most pertinent aims in the neuroimaging field, is the ability to interpret experimental findings in terms of their underlying neuronal mechanisms. Key to the realisation of this aim has been the use of computational models, encompassing realistic descriptions of neural dynamics, of which Dynamic Causal Modelling (DCM) is a commonly used example (Reis et al., 2019). Notably, in recent years, a growing numberof studies have employed DCM to investigate the underlying microcircuitry involved in generating cortical responses such as visually induced gamma oscillations (Shaw et al., 2017; Sumner et al., 2018; Shaw e al., 2019). A key strength of this method, touted as providing a “mathematical microscope”, lies in its ability to make inferences about cellular processes utilising non-invasive electrophysiological recordings (Moran et al., 2011). More specifically, using this technique it is possible to make inferences about laminar-specific aspects of cortical connectivity on the basis of MEG derived spectra (Shaw et al, 2017).

The key principle behind DCM is the conceptualisation of the brain as a dynamic system that can be influenced by inputs to produce certain outputs (Friston, Harrison, & Penny, 2003). The aim of this approach is to perturb this system and subsequently measure the

response (Friston, Harrison, & Penny, 2003). More specifically, DCM can be used to make inferences about the coupling of neuronal sources in the brain and how this relationship is influenced by experimental aspects (David et al., 2006). This modelling approach is based on the principles of effective connectivity, which can be defined as the influence a given neural system exerts over another (Friston, Harrison, & Penny, 2003). Of particular relevance to the study of visual gamma oscillations, DCM allows for inferences to be made about the connections between neuronal populations thought to be involved in their genesis, namely inhibitory interneurons and pyramidal cells (Moran, Stephan, Dolan & Friston, 2011, Shaw et al., 2017, Sumner et al., 2018). To date a number of studies have employed DCM approaches as a means to investigate the precise neurobiological mechanisms underlying individual differences in visual gamma oscillations. For example, Pinotsis et al. (2016) demonstrated that variability in visual gamma responses was related to changes in the balance of excitation and inhibition and furthermore that such variability is likely explained by inter-individual differences in the intrinsic connections involving interneurons in PING (pyramidal interneuron) networks. Furthermore, Shaw et al. (2017) showed that inter-individual differences in intrinsic connections between superficial pyramidal cells and inhibitory interneurons were the primary determinants of variation in visually induced gamma responses. Conversely, connections between interneurons and pyramidal cells in deeper layers of the cortex were found to mediate variations in beta responses.

A key advantage of modelling approaches such as DCM lies in its ability to afford greater mechanistic insights compared to more traditional analyses of physiological signals, including neural oscillations. Consequently, this approach has been suggested to have the potential to provide greater insights into the precise factors governing variability in neural dynamics (Shaw et al., 2017). Thus, in sum, it may be of benefit to extend the work documented in Chapter 3, by exploiting the greater specificity afforded by the DCM approach.

The present study therefore employed DCM in order to investigate the potential relationship between cortical myelin and individual variability in visual gamma oscillations in vivo. More specifically, there is evidence to suggest that the horizontal myelinated fibres of the cortex correspond to the axon collaterals of pyramidal cells, the primary generators of the MEG/EEG signal (e.g. Braitenberg, 1968).

In recent years, evidence has also emerged suggesting that the axons of inhibitory interneurons might also be myelinated (Micheva et al., 2016). According to the widely accepted PING model, it is reciprocally connected networks of pyramidal cells and inhibitory interneurons that contribute to the generation of gamma oscillations (Buzsaki and Wang, 2012). Thus, given the close relationship between these cell types and the cortical myeloarchitecture we sought to examine whether our myelin estimates might be related to the DCM model parameter estimates. The myelin estimates utilised in this study were derived using high resolution MRI, allowing for the estimation of R1 values at different cortical depths. Consequently, a further key aim of the present study was to examine the depth-specificity of any potential relationships between our R1 estimates and the DCM model parameters investigated in this study.

4.3 Methods

The 32 MEG and MRI datasets described in Chapter 3 were utilised in this study.

Virtual sensor data

In the previous chapter, an LCMV beamformer analysis was conducted in order to identify the location of the peak gamma response in the visual cortex for each participant. Virtual sensors were then constructed for each participant at the location of this peak response by multiplying the data by the corresponding beamformer weights. This resulted in the construction of an activity time-series for each trial at this peak location. These virtual sensor data were utilised as the input to the DCM model.

DCM

Dynamic causal modelling for steady state responses (DCM-SSR) was conducted on the virtual sensor data for all 32 participants. The DCM implementation adopted in the present study utilised the method outlined in Shaw et al. (2017). It is a modified version of the standard approach found in the SPM8 package (Moran et al., 2009) and is optimised to reflect the properties of the primary visual cortex. Full details of this DCM analysis approach can be found in the publication by Shaw et al. (2017). However, a summary of the methodology is provided below.

The neural model used in this instance was a variation of the canonical microcircuit (CMC) consisting of 4 laminar-resolved cell populations (see Figure 4.1). In the CMC model excitatory pyramidal cells are found in the both the superficial and deep cortical layers. These two populations of pyramidal cells are separated by stellate cells located in layer four. The final cell population in the model consists of inhibitory interneurons located in all layers. As noted by Shaw et al. (2017), such a model is undoubtedly a simplification of the actual cytoarchitecture of the cortex. However, it is important to strike a balance between complexity (in this case of the cortical microcircuitry), and model estimability, in order to ensure that a robust solution can be reached (Shaw et al., 2017). The approach outlined by Shaw et al. (2017) allows for such a balance to be attained and was guided by both the existing DCM literature, and anatomical evidence of the columnar structure of primary visual cortex. Notably, this approach has been shown to successfully capture neuronal dynamic perturbations induced by pharmacological manipulations, thus demonstrating the sensitivity and specificity of the model (Shaw et al., 2017).

Through DCM analysis it is possible to characterise the local synaptic connectivity between the 4 populations of cells included in the neural model, namely deep and superficial pyramidal cells, stellate cells, and inhibitory interneurons. These connections are shown in Figure 4.1 taken from Shaw et al. (2017) and includes both reciprocal and non-reciprocal connections. The full list of parameters included in the model and their corresponding functions are detailed in Table 4.1.

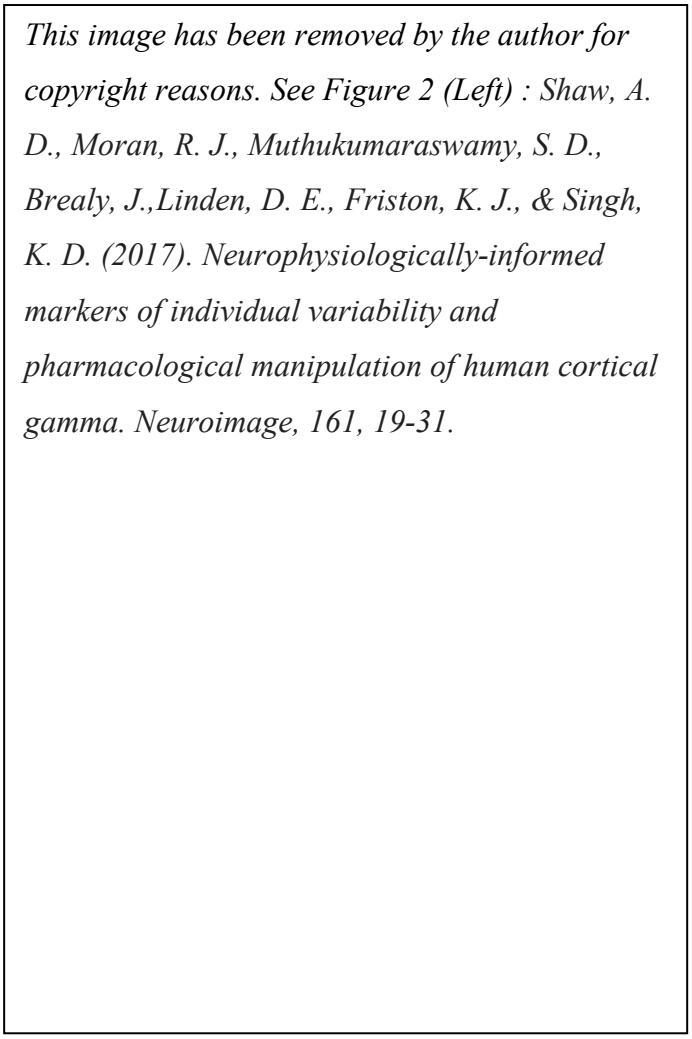

Figure 4.1: *Taken from - Shaw, A. D., Moran, R. J., Muthukumaraswamy, S. D., Brealy, J.,Linden, D. E., Friston, K. J., & Singh, K. D. (2017). Neurophysiologically-informed markers of individual variability and pharmacological manipulation of human cortical gamma. Neuroimage, 161, 19-31. This Figure depicts the canonical microcircuit (CMC) used in the DCM analysis in this study. Here, the excitatory connections are represented inblue, whilst the inhibitory connections are portrayed in red. Finally, the grey arrows are representative of self-inhibition of each of the excitatory cell populations.*

This image has been removed by the author for copyright reasons. See Figure 2 (right) : Shaw, A. D., Moran, R. J., Muthukumaraswamy, S. D., Brealy, J.,Linden, D. E., Friston, K. J., & Singh, K. D. (2017). Neurophysiologically-informed markers of individual variability and pharmacological manipulation of human cortical gamma. Neuroimage, 161, 19-31.

Table 4.1. *Taken from - Shaw, A. D., Moran, R. J., Muthukumaraswamy, S. D., Brealy,J., Linden, D. E., Friston, K. J., & Singh, K. D. (2017). Neurophysiologically-informed markers of individual variability and pharmacological manipulation of human cortical gamma. Neuroimage, 161, 19-31. This table describes each of the parameters utilised to define the model. The prior values (PI) and precision (sigma) of these parameters is also shown.*

In the CMC model time-differential equations are used to estimate the membrane potentials and postsynaptic currents of these interacting cell populations. In this way, a time course of the voltages and postsynaptic currents of the cell populations can be generated. In the context of the present study, DCM-SSR works by modifying these equations to also include a frequency-domain transfer function. Significantly, the resulting model output, which is in the frequency-domain, can then be compared with the spectra derived from each participant's virtual sensor data. The parameters of the model are then

optimised in order to achieve the best fit of the model spectra to the true data spectra derived from the MEG virtual sensors. This model fitting is achieved using a Bayesian inference procedure incorporated within DCM.

As noted in Shaw et al. (2017) the following parameters have been found to have a negligible effect on the fitted spectral density: G1, G3,G10 and G13. Hence, we chose to fix these parameters in our subsequent analysis. Similarly, the T1 parameter, which represents the time constant of the spiny stellate cells, was also fixed as even slight variations in this parameter have been demonstrated to have a profound impact on the model stability (Shaw et al., 2017).

The CMC model was first fitted to the mean spectra in order to derive initial starting values for the parameters included in the model. These values were then utilised as the priors when fitting the DCM-SSR model to each of the individual datasets. The DCM-SSR analysis output consisted of individual estimates of the model parameter strengths for each participant which were used in our subsequent multi-modal analysis.

The DCM analysis conducted in this study allows for the assessment of synaptic coupling between cell populations in the model. However, of particular interest, in the context of the present study, is that such an approach also confers the ability to conduct an exploration of the model parameters that best determine particular spectral features (Shaw et al., 2018). Thus, we sought to determine the model parameters influencing oscillatory dynamics, specifically the amplitude and frequency of visual gamma oscillations. Given our hypothesis of a potential relationship between oscillations and the cortical myeloarchitecture we also investigated whether the DCM model parameters, particularly those influencing visual gamma oscillatory dynamics, might therefore also be related to estimates of myelin density in the primary visual cortex.

Alpha, beta and gamma peaks can be recovered in the majority of participants' spectra, following the implementation of a pre-whitening procedure to remove the strong power law known to dominate neural signals (Shaw et al., 2017). Thus, akin to Shaw et al. (2017), we also chose to model the alpha frequency peak within each participant's spectral response utilising a gaussian function constrained between frequencies 8 Hz to 13 Hz. In contrast, the beta and gamma response peaks are recovered from the output of the CMC model itself.

More specifically, the beta and gamma peaks are generated by the synaptic rate constants and intrinsic connectivity of the CMC utilised in this study which is depicted in Figure 4.1.

In this way we were able to derive estimates of oscillatory dynamics for each participant and in particular the amplitude and frequency of the alpha, beta and gamma responses observed in participants' spectra.

Multi-modal Analysis

In order explore the existence of a potential relationship between the DCM analysis outputs and R1 estimates in primary visual cortex, a correlation analysis, across participants, was conducted. The R1 estimates utilised in this instance were sampled across the cortical depth as detailed in Chapter 3. Briefly, for each participant we extracted the mean R1 value of the Freesurfer-defined pericalcarine label, which approximates the primary visual cortex location of the visual gamma response, at each of the 7 cortical depths, derived using an equi-volume layering approach. In this way a mean R1 value for the primary visual cortex was derived for each subject at each of the 7 cortical depths investigated in this study. In this way it was possible to examine the depth-specificity of any potential relationship between the DCM model outputs and cortical myelin.

We sought to examine whether our myelin estimates might be related to the model parameter estimates. Hence, we assessed the relationship between the local synaptic connection parameter (G) outputs from the model (see Table 4.1 for descriptions of each parameter) and our myelin estimates. Of particular interest, were the G11 and G8 parameters given that these have previously been shown to correlate positively with gamma amplitude (Shaw et al., 2017). The Pearson's correlation coefficient was calculated between these parameters and the depth-specific myelin estimates.

The gamma amplitude and frequency estimates from the model showed a non-normal distribution. Hence in this instance, the Spearman's correlation coefficient was calculated between these values and our R1 estimates.

Given that axonal myelination should also influence the time constant of neuronal cell populations we also hypothesised that there might be a relationship between the time constant model parameter estimates and our myelin data. Thus, we also chose to calculate

the Pearson's correlation coefficient between the time constant parameters (T2, T3 and T4) and the depth specific cortical myelin estimates.

4.4 Results

Parameters influencing Gamma oscillatory dynamics

Akin to the results of Shaw et al. (2017) the correlation analysis revealed that the G11 parameter, which is representative of the inhibitory connection between the inhibitory interneurons and superficial pyramidal cells, was significantly correlated with the peak amplitude of visual gamma oscillations when correcting for multiple comparisons ($r = 0.78$, $p=<0.0001$). Similarly, a significant positive correlation was also observed between the G6 parameter (deep pyramidal cell connection to inhibitory interneurons) and peak gamma amplitude. A Positive correlation was observed between the G8 (spiny stellate connection to superficial pyramidal cells) and gamma amplitude; however, this relationship did not survive multiple comparisons correction.

We did not find any significant correlations between Gamma peak frequency and the model parameter estimates (Table 4.2). There was a negative correlation observed between T3 and peak gamma frequency, though this relationship would not survive multiple comparisons correction.

Parameter	Peak Gamma Frequency	Peak Gamma Amplitude
G4	0.36 (p=0.045)	-0.19 (p=0.290)
G7	0.32 (p=0.074)	-0.16 (p=0.385)
G11	0.07 (p=0.691)	**0.78 (p=<0.001)**
G12	-0.17 (p=0.349)	-0.35 (p=0.048)
G8	0.17 (p=0.359)	0.49 (p=0.005)
G5	-0.08 (p=0.664)	0.24 (p=0.186)
G6	0.09 (p=0.618)	**0.58 (p=0.001)**
G9	-0.19 (p=0.286)	-0.37 (p=0.036)
T2	0.26 (p=0.155)	0.36 (p=0.045)
T3	-0.42 (p=0.018)	-0.28 (p=0.116)
T4	-0.02 (p=0.926)	-0.36 (p=0.044)

Table 4.2. *Correlations between gamma oscillatory dynamics and the parameter estimates derived from the DCM model fitting and the corresponding p-values (uncorrected). The r- values highlighted in red are significant at p=<0.05, when using the Bonferroni correctionfor multiple comparisons (0.05/11=0.004).*

R1 and Oscillatory Parameters

As shown in Table 4.3 positive correlations were observed between Gamma amplitude and the R1 estimates. This relationship was strongest with R1 values sampled at the most superficial cortical depth investigated in this study (r=0.239, p=0.094), however none of these relationships were found to be statistically significant. We did not find evidence of a relationship between R1 estimates and either alpha or beta oscillatory amplitude.

With regards to the relationship between gamma frequency and R1, the majority of correlations were positive, with the strongest relationship being observed with R1 values sampled at mid-cortical depth. However, once again, none of these relationships met the threshold for statistical significance. Non-significant positive correlations were also found between the R1 estimates and alpha peak frequency at the majority of cortical depths.

A significant negative correlation was found between beta frequency and R1 estimates sampled superficially in the cortex (r = -0.345, p= 0.047). However, this relationship would not survive multiple comparisons correction.

Cortical Depth	Gamma Amplitude (R-val)	Gamma Amplitude (P-val)	Gamma Frequency (R-val)	Gamma Frequency (P-val)
1	0.239	0.094	-0.017	0.463
2	0.126	0.245	0.092	0.309
3	0.016	0.464	0.198	0.139
4	0.079	0.333	0.262	0.074
5	0.093	0.306	0.238	0.095
6	0.130	0.240	0.257	0.078
7	0.118	0.259	0.180	0.162

Table 4.3. *Correlations between gamma oscillatory dynamics and depth-specific R1 values and the corresponding p-value (uncorrected). Here depth 1 is the most superficial,whereas depth 7 is the closest to the white matter.*

R1 and Connection Parameters

Non-significant negative correlations were observed between the depth-specific R1 estimates and the G4 parameter (see Table 4.4). The relationships between G5 and R1 were found to be positive, however again these relationships did not meet the threshold for statistical significance. A negative correlation was observed between the G6 parameter and the depth-specific R1 estimates. These correlations were also observed to be strongest at deeper cortical depths. However, these relationships did not meet the corrected threshold for statistical significance. In the case of the G7, G8, G9 and G11 parameters , no significant relationships were once again found between the model estimates and the R1 values. Finally, negative correlations, strongest at mid-superficial cortical depths, were observed between the G12 parameter and the depth specific R1 values, though again these correlations did not meet the threshold for statistical significance.

Cortical Depth	G4 R-val	G4 P-val	G5 R-val	G5 P-val	G6 R-val	G6 P-val	G7 R-val	G7 P-val	G8 R-val	G8 P-val	G9 R-val	G9 P-val	G11 R-val	G11 P-val	G12 R-val	G12 P-val
1	-0.147	0.422	0.248	0.172	-0.183	0.317	-0.144	0.431	0.121	0.508	-0.025	0.892	-0.033	0.856	-0.066	0.718
2	-0.094	0.609	0.164	0.371	-0.161	0.378	-0.029	0.874	0.100	0.585	-0.100	0.585	-0.098	0.595	-0.201	0.270
3	-0.060	0.745	0.173	0.343	-0.186	0.307	0.053	0.772	0.113	0.538	-0.102	0.580	-0.141	0.443	-0.239	0.188
4	-0.053	0.772	0.203	0.265	-0.216	0.235	0.049	0.789	0.140	0.446	-0.074	0.687	-0.139	0.447	-0.203	0.265
5	-0.032	0.864	0.209	0.250	-0.240	0.185	0.060	0.744	0.142	0.437	-0.061	0.740	-0.132	0.471	-0.174	0.342
6	-0.046	0.803	0.207	0.255	-0.260	0.150	0.030	0.872	0.161	0.378	-0.029	0.877	-0.137	0.454	-0.134	0.463
7	-0.079	0.668	0.190	0.299	-0.269	0.137	-0.030	0.872	0.158	0.389	0.020	0.916	-0.172	0.347	-0.088	0.634

Table 4.4. *Correlations between Depth-specific R1 values and the parameter estimates derived from the DCM modelfitting. Depth 1 refers to myelin values sampled the most superficially in the cortex, whereas depth 7 refers to the R1values sampled closest to the white matter.*

R1 and Time Constant Parameters

Non-significant positive correlations were found between the T2 parameter and the depth specific R1 estimates (see Table 4.5). Similarly, no significant correlations were found between the R1 estimates and both the T3 and T4 time constant parameters.

Cortical Depth	T2 R-val	T2 P-val	T3 R-val	T3 P-val	T4 R-val	T4 P-val
1	0.090	0.623	0.159	0.386	-0.044	0.810
2	0.160	0.380	0.071	0.699	-0.024	0.897
3	0.187	0.306	0.025	0.893	0.004	0.983
4	0.174	0.341	0.024	0.897	-0.011	0.954
5	0.178	0.330	0.027	0.882	-0.012	0.946
6	0.159	0.386	0.055	0.767	0.025	0.894
7	0.113	0.537	0.084	0.649	0.051	0.782

Table 4.5. *Correlations between Depth-specific R1 values and the parameter estimates derived from the DCM model fitting. Depth 1 refers to myelin values sampled the most superficially in the cortex, whereas depth 7 refers to the R1 values sampled closest to the white matter.*

4.4 Discussion

Here, for the first time, we explored the relationship between aspects of the cortical microcircuitry derived using neurophysiologically informed modelling and myelin, a key feature of the cortical microstructure. However, we did not find evidence of a statistically significant relationship, across participants, between our depth-specific myelin values and the DCM model parameter estimates for any of the relationships explored in this study.

Akin to the results of Chapter 3, the present study also did not find evidence of a significant relationship between participants' peak gamma response amplitudes derived from the cortical microcircuit model and cortical myelin. However, it is notable that this relationship was found to be positive and was also strongest at more superficial cortical depths, from which gamma oscillations are thought to originate. Given the relatively small sample size employed in this study, it is possible that a further investigation of this relationship in a larger sample might provide further insight into the veracity of the trend observed here. We also explored the relationship between cortical myelin and the amplitude of participants' alpha and beta peaks, however no significant correlations between these factors were found.

With regards to the estimated oscillatory frequency parameters, alpha and gamma peak frequency estimates were also found to be non-significantly correlated with our myelin estimates. There was a trend towards a negative correlation between beta peak frequency and cortical myelin sampled superficially in the cortex. However, this relationship would not survive multiple comparisons correction. Again, further exploration in a larger sample size might be of benefit to further investigate the validity of this observed trend.

Akin to Shaw et al. (2017), we did find evidence of a relationship between gamma amplitude and relevant parameters of the DCM model, namely the G11 parameter, pointing to the success of the model fitting. However, unlike this previous investigation we did not find significant correlations between relevant model parameters and gamma peak frequency estimates in our sample of participants, although some trends were evident. One potential explanation for this slight discrepancy is that the study by Shaw et al. (2017) utilised a much larger sample of participants (93). Of note, it is possible that the looser coupling between oscillatory dynamics and the DCM model parameters in our

sample might in turn have led to a weakening of the relationships between our R1 estimates and the model parameters. Thus, this once again points to the potential utility of exploring these relationships in a further larger sample of individuals.

However, a number of other factors may have contributed to the null findings of this study. For example, a significant limitation of the present study, and indeed studies employing DCM in general, is that the neural models utilised in such investigations are likely an over-simplification of the true cytoarchitecture of the cortex. We employed the methods of Shaw et al. (2017), whose choice of neural model was optimised for the known neurophysiology of the visual cortex and was carefully selected in order to strike a balance between neurophysiological validity and model estimability. The model employed here has previously been validated in pharmacological manipulation studies (Muthukumaraswamy, et al., 2015; Shaw et al., 2017) that have demonstrated the sensitivity of the model to such perturbations. Furthermore, this particular model has also recently been shown to be sensitive to the effects of clinical disorders such as schizophrenia (Shaw et al., 2020). However, with regards to the specific aims of the present study, in future it may be of benefit to conduct further validation studies in order to investigate whether the model is sufficiently complex to accurately examine the impact of myelin perturbations on the model parameters. For example, one possibility would be to employ the model in a clinical population in which myelin abnormalities are well documented, such as Multiple Sclerosis. Of note, previous studies have demonstrated evidence of a diminished visual gamma band response in MS patients compared to healthy control subjects (Barratt et al., 2017).

On a related point, given that the present study employed a sample of healthy young adults, it is possible that individual differences in both our DCM parameter estimates and R1 measures may have been too subtle to allow for the detection of a relationship between these two variables. Thus, in future, investigating this relationship in a clinical population, in which demyelination represents a key feature, in addition to a healthy control group, would likely be of benefit. A further potential limitation of the present investigation is that the quantitative R1 estimates utilised in this study will likely be affected by multiple variations in the underlying microstructure (Weiskopf et al., 2015). Although validation against histological data has shown that cortical T1 (R1=1/T1) contrast is reflective of its myelin content, it should be noted that iron has also been shown to contribute to T1 contrast in the cortex (Stuber et al., 2014). However, as noted in Chapter 3, given that

myelin and iron are typically strongly co-localised in the cortex, it has been argued that, independent of the exact contribution of iron and myelin, T1 can be justified as largely reflecting the distribution of intracortical myelin (Huntenburg et al., 2017). That said, this issue points to the potential importance of employing multiple MR contrasts in order to accurately resolve specific in-vivo histological measures of the brain's microstructure (Weiskopf et al., 2015). Interestingly, of late, there has been increasing interest in using a novel quantitative and local contrast technique known as Quantitative Susceptibility Mapping (QSM) to investigate the microstructure of the brain (Deistung et al., 2013). The main contributors to contrast observed in QSM are iron and myelin (Deistung et al., 2013). However, a significant advantage of QSM lies in its potential to distinguish paramagnetic from diamagnetic contributions, given their different magnetic properties (Marques, Khabipova, & Gruetter, 2017). Intriguingly, utilising QSM in combination with T2* could thus help to disentangle the contribution of iron from myelin (Duyn, 2017). This is because whilst myelin, which is diamagnetic, has a negative magnetic susceptibility, iron is paramagnetic and has a higher magnetic susceptibility. Indeed, it has been demonstrated that modelling approaches utilising information from susceptibility values and R2* (combined with estimates of myelin content from magnetisation transfer contrast) can allow for the quantification of iron and myelin content (Schweser, Deistung, Lehr, Sommer, & Reichenbach., 2011). Thus this approach may be of value in future studies of cortical myelination and in combination with the T1 imaging approach employed here, might offer the potential to obtain cortical myelination maps clean of iron/paramagnetic contributions (Marques, Khabipova, & Gruetter, 2017).

Significantly, owing to recent innovations in the neuroimaging field, there is now also the potential to unify structural and functionally derived biophysical models (Freund et al., 2016). In the present study we explored the relationship between estimates of the cortical microstructure derived using high resolution quantitative MRI and the output of a functional biophysical model applied to MEG data. However, whilst beyond the scope of the present work, in future studies it may be of benefit to adopt a slightly different approach whereby information about the cortical microstructure derived from high field MRI is incorporated into this model. For example, the neural model used in the DCM analysis could be modified and further developed to incorporate myelin estimates as anatomically informed priors. One way to implement this might be to use myelin estimates as a proxy for pyramidal cell density in specific cortical layers, given that the axons of these cells are known to be myelinated. Such an approach might be able to further

elucidate the relationship between cortical myelin and neural dynamics as well as having the potential to enhance the DCM model itself and its sensitivity to such phenomena. Such an approach is not without precedent. For example, a previous study by Stephan et al. (2009) utilised diffusion imaging in combination with tractography in order to specify anatomically informed priors for DCM models of fMRI data. The studycompared this approach to DCM models that did not include such anatomically informed priors. Significantly, the authors found that the best DCM model was that which included the anatomically informed priors (Stephan et al., 2009).

In conclusion, this study did not find strong evidence of a relationship between potentially relevant aspects of the cortical microcircuitry and myelination of the cortex.However, it is possible that a number of limiting factors might have reduced our ability to detect the presence of any such relationships. Of particular importance is that further validation studies are required in order to evaluate the suitability of the modelling approach employed here, in the context of investigating the potential influence of cortical myelination and individual differences thereof on aspects of the cortical microcircuitry. Furthermore, future investigations might also wish to explore the utility of adopting an alternative approach whereby information about the cortical myeloarchitecture is explicitly included in the DCM model in the form of anatomically informed priors.

Chapter 5

An Investigation of the Relationship Between Inter-Individual Differences in Auditory Steady State Responses and the Cortical Microstructure

5.1 Abstract

Gamma band Auditory Steady State Responses (ASSRs) have been suggested to provide a window onto the ability of the auditory cortex to support oscillatory activity. Intriguingly, to date, considerable inter-individual differences in morphological aspects of these responses have been documented in both health and disease. Indeed, impaired gamma ASSRs have been demonstrated in a range of psychiatric and neurodevelopmental disorders. Thus, the understanding of the mechanisms underlying such individual variability can be seen to be of great clinical significance. Of particular interest is the relationship between a key aspect of the cortical microstructure, namely its myelin content, and variability in the gamma ASSR, owing to the close association between myelin and cell populations thought to be involved in the generation of gamma oscillations. Furthermore, a role for myelin in aiding neural synchrony has also been proposed. Thus, in a sample of healthy young adults, we conducted a novel investigation of the relationship between inter-individual variability in gamma band ASSRs elicited using an auditory chirp stimulus and myelination across the cortical depth. Significant correlations were not observed between either the amplitude, peak frequency, or phase consistency of participants' ASSRs and myelination (R1) of the primary auditory cortex. However, a trend indicative of a positive correlation between the amplitude of the ASSR and cortical myelination, particularly at lower cortical depths, was observed. Further

research will be essential to unravelling the significance of the trends observed here and their relevance to the understanding of the pathophysiology of clinical conditions.

5.2 Introduction

The auditory steady state response (ASSR) is a type of neural oscillatory activity that can be used to probe the functioning of auditory pathways and their capacity to generate synchronous activity at specific frequencies (O'Donnell et al., 2013). The ASSR occurs when neuronal activity synchronises or entrains to the frequency and phase of an auditory stimulus. Akin to visual gamma oscillations, discussed in Chapter 3 of this thesis, the amplitude of the gamma ASSR has been shown to demonstrate inter-individual variability (Ross *et al.*, 2000). That said, a strikingly consistent discovery in the literature, is that the amplitude of the ASSR in humans peaks in the 30-50 Hz gamma range, very close to 40 Hz (Galambos, Makeig, & Talmachoff, 1981; Picton et al., 2003). Such findings have been taken to suggest that the underlying neural populations in the auditory cortex may preferentially oscillate at this frequency. Thus this ~40 Hz response has been touted as the resonance or working frequency of networks in the auditory cortex (O'Donnell et al., 2013). Studies have also shown that participants can show a second, weaker peak response in the gamma range at approximately 80 Hz (Lins et al., 1995). Whilst the ASSR occurring at ~ 40 Hz has been localised to the primary auditory cortex in prior MEGinvestigations, at higher frequencies (~80 Hz), this activity has been found to be strongest in subcortical structures such as the brainstem (Herdman et al., 2002).

Significantly, the location of this resonant response in the gamma frequency range points to the likelihood that its generation might rely on some of the same circuit and neuronal properties as non-driven gamma band oscillations, such as those thought to be involved in cognition (Spencer, Salisbury, Shenton, & McCarley, 2008). Consequently, ASSR paradigms can be viewed as an ideal means of probing the ability of neural networks to generate and support oscillatory activity (Uhlhaas, Roux, Rodriguez, Rotarska-Jagiela, & Singer, 2010). Indeed, the 40 Hz steady response has been employed by numerous studies as an index of the ability for cortical networks to support synchronised oscillatory activity in the gamma band frequency range (Griskova et al., 2007).

A deficit in the ability of the auditory cortex to support neural synchrony at a particular frequency will be reflected in the amplitude of the ASSR response (O'Donnell et al., 2013).

Similarly, the phase variability of the ASSR also constitutes a useful measure of the ability of a cortical area to support neural synchrony. In the case of high frequency activity, such as that in the gamma range, it is of critical importance that neural synchrony entails a high degree of precision in order to allow for the effective summation of synaptic currents and the production of a measurable signal (Uhlhass & Singer, 2006). Whilst investigations of the amplitude of MEG responses certainly correlate with the degree of neural synchrony, a number of confounding factors make it difficult to draw firm conclusions regarding synchrony when considering amplitude measures in isolation (Uhlhass & Singer, 2006). In light of this, a variety of phase-based approaches have been developed that allow for the computation of the phase consistency of the timing of neural activity across trials (de Beeck & Nakatani, 2019). One such amplitude independent measure is the Inter Trial Phase Coherence (ITPC). Although an ITPC value close to 0 reflects a high variability of phase angles across trials, a value closer to 1 is indicative of all epochs having the same phase angle (Lachaux et al., 1999). Thus, a higher ITC value can be taken as an indicator of greater neural synchrony.

Abnormalities in the amplitude and phase coherence of gamma frequency ASSRs have been documented in a number of clinical conditions, including bipolar disorder (Isomura et al., 2016), autism (Seymour et al., 2020), and Fragile X syndrome (Ethridge et al., 2017), to name but a few. Interestingly, abnormalities in the 40 Hz ASSR have also been extensively implicated in schizophrenia in both chronic (Spencer et al., 2008b) and first episode (Spencer et al., 2008a) patients. For example, a meta-analysis by Thuné, Recasens, & Uhlhaas (2016) of the 40 Hz ASSRin schizophrenia found that of the 20 studies investigated, 17 reported a reduction in the amplitude of the ASSR in schizophrenic patients compared to controls. In light of the consistent findings of altered gamma ASSR's in schizophrenia reported in the literature, the ASSR has been suggested as a potentially useful biomarker of the condition (O'Donnell et al., 2013).

Typically, the ASSR is investigated using amplitude modulated tones or click trains at a particular frequency, usually 40 Hz (Artieda et al., 2004). However, akin to the literature regarding visual gamma oscillations, there is also evidence suggestive of the existence of inter-subject variability in the peak frequency of this response. Although testing participants' responses to different frequencies can be a prohibitively lengthy process if a single frequency is studied at one time, Artieda et al. (2004) demonstrated how ASSRs to multiple frequencies can be measured using a tone modulated in amplitude that increases

linearly in frequency over time, known as a 'chirp'. This study revealed the presence of inter-individual differences in participants' peak gamma band responses, suggesting that this methodology might represent a powerful tool for investigating inter-individual differences in cortical responses to auditory stimulation.

Studies in clinical populations have also employed chirp stimuli, as opposed to stimulating at a particular frequency, in order to investigate synchrony deficits in different populations. For example, an EEG study of autism spectrum disorder utilising an auditory chirp stimulus (1-100 Hz) documented evidence indicative of a decreased ability to support synchrony in the low gamma range in participants with autism spectrum disorders (ASD) compared to typically developing controls (De Stefano et al. 2019). The authors of this study point to their finding of a reduction in phase locking in the low gamma band in ASD as indicating the presence of abnormal inhibitory network function - given that these inhibitory networks are hypothesised to determine the ability to phase-lock to an oscillatory stimulus (De Stefano et al., 2019).

A further clinical study, utilising the chirp stimulus of Alegre et al. (2017), investigated steady-state responses in two different groups of schizophrenia patients, namely those who were drug naïve and those receiving treatment with atypical antipsychotics. Interestingly, the drug naïve group were found to exhibit reduced amplitude and inter-trial phase coherence in the low gamma band (30-50 Hz), in addition to reduced amplitude of the response in the higher 90-100 Hz gamma range, in comparison to control subjects. This disruption of low gamma activity was not found in the treated patient group, though a reduction in the higher 90-100 Hz gammarange was still evident in this cohort. Significantly the results of this study point to the fact that impairments in auditory steady state responses in schizophrenia may not be limited to 40 Hz, and in fact encompass a broader range of frequencies. Furthermore, the results of this study provide some indication that treatment with atypical antipsychotics may normalise these responses to some extent, at least in the low gamma range.

Finally, potentially significant individual differences in the peak frequency of oscillatory activity in response to chirp stimuli have also been reported. For example, Arrondo et al. (2009) reported evidence of a lower peak frequency of the auditory steady state response in MS patients exhibiting cognitive impairment in comparison to those without cognitive impairment and healthy control subjects. Furthermore, the study found a negative

correlation between the frequency of the ASSR (in the 40 Hz range) and cognitive impairment. The results of this study can be taken to suggest that variability in the peak frequency of ASSR may be of functional significance. Indeed, the authors suggest that the demyelinating lesions characteristic of MS might be implicated in both the slowing of oscillatory activity and subsequent efficiency of cognitive processing.

In sum, there is a considerable body of evidence pointing to the existence of potentially significant individual variability in ASSR responses, particularly in clinical populations. Yet, in contrast, there has been a relative dearth of research conducted into the potential structure-function relationships underlying such variability. In particular, to date, only a handful of studies have investigated the dependence of the ASSR on the underlying structure of the auditory cortex in human participants. For example, building on previous findings of altered structural and functional parameters in auditory regions in schizophrenia, Edgar et al. (2014) examined the relationship between the structure of the STG and the 40 Hz ASSR in both healthy controls and schizophrenia patients. In accordance with the findings of previous studies, they reported evidence of reduced power and inter-trial coherence in schizophrenia in the left STG. The study also reported a positive association between cortical thickness of the left STG and both the 40 Hz ASSR and ITC, however this relationship was not evident in the schizophrenia cohort. The authors speculated that one possible explanation for their findings is that the presence of grey matter abnormalities in schizophrenia may preclude the development of typical structure-function relationships in this population.

A further study of structure-function relationships in the auditory cortex by Kim et al., (2019) investigated the 40 Hz ASSR and its association with anatomical characteristics, such as brain volume, in a cohort of schizophrenic patients and healthy controls. In contrast to the aforementioned studies, this investigation found evidence of an increased gamma response in schizophrenic patients. Echoing the findings of Edgar et al. (2014) this study also found evidence of an association between the volume of the right superior temporal gyrus (STG) and evoked power in control subjects but not those with schizophrenia. The authors hypothesize that one potential explanation for the absence of this association in patients with schizophrenia may be due to anatomical differences previously noted in this population, such as a reduction of pyramidal cell volume, specifically in deep layer 3 of the auditory association cortex (Sweet et al., 2003). However, given that only STG volume was considered in this study, it is not possible to

draw concrete conclusions regarding the precise neuroanatomical origins of this difference. Future studies employing more advanced MRI techniques designed to afford greater specificity with regards to the underling cortical microstructure could provide greater insight into the association between microstructural properties of the auditory cortex,the morphology of ASSRs and individual differences thereof.

Adopting a developmental perspective might also provide some clues as to the potential significance of inter-individual differences in ASSRs and their relation to the underlying neuroanatomy. Significantly, akin to other types of gamma oscillations, the ASSR is known to undergo profound changes during childhood and adolescence. Such changes have been suggested to reflect the maturation of neural circuits in the cortex (Uhlhaas et al.,2009; Uhlhaas & Singer, 2010). Of note, similar to gamma oscillations, the cortical myeloarchitecture also undergoes profound changes during childhood and adolescence (Glasser & Van Essen, 2011; Lebenberg et al., 2019; Grydeland et al., 2019). Furthermore, the timing of these changes coincides with the aforementioned development of oscillatory processes and transitions in cognitive development.

Significantly, converging lines of evidence have pointed to individual variability in the cortical myeloarchitecture as being of potential importance in understanding variability in neural responses such as the gamma ASSR. For example, building upon the close association between the cyto and myeloarchitecture of the cortex, previous studies have shown evidence of a positive association between the amplitude of MEG responses derived from the auditory cortex and cortical myelination (R1). In Chapter 3 of this thesis, we also observed an association between visual gamma activity at approximately 40 Hz and myelination of the primary visual cortex. Furthermore, a growing body of evidence suggests that the cortical myeloarchitecture is likely adaptively influenced to support oscillations (Hunt et al., 2016). Finally, whilst the role of white matter myelination in aiding neural synchronisation has been widely discussed, it is possible that cortical myelination might also have a role to play in facilitating neural synchrony at a more local level (Grydeland, Westlye, Walhovd & Fjell, 2015).

Significantly, altered ASSR responses, abnormalities in their purported neural generators (pyramidal cells and inhibitory interneurons whose axons are known to be myelinated) and aberrant myelination have all been implicated in a wide range of clinical disorders. Consequently, an investigation of the relationship between cortical myelin and ASSRs has

the potential to provide novel mechanistic insights into these neural responses that might ultimately be of great clinical significance.

Hence, the current study employed high resolution MRI to explore the relationship between the cortical microstructure, particularly its myelin content, and the peak amplitude and ITPC of gamma band ASSRs derived using a linearly increasing auditory chirp stimulus. It was hypothesised that a positive correlation might exist between the amplitude of gamma band ASSRs and myelination of the auditory cortex. Furthermore, the phase-based ITPC metric was used in order to test the specific hypothesis that cortical myelination might influence the synchrony of neural activity occurring in more local neural networks. Finally, given the use of a chirp stimulus we were also able to conduct an exploratory analysis of the relationship between the peak gamma frequency of the ASSR and cortical myelin. Similar to the previous chapters of this thesis, we also exploited the high resolution of our MRI datasets in order to explore the depth specificity of these potential relationships.

5.3 Methods

Participants

38 healthy participants took part in this study. All participants were aged between 18-30 years. They had normal hearing and no history of psychological or neurological disorders. Ethical approval was obtained from the Cardiff University School of Psychology Ethics Committee and all participants provided written informed consent prior to their participation.

MRI Data Collection

The MRI data and processing outlined here is the same as that included in Chapter 3 of this thesis. However, for the purpose of clarity the methodology employed will be outlined again below.

Quantitative T1 maps and T1-weighted images were acquired for each participant ona 7T MR system (Magnetom, Siemens healthcare) at submillimetre resolution using the MP2RAGE sequence (MP2RAGE acquisition parameters: TR =6s, TD1/TD2= 0.8/2.7s, α1/α2=7/5 degrees, TRGRE=6.4 ms, iPAT=3 and 6/8 partial). Fourier sampling was used in the phase encoding direction and 6/8 partial Fourier inthe slice encoding direction. Resolution = 0.65mm isotropic. TA = 10 min 44s. A tailored adiabatic inversion pulse was also used for inversion (Hurley et al. 2010). This sequence outputs 4 different imaging volumes (1st inversion image INV1, second inversion image INV2, a T1-weighted image (UNI image) and finally a quantitative T1 MAP). Given that the T1 maps derived from the MP2RAGE sequence can show some residual sensitivity to inhomogeneities in the B_1^+ field, the B_1^+ field was also measured separately using the SA2RAGE sequence (SA2RAGE acquisition parameters: TR = 2.4s,TD1/TD2 = 0.042/1.8 s, α1/α2 = 4/11 degrees, TRGRE= 2.1 ms, iPAT= 2 and 6/8 partial Fourier sampling was used in the phase encoding direction and 6/8 partial Fourier in the slice encoding direction. Resolution = 2x2x2.5mm.TA = 2 min 16s).

Calculation of R1maps and B_1^+ correction procedure

The SA2RAGE derived maps of the B_1^+ field were used to correct the T1 maps produced by the MP2RAGE sequence for residual transmit field biases, in order to produce bias free high resolution T1 maps. Each participant's SA2RAGE derived B_1^+ map was first registered and interpolated to the same resolution as the MP2RAGE volumes using FSL's FLIRT registration algorithm. Subsequently, these registered and interpolated B_1^+ maps were used to correct the high resolution MP2RAGE Uniform images and T1 maps for residual RF transmit field biases using the methodology outlined in Marques & Gruetter (2013).

Following this correction procedure each participant's corrected T1 map was converted to an R1 map (R1=1/T1) for ease of interpretation given the hypothesised positive correlation between R1 and myelin.

MRI Pre-processing and Analysis

In order to improve segmentation outcomes a number of pre-processing steps, including a selection of those recommend by Haast et al. (2018), were performed on the different volumes produced by the MP2RAGE sequence (e.g. INV2, UNI). In brief, each participant's second inversion volume (INV2) was first bias corrected using the N4 algorithm. This volume was subsequently skull stripped using FSL's BET routine in order to produce a brain mask. Finally, the CBS tools software package was also used to remove additional non-brain tissue (arteries and dura) from the corrected T1-weighted image (UNI image). A common issue encountered during the processing of these images is the misclassification of CSF as grey matter in some brain regions. Thus, a CSF mask was also created using the first inversion image (INV1) and applied to the corrected T1-weighted image.

Each participant's pre-processed B_1^+ corrected T1-weighted image was then processed at native 0.65 mm resolution using the Freesurfer 7 'recon all' pipeline in order to construct a representation of the cortical surface. The resultant surfaces were visually inspected for quality control purposes and manual corrections were performed where necessary. Following quality assessment of participants' MRI scans and Freesurfer surfaces 3 scans were found to be unusable and were excluded from the ensuing analysis. Thus only 35 datasets were available for comparison with our MEG datasets.

Following Freesurfer processing, participants' individual quantitative R1 maps were then mapped onto the cortical surfaces. Initially, each subject's quantitative R1 map was sampled on their cortical surface using the Freesurfer mri_vol2surf function by averaging between 20-80% of the cortical depth to reduce the risk of partial voluming.

Cortical depth analysis - A cortical depth analysis was also performed by projecting the R1 maps onto the cortical surface using an equi-volume layering approach (Waehnert, et al., 2014). This involved the creation of 11 different surfaces. R1 values were then systematically sampled along these surfaces. Again, to reduce the risk of partial voluming only 7 of these surfaces were included in the subsequent analyses (the 2 surfaces closest to the pial and white matter surfaces were excluded from the subsequent analysis). Thus, we chose to only use equi-volume surfaces at the following fractional cortical depths

(projecting from the pial surface):0.2, 0.3, 0.4, 0.5, 0.6, 0.7, 0.8. Accordingly, estimates of myelin content at 7 cortical depths were derived. In the remainder of this chapter the following naming convention will be used to refer to the different cortical depths investigated depths: 1, 2, 3, 4, 5 ,6, 7. Here depth 1 is closest to the pial surface whereas depth 7 is the closest to the GM/WM border.

Myelination of primary auditory cortex

In order to examine myelination of the primary auditory cortex, we chose to define our region of interest using the right transverse temporal label from the Desikan- Killiany Atlas (Desikan et al., 2006) included in Freesurfer. This choice was guided by the fact that the transverse temporal gyrus, also known as Heschl's gyrus, is known to contain the primary auditory cortex (Brodmann areas 41 and 42) (Johns, 2014). For each participant we first extracted the mean R1 value (sampling at 20-80 % of the cortical depth, from the white matter surface) in the transverse temporal label to give an estimate of the myelin in the primary auditory cortex. Depth specific myelin estimates for the transverse temporal cortex were then derived by repeating this process for each of the 7 equi-volume surfaces. In this way we were able to obtain mean R1 values for the transverse temporal region of interest at each of the 7 cortical depths investigated in this study.

MEG Data and Processing

Auditory Click Chirp Experiment Design

The auditory stimulation paradigm utilised in this investigation was developed and tested by Brealy (2015) and was based on the stimulus paradigm outlined in Artieda et al. (2004). The stimuli consisted of a series of 1 millisecond long clicking sounds, known as chirps, that either increased linearly in frequency from 1-120 Hz (325 trials) or decreased in frequency from 120-1 Hz (25 trials). Each chirp sound lasted for 1.62 seconds and was followed by a baseline period of 0.5 seconds. These auditory stimuli were delivered binaurally through insert earphones and were presented at approximately 92 dbSPL (this sound level was calibrated in the MEG lab using a KEMAR mannequin microphone).

Participants were directed to passively listen to these auditory stimuli during the experiment. However, in order to maintain attention, participants were asked to count the number of descending chirps they heard. In total the paradigm consisted of 325 trials, however only the ascending chirps were utilised in the subsequent analysis. The experimental duration was approximately 12 minutes.

MEG Data Acquisition

Whole head MEG recordings were acquired using a 275-channel CTF axial gradiometer system housed in a magnetically shielded room. Participants were seated in an upright position during the recording sessions. Prior to the MEG recording, participants were fitted with three electromagnetic head coils located at a fixed distance from the nasion and the two pre-auricular points. The location of these markers was verified afterwards using high resolution digital photographs.

Due to a technical fault with the equipment used to deliver the auditory stimuli, data collection was unsuccessful for 3 subjects. Thus only 32 subjects were included in the MEG analysis (2 participants were also removed following QA of their MRI datasets and an MRI dataset was not available for one participant).

MEG pre-processing

Data were epoched from -0.2 s before stimulus onset to 1.9 seconds after the onset of the stimulus. The individual trials were then visually inspected for the presence of gross artefacts such as muscle movements and head motion. Trials found to be affected by such artefacts were excluded from the subsequent analysis.

Further pre-processing was performed using the Brainstorm Software (Tadel et al., 2011). As outlined in Chapter 2 of this thesis, we chose to use a minimum norm implementation within Brainstorm for this analysis, rather than a beamformer, as minimum norm methods do not suffer from the same limitations regarding the presence of correlated sources. Participants' raw data was first imported into the Brainstorm database and again epoched from -0.2 s before stimulus onset to 1.9 seconds after the onset of the stimulus. For each subject's data a number of processing steps were then applied. More specifically, the noise covariance matrix was calculated based on the baseline period and the trials were also averaged in order to produce an average response for each subject.

Each participant's T1-weighted image (MPRAGE UNI), with background noise removed (using a regularisation function), was downsampled to 1mm isotropic resolution and subsequently processed using the Freesurfer recon-all pipeline. The decision was made to downsample the data for this part of the analysis because the pre-processing steps utilised in our high-resolution MRI processing pipeline created challenges when using the resultant Freesurfer output in Brainstorm. For example, we performed skull stripping prior to Freesurfer processing for our high-resolution data as this produced more favourable results. However, this presents a substantial problem when trying to co-register the MEG and MRI data in Brainstorm based on the fiducial locations - given that the skull has been removed and so key anatomical landmarks that would usually be utilised to guide the placement of these locations are no longer available.

Following Freesurfer processing of the downsampled MRI data, the resulting Freesurfer anatomy folders, which included the cortical surfaces, were subsequentlyloaded into Brainstorm. However, the data from one subject was excluded due to poor reconstruction of the cortical surface, leaving a final sample size of 31 participants.

Co-registration of the MEG and MRI data was then performed by marking the points on the MR image corresponding to the position of the three fiducial coils (nasion, right ear, left ear). Brainstorm also requires the inclusion of three additional reference points in order to ensure that all subjects are aligned the same way. These three points are the anterior commissure, posterior commissure and the interhemispheric point. These locations were again marked on each subject's individual MRI.

The co-registered MRIs were then segmented into the following tissue types: brain, skull and scalp. Head models were the then constructed for each participant using the overlapping spheres method (Huang et al.,1999). This head model was chosen as it is the default option for MEG data in the Brainstorm software.

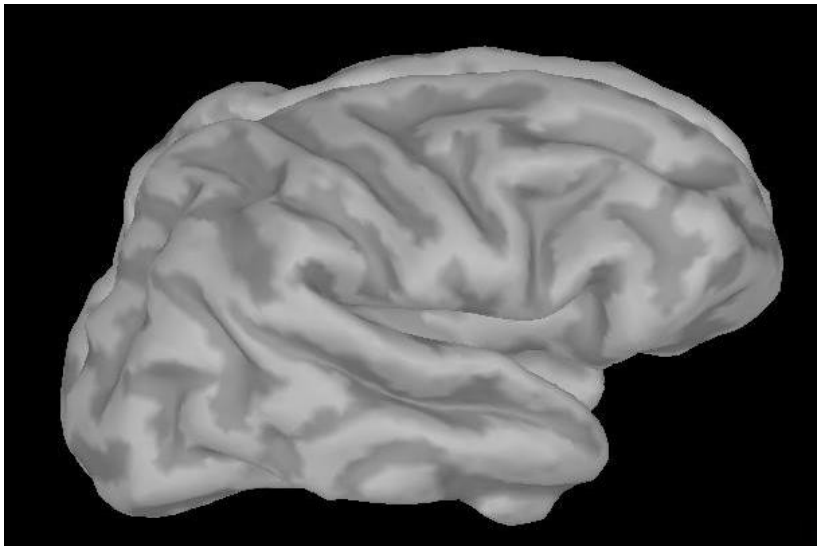

Figure 5.1: *Cortical surface representation derived using Freesurfer and displayed in Brainstorm.*

Source localisation was then performed using minimum-norm source reconstruction. More specifically, we employed the weighted minimum-norm estimation of the amplitude of distributed sources, as implemented in the Brainstorm software, using default settings. This method produces a depth-weighted linear L2-minimum norm estimate of current density. The amplitude of these current density maps is given in units of picoampere-meter (pA-m) which is the naming convention used by the Brainstorm software.

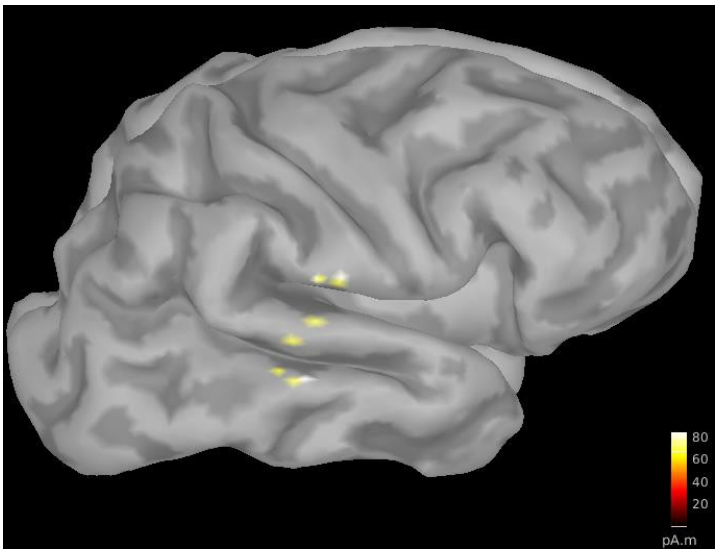

Figure 5.2: *Cortical surface representation displayed in Brainstorm with the minimum norm reconstruction overlaid.*

Regions of interest corresponding to the auditory cortex were then created using the Freesurfer defined right transverse temporal label. The terminology used for these regions of interest in the Brainstorm software is ‘scouts’. The time series for this scout region was

then extracted by finding, for each time point, the absolute maximum value across all the vertices in the transverse temporal label. Each participant's 'scout' time series was then imported into Matlab for further analysis using Fieldtrip.

Although our stimuli were delivered bilaterally, we chose to focus on the ASSR in the right hemisphere given that previous investigations have shown that the majority of participants show the strongest ASSR response in the right auditory cortex (Ross et al., 2005; Oda et al., 2012; Brealy 2015).

The scout time series were first converted into Fieldtrip virtual sensor format for further processing. We then conduced a time frequency analysis on these virtual sensor data. More specifically, a wavelet analysis was conducted using a DPSS taper and 8 Hz smoothing. We also baseline corrected this time frequency data by calculating the percentage change between the baseline and stimulation periods.

For each participant, the maximum response in the 0.35 to 0.75s time window was then calculated. This time frame corresponds to the presentation of frequencies in the gamma band (30-50 Hz). This range of frequencies was chosen as the majority of participants showed a peak response within this range. In this way we were able to derive the peak amplitude and frequency of participants' ASSRs within this frequency range.
Inspection of participants' time frequency plots revealed that the majority of participants did not show a further peak response in the higher gamma range (i.e. 70-100 Hz). Hence, we chose not to explore the responses in the higher gamma band.

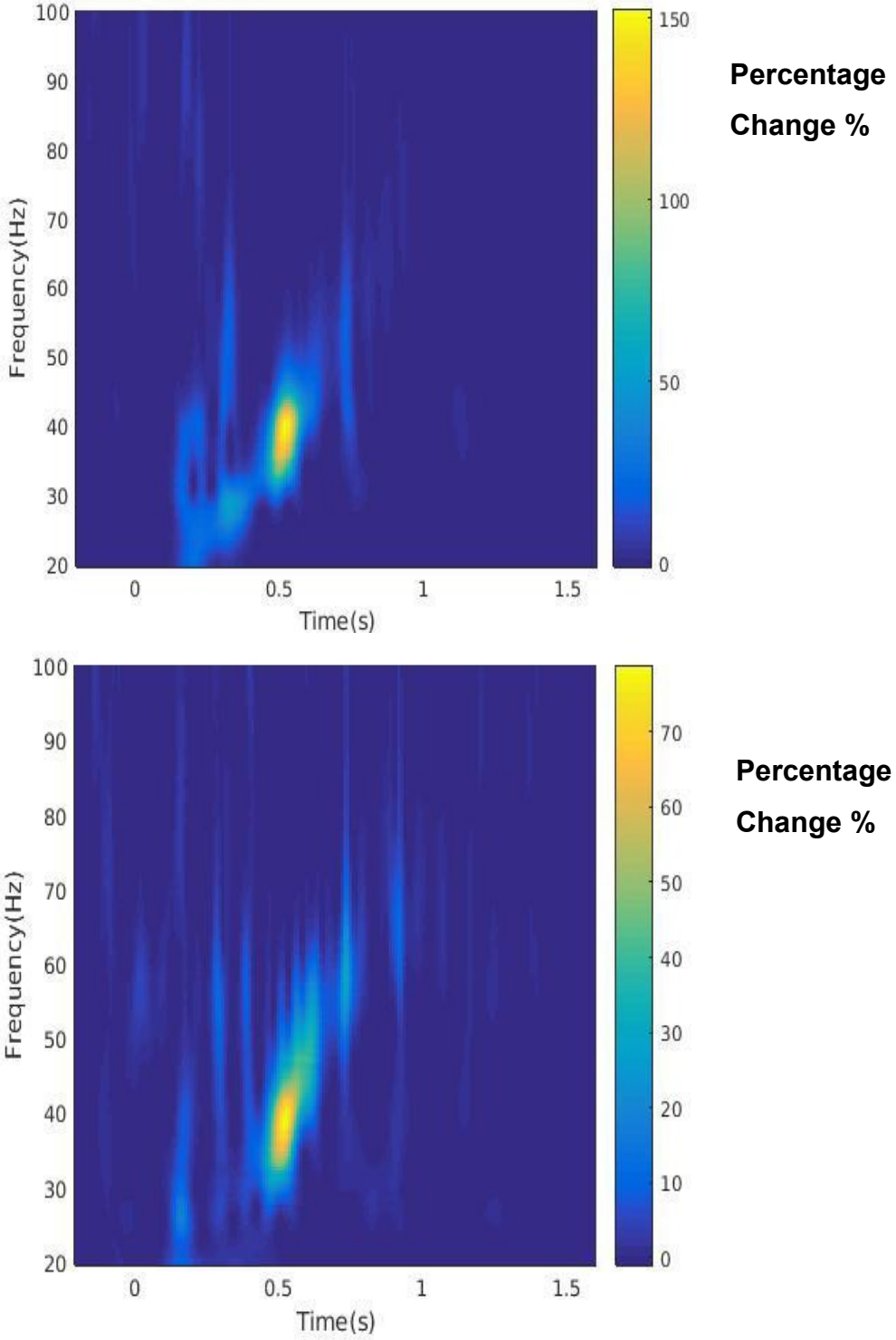

Figure 5.3: *Time-frequency representations of the amplitude of the ASSR responses (calculated as the percentage change from baseline) derived using the auditory chirpstimulus from two representative subjects.*

ITC Analysis

A further ITC analysis was also conducted. The procedure for this analysis broadly followed that of the previous amplitude base analysis. However, the key difference is that, in this instance, the trials were not averaged in order to allow for the investigation of inter-trial coherence. The same head model was used in this analysis and source localisation was performed using the minimum norm procedure outlined above. Following source localisation, for each participant, the scout time series were once again extracted for the transverse temporal label and imported into Matlab.

The imported data were converted into a Fieldtrip style format and a frequency decomposition of the data performed in Fieldtrip using a wavelet analysis in order to derive the Fourier spectrum. A new Fieldtrip style data structure was then made using the information from this frequency decomposition. The inter-trial phase coherence (ITPC) was then calculated as defined in the EEGLAB toolbox (Delorme & Making, 2004). Following the calculation of the ITPC values, for each participant,we once again extracted the maximum response in the 0.35 to 0.75s time window corresponding to the low gamma band (30-50 Hz).

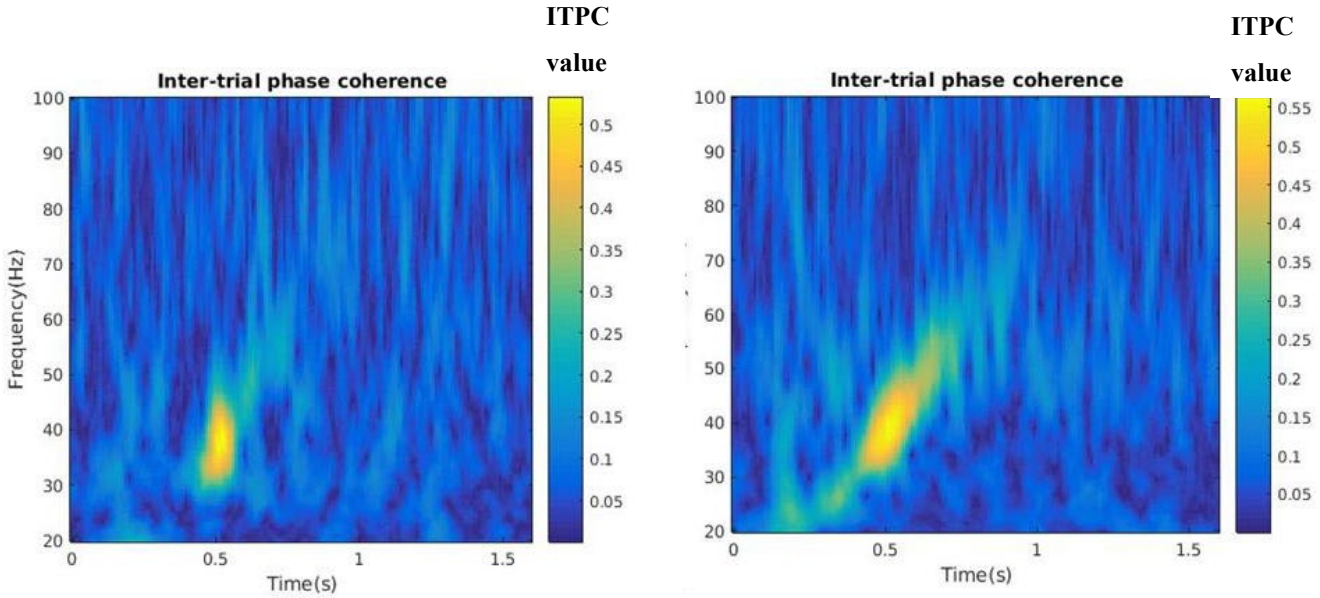

Figure 5.4: *Time-frequency representations of the ITPC of the ASSR (calculated as the percentage change from baseline) derived using the auditory chirp stimulus from two representative subjects.*

Multimodal Analysis

Once each participant's peak amplitude and ITPC values had been determined, a multimodal analysis was conducted in order to investigate the relationship between these measures and cortical myelination (R1).

R1 and Gamma ASSR Amplitude

Inspection of participants' time-frequency plots was conducted for quality control purposes. From this examination it was evident that a clear response to the chirp stimulus, in the low gamma range, was not evident for all subjects. Thus, we chose to exclude the data from 7 subjects, who did not show a gamma response to the stimulus, from the subsequent statistical analysis.

A correlation analysis was first conducted between participants' R1 values sampled at 20-80% of the cortical depth and the peak gamma amplitude estimates. Given the non-normal distribution of the data (Shapiro-Wilk Test sig. = < 0.05) Spearman's correlation coefficient was used in this instance.

On the basis of the aforementioned close relationship between the cyto and myeloarchitecture of the cortex, it was hypothesised that a positive relationship might therefore exist between cortical myelin, indexed by R1 and the amplitude ofthe gamma ASSR.

An exploratory analysis was also conducted to investigate the relationship between depth-specific R1 estimates and the amplitude of the gamma ASSR. This was achieved by calculating the Spearman correlation coefficient between participants'peak ASSR responses and R1 values sampled at each of the 7 cortical depths investigated in this study.

R1 and Gamma ASSR Peak frequency

A further exploratory analysis was also conducted to investigate the relationship between R1 estimates and the peak frequency of the gamma ASSR. This was achieved by calculating the Spearman correlation coefficient between participant's peak ASSR

responses and R1 values averaged over 20-80% of the cortical depth, in addition to those sampled at each of the 7 cortical depths investigated in this study.

R1 and ITPC

Again, inspection of participants' ITPC data, plotted in the format of a regular time-frequency representation, revealed that a clear gamma band response to the chirp stimulus was not evident in all subjects. Thus, for quality control purposes we chose to exclude the data from 5 subjects (for whom a response in the gamma range was not discernible) from the subsequent correlation analysis. A Further correlation analysis was then conducted between participants' R1 valuessampled at 20-80% of the cortical depth and their peak ITPC values for the low gamma band (30-50 Hz). Again, the data was found to be non-normally distributed (Shapiro-Wilk Test sig. = < 0.05) and thus Spearman's correlation coefficient was used in this instance.

Akin to the amplitude analysis, a further exploratory analysis was also conducted to investigate the relationship between depth-specific R1 estimates and participants' peak ITPC responses in the low gamma range. In order to do so the Spearman correlation coefficient between participants' peak ASSR responses and R1 values sampled at each of the 7 cortical depths investigated in this study was calculated.

5.4 Results

R1 and Gamma ASSR Amplitude

The results of the correlation analysis revealed evidence of a positive correlation between the amplitude of the ASSR and R1 values sampled at 20-80% of the cortical depth ($r=0.330$, $p=0.057$). However, this relationship did not meet the threshold for statistical significance. As detailed in Table 5.1, non-significant positive correlations were also observed between depths 1-4, representing the superficial and mid cortical depths and the amplitude of the ASSR.

Cortical Depth	R-val	P-val
20-80	0.330	0.057
1	0.201	0.173
2	0.157	0.231
3	0.169	0.215
4	0.289	0.086
5	0.363	0.041
6	0.423	0.020
7	0.393	0.029

Table 5.1: *Table showing the correlations (R-values) and corresponding p-*values for *the relationship between amplitude of the ASSR in the 30-50 Hz range and R1 values in primary auditory cortex at each cortical depth.*

Significant positive correlations between depth specific R1 values and the amplitude of participants' ASSR responses were however observed in the case of depth 6 (r=0.363, p=0.41), depth 7 (r=0.423, p=0.20) (see Figure 5.5) and depth 8 (r=0.393, p=0.29), when considering an alpha level of p=0.05. Note that these relationships do not survive multiple comparisons correction (0.05/8 =0.006).

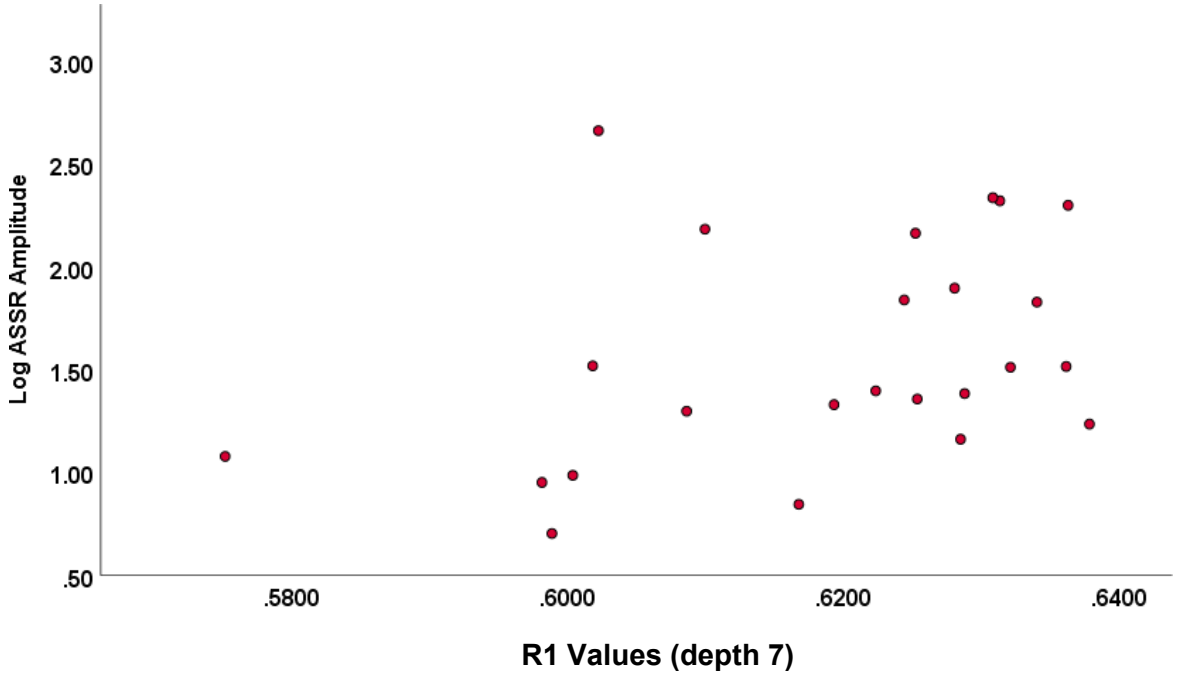

Figure 5.5: *Scatter plot of the relationship between gamma ASSR amplitude and R1 values sampled at depth 7. Note the log amplitude is plotted here for display purposes.*

R1 and Gamma ASSR Peak Frequency

Non-significant positive correlations were found between the peak frequency of the gamma ASSR and R1 values at all cortical depths. Though weak in the majority of cases, as outlined in Table 5.2, stronger correlations were observed between peak frequency and R1 values sampled at superficial cortical depths compared to those sampled deeper in the cortex (e.g. see Figure 5.6).

Cortical Depth	R-val	P-val
20-80	0.014	0.948
1	0.185	0.386
2	0.229	0.282
3	0.116	0.591
4	0.021	0.921
5	0.012	0.956
6	0.029	0.894
7	0.060	0.782

Table 5.2: *Table showing the correlations (R-values) and corresponding p-values for the relationship between peak frequency of the ASSR in the 30-50 Hz range* and R1 *values in primary auditory cortex at each cortical depth.*

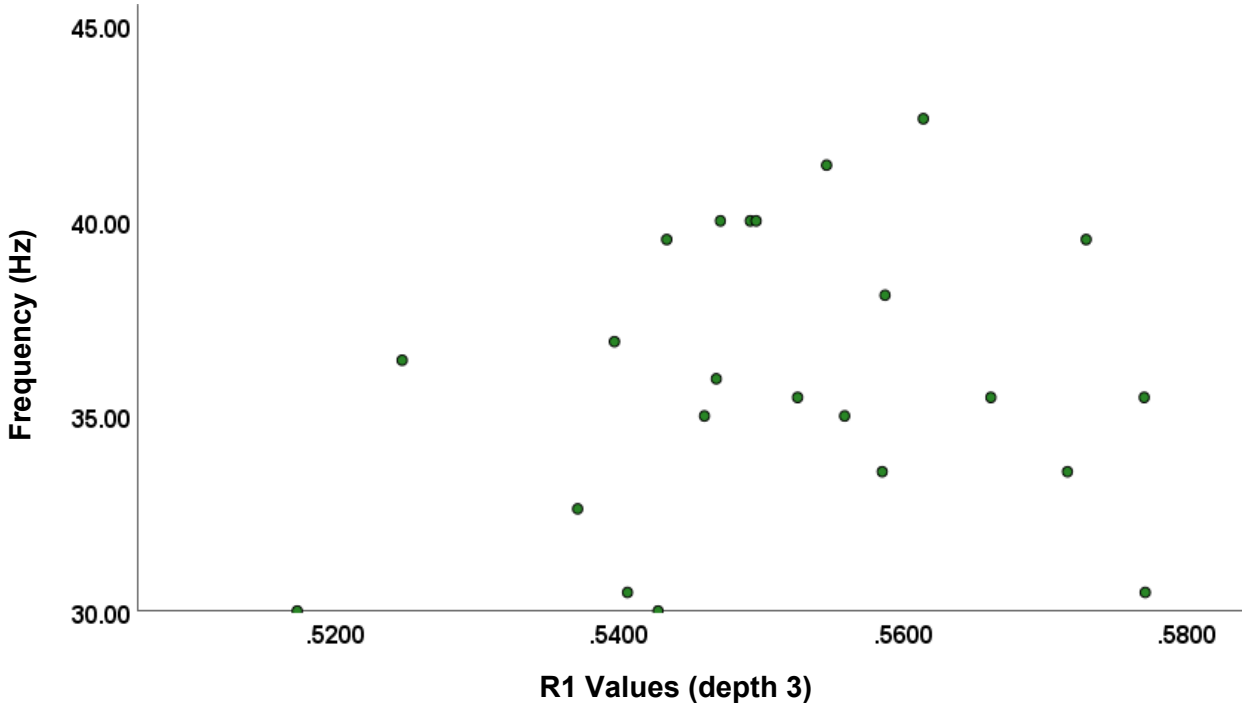

Figure 5.6: *Scatter plot of the relationship between gamma ASSR peak frequency and R1values sampled at depth 3.*

R1 and ITPC

A weak, non-significant, negative correlation was observed between participants' peak ITPC values and R1 values sampled at 20-80% of the cortical depth (r=-0.125, p=0.272). Non-significant negative correlations were also observed between the depth specific R1 estimates and the ITPC values (see Table 5.3). The strongest correlation was found between R1 values sampled at depth 4 (approximate to mid cortical depth) and participants' ITPC values (r=-0.210, p=0.152)(see Figure 5.7), though as aforementioned this relationship was relatively weak and consequently did not meet the threshold for statistical significance.

Cortical Depth	R-val	P-val
20-80	-0.125	0.272
1	-0.064	0.378
2	-0.120	0.280
3	-0.210	0.152
4	-0.166	0.209
5	-0.134	0.258
6	-0.153	0.228
7	-0.177	0.193

Table 5.3: *Table showing the correlations (R-values) and corresponding p-valuesfor the relationship between participants peak ITPC values in the 30-50 Hz range and R1 values in primary auditory cortex at each cortical depth.*

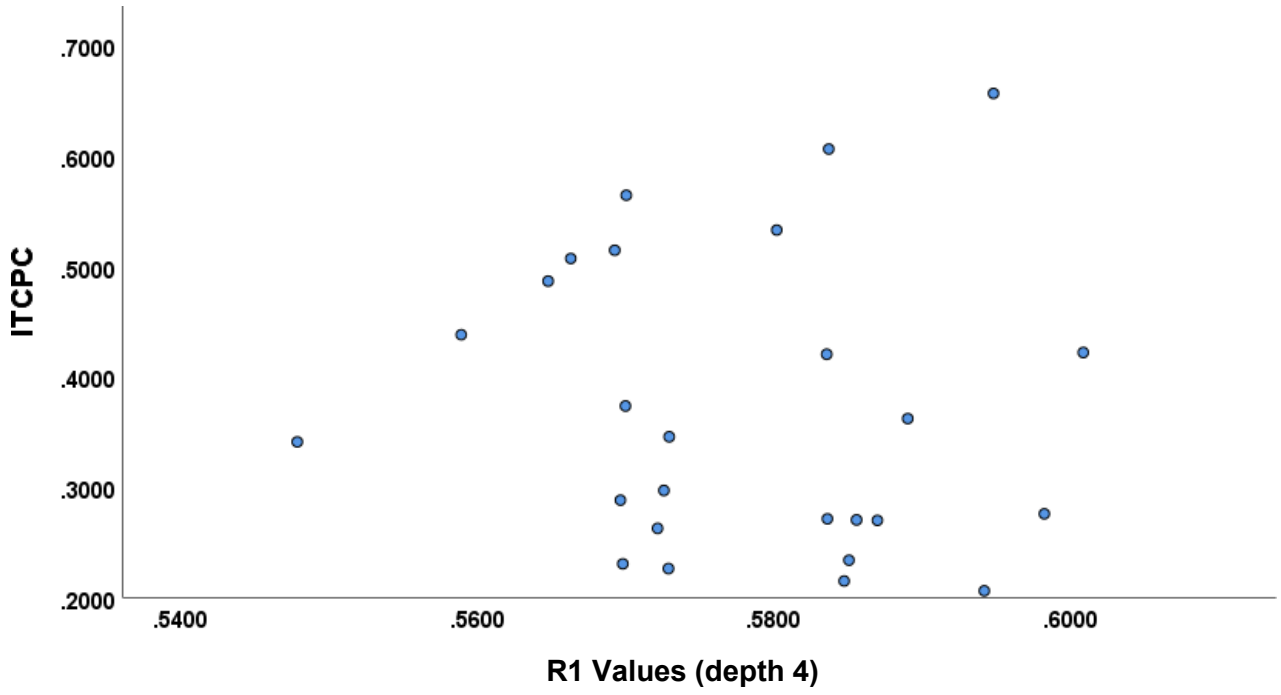

Figure 5.7: *Scatter plot of the relationship between gamma ASSR ITPC and R1* values sampled *at depth 4.*

5.4 Discussion

This study investigated the relationship between gamma frequency ASSRs and myelination of the primary auditory cortex using an auditory click-chirp stimulus. A key strength of the auditory paradigm employed in the present study is its ability to probe the cortical response to a broad range of frequencies. However, in line with previous investigations, we found that the majority of participants produced a maximal ASSR in the 30-50 Hz (low gamma) range.

Interestingly, our multimodal analysis identified a trend towards a positive correlation between the peak amplitude of participants' ASSRs in the low gamma range (30-50 Hz) and myelination of the primary auditory cortex. Furthermore, there also appeared to be an element of depth-specificity to this relationship, given that the strongest correlations were found with R1 values sampled deeper in the cortex. However, further exploration of the trends observed in the present dataset, in a larger sample of subjects, would likely be of benefit in order to accurately probe their validity and repeatability.

That said, the relationships observed in the current dataset are nevertheless intriguing. Of particular interest, is that they can be seen to provide some evidence insupport of our hypothesis of a positive correlation between cortical myelin and amplitude of gamma band ASSRs. Furthermore, the results of the present study are also in-line with that of a previous multi-modal MEG and MRI investigation by Helbling et al. (2015), that provided a source of inspiration for the current work. The authors of this earlier study also employed an auditory paradigm and found evidence of a positive correlation between MEG dipole strength and R1 in relevant auditory cortical regions.

However, somewhat unexpected, was the finding that the strongest relationships were observed between the amplitude of gamma ASSRs, and myelin sampled at lower cortical depths. Gamma band activity is typically thought to arise from the coordinated interaction of inhibitory interneurons and excitatory pyramidal cells in the superficial layers of the cortex (layers 2 and 3). Thus, it was expected that stronger relationships might therefore be found between our myelin values sampled superficially in the cortex and participants' peak gamma ASSRs. However, it is interesting to note that low and high frequency gamma oscillations have been argued to differ with regards to their layer specificity.

Indeed, a study by Oke et al. (2010), that explored gamma oscillatory dynamics, albeit in the visual cortex of rats, found that although high frequency gamma oscillations (>70 Hz) were generated in the superficial layers of the cortex (layer 3), lower frequency gamma oscillations actually occurred in the deeper layers of the cortex (layer 5) in this rat model. While speculative, this distinction between the layer specific origins of different types of gamma activity might be seen to provide one potential explanation for the pattern of results observed in the present study.

Interestingly, thalamocortical pathways have also been hypothesised to be involved in the generation of 40 Hz ASSR activity Ribary et al. (1991). Thalamocortical fibres, originating from the thalamus, are known to terminate in layers 4 and 6 of the primary auditory cortex Lee et al. (2013). These thalamic projections innervating the auditory cortex are also known to be myelinated. Significantly, there is evidence from animal models to suggest that demyelination of these fibres has a significant impact on the function of neural activity in the thalamocortical system, most notably in thalamo-recipient layer 4 (Ghaffarian et al., 2016). Furthermore, cortical synaptic transmission in layer 3 of the auditory cortex was also found to be affected by the process of demyelination. Of particular relevance to the present study is that demyelination of these pathways also reduced the amplitude of excitatory postsynaptic potentials recorded from the auditory cortex (Ghaffarian et al., 2016).

Thus, it might also be tempting to speculate that the relationship between cortical myelin sampled at lower cortical depths and the amplitude of the ASSR observed in the present study might have been driven, at least in part, by individual differences in the myelination of thalamocortical projections. However, as noted previously, further work is needed in order to establish the validity of the trends observed in the present study before a stronger interpretation of the findings presented here can be considered.

In this investigation an exploratory analysis was also conducted to examine the relationship between the peak frequency of participants' ASSRs in the low gamma band and cortical myelination. No significant relationships were observed between these variables. The predominant direction of this relationship was also negative. This is a somewhat surprising finding given the positive relationship observed with amplitude. However, this discrepancy is likely explained by the fact that in a small number of cases some participants displaying an ITPC response in the low gamma range did not show a

clear response in the amplitude analysis and vice versa. Thus, there was a slight discrepancy in the subjects included in these respective analyses. The point speaks to the well-documented challenges associated with correlational methods, particularly in the case of relatively small sample sizes such as that employed here. Hence these results should be interpreted with caution.

That said, of potential interest is that, in direct contrast to the results of our amplitude analysis, the relationship between peak gamma frequency and R1 appeared to be strongest at more superficial cortical depths. Significantly, previous studies utilising neurophysiological modelling of gamma oscillations in the visual cortex have shown that the primary determinants of the gamma response properties, such as peak frequency, relate to the connections between pyramidal cells and inhibitory interneurons in the superficial layers of the cortex (Shaw et al., 2017).

The final analysis presented in this chapter investigated the relationship between the ITPC of participants' peak ASSRs in the low gamma band and cortical myelination. Notably, no significant relationships were found between participants' ITPC values and R1 values sampled at any of the cortical depths investigated in this study. A key feature of the ITPC measure is that it is amplitude independent and is thus arguably less susceptible to noise compared to amplitude-based approaches (McFadden et al.,2014). It has also been shown to be a more reliable measure of the ASSR between sessions than spectral measures such as evoked power (McFadden et al., 2014; Tan, Gross, & Uhlhaas, 2015). Consequently, it could be argued that the ITPC measure is a more robust measure of ASSRs than our amplitude-based measure, which was calculated as the percentage change in spectral power from baseline.

However, it should be noted that a number of caveats exist with regards to the application and interpretation of the ITPC metric. For example, utilising simulations,van Diepen & Mazaheri (2018) showed that ITPC values are in fact susceptible to the influence of a number of undesirable factors including oscillatory power and both the amplitude and latency of evoked responses. Their study revealed that oscillations with larger amplitudes have higher SNR. This in turn allows for more accurate phase estimations, less variability, and consequently higher estimates of ITPC values. As argued by Van Diepen & Mazaheri (2018), caution should therefore be taken when interpreting differences in ITPC values in the presence of differences in oscillatory power (Muthukumaraswamy & Singh, 2011).

Given that there was evidence of considerable inter-individual variability in the amplitude of participants' oscillatory responses in the present study, it is possible that this may have influenced the ITPC values observed to some extent.

There are a number of other limitations associated with this study that might also have acted to diminish our ability to accurately detect a significant relationship between the amplitude and ITPC of gamma band ASSRs and cortical myelination. For example, we chose to delineate the primary auditory cortex using the transverse temporal label from the Freesurfer Desikan-Killiany atlas (Desikan et al., 2006). Accordingly, it is important to note that the precise delineation of the auditory cortex in individual subjects remains both challenging and controversial (De Martino et al., 2015).

A key source of this difficulty is the fact that the position of the primary auditory cortex relative to key anatomical landmarks, such as the cortical gyri and sulci, has been shown to vary across subjects (De Martino et al., 2015). Furthermore, the anatomy of Heschl's gyrus, also known as the transverse temporal gyrus, which includes the primary auditory cortex, varies considerably across both individuals and hemispheres (Marie et al., 2015). These differences are evident in terms of both the size and morphological aspects of this structure, such as its gyrification patterns (Marie et al., 2015). In sum, unlike in other regions of the brain, such as the visual cortex, the borders of the primary auditory cortex cannot be defined solely using anatomical methods (Dick et al., 2012). Similarly, efforts to produce a functional delineation of the primary auditory cortex, for example by using fMRI to obtain tonotopic maps, has also thus far proven fraught with challenges (De Martino et al., 2015). Hence, ex-vivo post-mortem analysis of the cyto and myeloarchitecue of the brain remains the most anatomically precise method of determining the location of primary auditory cortex in a specific individual (De Martino et al., 2015).

That said, high resolution MRI of cortical myelin content, in combination with functional methods, is beginning to show great promise with regards to accurately establishing the precise boundaries of cortical areas in-vivo (Sereno et al., 2013; Dick et al., 2012). Thus, it may be of benefit, for future studies, to explore the possibility using information from the cortical myeloarchitecture, obtained using high resolution MRI in combination with an fMRI-based functional localiser sequence, in order to define the precise location of the primary auditory cortex on an individual subject basis. The feasibility of such an approach

has already been demonstrated. For example, De Martino et al. (2015) utilised high-resolution myelin sensitive MRI contrast maps to derive depth-dependent anatomical profile contrasts. Using this methodology, they were able to identify a highly myelinated region in Heschl's gyrus. Significantly, functional data derived using fMRI showed that this highly myelinated region possessed functions typically associated with the primary auditory cortex, such as narrow frequency tuning. Thus, in sum, this combination of high-resolution MRI and functional imaging provided compelling evidence that such an approach can be used to identifying the region homologous to the primary auditory cortex in vivo.

Of note, a second, weaker peak ASSR response in the high gamma range (70-100 Hz), has also been documented in previous investigations (Artieda et al., 2004, Hamm et al., 2011; Alegre et al., 2017). However, a clear response in this frequency range was not observed in the present study. One potential explanation for this is that due to experimental time constraints, it was necessary to use a smaller number of trials than previous investigations, thus decreasing the available SNR of our data. For example, a prior investigation by (Artieda et al., 2004), on which the chirp stimulus utilised in the present study was based, recorded a minimum of 500 trials per participant, whereas only 300 trials were available for analysis in the present study. Thus, it is possible that increasing the number of experimental trials might have allowed for the observation of the higher gamma frequency ASSR in the present study. Nevertheless, there is evidence to suggest that the high frequency gamma ASSR originates from subcortical sources to which MEG and indeed the minimum norm imaging are less sensitive, given their inherent bias towards superficial sources. Indeed, whilst EEG, MEG and animal studies have all pointed to the auditory cortex as the most likely source of ASSRs occurring below 50 Hz (O'Donnell et al., 2013), those occurring at higher frequencies have been proposed to originate from brainstem areas (Herdman et al., 2002) in addition to other subcortical sources (Farahani, & van Wieringen, 2020). Hence it is possible that our decision to use a minimum-norm approach for source localisation purposes might also have impacted our ability to measure higher frequency gamma ASSR activity.

In conclusion, the present study demonstrated a positive relationship between myelination (R1) of the primary auditory cortex and the amplitude of the gamma ASSR. Furthermore, there appeared to be an element of depth specificity to this relationship, once again highlighting the importance of considering how the microstructure of the cortex varies

across its depth. Although further replication and investigation of these trends is required, the results of the present study can nevertheless be seen to provide potentially interesting insights into the relationship between a key feature of the cortical microstructure, namely its myelin content, and the amplitude of the gamma ASSR. Given the implication of aberrant ASSRs in a variety of clinical disorders, the approach employed in the present study might therefore provide a useful framework for exploring the pathophysiology of clinical conditions such as schizophrenia in which both myelin abnormalities and aberrant oscillatory dynamics have been observed.

Chapter 6

Depth Dependent Relationships between Cortical Myelin and Frequency-Specific Oscillatory Resting-State Networks

6.1 Abstract

Inter-areal communication and the establishment of neural networks is of pivotal importance for brain functioning, yet many questions remain regarding how the structural architecture of the brain supports the formation of these complex channels of communication. Converging lines of evidence now point to myelin as playing a pivotal role in shaping and supporting neural activity and cortical communication. Recent years have witnessed a renewal of interest in examining the cortical myeloarchitecture in-vivo and studies have documented a close association between structural networks indexed by cortical myelin and their MEG derived functional counterparts, suggesting an intricate relationship between the two. However, the cortical myeloarchitecture is also known to vary across the cortical depth. Furthermore, frequency-specific MEG oscillatory networks are thought to arise from different layers of the cortex. Hence, here we utilised high resolution MRI at 7T, in combination with MEG, to explore the relationship between depth specific estimates of intra-cortical myelin and MEG derived functional connectivity estimates. For the first time we were able to show evidence of a cortical depth-dependent relationship between cortical myelin and frequency- specific resting-state MEG networks. These results demonstrate the value of considering how the microstructure of the cortex varies with cortical depth and shed new light on brain structure-function relationships.

6.2 Introduction

Inter-areal communication and network formation is of critical importance for brain functioning. Owing to its rich temporal resolution, MEG represents a valuable tool for investigating the nature of such networks, with numerous MEG studies pointing towards

the pivotal role of neural oscillations in the establishment of brain networks (Brookes, Tewarie & Hunt et al., 2016). The study of oscillatory dynamics, and the networks of communication to which they give rise, thus represents an important avenue of research, with the potential to significantly enhance our understanding of the brain and cognition, in health and disease (Hinkley at al., 2011; Cornew, Roberts, Blaskey & Edgar, 2012; Engels et al., 2017).

To date a number of studies have utilised diffusion MRI methods in order to shed new light on the question of how the structural white matter pathways of the brain might relate to their functional counterparts, such as those derived using fMRI and MEG (Honey et al., 2009; Messaritaki et al., 2020). Less understood is how the microstructure of the cortical grey matter might relate to functional networks in the brain (Hunt et al., 2016). However, a key aspect of the cortical microstructure, namely its myelin content, has received increasing attention in recent years, owing to its ability to be investigated using MRI, opening up a wealth of new opportunities in this regard.

Although most common in the brain's white matter, the cortical grey matter is also myelinated. Furthermore, individual cortical areas demonstrate unique myelin profiles (Nieuwenhuys, 2013), raising the intriguing question of what the functional significance of this might be. In recent years, in line with the aforementioned advances in MRI, cortical myelin has become the subject of increasing attention, with a number of studies having shown the feasibility of using MRI techniques to investigate cortical myelination in vivo. Such studies are already beginning to provide key insights into the brain's myeloarchitecure. For example, in line with classical histological studies, MRI investigations of cortical myelin have consistently demonstrated a pattern of increased myelination of primary sensory areas in comparison to frontal and higher association areas (Waehnert et al., 2016).

To date there has been particular interest in using T1 (or R1) as a marker of cortical myelination (Tardif et al., 2016). In healthy subjects, T1 is thought to principally reflect variations in myelin content (Lutti, Dick, Sereno, & Weiskopf, 2014), with histological investigations concluding that myelin is likely the dominant source of contrast in T1 maps (Stüber et al., 2014). Robust differences in T1, linked to variations in myelin density, have also been demonstrated (Waehnert et al., 2016).

Within the cortex, myelin density is also known to vary across the cortical laminae. For example, myelination is higher in deeper cortical layers compared to those occurring more superficially. Recent studies employing high field MRI have now also demonstrated evidence of depth-specific cortical myelination patterns in vivo (Sprooten et al., 2019). Intriguingly, cortical regions are also known to myelinate at different rates during development (Glasser & Van Essen, 2011; Lebenberg et al., 2019; Grydeland et al., 2019) and these differing developmental trajectories have also been shown to extend to the level of cortical layers. Whitaker et al. (2016) report that the location of the strongest changes in cortical myelination during adolescence corresponded to the boundary between layers V and V1. Similarly, Paquola et al. (2019) report evidence of layer specific microstructural changes during adolescence, with their finding pointing to the preferential accumulation of myelin in mid-to-deeper cortical layers. This finding was particularly evident in heteromodal and unimodal association cortices pointing to a process of fine tuning of hierarchical gradients of cortical networks during adolescence (Paquola et al., 2019).

Significantly, a close relationship also exists between the cytoarchitecture and myeloarchitecture of the brain. For example, Helbling et al (2015) demonstrated that estimates of cortical myelin could be used both refine MEG derived source localisation estimates and predict the magnitude of MEG derived electrophysiological signals. Growing evidence also points to inter-individual differences in cortical myelination as being of functional relevance (Gryndeland etal., 2013, Kim & Knösche, 2016). Furthermore, far from being merely a passive feature of the brain's microstructure, it has been proposed that myelin plays an important role in shaping neural activity and synchrony (Pajevic, 2014). In support of this there is compelling evidence, largely from animal models, of the role of neural activity in shaping myelination (Gibson et al., 2014, Mitew et al. (2018). Building on such evidence a multi-modal MEG/MRI study by Hunt et al. (2016) reported a relationship between the microstructure of the brain and its function at the network level. More specifically, functional networks in the beta and gamma bands significantly predicted the spatial pattern of structural covariance in this study, given that brain areas that were found to be highly functionally connected also exhibited cross-subject covariation in their myeloarchitecture. This raises the intriguing possibility that given the role of myelin in speeding neuronal conduction, cortical myelination might therefore be shaped to support functional networks.

A considerable body of research in monkeys has also suggested that an intricate relationship likely exists between the microstructure of the brain and connectivity

(Huntenberg et al., 2017). For example, long range connections have been preferentially found between brain regions that demonstrate similar microstructural properties. As such it has been suggested that microstructural features of the cortex, such as its myelin content, may also be related to functional connectivity patterns. In line with this suggestion, a multi-modal 7T MRI –fMRI study by Huntenberg et al. (2017) found that regions that exhibit similar myelin content showed higher functional connectivity than regions that differ in their myelin content. This further suggests that the cortical myeloarchitecture might indeed be adapted to support communication between brain regions.

Given that the cortical myeloarchitecture is known to vary not only between brain regions but also across the cortical depth, exploring depth specific relationships between the cortical microstructure and functional connectivity may also be of great benefit. Such depth-specific estimates may have greater sensitivity to inter- individual differences in patterns of cortical myelination as well as inter-regional differences.

The ability to derive depth-dependent estimates of cortical myelin can be seen to be of particular importance when considering the relationship between the cortical myeloarchitecture and oscillatory networks, given that different oscillatory frequencies are thought to arise from specific layers of the cortex. Evidence derived largely from animal models has suggested that synchronisation in the gamma band is strongest in the superficial layers of the cortex, from which feedforward projections typically originate (Buffalo et al., 2011). Such evidence indicates that gamma oscillations may sub-serve feedforward processing in the brain (Michalareas et al., 2016). Conversely, lower frequency oscillations in the alpha and beta ranges have been suggested to originate from deeper layers of the cortex (Buffalo et al., 2011). and are typically implicated in feedback mechanisms (Michalareas et al., 2016). However, evidence of the layer specific origins of these signals in humans remains lacking.

Thus, building on previous findings of a relationship between the cortical myeloarchitecture, functional connectivity patterns and electrophysiology, here, for the first time, we propose to use high resolution quantitative myelin imaging at 7T in combination with MEG to explore the depth-specific relationship between cortical myelin and resting state oscillatory networks. In order to do so we first explored the link between microstructural similarity and connectivity. Akin to Hunt et al., (2016) we derived a structural myelin network using the principles of structural covariance. This is based on the frequent finding that inter-individual differences in structural properties of brain

regions are coordinated within communities of brain regions that fluctuate together in size across the population (Alexander-Bloch, Giedd, & Bullmore, 2013). In a related, complementary approach, we also created R1 difference matrices, similar to Huntenberg et al (2017). These matrices represent the difference in R1 (myelin) between brain regions, allowing us to test whether regions with more similar myelin content display higher functional connectivity. Finally, we also examined the association between MEG connectivity strength and depth dependent cortical myelination.

Thus, here we investigate how both the amount and similarity in myelin content between brain regions relates to cortical connectivity patterns.

6.3 Methods

Participants

38 healthy participants took part in this study. All participants were aged between18-30 and had no history of psychological or neurological disorders. Ethical approval was obtained from the Cardiff University School of Psychology Ethics Committee and all participants provided informed consent prior to their participation.

MRI Data Collection

Quantitative T1 maps and T1-weighted images were acquired for each participant on a 7T MR system (Magnetom, Siemens healthcare) at submillimetre resolution using the MP2RAGE sequence (MP2RAGE acquisition parameters: TR =6s, TD1/TD2=0.8/2.7s, α1/α2=7/5 degrees, TRGRE=6.4 ms, iPAT=3 and 6/8 partial Fourier sampling was used in the phase encoding direction and 6/8 partial Fourier in the slice encoding direction. Resolution = 0.65mm isotropic. TA = 10 min 44s. Atailored adiabatic inversion pulse was also used for inversion (Hurley et al. 2010). This sequence outputs 4 different imaging volumes (first inversion image INV1, second inversion image INV2, a T1-weighted image (UNI image) and finally a quantitativeT1 map). T1 maps derived from the MP2RAGE sequence can show some residual sensitivity to inhomogenities in the B_1^+ field (Marques & Gruetter, 2013), especially when acquired at 7T. Thus, in this study the B_1^+ field was

also measured separately using the SA2RAGE sequence (SA2RAGE acquisition parameters : TR = 2.4s,TD1/TD2=0.042/1.8 s, α1/α2=4/11 degrees, TRGRE=2.1 ms, iPAT=2 and 6/8 partial Fourier sampling was used in the phase encoding direction and 6/8 partial Fourier in slice encoding direction. Resolution = 2x2x2.5mm.TA = 2 min16s).

Calculation of R1maps and B_1^+ correction procedure

The SA2RAGE derived maps of the B_1^+ field were used to correct the T1 maps for residual transmit field biases, in order to produce bias free high resolution T1 maps. Each participant's SA2RAGE derived B_1^+ map was first registered and interpolated to the same resolution as the MP2RAGE volumes using FSL's FLIRT registration algorithm. Subsequently these registered and interpolated B_1^+ maps were utilised to correct the high resolution MP2RAGE Uniform images and T1 maps for residual RF transmit field biases using the methodology outlined in Marques & Grutter (2013).

Following this correction procedure each participant's T1 map was converted to an R1 map (1/T1) for ease of interpretation, given the positive relationship between myelin and R1. Thus, in the rest of this chapter the term R1 map will be used to refer to the myelin maps collected in this study.

MRI Pre-processing and Analysis

MRI datasets from two participants were found to be contaminated by motion artefacts and were thus excluded from the subsequent analysis. A further MRI scan was also unavailable for one participant. Thus, the final sample size consisted of 35 participants. In order to improve segmentation outcomes a number of pre-processing steps recommend by Haast et al (2018) and adapted for the data utilised in this study were performed on the different imaging volumes produced by the MP2RAGE sequence (e.g. INV2,UNI). In brief, each participant's second inversion volume (INV2) was first bias corrected using the N4 algorithm. This volume was subsequently skull stripped using FSL's BET routine in order to produce a brain mask. The CBS tools software package was also used to remove additional non- brain tissue (arteries and dura) from the corrected T1-weighted image

(UNI image). A mask of the CSF was also produced using the INV1 image. The brain extracted, B_1^+ corrected image with dura, arteries and CSF removed was then used as the input for the subsequent Freesurfer analysis.

Each participant's pre-processed, B_1^+ corrected, T1-weighted image was then processed at native 0.65 mm resolution using the Freesurfer 7 'recon all' pipeline in order to construct a representation of the cortical surface. The resulting Freesurfer surfaces were then visually inspected for quality control purposes and manual corrections performed where necessary. Following Freesurfer processing, we generated 11 intracortical equi-volume surfaces corresponding to 11 different cortical depths. However, given the risk of partial-volume effects, that could introduce bias due to high R1 values from the white matter bleeding into deeper regions of the cortex for example, we chose to exclude four of these surfaces from the subsequent analysis given their proximity to the grey/pial and grey/white borders respectively.

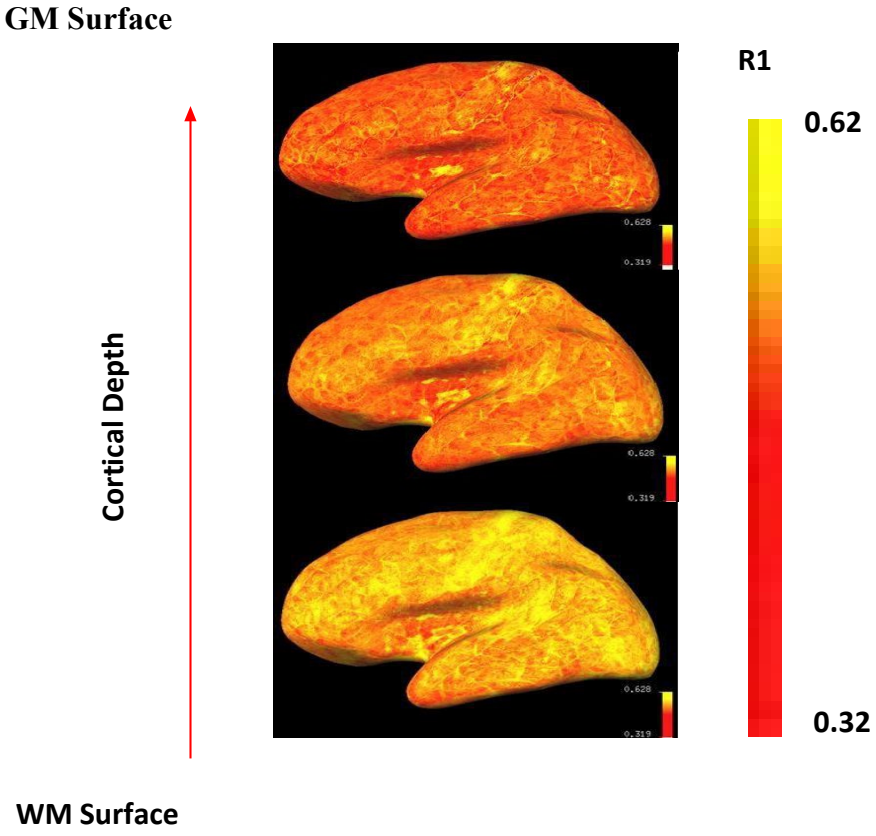

Figure 6.1: *Example R1 maps sampled at different depths overlaid on the cortical surface.*

Volume to surface mapping– Each individual participant's quantitative R1 map was then mapped onto the equi-volume surfaces using Freesurfer's 'mri_vol2surf' function (this

function assigns values from a volume to each vertex of a surface). This resulted in the creation of R1 maps sampled at 7 cortical depths corresponding to the 7 equi-volume surfaces used in this analysis. These are subsequently referred to as depths 1-7 in the remainder of this chapter. Depth 1 corresponds to the most superficial cortical depth and depth 7 corresponds to the deepest cortical depth from which the R1 values were sampled.

R1 of Desikan-Killian ROIs

Mean R1 values were then calculated for each of the Desikan-Killian atlas (Desikan et al., 2006) ROIs using the Freesurfer output aparc+aseg (cortical and subcortical parcellation) volume to define the atlas labels. This procedure was repeated for each of the 7 cortical depths under investigation. In this way a single R1 value was derived for each node in the Desikan-Killian atlas at each depth for each subject.

Quality Check of Freesurfer ROIs

Inspection of the R1 data revealed a pattern of higher R1 in right hemisphere ROIs compared to the left hemisphere ROIs. In order to mitigate any potential bias introduced by this asymmetry when comparing to the comparatively symmetric MEG connectivity data we normalised the R1 values for the MRI values in each hemisphere. This was achieved by z-scoring the left and right hemisphere R1 data independently for each of the cortical depths. These normalised R1 values were used in the subsequent analyses in this chapter.

Despite the improvements rendered by the B_1^+ correction procedure inferior temporal regions can still show artificially high R1 values due to the low signal in these regions, thus we chose to remove the following regions from the analysis: Inferior Temporal, Temporal Pole. The fusiform label was also found to be affected in a similar way and was thus also removed from the subsequent analysis.

As a final quality control procedure, we also calculated the coefficient of Variance (COV) for the mean R1 values for each ROI at each depth. Inspection of this data led to the

additional removal of the following labels: rostral anterior cingulate and the frontal pole as their COV was more than 3 standard deviations above the mean.

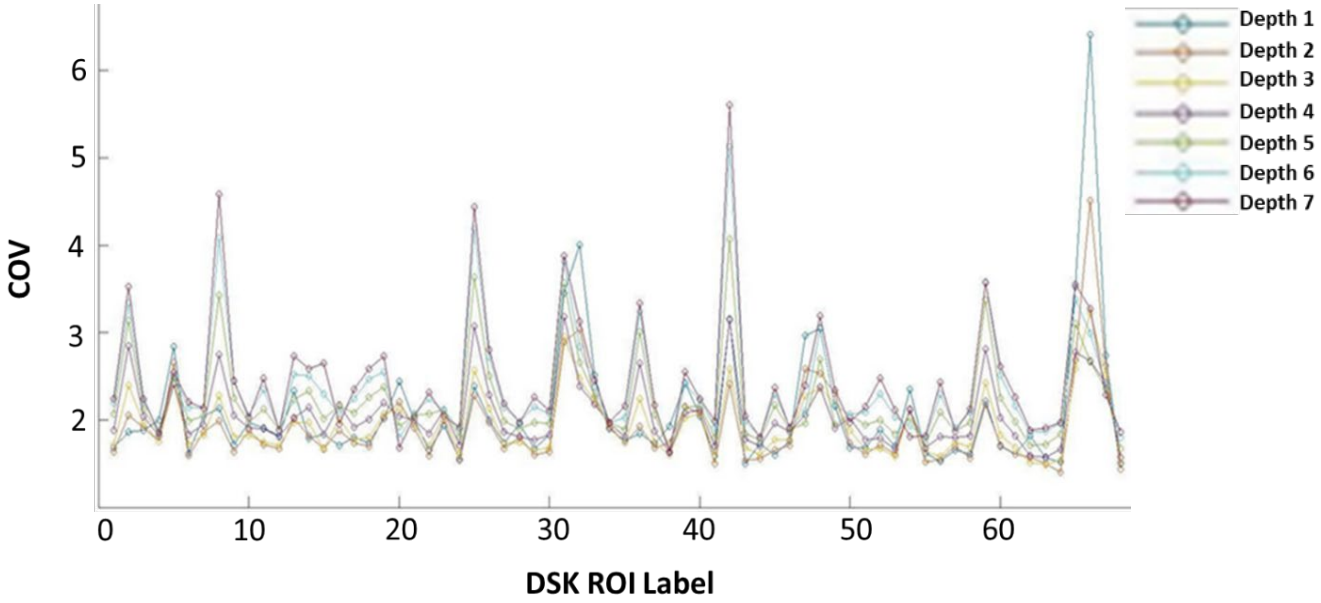

Figure 6.2: *Figure showing the COV of R1 values calculated for each of the ROIs in the Desikan-Killian atlas.*

Structural Covariance Matrices

To investigate the structural covariance of myelin, Pearson's correlation across subjects was used to measure the relationship between R1 values in each pair of nodes in the Desikan-Killian atlas. This procedure was repeated for each of the cortical depths resulting in the creation of 7 structural covariance matrices. Each entry in these matrices represents the correlation across subjects between a particular node pair.

R1 Difference Matrices – Similar to Huntenberg et al. (2017) an R1 difference matrix was also generated for each participant by calculating the absolute difference in R1 for each pair of nodes in the Desikan-Killian atlas. High values in this matrix therefore indicate node pairs that show large differences in their R1 values while values closer to zero indicate node pairs with more similar R1 values. This approach represents another way of probing myelin structural 'connectivity', complementary to the structural covariance approach outlined above. Notably, the motivating assumption of this analysis is that regions that have more similar myelin content are likely to be structurally related.

MEG Resting State Paradigm

7 minutes of eyes open resting state MEG recording were acquired from participants. During this task participants were instructed to simply relax and let their minds wander.

MEG Data Acquisition

Whole head MEG recordings were acquired using a 275 channel CTF axial gradiometer system housed in a magnetically shielded room. Participants were seated in an upright position during the recording sessions. Prior to the MEG recording, participants were fitted with three electromagnetic head coils located at a fixed distance from the nasion and the two pre-auricular points, the location of which was recorded continuously for MRI co-registration purposes. The location of these markers was verified afterwards using high resolution digital photographs.

Pre-processing

Datasets were first downsampled to 600 Hz prior to filtering with high-pass (1 Hz) and low-pass (150 Hz) filters and subsequently split into 2 second epochs. Artefact rejection was performed manually. Specifically, the data was visually inspected to identify eye, muscle and head movement artefacts, which were subsequently removed and thus excluded from the ensuing analysis.

Co-registration – co-registration was performed using the T1-weighted UNI image from the MP2RAGE sequence (see MRI methods). Each subject's UNI image was co-registered to the MEG data by marking the points on the MRI image corresponding to the position of the fiducial coils.

Template Atlas Source Model Construction

In order to define the source model a template atlas was built based on the Freesurfer Desikan-Killian cortical atlas (Desikan et al., 2006). Initially each participant's surface defined aparc+aseg parcellation was converted to a volume using AFNI's surface mapper program, SUMA, resulting in a Desikan-Killian cortical atlas volume defined for each participant in individual space. Subsequently, each participant's data was registered to MNI space by first registering their T1-weighted volume to a 1mm MNI template brain

available in FSL. The resultant transformation matrices were then applied to the atlas volumes in order to derive, for each participant, a Desikan- Killian cortical atlas volume in MNI space. These atlas volumes were then loaded into Matlab and a probabilistic atlas defined by finding the most common atlas label for each MNI coordinate. This probabilistic atlas was used as the source model for the subsequent MEG source reconstruction analysis.

Desikan-Killian Atlas Labels

1	lh.bankssts.label	35	rh.bankssts.label
2	lh.caudalanteriorcingulate.label	36	rh.caudalanteriorcingulate.label
3	lh.caudalmiddlefrontal.label	37	rh.caudalmiddlefrontal.label
4	lh.cuneus.label	38	rh.cuneus.label
5	lh.entorhinal.label	39	rh.entorhinal.label
6	lh.fusiform.label	40	rh.fusiform.label
7	lh.inferiorparietal.label	41	rh.inferiorparietal.label
8	lh.inferiortemporal.label	42	rh.inferiortemporal.label
9	lh.isthmuscingulate.label	43	rh.isthmuscingulate.label
10	lh.lateraloccipital.label	44	rh.lateraloccipital.label
11	lh.lateralorbitofrontal.label	45	rh.lateralorbitofrontal.label
12	lh.lingual.label	46	rh.lingual.label
13	lh.medialorbitofrontal.label	47	rh.medialorbitofrontal.label
14	lh.middletemporal.label	48	rh.middletemporal.label
15	lh.parahippocampal.label	49	rh.parahippocampal.label
16	lh.paracentral.label	50	rh.paracentral.label
17	lh.parsopercularis.label	51	rh.parsopercularis.label
18	lh.parsorbitalis.label	52	rh.parsorbitalis.label
19	lh.parstriangularis.label	53	rh.parstriangularis.label
20	lh.pericalcarine.label	54	rh.pericalcarine.label
21	lh.postcentral.label	55	rh.postcentral.label
22	lh.posteriorcingulate.label	56	rh.posteriorcingulate.label
23	lh.precentral.label	57	rh.precentral.label
24	lh.precuneus.label	58	rh.precuneus.label
25	lh.rostralanteriorcingulate.label	59	rh.rostralanteriorcingulate.label
26	lh.rostralmiddlefrontal.label	60	rh.rostralmiddlefrontal.label
27	lh.superiorfrontal.label	61	rh.superiorfrontal.label
28	lh.superiorparietal.label	62	rh.superiorparietal.label
29	lh.superiortemporal.label	63	rh.superiortemporal.label
30	lh.supramarginal.label	64	rh.supramarginal.label
31	lh.frontalpole.label	65	rh.frontalpole.label
32	lh.temporalpole.label	66	rh.temporalpole.label
33	lh.transversetemporal.label	67	rh.transversetemporal.label
34	lh.insula.label	68	rh.insula.label

Table 6.1 : *Table showing the order of ROI labels in the Desikan-Killian cortical atlas.*

Source reconstruction

Source reconstruction was performed using the FieldTrip Toolbox (Oostenveld, Fries, Maris, & Schoffelen, 2010). The data were filtered into six frequency bands of interest (Delta 1-4, Theta 4-8, Alpha 8-13, Beta 13-30, Low Gamma 40-60 and HighGamma 60-80 Hz). (The decision to exclude frequencies 31-39 from the gamma band was made here in order to reduce the risk of overlap with the beta frequency range). Source localisation was then performed utilising a Linear Constrained Minimum Variance (LCMV) beamformer on a 6x6x6 mm grid, using a local-spheres conductor model. The local-spheres model was used in this instance as it constitutes the default option in the CUBRIC resting-state MEG pipeline. Seed regions were defined using 68 regions from the Desikan-Killian cortical atlas (Desikan et al., 2006). In each of the 68 atlas regions, the beamformer voxel with the highest temporal standard deviation of its band-pass filtered Hilbert envelope was chosen to represent that region and included in the subsequent analysis. In order to correct for zero-lag source leakage in these time courses symmetric orthogonalization was applied (Colclough, Brookes, Smith & Woolrich, 2015). Hilbert amplitude envelopes were then calculated from these virtual sensor time series for each of the nodes, for each frequency band. Amplitude-amplitude connectivity matrices were then constructed by correlating the amplitude envelopes of each node with every other node, resulting in the generation of a 68x68 matrix for each subject, for each frequency band. The individual entries in these matrices represent the amplitude correlation coefficients between nodes in the Desikan-Killian atlas. These correlation coefficients were then converted to variance-normalised Z-scores using a Fisher Z transform in order to correct for potential effects induced by variability in data quality among participants (Koelewijn et al., 2019).

Connectivity Strength

For each node in the Desikan-Killian atlas a connectivity strength metric was also calculated by summing across connectivity values. This procedure was repeated for each of the six frequency bands under investigation (delta, theta, alpha, beta, low gamma, high gamma).

Multimodal Analysis

R1 Structural Covariance Matrices and MEG networks

To assess the spatial-similarity between the frequency specific resting state networks and the myelin structural covariance networks, the Pearson's correlation coefficient between the myelin networks and the frequency specific resting state MEG networks, which were averaged across participants, was calculated. This procedure was repeated for the R1 matrices sampled at each of the cortical depths. To determine the robustness of the resulting correlation values, 95% confidence intervals were also calculated by implementing a bootstrapping with replacement procedure. The bootstrapping method is a resampling procedure first introduced by Efron (1979), in which the data from a known sample is used to generate a sampling distribution by randomly sampling (with replacement) from the original sample. The effect of interest, (in this case the correlation coeffiecient) can be calculated at every resampling iteration allowing for the generation of a sampling distribution which can be used to calculate confidence intervals. In the present study, for each of 10000 iterations the Matlab bootstrap function was used to determine the subject sample to include in the construction of the structural covariance matrix. As before, the resulting structural covariance matrix was then correlated with the mean frequency specific resting state MEG networks. In this way, correlation coefficients were derived for each of the 10000 iterations and from this data 95% confidence intervals were calculated in order to determine the robustness of the correlations. Again, this procedure was repeated for each frequency band and cortical depth combination.

R1 difference matrices and MEG networks

We next assessed the relationship between the frequency-specific resting-state networks and the R1 difference matrices. For this analysis, the data were againaveraged across participants. The mean R1 difference matrix was correlated with the frequency specific resting state MEG networks using the Pearson's correlation coefficient. Akin to the structural covariance analysis outlined above, in order to determine the robustness of these correlations, 95% confidence intervals were also calculated by implementing a bootstrapping with replacement procedure. More specifically, for each of 10000 iterations

the Matlab *bootstrap* function was used to determine the subject sample to include in the analysis. Average R1 difference and MEG connectivity matrices were then created using the data from these subjects. As before, the mean R1 difference matrix was then correlated with the mean frequency specific resting state MEG network. In this way, correlation coefficients were derived for each of the 10000 iterations and from this data 95% confidence intervals were calculated. Again, this procedure was repeated for each frequency band and cortical depth combination.

Myelin and connectivity strength

Finally, we also sought to determine whether a relationship might exist between the connectivity strength of the nodes in the functional connectivity network and the myelin content (R1). In the first instance, the R1 values for each node in the Desikan-Killian atlas were averaged across subjects to derive a mean R1 value for each node, at each depth. Pearson's correlation coefficient was then calculated between the mean connectivity strength for each frequency band and the normalised depth-specific R1 values.

Additional Cohort – In order to validate our findings, we also calculated the MEG connectivity strength for an additional cohort of 183 participants for whom R1 maps were not available and again correlated these values with the mean R1 matrices from the present study. Full details of this cohort and the analysis pipeline used to derive their MEG connectivity matrices can be found in Koelewijn et al. (2019).

6.4 Results

Structural covariance

The structural covariance analysis revealed evidence of a positive relationship between the structural myelin networks and MEG connectivity in all frequency bands. Interestingly, the pattern of correlations also appeared to demonstrate a depth specific pattern (Figure 6.3). In the delta, theta, alpha and beta bands stronger correlations were found between the myelin covariance matrices at deeper cortical depths and MEG functional connectivity

networks. In both the low and high gamma bands the strongest correlations were also found between the MEG functional networks and the myelin structural networks sampled at deeper cortical depths, however these relationships were weaker than those observed for the other frequency bands investigated in this study. Given the large number of data points the p-values in this analysis were very small(<0.0001 in the majority of cases) and thus the results of the bootstrap test were examined to establish the robustness of the observed correlations.

Significantly, the results of the bootstrapping procedure pointed to the robustness of these relationships. For all frequency bands and cortical depths, the 95% confidence intervals did not contain 0.

Cortical Depth	Delta	Theta	Alpha	Beta	Low Gamma	High Gamma
1	0.293	0.271	0.330	0.372	0.175	0.093
2	0.324	0.328	0.358	0.395	0.184	0.111
3	0.339	0.372	0.381	0.419	0.187	0.122
4	0.354	0.399	0.398	0.439	0.197	0.134
5	0.386	0.438	0.426	0.465	0.211	0.146
6	0.413	0.474	0.459	0.488	0.223	0.159
7	0.431	0.500	0.492	0.511	0.229	0.169

Table 6.2: *Correlations between the Myelin structural covariance matrix and MEG connectivity at each of the 7 cortical depths investigated in this study. Depth 1 is located the most superficially in the cortex, whereas depth 7 is the closest to the grey matter/white matter border.*

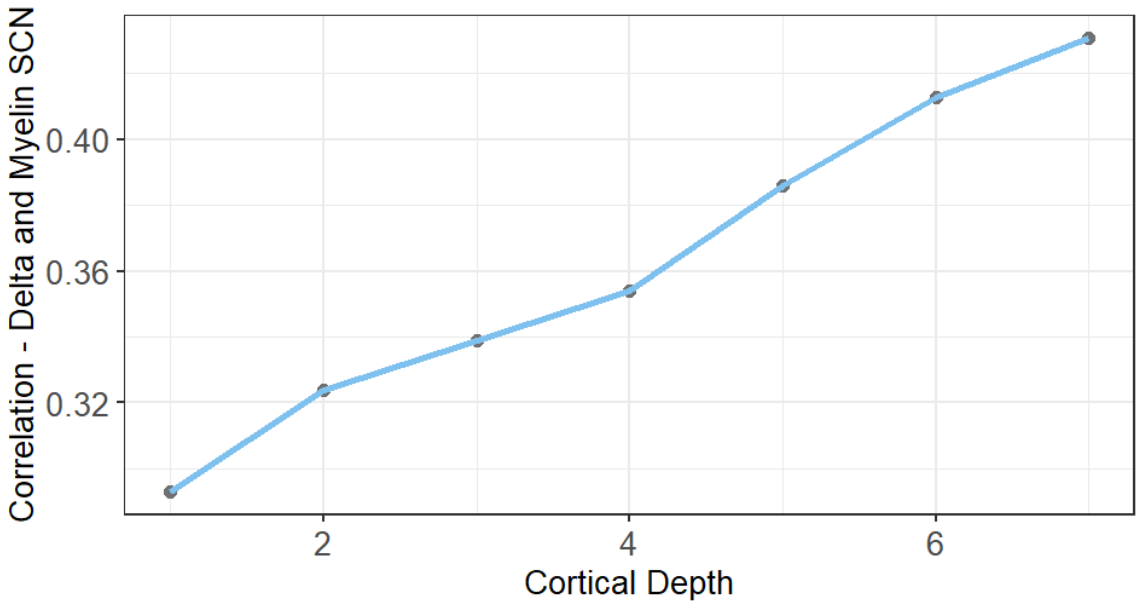

Figure 6.3: *Figure showing the correlations between delta resting state networks and networks of myelin structural covariance sampled at different cortical depths. Depth 1 is located the most superficially in the cortex, whereas depth 7 is the closest to the grey matter/white matter border.*

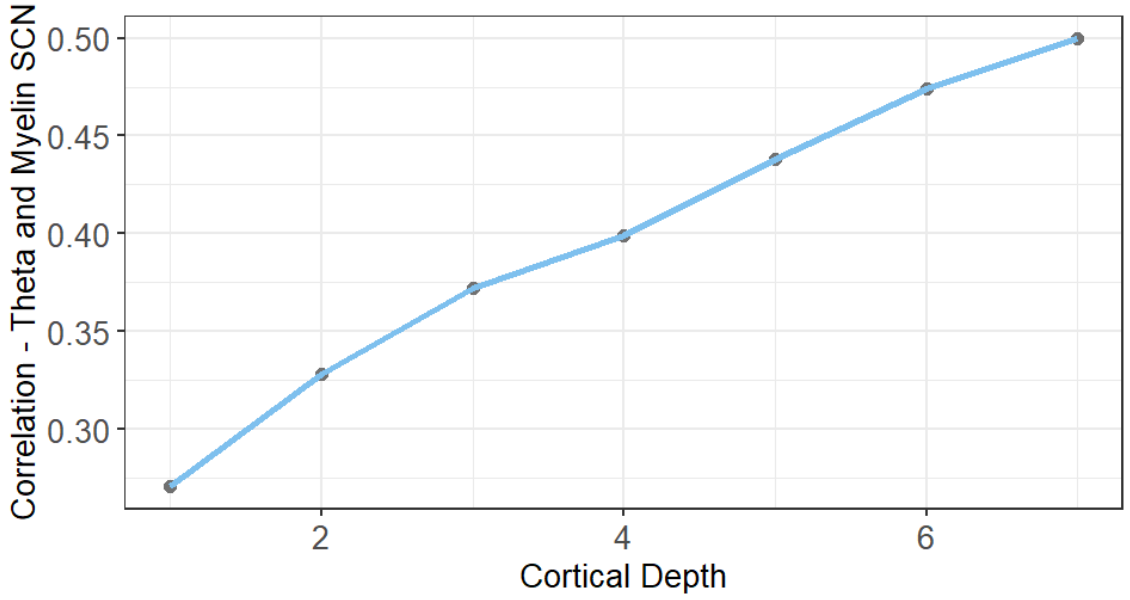

Figure 6.4: *Figure showing the correlations between theta resting state networks and networks of myelin structural covariance sampled at different cortical depths. Depth 1* is *located the most superficially in the cortex, whereas depth 7 is the closest to the grey matter/white matter border.*

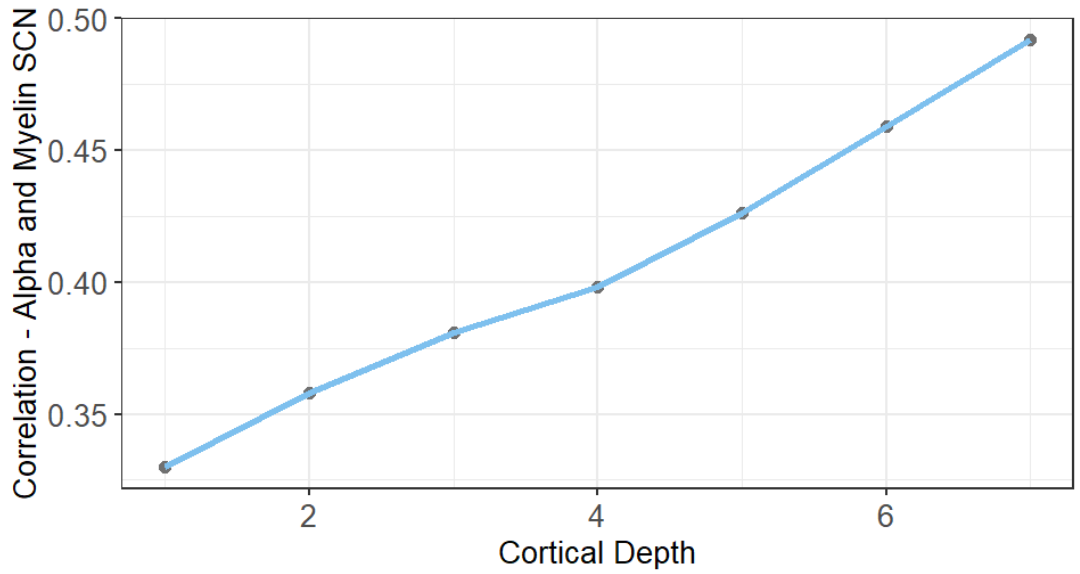

Figure 6.5: *Figure showing the correlations between alpha resting state networks and networks of myelin structural covariance sampled at different cortical depths. Depth 1 is located the most superficially in the cortex, whereas depth 7 is the closest to the grey matter/white matter border.*

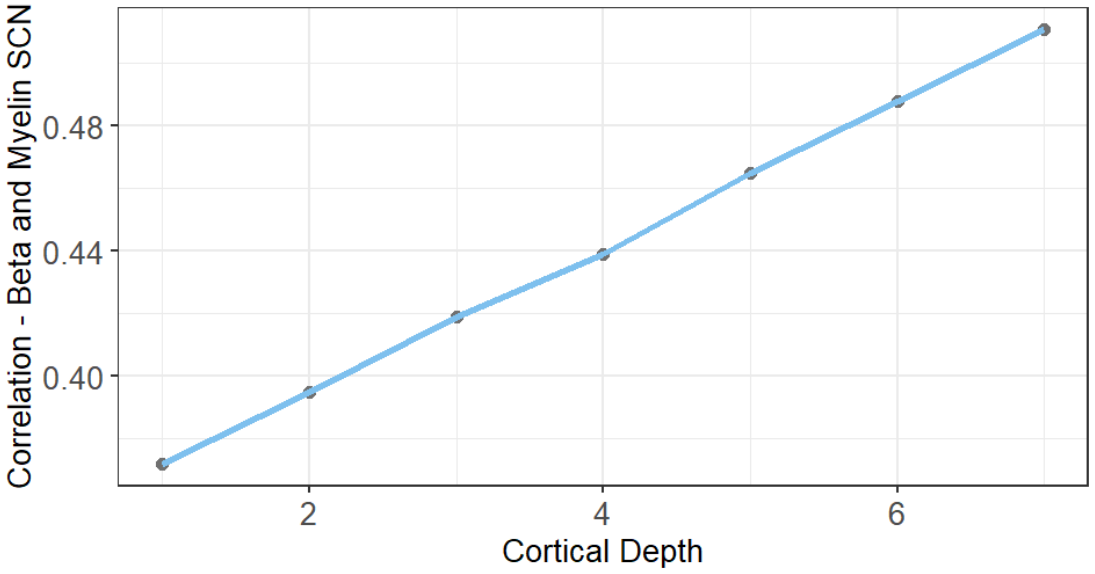

Figure 6.6: *Figure showing the correlations between beta resting state networks and networks of myelin structural covariance sampled at different cortical depths. Depth 1 is located the most superficially in the cortex, whereas depth 7 is the closest to the grey matter/white matter border.*

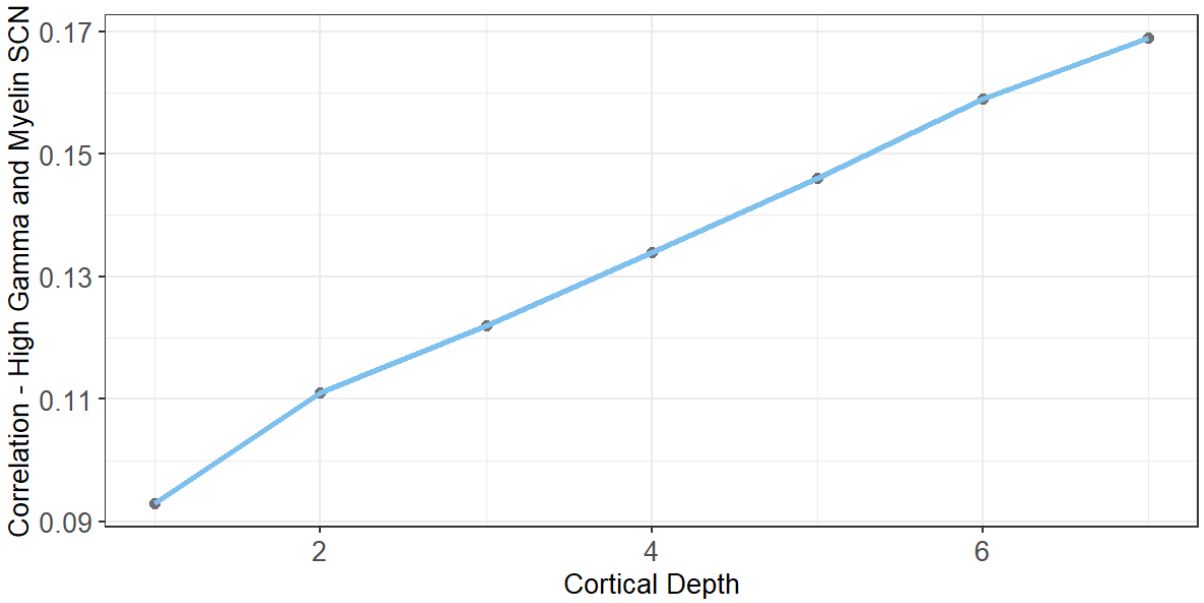

Figure 6.7: *Figure showing the correlations between low gamma resting state networks and networks of myelin structural covariance sampled at different cortical depths. Depth 1 is located the most superficially in the cortex, whereas depth 7 is the closest to the grey matter/white matter border.*

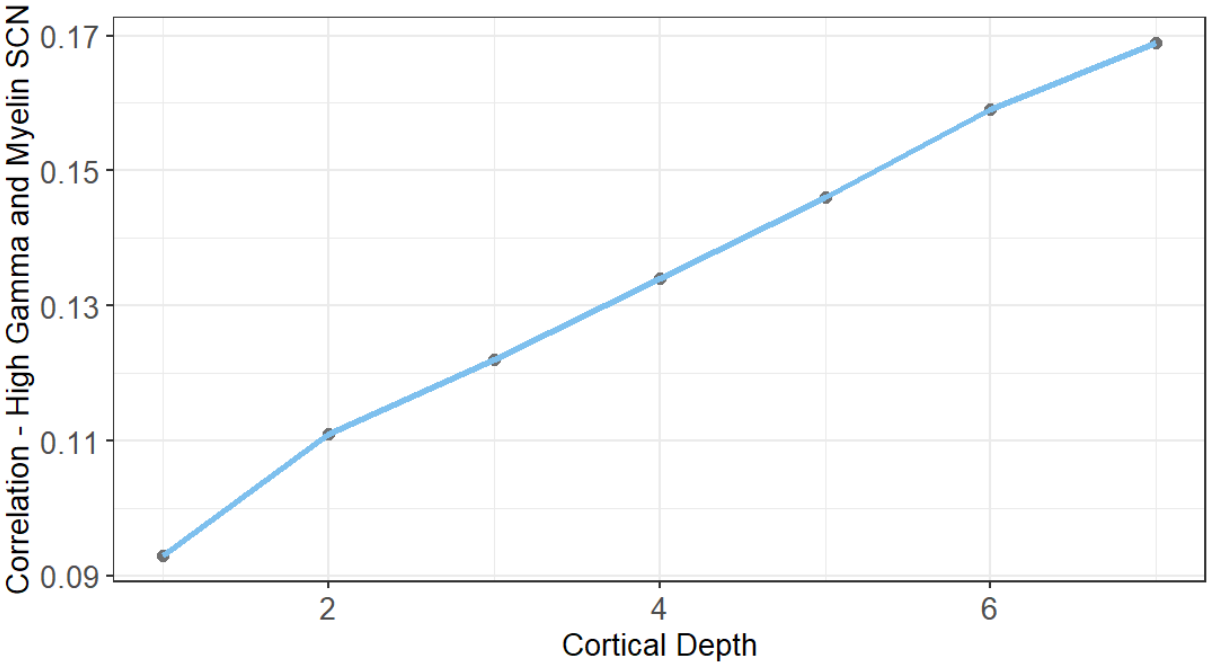

Figure 6.8: *Figure showing the correlations between high gamma resting state networks and networks of myelin structural covariance sampled at different cortical depths. Depth 1 is located the most superficially in the cortex, whereas depth 7 is the closest to the grey matter/white matter border.*

In Figure 6.9 visual representations of examples of the depth-specific structural covariance matrices can be observed. In these matrices the cortical regions in the Desikan-Killian atlas are plotted along both the X and Y axes. Each element in the matrices denotes the cross-subject correlation in R1 values between two brain regions.

Figure 6.10 shows the frequency-specific MEG connectivity matrices. In these matrices the cortical regions in the Desikan-Killian atlas are plotted along both the X and Y axes. Each element in the matrices represents the amplitude coupling between two brain regions.

From a visual standpoint it could be suggested that depth 7 bears the closest similarity to the alpha, beta and theta connectivity bands. For example, akin to these MEG matrices, the depth 7 structural covariance networks also seem to show a pattern of higher values towards the bottom right-hand corner.

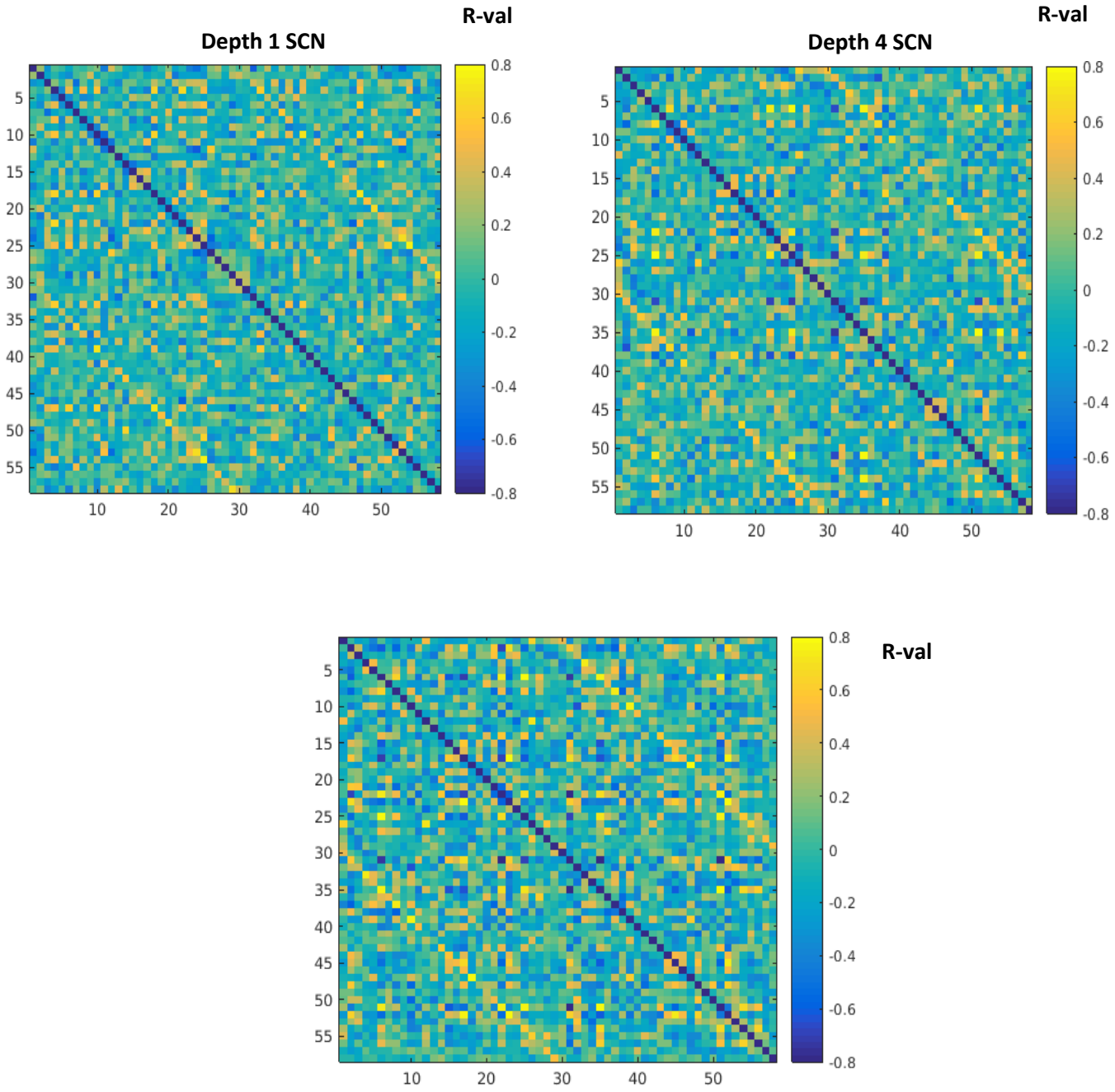

Figure 6.9: *Correlations matrices for 3 of the depths investigated in this study. Depth 1 represents the most superficial cortical depth investigated, depth 4 represents the middle cortical depth and depth 7 represents the deepest cortical depth. In these matrices the cortical regions in the Desikan-Killian atlas are plotted along both the X and Y axes. Each element in the matrices denotes the cross-subject correlation in the z-scored R1 values between two brain regions. The colour bar shows the Pearson's correlation coefficient (r-value). Note that although the Desikan atlas incudes 68 nodes, only 58 are shown here as some nodes were removed from the R1 analysis for quality control purposes.*

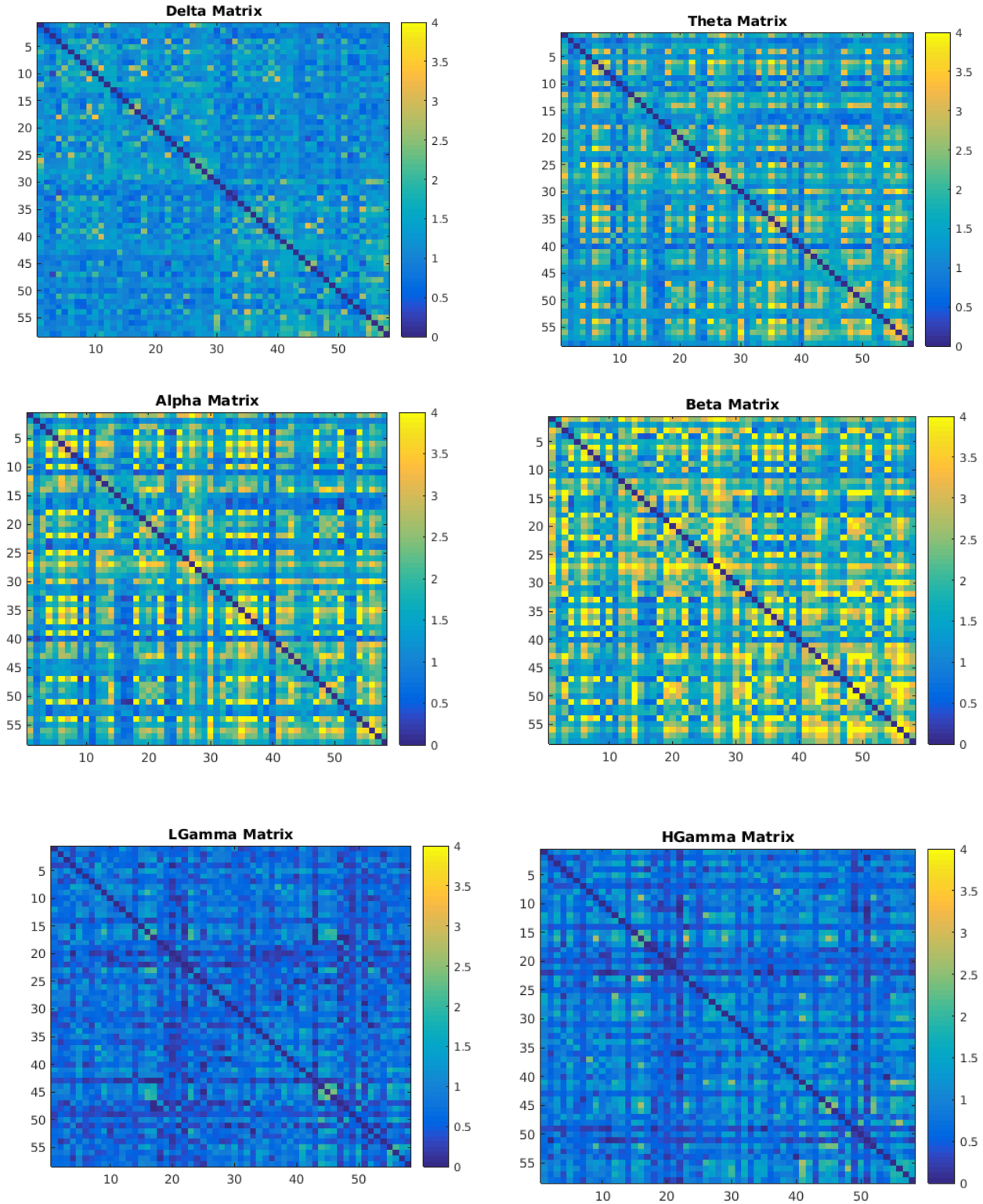

Figure 6.10: *Correlations matrices for the six MEG frequency bands investigated in this study. In these matrices the cortical regions in the Desikan-Killian atlas are plotted along both the X and Y axes. The individual entries in these matrices represent the amplitude correlation coefficients between nodes in the Desikan-Killian atlas, which have been converted to variance-normalised Z-scores using a Fisher Z transform. The colour bars thus show the Z-score values. Note that for comparison purposes akin to the myelin matrices, although the Desikan atlas incudes 68 nodes, only 58 are shown here as some nodes were removed from the R1 analysis for quality control purposes.*

R1 difference matrices and MEG networks

In all frequency bands the relationship between the R1 difference matrices and MEG connectivity matrices was found to be negative (see Table 6.3). Thus, regions with more similar myelin content demonstrated higher functional connectivity. In the delta band, the strongest correlation was found between the MEG Networks and the R1 difference matrices sampled at lower cortical depths.

In the theta band the relationship was strongest between the R1 difference matrices at depths 2 and 7 and the MEG connectivity network. In the beta band the relationship was strongest between the R1 difference matrices sampled at both superficial and deep cortical depths with a notable weakening of this relationship at mid-cortical depths. A similar pattern was also observed in the alpha band.

In the low gamma band, the strongest correlation was found with the R1 difference matrices at mid cortical depths. Similarly, in the high gamma band the strongest correlation was also found with the R1 difference matrices sampled at superficial-mid cortical depths.

Again, given the large number of data points the p-values observed in this analysis were very small (<0.0001 in the majority of cases). However, the bootstrapping procedure revealed that the relationships between the R1 difference matrices derived from each of the cortical depths investigated and the delta, theta, beta, and gamma bands were robust as the 95% confidence intervals did not contain zero.

However, in the case of the alpha band, only weak relationships were observed. Furthermore, these relationships were not significant when correcting for multiple comparisons ($p=0.05/7=0.007$), except for in the case of depths 1 and 2.

Cortical Depth	Delta	Theta	Alpha	Beta	Low Gamma	High Gamma
1	-0.052	-0.074	-0.050	-0.123	-0.127	-0.125
2	-0.072	-0.105	-0.052	-0.116	-0.140	-0.158
3	-0.082	-0.097	-0.041	-0.098	-0.151	-0.162
4	-0.094	-0.093	-0.037	-0.094	-0.156	-0.162
5	-0.107	-0.093	-0.036	-0.097	-0.158	-0.159
6	-0.120	-0.096	-0.039	-0.106	-0.155	-0.154
7	-0.124	-0.103	-0.044	-0.120	-0.140	-0.135

Table 6.3: *Correlations between the R1 difference matrices and MEG connectivity at each of the 7 cortical depths. Depth 1 is located the most superficially in the cortex, whereas depth 7 is the closest to the grey matter/white matter border.*

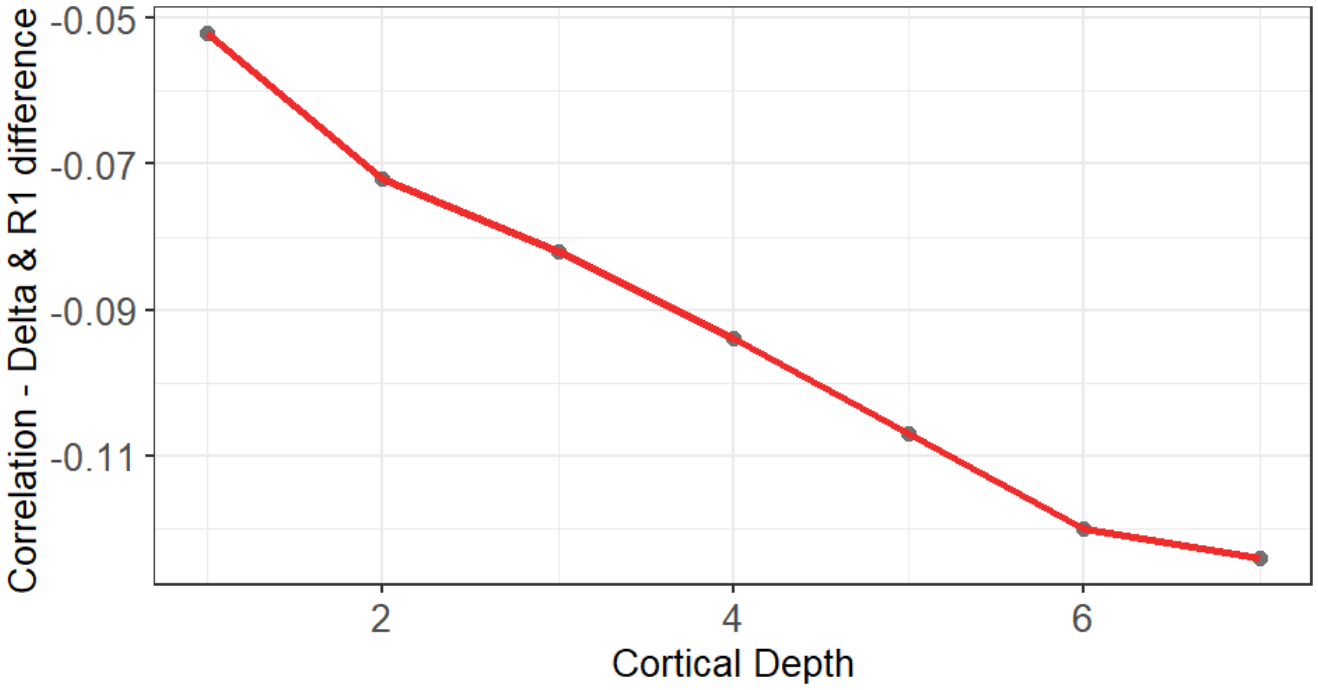

Figure 6.11: *Figure showing the correlations between delta resting state networks and R1 difference matrices sampled at cortical depths 1-7. Depth 1 is located the most superficially in the cortex, whereas depth 7 is the closest to the grey matter/white matter border.*

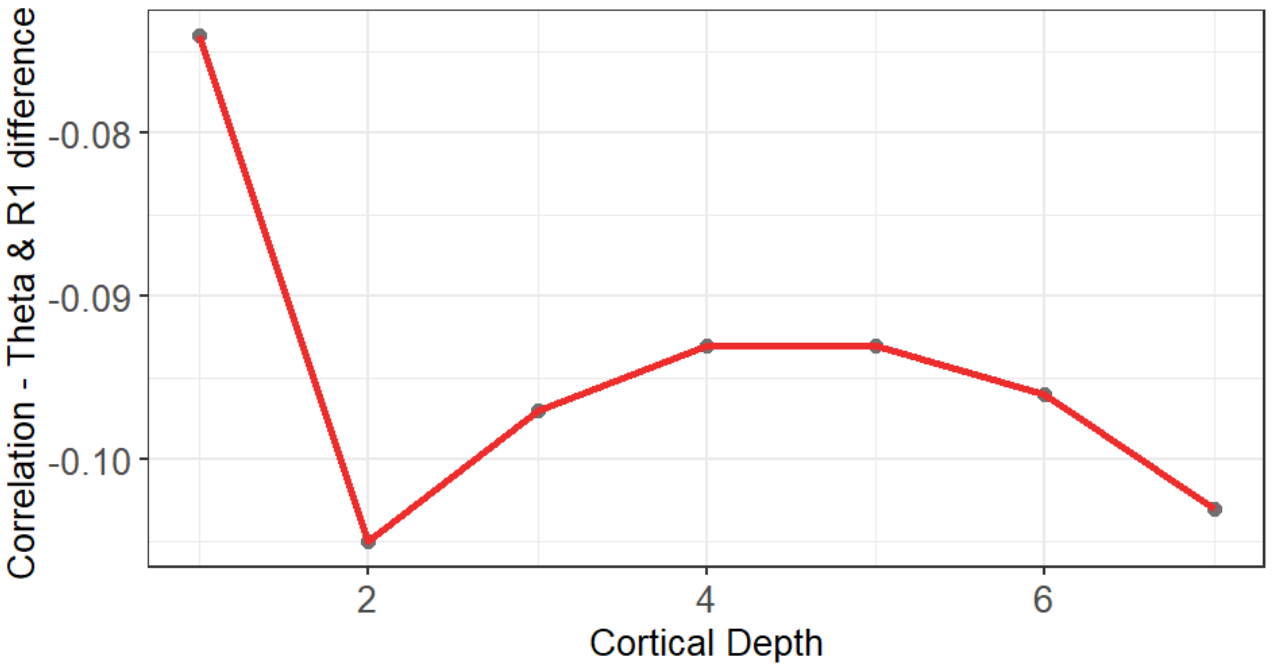

Figure 6.12: *Figure showing the correlations between theta resting state networks and R1 difference matrices sampled at cortical depths 1-7. Depth 1 is located the most superficially in the cortex, whereas depth 7 is the closest to the grey matter/white matter border.*

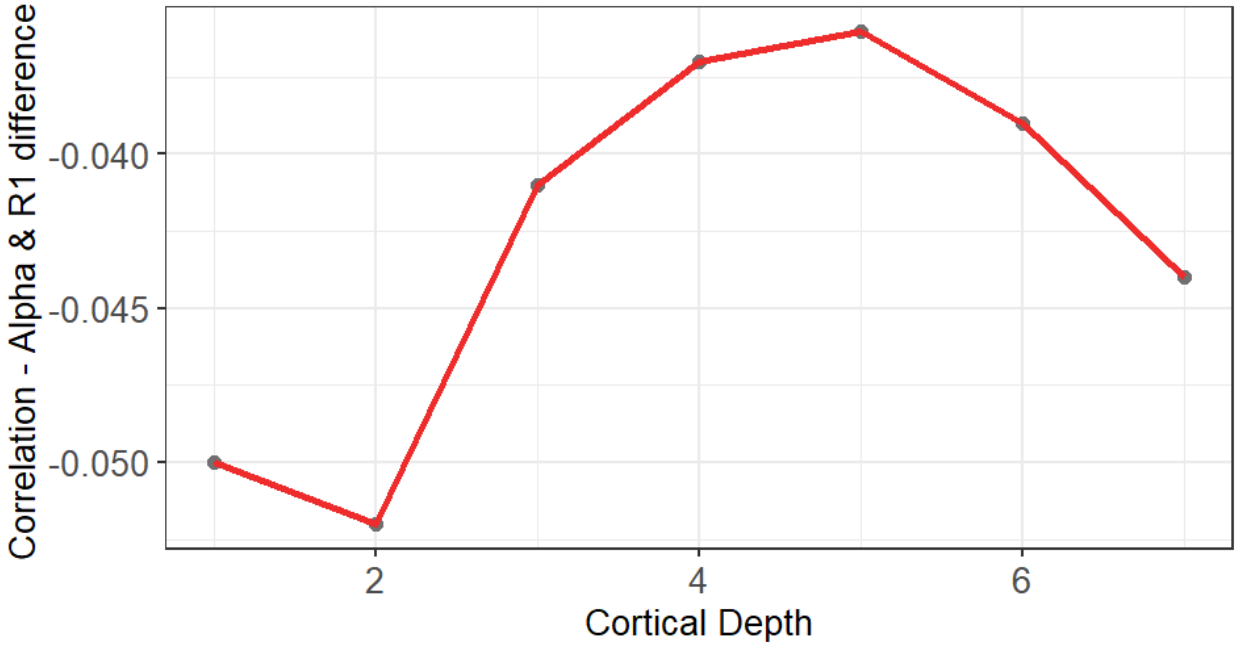

Figure 6.13: *Figure showing the correlations between alpha resting state networks and R1 difference matrices sampled at cortical depths 1-7. Depth 1 is located the most superficially in the cortex, whereas depth 7 is the closest to the grey matter/white matter border.*

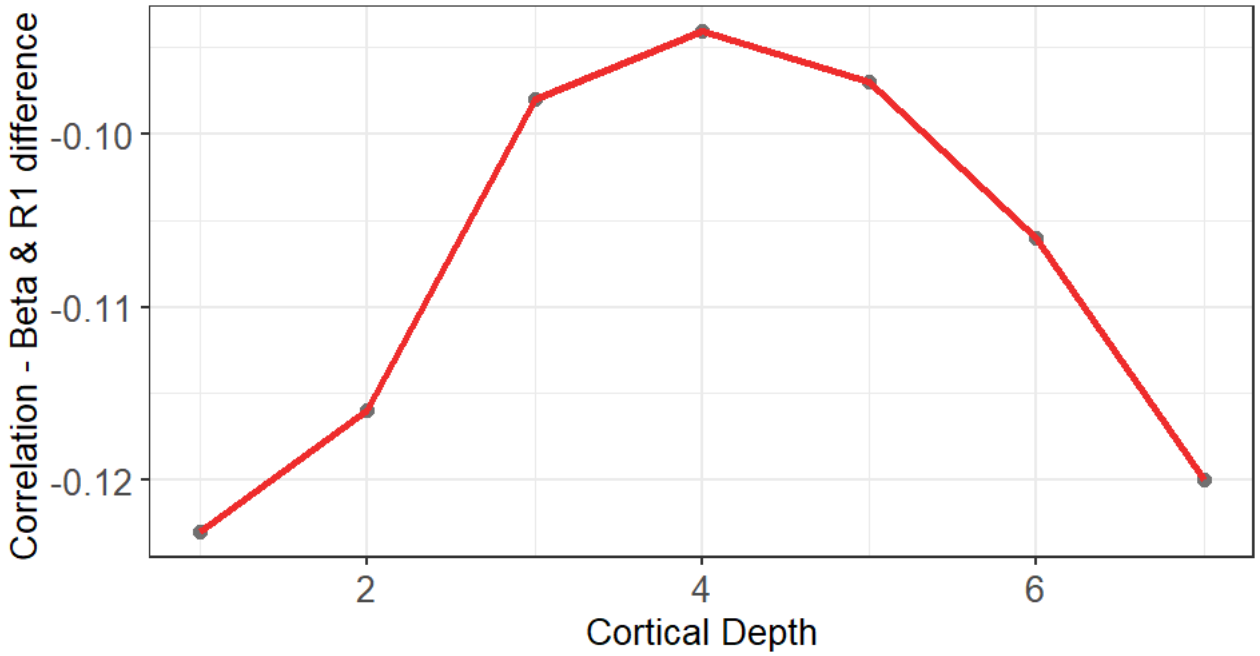

Figure 6.14: *Figure showing the correlations between beta resting state networks and R1 difference matrices sampled at cortical depths 1-7. Depth 1 is located the most superficially in the cortex, whereas depth 7 is the closest to the grey matter/white matter border.*

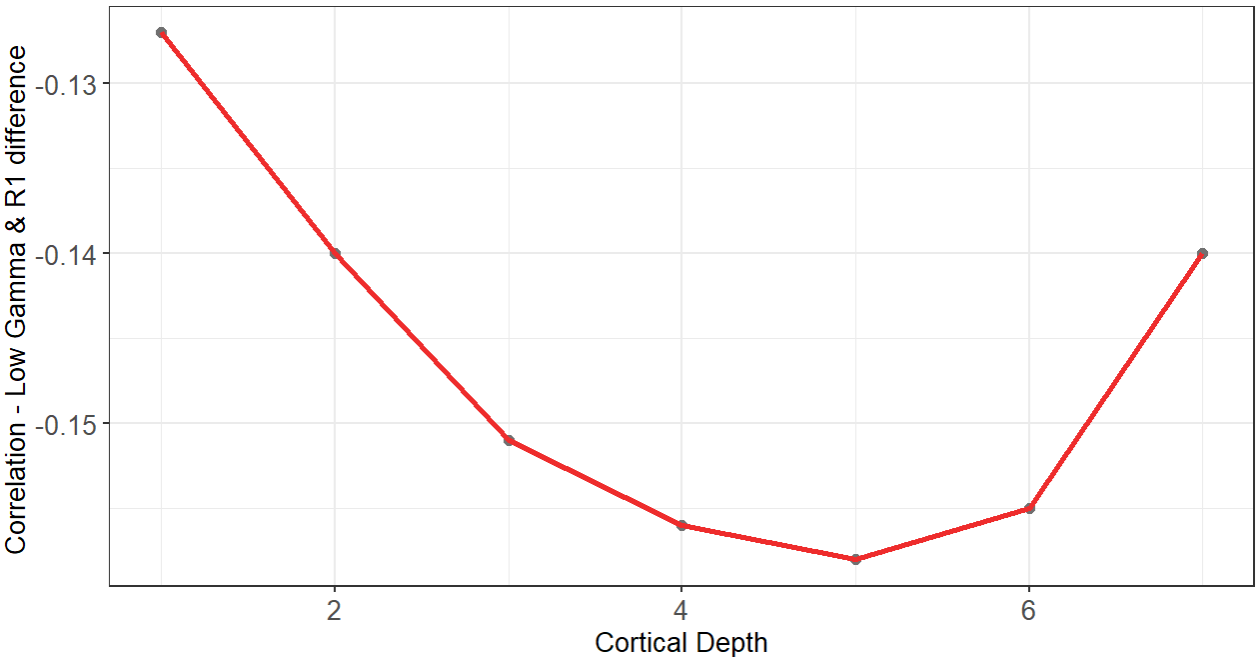

Figure 6.15: *Figure showing the correlations between low gamma resting state networks and R1 difference matrices sampled at cortical depths 1-7. Depth 1 is located the most superficially in the cortex, whereas depth 7 is the closest to the grey matter/white matter border.*

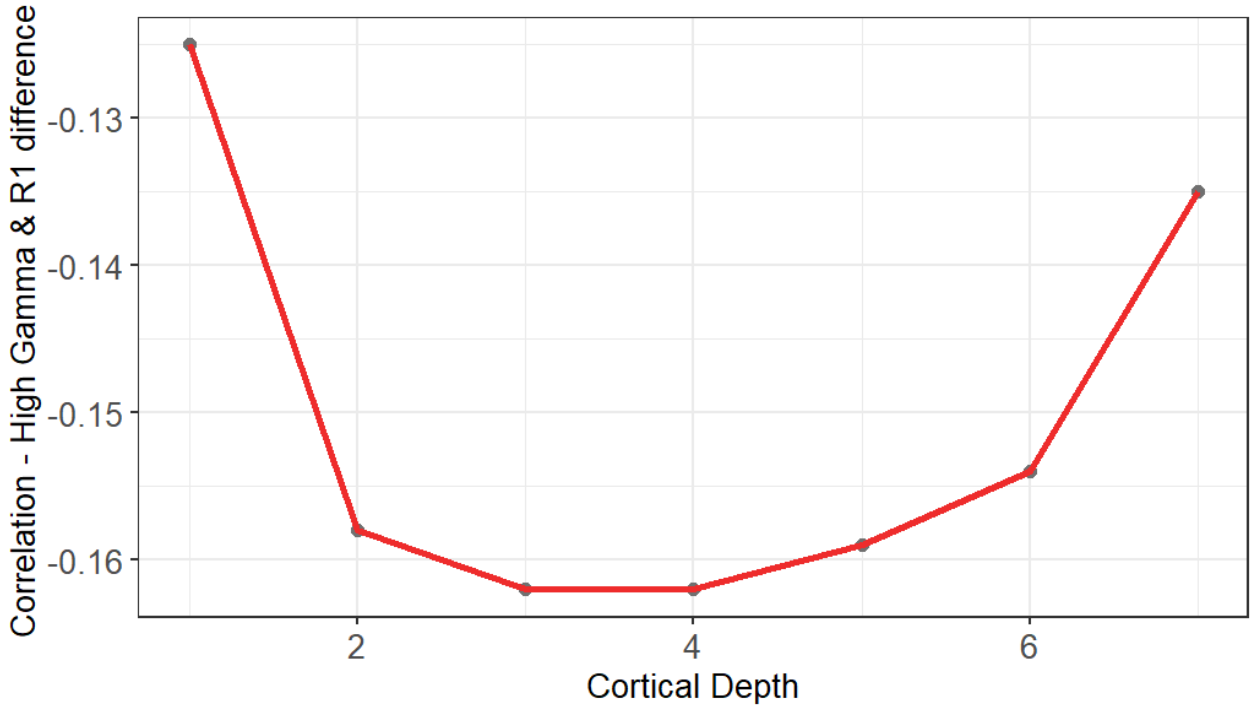

Figure 6.16: *Figure showing the correlations between high gamma resting state networks and R1 difference matrices sampled at cortical depths 1-7. Depth 1 is located the most superficially in the cortex, whereas depth 7 is the closest to the grey matter/white matter border.*

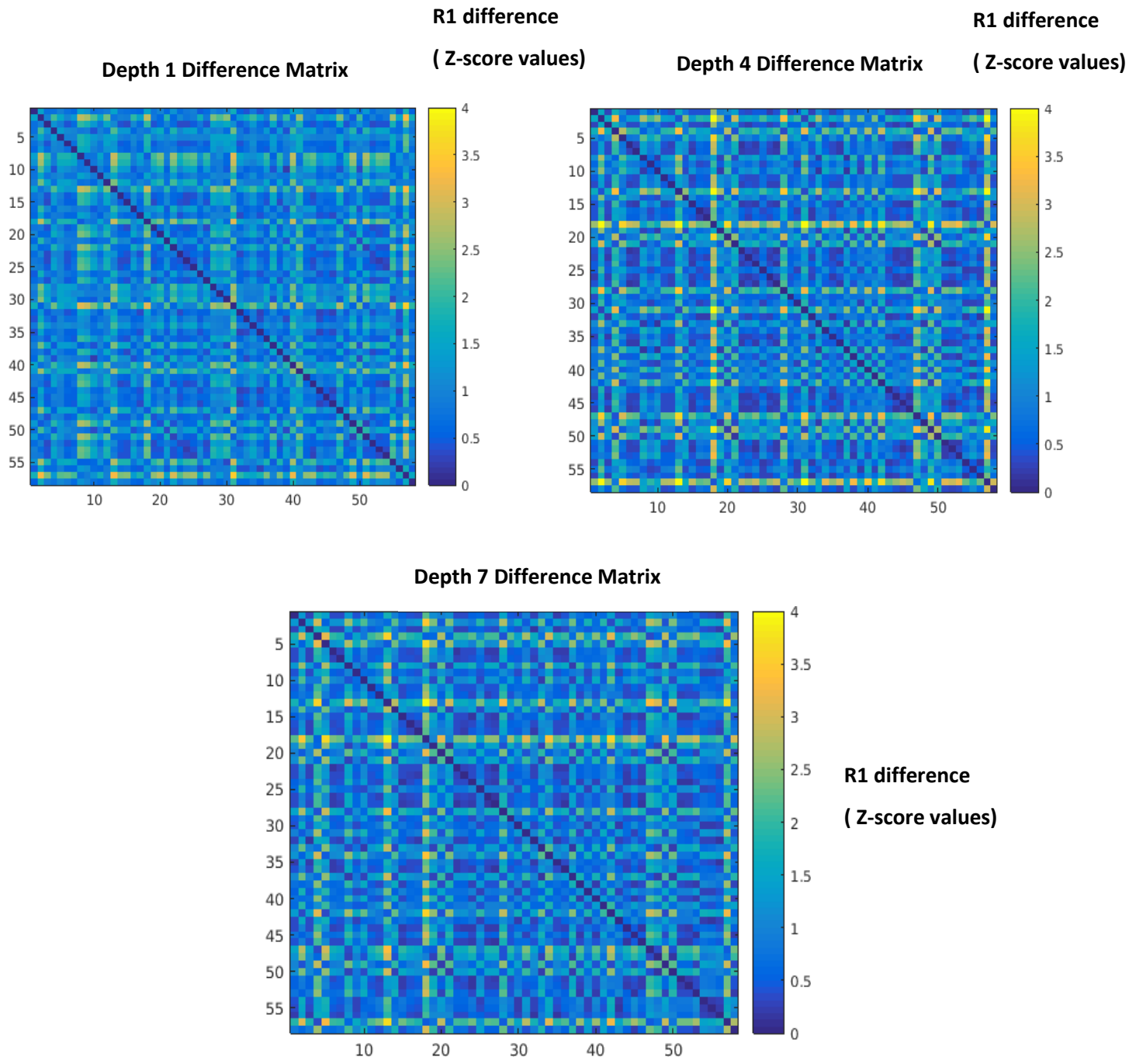

Figure 6.17: *R1 difference matrices for 3 of the depths investigated in this study. These matrices were* generated *by calculating the absolute difference in the z-scored R1 values for each pair of nodes in the Desikan-Killian atlas. The colour bars thus show the difference in the z-scored R1 values. High values in this matrix therefore indicate node pairs that show large differences in their R1 values while values closer to zero indicate node pairs with more similar R1 values. Although the Desikan atlas incudes 68 nodes, only 58 are shown here as some nodes were removed from the R1 for quality control purposes.*

Strength Analysis

Spatial Similarity

As depicted in *Figures 6.18 and 6.19* it is evident that the spatial pattern of R1 sampled deep in the cortex demonstrates greater similarity with the spatial pattern of MEG connectivity strength in the theta, alpha and beta bands than does that of R1 sampled more superficially.

Conversely, in both the low and high gamma bands the opposite relationship is observed with the spatial pattern of superficial R1 demonstrating greater similarity with the spatial pattern of MEG connectivity strength in the gamma bands.

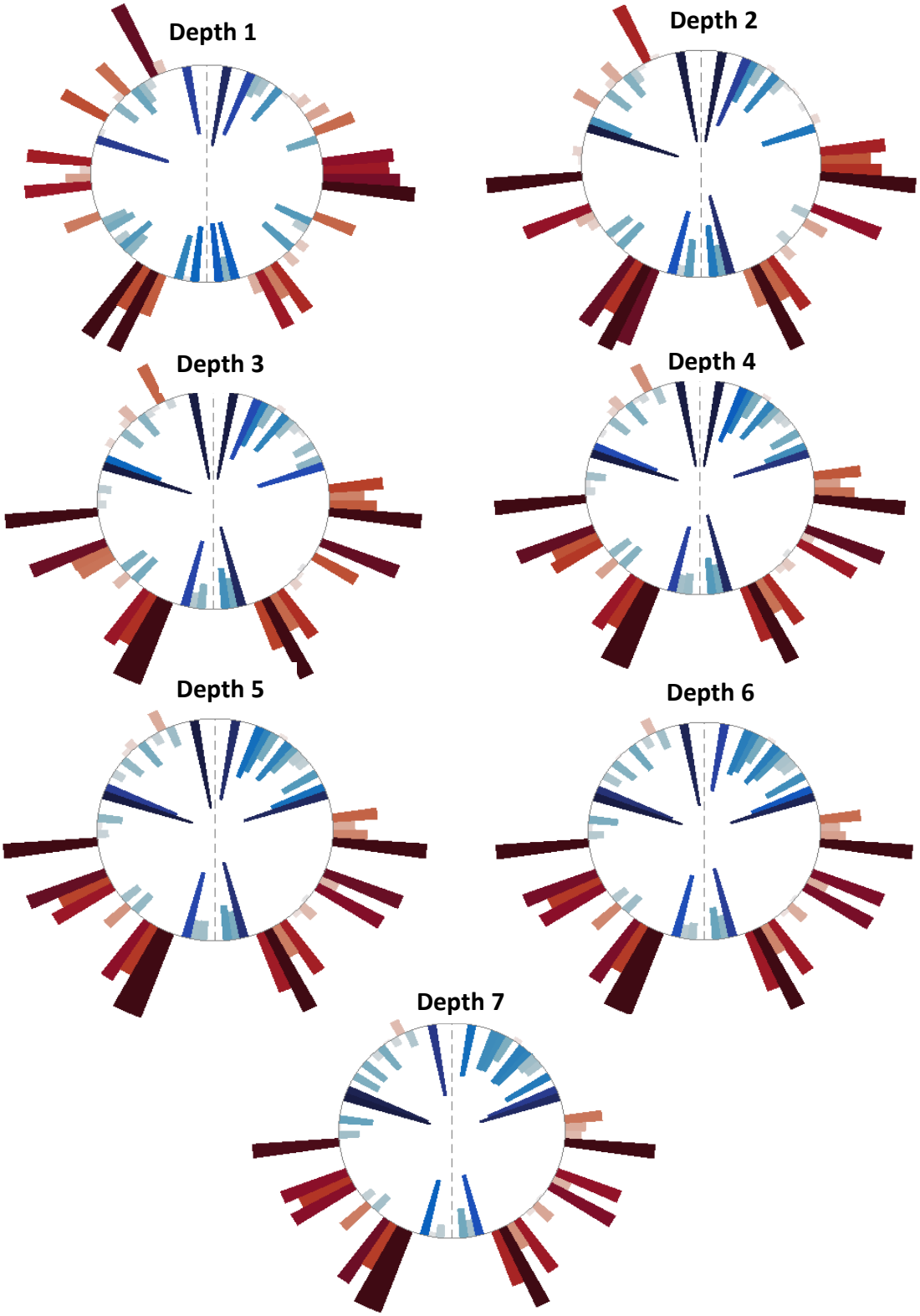

Figure 6.18: *Circle plots demonstrating the Depth-specific R1 distributions for depths 1-7. Depth 1 is the most superficial, whereas depth 7 is the closest to the grey matter/white matter border. Each bar in the circle plots depicts the amplitude of the Z-scored R1 values of each node in the Desikan-Killian atlas. The regions with the highest R1 values are depicted in Red.* The *Desikan-Killian atlas areas are split into left and right and grouped around the plot as follows from top to bottom: cingulate cortex (top), frontal regions, insula, temporal lobe, sensorimotor regions, parietal, occipital cortex and precuneus (bottom).*

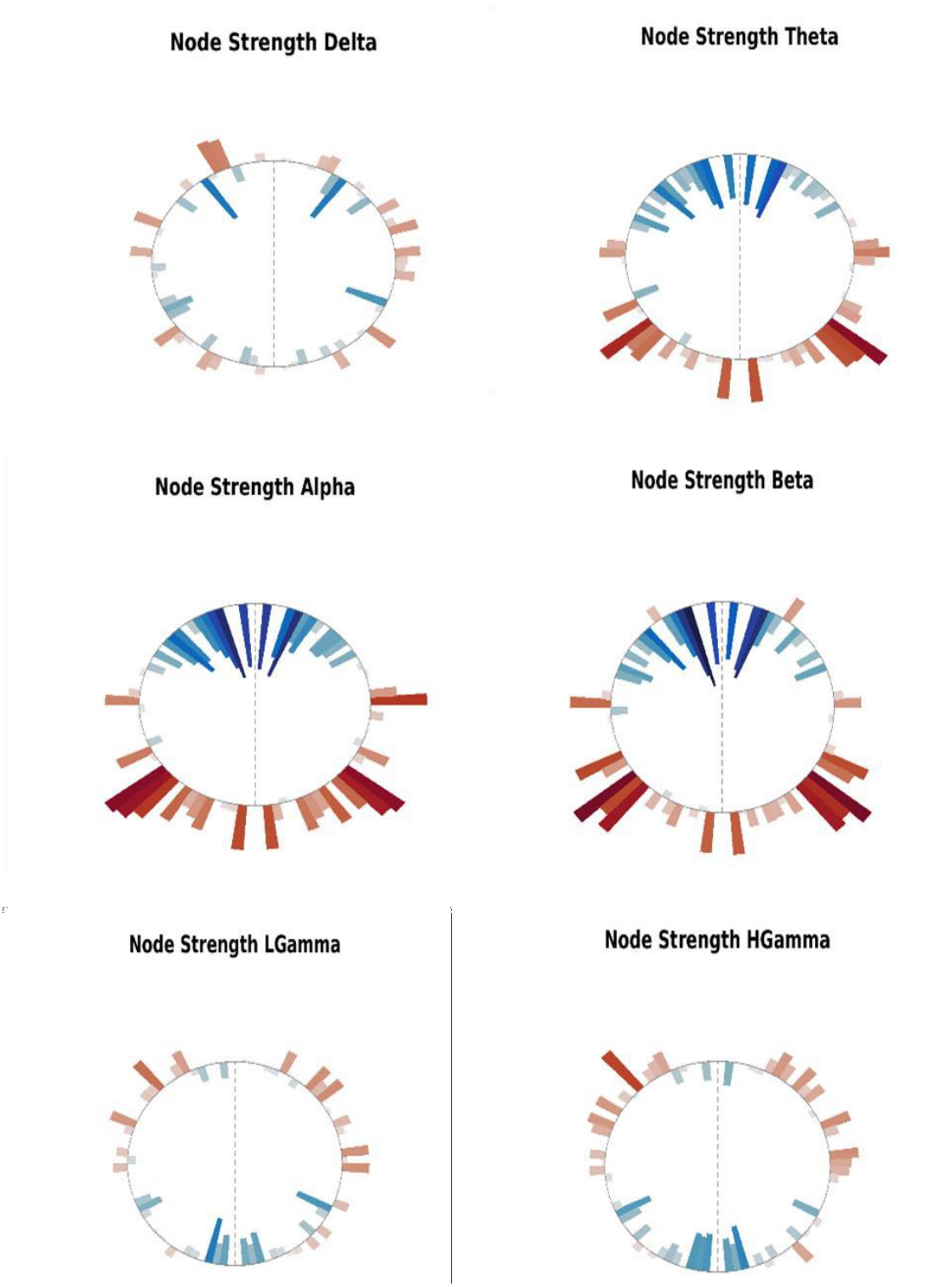

Figure 6.19: *Circle plots demonstrating the patterns of Node connectivity strength for all MEG frequency bands. Each bar in the circle plots depicts the amplitude of the strength of each node in the Desikan-Killian atlas. The regions with the highest connectivity strength are depicted in Red.* The *Desikan-Killian atlas areas are split into left and right and grouped around the plot as follows from top to bottom: cingulate cortex (top), frontal regions, insula, temporal lobe, sensorimotor regions, parietal, occipital cortex and precuneus (bottom).*

Myelin and MEG-derived functional Connectivity Strength

When correcting for multiple comparisons (threshold of 0.05 corrected for multiple comparisons across depths p-value =0.05/42 = 0.0071) significant positive correlations were found between connectivity strength and R1 in the theta, alpha and beta frequency bands at the deeper cortical depths, where these relationships were the strongest (see Table 6.4 and Figures 6.21-6.23). However, in the delta band, non-significant positive correlations were found between connectivity strength and R1 at all cortical depths investigated (see Table 6.4 and Figure 6.20).

In the low-gamma band a significant positive correlation was found between connectivity strength and R1 sampled superficially in the cortex (depth 1), see Figure 6.24. Finally, when considering the high-gamma band the strongest relationship was again found with the more superficial cortical depths, with a significant correlation documented between R1 values at depth 1 and MEG connectivity strength (see Table 6.4 and Figure 6.25).

Cortical Depth	Delta	p-val D	Theta	p-val T	Alpha	p-val A	Beta	p-val B	Low Gamma	p-val LG	High Gamma	p-val HG
1	0.323	0.013	0.124	0.352	0.137	0.304	-0.009	0.945	0.435	0.001	0.427	0.001
2	0.262	0.047	0.231	0.082	0.269	0.042	0.160	0.230	0.202	0.128	0.199	0.135
3	0.217	0.103	0.274	0.037	0.319	0.015	0.244	0.065	0.078	0.563	0.082	0.543
4	0.190	0.153	0.300	0.022	0.346	0.008	0.290	0.028	0.014	0.915	0.023	0.867
5	0.174	0.192	0.323	0.013	0.371	0.004	0.326	0.013	-0.033	0.808	-0.024	0.857
6	0.162	0.224	0.342	0.009	0.394	0.002	0.355	0.006	-0.079	0.554	-0.074	0.579
7	0.144	0.280	0.355	0.006	0.411	0.001	0.379	0.003	-0.127	0.342	-0.130	0.332

Table 6.4: *Correlations between R1 (myelin) and MEG connectivity strength at the 7 different cortical depths. Depth 1 is located the most superficially in the cortex, whereas depth 7 is the closest to the grey matter/white matter border.*

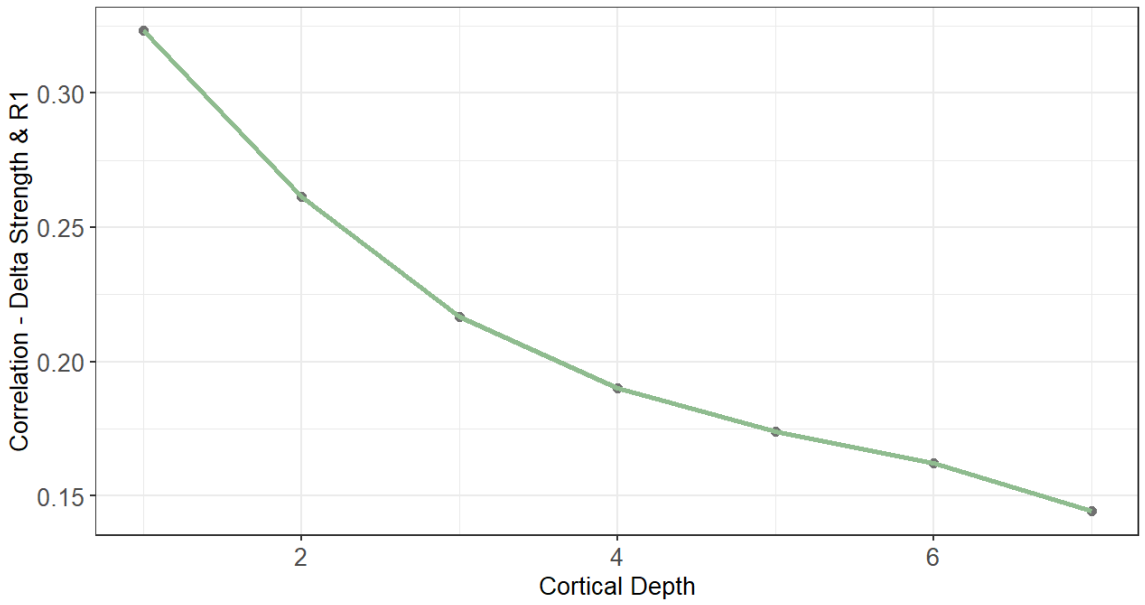

Figure 6.20: *Figure showing the correlations between Delta connectivity strength and R1 values sampled at different cortical depths. Depth 1 is located the most superficially in the cortex, whereas depth 7 is the closest to the grey matter/white matter border.*

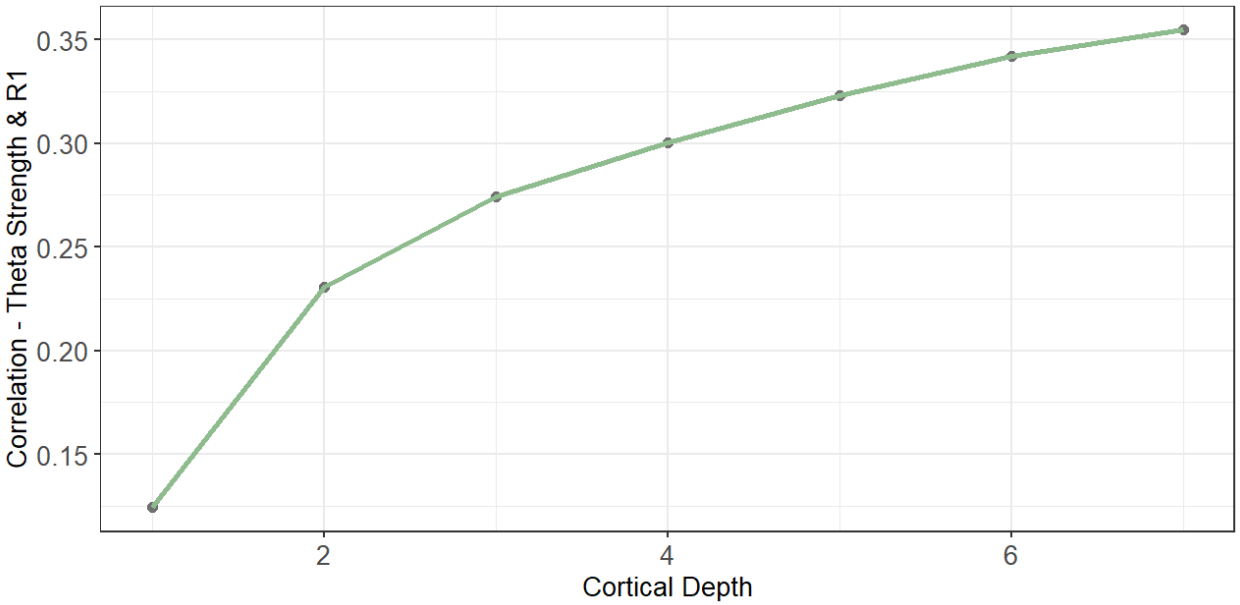

Figure 6.21: *Figure showing the correlations between Theta connectivity and R1 values sampled at different cortical depths. Depth 1 is located the most superficially in the cortex, whereas depth 7 is the closest to the grey matter/white matter border.*

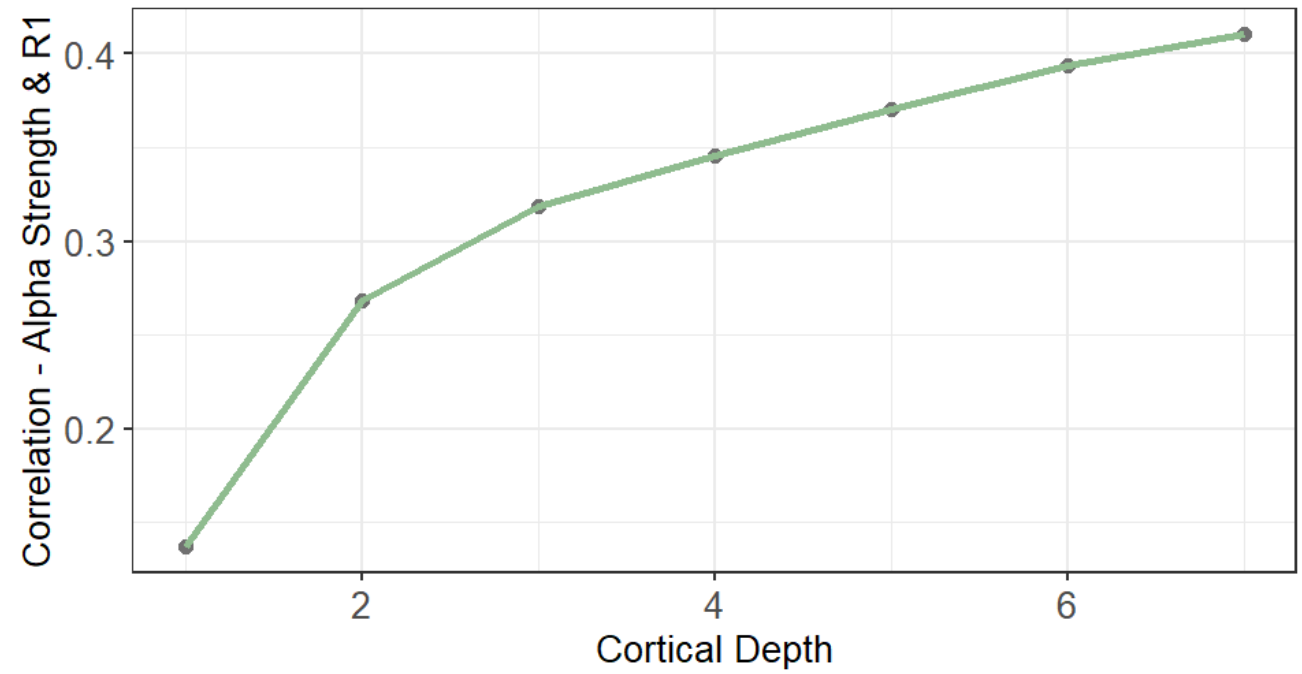

Figure 6.22: *Figure showing the correlations between Alpha connectivity strength and R1 values sampled at different cortical depths. Depth 1 is located the most superficially in the cortex, whereas depth 7 is the closest to the grey matter/white matter border.*

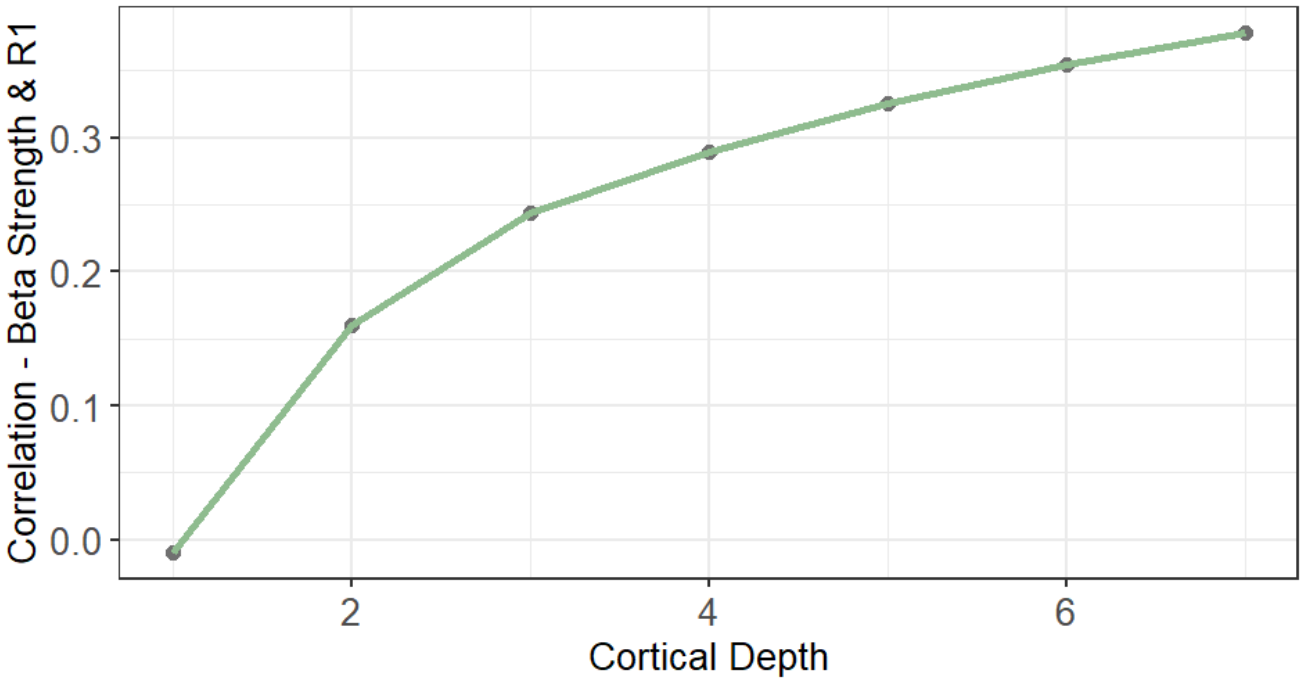

Figure 6.23: *Figure showing the correlations between Beta connectivity strength and R1 values sampled at different cortical depths. Depth 1 is located the most superficially in the cortex, whereas depth 7 is the closest to the grey matter/white matter border.*

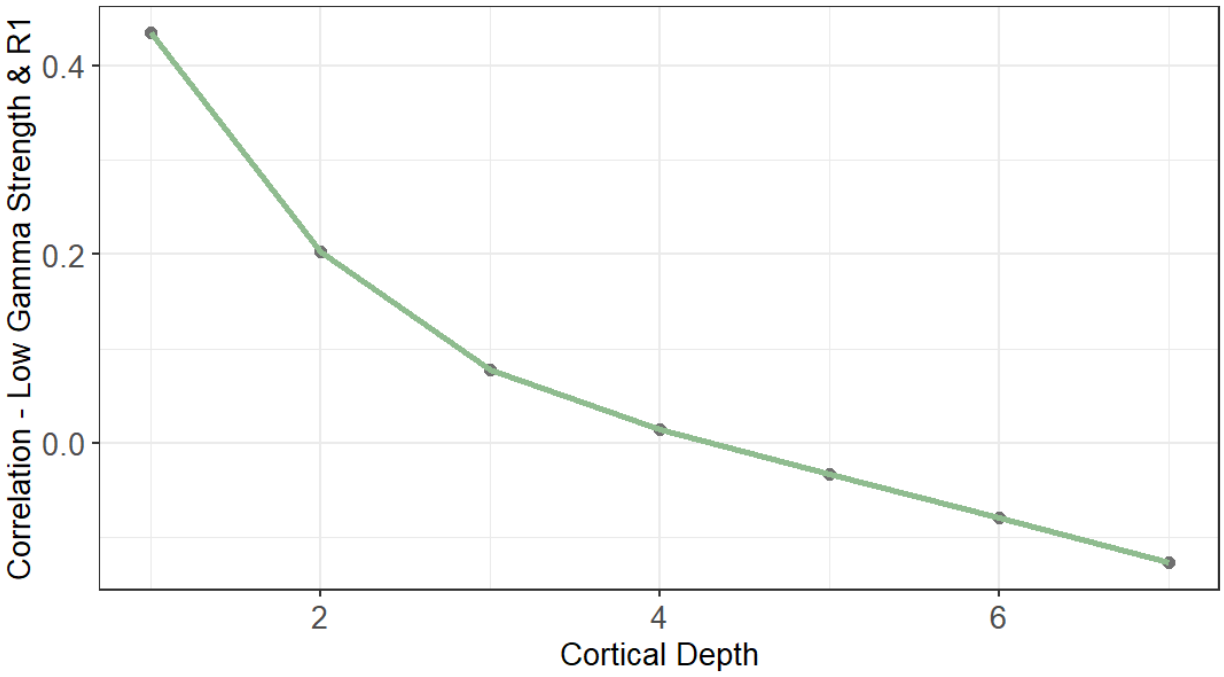

Figure 6.24: *Figure showing the correlations between Low Gamma connectivity strength and R1 values sampled at different cortical depths. Depth 1 is located the most superficially in the cortex, whereas depth 7 is the closest to the grey matter/white matter border.*

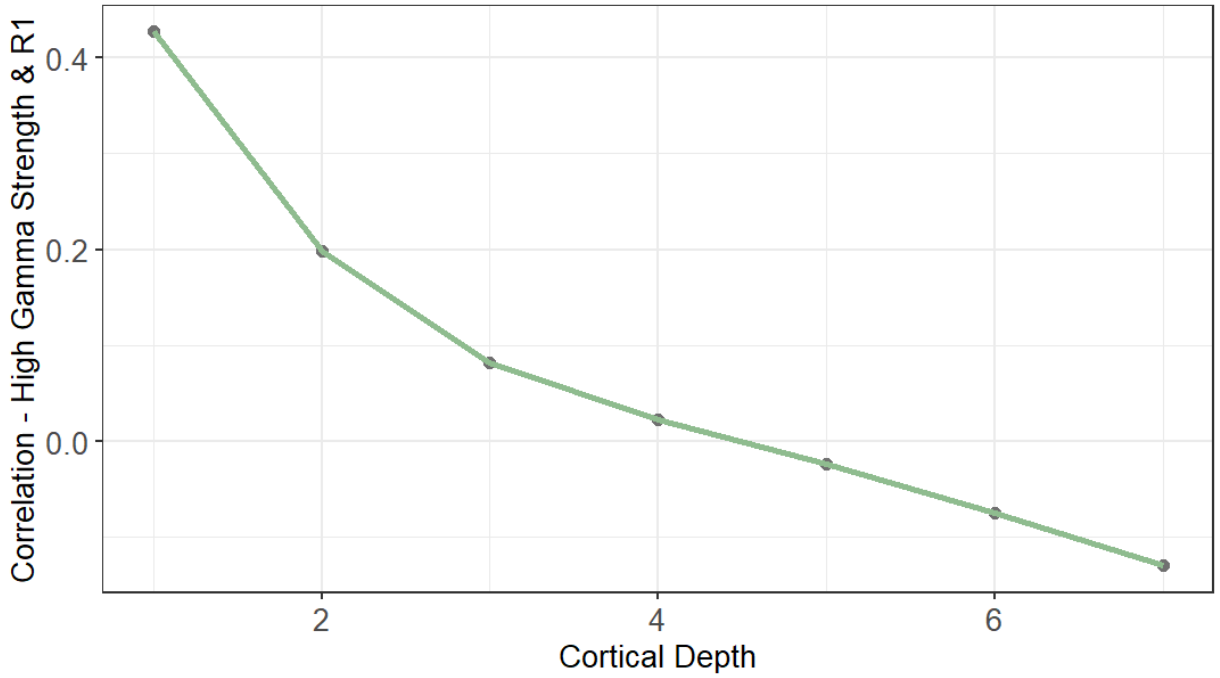

Figure 6.25: *Figure showing the correlations between High Gamma connectivity strength and R1 values sampled at different cortical depths. Depth 1 is located the most superficially in the cortex, whereas depth 7 is the closest to the grey matter/white matter border.*

183 Sample

Interestingly, a similar pattern to that outlined above is also observed when the myelin values were correlated with the connectivity matrices derived from the larger cohort study of 183 participants (see Table 6.5 and Figures 6.26-6.31).

Cortical Depth	Delta	p-val D	Theta	p-val T	Alpha	p-val A	Beta	p-val B	Low Gamma	p-val LG	High Gamma	p-val HG
1	0.078	0.563	0.122	0.361	0.110	0.110	-0.061	0.650	0.442	0.001	0.472	0.000
2	-0.052	0.701	0.205	0.123	0.270	0.270	0.126	0.345	0.169	0.204	0.210	0.113
3	-0.113	0.401	0.235	0.075	0.332	0.332	0.219	0.098	0.029	0.827	0.073	0.585
4	-0.141	0.290	0.255	0.054	0.364	0.364	0.269	0.041	-0.040	0.768	0.007	0.959
5	-0.159	0.234	0.273	0.038	0.390	0.390	0.306	0.020	-0.092	0.495	-0.043	0.747
6	-0.167	0.211	0.288	0.028	0.414	0.414	0.333	0.011	-0.146	0.275	-0.097	0.470
7	-0.177	0.184	0.295	0.025	0.428	0.428	0.354	0.007	-0.211	0.112	-0.159	0.234

Table 6.5: *Table depicting the correlations between R1 (myelin) and MEG connectivitystrength at each of the 7 cortical depths for the cohort of 183 subjects.*

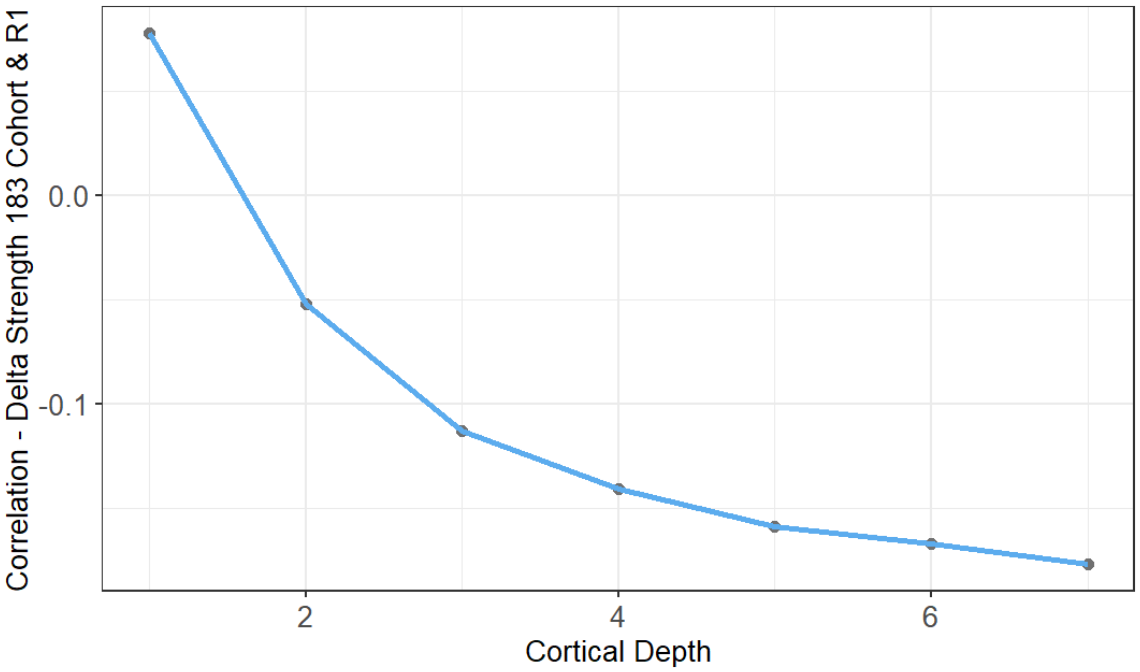

Figure 6.26: *Figure showing the correlations between Delta connectivity strength and R1 values sampled at the 7 cortical depths for the cohort of 183 subjects.*

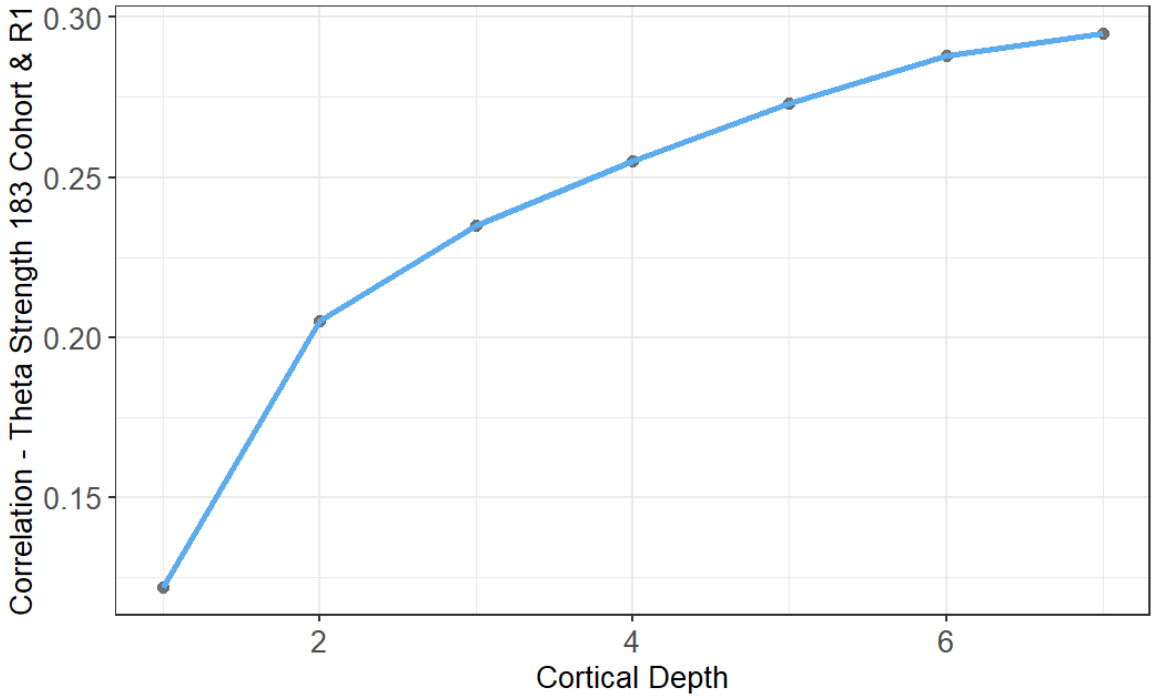

Figure 6.27: *Figure showing the correlations between Theta connectivity strength and R1 values sampled at the 7 cortical depths for the cohort of 183 subjects.*

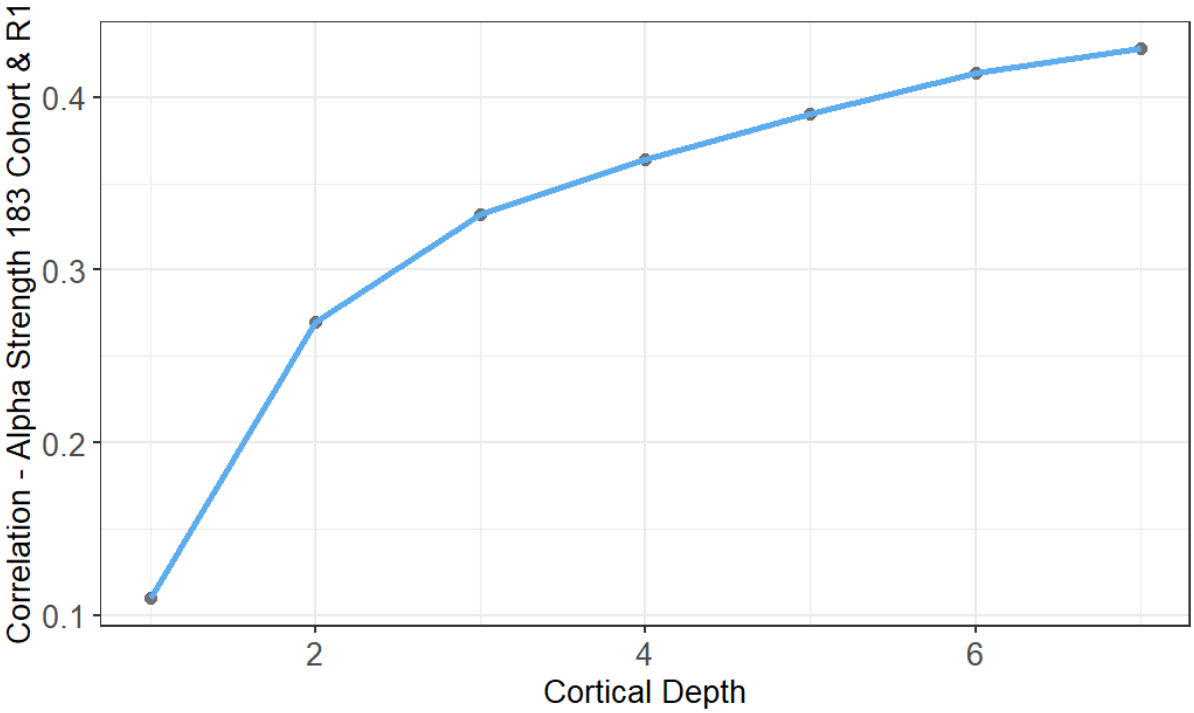

Figure 6.28: *Figure showing the correlations between Alpha connectivity strength and R1 values sampled at the 7 cortical depths for the cohort of 183 subjects.*

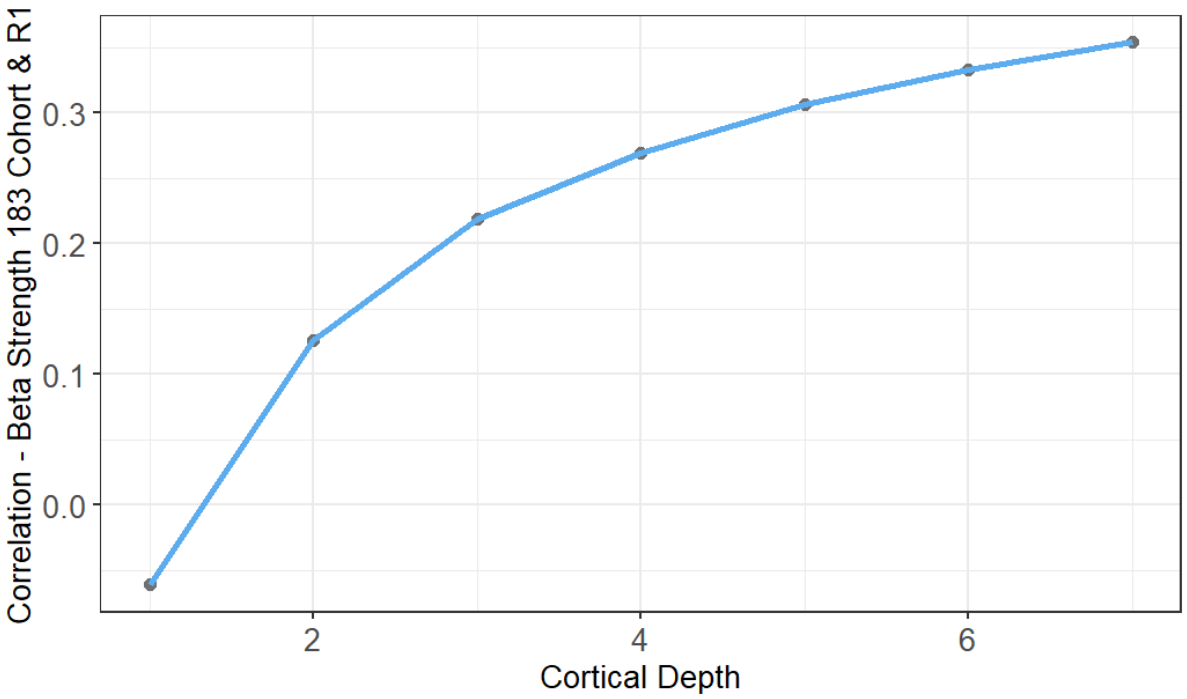

Figure 6.29: *Figure showing the correlations between Beta connectivity strength and R1 values sampled at the 7 cortical depths for the cohort of 183 subjects.*

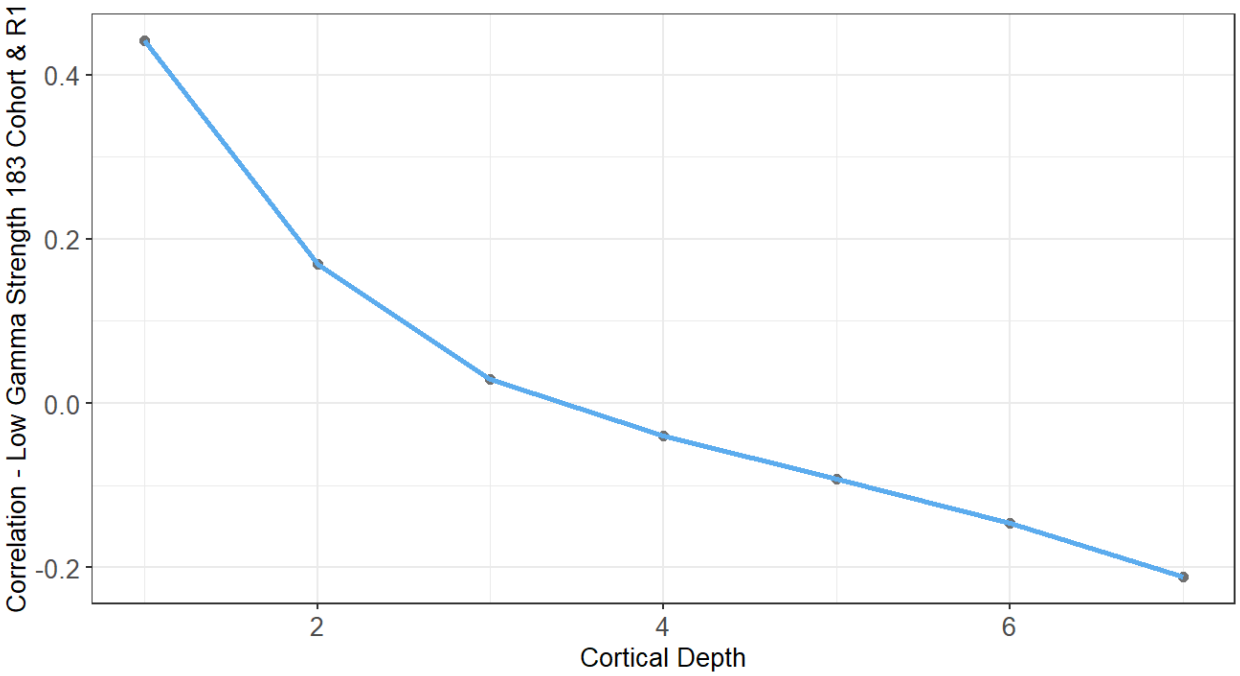

Figure 6.30: *Figure showing the correlations between Low Gamma connectivity strength and R1 values sampled at the 7 cortical depths for the cohort of 183 subjects.*

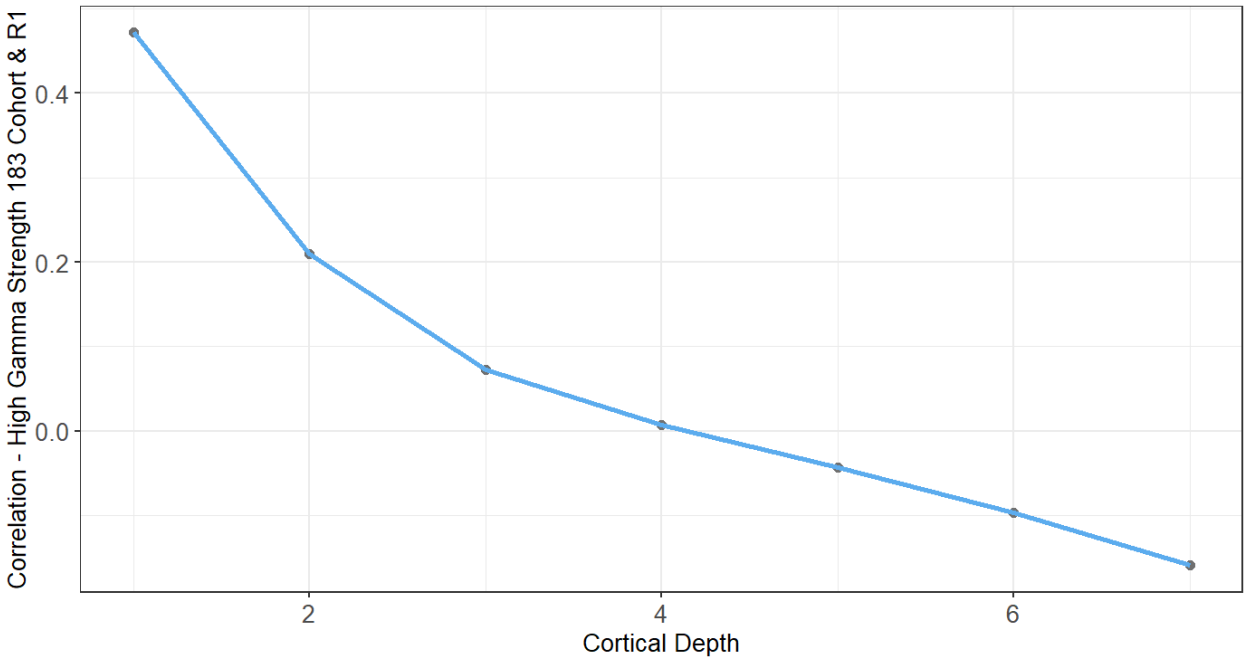

Figure 6.31: *Figure showing the correlations between High Gamma connectivity strength and R1 values sampled at the 7 cortical depths for the cohort of 183 subjects*

6.5 Discussion

Despite decades of research, the question of how the unique structure of the brain relates to its function, at both the local and network level, remains largely unanswered. However, recent advances in neuroimaging are bringing us ever closer to unravelling the precise nature of this intricate relationship. By exploiting the highresolution of 7T MRI in combination with MEG, here, for the first time, we report evidence of a cortical depth-dependent relationship between frequency specific oscillatory networks and the cortical myeloarchitecture.

The results of our structural covariance analysis revealed evidence of a positive relationship between R1 and MEG connectivity in all frequency bands, pointing to the existence of a relationship between functional connectivity indexed by oscillatory networks and structural connectivity indexed by myelin within the grey matter.

Interestingly, the present study also found that the relationships between the myelin structural covariance networks and the frequency specific MEG networks demonstrated a depth-specific pattern. Notably, in all frequency bands, stronger correlations were found between the myelin covariance matrices at deeper cortical depths and the functional MEG networks. Thus, these data suggest that the variation in myelination observed across the cortical depth might be of functional significance.

With regards to the relationship between cortical myelination and MEG connectivity strength an interesting, and largely concordant, pattern of results was also observed. In the theta, alpha and beta bands we observed a significant positive correlation between MEG connectivity strength and R1 sampled at lower cortical depths. Thus, regions with greater myelination in deeper layers of the cortex were found to demonstrate higher functional connectivity in these frequency bands. This finding adds to a growing body of evidence suggesting that an intricate relationship exists between the brain's microstructure, indexed by myelin, and functional oscillatory networks. Our results also revealed that in both the high and low gamma bands a significant positive correlation was found between MEG connectivity strength and cortical myelination when considering the more superficial cortical depths investigated in this study. Notably, this pattern of findings was also broadly replicated when the R1 data collected as part of this investigation was correlated with MEG strength data derived from a further sample of 183 individuals from a larger cohort

study. Whilst further replication in a sample of participants in which both MEG connectivity and R1 data are available would be beneficial, this can nevertheless be seen to lend considerable weight to the robustness of the findings of this investigation.

In light of these findings, the results of the present study pose a number of important questions with regards to not only how but also why some cortical regions might come to be more heavily myelinated than others and in what way this might relate to their function and connectivity patterns. Notably, the results of the present study also concur with that of Hunt et al. (2016) in pointing to a close relationship between the cortical myeloarchitecture and electrophysiological networks. As such it can be seen to add to the growing body of evidence suggesting that the cortical myeloarchitecture is likely shaped to support neural activity and synchrony.

To date, myelin has been extensively implicated in sub-serving brain communication through its ability to help speed nerve conduction (Fields, 2014). However, the majority of studies to date have focused on the importance of white matter myelination and its role in neuronal synchronisation, with little attention paid to its grey matter counterpart. Yet, intra-cortical myelin is also suggested to play a key role in optimizing the timing and synchrony of action potentials, a necessity for the optimal functioning of neuronal networks (Tardif et al. 2015). As argued by Hunt et al. (2016), given the vital role myelin plays in increasing the speed of neural communication in the brain, it is likely that cortical myelination may therefore be shaped to support oscillatory networks, allowing these to form with greater efficiency.

However, whilst the role of myelin in speeding the conduction of action potentials, a factor that could indeed facilitate oscillatory communication and synchrony, remains undisputed, other theories regarding the role of myelination in the cortex have been suggested. For example, Braitenberg (1968) suggested that a principle motivation for the myelination of axons in the cortex may be to prevent the formation of aberrant synaptic connections given that new connections cannot be formed on already myelinated axons. Furthermore, myelination has been shown to suppress synaptic plasticity by inhibiting neurite growth (Lozano, Schmidt & Roach, 1995; Thallmair et al., 1998). Thus, it has been suggested that heavily myelinated regions may be less plastic than their lightly myelinated counterparts. A key piece of evidence in support of this assertion, pointed to by Glasser et al. (2014), comes from observations of congenitally blind patients whose primary visual

cortices also show an important myeloarchetonic feature, the highly myelinated stria of Gennari. This suggests its development is independent of visual experience, it does not require such experience to be maintained, and is thus not strongly influenced by plasticity (Trampel et al., 2011). Hence, there may be additional benefits to myelination in the cortex that may be of relevance to understanding the contribution of cortical myelination to the function of cortical areas and in particular their microcircuitry and connectivity patterns. Additional research is required to further explore these intriguing possibilities.

Regardless, the results presented here can be taken to suggest that higher myelination is likely an adaptation designed to facilitate oscillatory connectivity between brain regions. However, it is also true that in addition to myelinated tangential intra-cortical axons, it is possible that more densely connected regions may also have a greater proportion of radial fibres originating from the white matter. Naturally, this would also increase the concentration of myelin in such regions. Hence, this might also have contributed to the observed relationship between connectivity strength and myelination to some extent. Further work encompassing histology-based investigations of the relative proportions of myelinated radial and axial fibres in the cortex may have the potential to shed further light on the contributions of particular axonal populations to the R1 values measured in the cortex. Similarly, with continued advances in diffusion imaging methods targeting the visualisation of the cortex (Balasubramanian et al., 2020) it might also be feasible to one day utilise high-resolution diffusion acquisitions to explore and disentangle the contributions and origins of the various fibre populations in the cortex.

A further possibility explored by the present study is that microstructural similarity might also be a driver of connectivity, and thus, regardless of the absolute concentration of myelin, connections may preferentially occur between regions with a similar myelin distribution. In support of this, we found evidence suggestive of a relationship between microstructural similarity and connectivity. In the delta, theta beta and gamma bands, significant negative correlations were found between the connectivity matrices and R1 difference matrices sampled at each of the cortical depths. Similarly, significant negative relationships were found between alpha networks and the R1 difference matrices at the majority of cortical depths. Thus, regions with more similar intracortical R1 (myelin) showed higher functional connectivity than did regions that differ in their intracortical R1 values. Furthermore, these relationships also demonstrated a depth-specific pattern. For

example, there was a stronger correlation between oscillatory networks in both the low and high gamma bands and the R1 difference matrices sampled from mid- superficial regions of the cortex compared to those sampled deep in the cortex.

These findings echo that of a previous study by Huntenberg et al. (2017) that used fMRI in combination with T1 imaging and found that regions with similar myelin content showed higher functional connectivity. Our findings can be seen to further support the idea that microstructural similarity may enhance communication between brain regions or may at least be predictive of this. Intriguingly, a growing number of studies are now also beginning to look at the development of the cortical myeloarchitecture. This provides a unique opportunity to explore the possibility that common patterns of myelination may be related to shared developmental trajectories and experiences during development, which might in turn facilitate both the formation of and communication within cortical networks.

For more than a century the existence of waves of myelination in the brain have been hypothesised, with the early writings of Flechsig (1901) proposing that rather than developing simultaneously across brain regions, cortical myelin instead develops in a succession of stages. For example, heavily myelinated areas such as the primary sensory and motor areas typically myelinate earlier than the more lightly myelinated association areas (Glasser and Van Essen, 2011). Utilising an impressive sample of 484 participants, aged 8-85 years, a further study by Grydeland et al. (2019) also documented evidence of waves of intracortical myelinogenesis. In this study early maturing regions were again largely identified as the heavily myelinated primary motor and sensory cortices, whereas later maturing regions were chiefly association, limbic and insular cortices. Furthermore, these changes have also been demonstrated at the level of the cortical laminae with specific changes in myelination having been reported during adolescence (Paquola et al., 2019).

Intriguingly, it is notable that sensory regions, known to show high myelin concentrations and similar developmental trajectories, typically dominate networks in the alpha and beta bands. This raises the possibility that the development of cortical myelination may have a profound effect on the developmentof oscillatory networks in the brain and vice versa, again pointing to the close relationship between the cortical myeloarchitectural and neural

activity. Further studies employing longitudinal assessments of the development of oscillatory networks and the cortical myeloarchitectural will be of great benefit to further exploring this possibility.

The results of all three analyses presented in the current investigation further extend previous work to show that the relationship between the cortical myeloarchitecture and oscillatory networks follows a depth-specific pattern. The findings of the present study therefore point to the importance of considering how the microstructure of the cortex varies with cortical depth. This work can thus be seen to have important implications, particularly in the context of attempts to link the cortical microstructure to its functional dynamics. Significantly, our finding of a depth specific relationship between cortical myelin and oscillations supports the results of animal studies suggesting that lower frequency oscillations including alpha and beta, originate from deeper layers of the cortex (Bonaiuto et al., 2018; Michalareas et al., 2016; Scheeringa, & Fries, 2017; Buffalo et al., 2012). On the basis of this evidence these different frequencies have been ascribed specific functional roles within the brain. Specifically, lower frequency oscillations, originating from the infragranular layers of the cortex, have been implicated in top-down feedback communication within the brain. Whereas higher frequency signals arising from the supragranular layers have been implicated in bottom-up feedforward communication (Michalareas et al., 2016) .

In humans, evidence for this theory has been obtained largely indirectly, however recent MEG studies have attempted to investigate this laminar specific hypothesis non-invasively utilising modelling approaches in combination with improvements in SNR gained through the use of subject specific head masks (Bonaiuto et al.,2018). However, it should be noted that much of the evidence to date, in both human and animal models alike, has focused on primary sensory and sensory motor regions of the brain (Bonaiuto et al., 2018). The results presented here support the findings of previous studies suggestive of a laminar pattern of frequency specific communication in the brain whilst further suggesting that this pattern likely extends to networks across the brain.

Significantly, abnormalities in myelin, oscillatory dynamics, connectivity, and laminar-specific microstructural parameters have all been extensively implicated in a wide array of clinical conditions. The present study can therefore be seen to provide an interesting framework to investigate clinical populations. For example, the demyelination of cortical

grey matter observed in patients with MS is thought to impact cognitive functioning by disturbing the co-ordinated interaction between neurons both within and across brain areas. Schoonhoven et al. (2018) showed that slowing of neuronal activity, particularly in the alpha band, as measured by resting-state MEG, correlated with cognitive impairment in patients with MS. However, in such studies the cortical myeloarchitecture was not investigated.

Thus, applying the approach of the present study to investigate the relationship between the cortical myeloarchitecture and oscillatory networks in conditions such as MS could have the potential to provide valuable new insights into the pathophysiology of such conditions.

That said, there are a number of limitations regarding the present study that must be take into consideration. In particular, it should be noted that the myelin estimates in this study were based on the measurement of T1 which is an indirect measure of myelin. Accordingly, these results should be interpreted with caution. Validation against histological data has shown that cortical T1 contrast is reflective of its myelin content, however it should be noted that iron has also been shown to contribute to T1 contrast in the cortex (Stuber et al., 2014). Thus, it is possible that our T1 estimates may also reflect the degree of intracortical iron to some extent. However, given that myelin and iron are typically strongly co-localised in the cortex, it has been argued that independent of the exact contribution of iron and myelin, T1 can be justified as largely reflecting the distribution of intracortical myelin (Huntenburg et al., 2017). Moreover, in contrast to several other approaches quantitative T1 has been shown to demonstrate the highest intrasubject and intersubject reliability with regards to mapping intracortical myelin (Haast et al. 2016).

It is also of note that in this study the right hemisphere ROIs showed higher R1 than their left hemisphere counterparts. However, rather than reflecting a true hemispheric asymmetry in cortical myelination this is likely to have been driven by variation in cortical thickness. In line with previous investigations (e.g. Luders et al., 2006), participants in this study displayed a pattern of greater cortical thickness in the left hemisphere compared to the right hemisphere. Furthermore, we also noted a negative correlation between cortical thickness and R1 in this dataset. Thus, it may be speculated that the greater R1 values in the right hemispheres ROIs in this study may in fact have been driven by hemispheric

differences in cortical thickness. The thinner cortex in the right hemisphere may have led to increased partial voluming with the white matter surface and thus the placement of the surfaces deeper in the cortex in the right hemisphere. This would explain why higher R1 values were observed in the right hemisphere ROI's.

In this study we also chose to use the Desikan-Killian atlas to parcellate our datasets. The Desikan-Killian atlas consists of 68 cortical regions and can thus be seen to provide a relatively small number of regions, especially given the high resolution of our MR datasets. However given the much lower spatial resolution ofour MEG datasets it would likely prove challenging to adopt a finer parcellation scheme and thus it is important to strike a balance between the capabilities of each technique in the context of multi-modal imaging approaches such as this.

Finally, performing an un-biased statistical analysis on the results outlined in this chapter presents a significant challenge. Indeed, given the large number of data points the p-values presented for the structural covariance and R1 difference analysis are essentially meaningless and thus confer little information with regards to the significance of the correlation values. Other statistical approaches such as the use of randomisation tests to estimate a null distribution are also fraught with challenges in this context given that attempts to randomise the MEG or Myelin correlation matrices destroys their structure rendering any such analysis inherently biased. Thus, investigating possible alternative approaches for determining statistical significance in the context if the analyses presented here will necessarily be a key focus for future investigations.

In conclusion, the present study demonstrates, for the first time, non-invasive evidence of a depth specific relationship between oscillatory networks and the cortical myeloarchitecure in humans. These results can be seen to demonstrate the value of considering how the microstructure of the cortex varies with cortical depth given that this might have important implications for attempts to investigate the relationship between brain structure and function. Ultimately, this research might also pave the way for a greater understanding of the pathophysiology of clinical conditions in which myelin abnormalities and aberrant connectivity are implicated.

Chapter 7

General Discussion

The principle aim of this thesis was to explore the relationship between cortical myelination and neural oscillatory dynamics. To this end we leveraged high resolution 7T MRI in combination with a variety of MEG paradigms, in order to investigate the relationship between R1 (1/T1), an MRI-derived proxy for cortical myelination, and oscillatory dynamics. This relationship was explored at both the local level, in the primary visual and auditory cortices, and using a whole brain network-based approach. In this chapter the main findings of this thesis and their interpretation and limitations are discussed. Finally, we look forward to possible future avenues of research.

7.1 Summary of findings

In **Chapter 3** of this thesis we investigated the relationship between the amplitude of visual gamma oscillations and myelination (R1) of the primary visual cortex. We did not find evidence of a significant positive correlation between gamma amplitude and R1 as hypothesised. However, the results of our analysis of the relationship between the full frequency spectra and our myelin estimates were certainly intriguing. More specifically, we found evidence of a relationship between superficial myelin content and gamma oscillations occurring at a frequency of approximately 40 Hz. Furthermore, in the baseline period, the strongest correlations were found between lower frequency beta activity (~15-20 Hz) and R1 values sampled deep in the cortex.

In **Chapter 4** we explored the relationship between visual gamma oscillatory dynamics and cortical myelination further through the use of a neurophysiologically informed modelling approach (DCM). The aim of this chapter was to harness the greater specificity of this computational modelling approach to probe the potential existence of a relationship between cortical myelin and specific aspects of the cortical microcircuitry involved in the generation of visual gamma oscillations. We did not find evidence of a significant relationship between any of the DCM model parameters and our myelin estimates at any of the cortical depths investigated in this

study. However, there were some interesting trends observed in the data. For example, the relationship between the peak gamma amplitude derived from the DCM model and R1 was found to be positive and was also strongest at more superficial cortical depths. Furthermore, a trend towards a negative correlation between the beta peak frequency and superficial cortical myelin estimates was also observed.

In **Chapter 5** of this thesis, we moved beyond the visual cortex and explored the relationship between gamma auditory steady state responses (ASSRs) and myelination of the primary auditory cortex. Again, we were not able to detect statistically significant relationships between our myelin estimates and the amplitude of gamma band ASSRs. However, a trend indicative of a positive correlation between the amplitude of the ASSR and cortical myelination, particularly at lower cortical depths, was observed.

The aforementioned chapters explored the relationship between oscillatory dynamics and cortical myelination in local regions of interest, namely the primary visual and auditory cortices. However, in the final experimental chapter of this thesis, **Chapter 6,** we explored the relationship between cortical myelination and oscillatory dynamics at the network level. In this chapter we investigated, for the first time, the relationship between depth specific estimates of intra-cortical myelin and functional oscillatory networks. Notably, we were able to demonstrate the novel finding of a cortical depth-dependent relationship between cortical myelin and frequency-specific resting-state MEG networks.

7.2 Interpretation

Taken together the results of this thesis can be seen to raise some interesting questions with regards to the relationship between MEG oscillatory dynamics and the cortical myeloarchitecure. In Chapters 3 and 4, we did not replicate Helbling et al's (2015) finding of a significant positive correlation between MEG derived electrophysiological responses and cortical myelin content, at least in the case of peak amplitude estimates. However, this could be interpreted as an interesting finding in and of itself. Although some interesting trends were observed, these did not survive appropriate correction for multiple comparisons. As discussed in Chapter 3, there are methodological factors at play that might have influenced this null finding. Nevertheless, it is interesting to note that whilst our investigation focused on the visual cortex and oscillatory dynamics thereof, auditory evoked response fields and thus auditory cortical areas were the substrate of interest in the

investigation by Helbing et al. (2015). Thus, one potential interpretation of our findings is that they might speak to the presence of inherent differences in the mechanisms of generation of these two distinct types of neural activity and/or a different coupling of structure and function in these areas.

The results of Chapter 3's whole spectra analysis did point to a potential relationship between lower frequency gamma activity, occurring at approximately 40 Hz, and myelination of primary visual cortex. Interestingly, activity around 40 Hz has been proposed to represent a resonance frequency, at least in the case of the auditory cortex. Furthermore, in Chapter 5 of this thesis we were able to observe a trend indicating a potential relationship between low gamma ASSRs, occurring at around 40 Hz and cortical myelination. Thus, taken together, the results of Chapters 3and 5 converge to suggest that 40 Hz activity in particular might be related to the cortical myeloarchitecture. The findings of Chapters 3 and 5 regarding 40 Hz activity can also be seen to be of particular pertinence given that 40 Hz activity is slowly emerging as being of special neurological importance (McDermott et al., 2018). In Chapter 5 of this thesis the fact that 40 Hz ASSRs have been extensively implicated in a wide array of psychiatric disorders including schizophrenia (Thuné, Recasens, & Uhlhaas, 2016) and autism was discussed (Seymour et al., 2020).

Activity at 40 Hz has also been the subject of increasing attention of late, owing to the emergence of a novel therapeutic technique. This involves light stimulation at 40 Hz which has been found to reduced amyloid levels in mouse models of Alzheimer's disease. For example, using optogenetics and a non-invasive light flicker treatment Iaccarino et al. (2016) found that gamma frequency entrainment at40 Hz, but not at other frequencies, led to a noticeable reduction in amyloid beta peptides in multiple mouse models and was also accompanied by increased microglia activity. Although much future work is needed to uncover the meaning of these results, and indeed how they might translate to humans, results such as these are certainly interesting.

In sum, the results presented in this thesis, and their suggestion of a potential relationship between gamma frequency activity at ~ 40 Hz and cortical myelin content, could ultimately be of great clinical relevance. Thus, further replication of the trends reported here is definitely warranted.

A key achievement of the present thesis was the novel finding, documented in Chapter 6, of a cortical depth-dependent relationship between oscillatory MEG networks and intra-cortical myelin. Akin to Hunt et al., (2016) we speculate that one interpretation of this

finding is that the cortical myeloarchitecture may be shaped in order to facilitate oscillatory communication between brain regions. Moreover, our results go one step further to suggest that this relationship also extends to the level of individual cortical layers. Similarly, Chapters 3-5 of this thesis also provide some indication of depth specificity to the observed effects. Thus, the results of this thesis can be seen to have important implications for other research in this field and point to the importance of considering the rich variability of the microstructural patterns observed across the cortical depth, rather than treating it as a uniform whole.

7.3 Limitations and Methodological considerations

Study specific methodological limitations are discussed within each experimental chapter of this thesis. However, in this section we provide a more general overview of some of the key methodological considerations that may be deemed particularly pertinent to the experiments conducted in this thesis.

Samples and Statistics

A significant limitation of the investigations employed in this thesis is their reliance on correlational methods. Consequently, it is not possible to draw conclusions about causal relationships between the variables investigated in the experiments presented here. Furthermore, as highlighted in Chapters 3, 4 and 5, our sample size was somewhat limited. Thus, it is likely that we may have been underpowered to detect statistically significant relationships. Compounding this issue is the fact that we employed a sample of healthy young adults, in which variations in cortical myelin content are highly likely to be subtle. Thus, it will be important for future studies to consider employing larger samples sizes. Finally, it will likely also be of benefit to explore the relationship between cortical myelin and oscillatory dynamics in a population in which myelin abnormalities are known to be present, in addition to a healthy control group. In such a population, larger inter-individual differences in cortical myelination are likely to be present, thus providing greater potential to explore how such differences might relate to functional oscillatory dynamics. Furthermore, in the context of such a group comparison, the ability to draw upon potentially more powerful statistical methods, rather than correlation-based analyses, would be a possibility.

Cortical parcellation schemes

In this thesis we chose to use the Desikan atlas, included in the Freesurfer software distribution, in order to define our regions of interest. The Desikan atlas consists of atotal of 68 regions (34 for each hemisphere). In light of the high-resolution of our datasets it might therefore be argued that utilising a finer parcellation scheme than this would have allowed for a more accurate and precise delineation of our regions of interest. This point can be seen as of particular pertinence when considered in light of the fact that studies of the cortical myeloarchitecture have distinguished approximately 200 different cortical areas (Nieuwenhuys, 2013). In addition to adopting a finer parcellation scheme, it might also have been of benefit to utilise an atlas explicitly derived from the myeloarchitecture in order to ensure that our myelin estimates follow true myeloarchitectural boundaries. Prior studies have previously shown the utility of such an approach. For example, utilising a multi-modal imaging approach that incorporated analysis of the cortical myelin content Glasser et al., (2016) produced a population based cortical parcellation consisting of 180 areas per hemisphere.

However, the mismatch in spatial resolution between our high-resolution MRI images and MEG data presents a significant challenge in this respect. Indeed, whilst MEG possesses excellent temporal resolution, on the order of milliseconds, its spatial resolution is more limited in comparison to what can now be achieved using 7T MRI and is thought to approach only a few millimetres. That said, recent methodological developments may hold the key to this predicament. In particular, optically pumped magnetometers (OPM's) represent an exciting emerging technology in the MEG field. In contrast to traditional MEG systems OPMs can be placed in close proximity to the scalp and thus have the potential to boost both sensitivity to neural dynamics, and importantly, spatial resolution (Iivanainen,Zetter, & Parkkonen , 2020).

Myelin and T1 – a troubled relationship?

The measurement of T1 represents a popular MRI method for investigating cortical myelin content in-vivo. However, as with all such MRI-derived measures, it is ultimately an indirect measure of myelin. T1 is also known to be sensitive to other aspects of the cortical

microstructure including its iron content, which has been found to show strong colocalization with myelin in the cortex (Fukunaga, et al., 2010).

It is also notable that large variations in T1 values have been reported in the literature (Stikov et al., 2015), even in instances where similar methods have been used. As argued by Rioux, Levesque, & Rutt (2016) this raises the troubling prospect that there might be some further sources of variability contributing to the measurement of T1 that are as yet unaccounted for.

In this thesis we chose to use the MP2RAGE sequence in order to derive high- resolution T1 maps of the cortex. This decision was largely driven by the suitability of this technique for use at high field and its ability to produce high-resolution T1 maps in feasible acquisition times. Although T1 values derived using the MP2RAGEhave been shown to demonstrate good reproducibility in a number of investigations, including our own, concerns have been raised regarding the ability of the MP2RAGEsequence to accurately measured T1 due to the effect of magnetisation transfer (MT) which causes biexponential relaxation. For example, Rioux, Levesque, & Rutt (2016) found that assuming a monoexponential recovery (as is the case with most T1 measurements) can lead to parameter-dependent variability in T1 especially when imaging at 7T.

While Rioux, Levesque, & Rutt (2016) propose corrections that can be applied to mitigate this problem, these are not applicable to the MP2RAGE in its current form given that it relies on only two points to characterise the T1 curve and thus cannot characterise the biexponential recovery that occurs due to the presence of multi-compartment tissue types (Marques, & Norris, 2018). Consequently, depending on the particular sequence parameters used, such as the inversion times, there might be a variable contribution of different tissue compartments to the estimated T1 values (Marques &Norris, 2018).

Importantly, the study by Rioux, Levesque, & Rutt (2016) outlined above, focused on estimates of T1 in the white matter, which would be expected to have a larger MT effect given that higher MT effects are typically found in the white matter as compared to the grey matter (Tofts, Steens & van Buchem, 2003). However, previous reports have documented evidence of biexponential longitudinal relaxation in the cortical grey matter (e.g. Prantner et al., 2008). Thus, it may be of value to investigate the potential effects of biexponential recovery in the grey matter on T1 estimates derived using the MP2RAGE. Were such effects to be found, this is likely to have a particular impact on comparison of T1 values derived using different acquisition protocols. The points raised here can be seen

to speak to the fact that T1 maps derived using the MP2RAGE may exhibit greater precision than accuracy (Marques, & Norris, 2018).

There continues to exist an ongoing debate within the neuroimaging field regarding which MRI measure might provide the most accurate assessment of the brain's myelin content. Nevertheless, it is possible that other MRI methods, such as qMT, may show greater specificity to cortical myelin. Indeed, a recent meta-analysis of quantitative MRI-histology comparisons by Mancini et al. (2020) found that the myelin proton fraction (MPF) and myelin water fraction (MWF) tended to be more specific to myelin than the other measures investigated, with coefficient of determination values of 0.7657 and 0.6997 respectively (Mancini et al., 2020). T1 was found to have the next highest coefficient of determination at 0.5321. It is somewhat unsurprising that the strongest values were found for the MPF and MWF in this investigation as theoretically speaking, they should be more specific to myelin. However, akin to the other methods investigated, even these metrics showed fairly large prediction intervals, calling into question the robustness of these measures and thus their validity as a true myelin biomarker. Consequently, the authors conclude that there is still much work to be done with regards to determining the specificity of MR measures (Mancini et al., 2020).

A further meta-analysis of histological validation studies of MRI-derived myelin measures by Lazari, & Lipp (2020) paints a somewhat similar picture. In this study a number of markers including R1 were found to correlate with myelin. However, again the authors argue that it is difficult to answer the question as to how the investigated MR measures compare to one another with regards to their myelin sensitivity. This is due to the observed large degree of heterogeneity in methodologies employed by studies in the field, which could have influenced the reported effect sizes. Echoing this sentiment, a further recent review of available MRI methods came to the rather sobering conclusion that due to the lack of reproducibility studies and available data from animal and ex-vivo studies, reaching a definitive conclusion and recommendation regarding the optimal MRI method for quantifying myelin in the brain is not currently feasible, or indeed advisable (van der Weijden et al., 2020).

In sum, although demonstrated to be highly reproducible, MP2RAGE and indeed T1 measurements more broadly may be argued to possess a number of limitations with regards to their ability to accurately quantify myelin content in the brain. However, as outlined above, all in-vivo MRI derived measures of cortical myelin are by their very nature indirect and thus we must rely on histological validation in order to assess their

utility as a myelin biomarker. Consequently, further validation studies and comparisons of the available methods are required. To date myelin abnormalities have been well documented in an array of psychiatric and neurological disorders, such as multiple sclerosis (MS). Thus, the ability to accurately characterise myelin in-vivo is of great clinical significance, highlighting the vital importance of continued research in this area.

Until such a time as a consensus has been reached in the field regarding the most appropriate choice of myelin biomarker, adopting multiple myelin sensitive image contrasts in MRI acquisitions might be considered a particularly attractive option. Indeed Lazari, & Lipp (2020) argue that, for now at least, this might represent the best way to verify myelin related hypotheses. Of note, employing multiple myelin markers has been shown to provide complementary information, useful in investigations of pathology (Lipp et al., 2019). Furthermore, as discussed in Chapter 6 of this thesis, utilising QSM in combination with T2* could help to disentangle the contribution of iron from myelin Duyn (2017) due to their different magnetic properties. Indeed, it has been demonstrated that modelling approaches utilising information from susceptibility values and R2* (combined with estimates of myelin content from magnetisation transfer contrast) can allow for the quantification of iron and myelin content (Schweser, Deistung, Lehr, Sommer, & Reichenbach, 2011). Thus, utilising multiple image contrasts may offer the potential to obtain myelin/diamagnetic cortical maps clean of iron/paramagnetic contributions (and vice versa) (Marques, Khabipova, & Gruetter, 2017).

7.4 Future research directions

The results of this thesis point to a number of exciting future avenues of research. In particular, given that both myelin abnormalities and aberrant oscillatory dynamics have been widely implicated in a variety of psychiatric disorders, such as schizophrenia, adopting the methods employed here to investigate the relationship between cortical myelin and oscillatory dynamic in such populations has the potential to provide further insights into the pathophysiology of such conditions.

Similarly, as discussed in Chapter 6, the cortical myeloarchitecture undergoes profound changes during childhood and adolescence, with different developmental trajectories of cortical myelin evident at the level of both cortical regions and layers (Lebenberg et al.,

2019; Grydeland et al., 2019; Whitaker et al., 2016; Paquola et al., 2019). In line with the results of previous studies, and indeed the findings presented here, suggesting a potentially intricate link between cortical myelin and oscillatory dynamics, it may be argued that the maturation of cortical myelination is likely of great functional significance. However, no studies have yet investigated how the timing of changes in cortical myelin during development might relate to oscillatory dynamics, the onset of developmental disorders and the acquisition of cognitive milestones. To date, a key barrier to the wider uptake of neurodevelopmental studies of oscillatory dynamics has been the lack of suitable measurement technologies, given the significant constraints of both EEG (e.g. spatial resolution) and MEG (e.g.head size, movement). However, as aforementioned, recent years have witnessed the emergence of new, wearable, MEG technologies based on optically pumped magnetometers (OPMs). Critically, these devices can be placed closer to the scalp surface, increasing sensitivity and are robust to head-movement. Thus, one potentially fruitful avenue of research would be to adopt a multi-modal approach similar to that utilised here, combining electrophysiological measures (e.g. MEG or OPMs) of neural oscillations with high-resolution MRI imaging of the cortical microstructure, in order to investigate structural and functional aspects of brain maturation and the intricate relationships between them. Such an approach might ultimately pave the way for greater insights into neurodevelopmental disorders and eventually help guide the development of effective therapeutic approaches and identify key strategic timepoints for intervention.

However, crucial to the interpretation of the potential findings of such research, will be further experimental explorations with the specific aim of disentangling the multiple proposed functional roles of myelin highlighted in the introduction of this thesis.

7.5 Concluding Remarks

In conclusion, the principle aim of this thesis was to investigate the relationship between the cortical myeloarchitecture and neural oscillatory dynamics, with the goal of gaining further insights into these key aspects of brain structure and function.To this end we conducted novel investigations of the relationship between depth- specific cortical myelin estimates and the morphology of neural oscillations in the primary auditory and visual cortices. Significantly in these investigations, we were able to document some trends in the data indicative of a relationship between oscillatory activity, particular in the low

gamma (~40 Hz) range and cortical myelination. Here, for the first time, we also found evidence of depth-dependent relationships between oscillatory networks and cortical myelin. Further investigationand replication of the findings presented here in a larger sample is needed.

Furthermore, there are a number of methodological limitations that should be taken into consideration when interpreting these findings. Ultimately, the approaches presented in this thesis provide a potentially useful framework for investigating the pathophysiology of clinical conditions and atypical development and can thus be seen to pave the way for a number of exciting avenues of future research.

References

Abragam, A. (1961). The Principles of Nuclear Magnetism. Clarendon Press

Adaikkan, C., & Tsai, L. H. (2020). Gamma entrainment: impact on neurocircuits,glia, and therapeutic opportunities. *Trends in Neurosciences*, *43*(1), 24-41.

Alegre, M., Molero, P., Valencia, M., Mayner, G., Ortuño, F., & Artieda, J. (2017). Atypical antipsychotics normalize low-gamma evoked oscillations in patients with schizophrenia. *Psychiatry research*, *247*, 214-221.

Alexander-Bloch, A., Giedd, J. N., & Bullmore, E. (2013). Imaging structural co- variance between human brain regions. *Nature Reviews Neuroscience*, *14*(5), 322-336.

Allen, M., Glen, J. C., Müllensiefen, D., Schwarzkopf, D. S., Fardo, F., Frank, D., ...& Rees, G. (2017). Metacognitive ability correlates with hippocampal and prefrontalmicrostructure. *NeuroImage*, *149*, 415-423.

Amunts, K., & Zilles, K. (2015). Architectonic mapping of the human brain beyond Brodmann. *Neuron*, *88*(6), 1086-1107.

Arrondo, G., Alegre, M., Sepulcre, J., Iriarte, J., Artieda, J., & Villoslada, P. (2009). Abnormalities in brain synchronization are correlated with cognitive impairment in multiple sclerosis. *Multiple Sclerosis Journal*, *15*(4), 509-516.

Artieda, J., Valencia, M., Alegre, M., Olaziregi, O., Urrestarazu, E., & Iriarte, J. (2004). Potentials evoked by chirp-modulated tones: a new technique to evaluate oscillatory activity in the auditory pathway. *Clinical neurophysiology*, *115*(3), 699-709.

Ashburner, J., Barnes, G., Chen, C. C., Daunizeau, J., Flandin, G., Friston, K., ... & Penny, W. (2014). SPM12 manual. *Wellcome Trust Centre for Neuroimaging, London, UK*, *2464*.

Baillet, Sylvain. (2017) Magnetoencephalography for brain electrophysiology and imaging. *Nature neuroscience 20*(3), 327-339.

Baillet, S., Mosher, J. C., & Leahy, R. M. (2001). Electromagnetic brain mapping. *IEEE Signal processing magazine*, *18*(6), 14-30.

Baillet S. (2010). The dowser in the fields: searching for MEG sources.In Hansen, P., Kringelbach, M., & Salmelin, R. (Eds.).*MEG: An introduction to methods*.pp. 83-123.Oxford University Press.

Balchandani, P., & Naidich, T. P. (2015). Ultra-high-field MR neuroimaging. *American Journal of Neuroradiology*, *36*(7), 1204-1215.

Balasubramanian, M., Mulkern, R. V., Neil, J. J., Maier, S. E., & Polimeni, J. R. (2020). Probing in vivo cortical myeloarchitecture in humans via line-scan diffusionacquisitions at 7 T with 250-500 micron radial resolution. *Magnetic resonance in medicine*, *85*(1), 390-403.

Barbier, E. L., Marrett, S., Danek, A., Vortmeyer, A., Van Gelderen, P., Duyn, J., ... & Koretsky, A. P. (2002). Imaging cortical anatomy by high-resolution MR at 3.0 T: detection of the stripe of Gennari in visual area 17. *Magnetic Resonance in Medicine: An*

Official Journal of the International Society for Magnetic Resonance in Medicine, *48*(4), 735-738.

Barnes, G. R., & Hillebrand, A. (2003). Statistical flattening of MEG beamformerimages. *Human brain mapping*, *18*(1), 1-12.

Barratt, E. L., Tewarie, P. K., Clarke, M. A., Hall, E. L., Gowland, P. A., Morris, P.G., ... & Brookes, M. J. (2017). Abnormal task driven neural oscillations in multiplesclerosis: A visuomotor MEG study. *Human Brain Mapping*, *38*(5), 2441-2453.

Başar, E., Femir, B., Emek-Savaş, D. D., Güntekin, B., & Yener, G. G. (2017).Increased long distance event-related gamma band connectivity in Alzheimer'sdisease. *NeuroImage: Clinical*, *14*, 580-590.

Bastos, A. M., Vezoli, J., Bosman, C. A., Schoffelen, J. M., Oostenveld, R., Dowdall, J. R., ... & Fries, P. (2015). Visual areas exert feedforward and feedbackinfluences through distinct frequency channels. *Neuron*, *85*(2), 390-401.

Bartoli, E., Bosking, W., Chen, Y., Li, Y., Sheth, S. A., Beauchamp, M. S., ... & Foster, B. L. (2019). Functionally distinct gamma range activity revealed by stimulus tuning in human visual cortex. *Current Biology*, *29*(20), 3345-3358.

Bauer, M., Stenner, M. P., Friston, K. J., & Dolan, R. J. (2014). Attentional modulation of alpha/beta and gamma oscillations reflect functionally distinct processes. *Journal of Neuroscience*, *34*(48), 16117-16125.

Bazin, P. L., Weiss, M., Dinse, J., Schäfer, A., Trampel, R., & Turner, R. (2014). A computational framework for ultra-high resolution cortical segmentation at 7Tesla. *Neuroimage*, *93*, 201-209.

Beul, S. F., Barbas, H., & Hilgetag, C. C. (2017). A predictive structural model ofthe primate connectome. *Scientific Reports*, *7*

Bok, S. T. (1929).Der Einfluß der in den Furchen und Windungen auftretenden Krümmungen der Großhirnrinde auf die Rindenarchitektur. *Zeitschrift für die gesamte Neurologie und Psychiatrie*, *121*(1), 682.

Bonaiuto, J. J., Rossiter, H. E., Meyer, S. S., Adams, N., Little, S., Callaghan, M. F.,... & Barnes, G. R. (2018). Non-invasive laminar inference with MEG: Comparison of methods and source inversion algorithms. *NeuroImage*, *167*, 372-383.

Bock, N. A., Hashim, E., Janik, R., Konyer, N. B., Weiss, M., Stanisz, G. J., ... & Geyer, S. (2013). Optimizing T 1-weighted imaging of cortical myelin content at 3.0 T. *Neuroimage*, *65*, 1-12.

Braitenberg, V. (1962). A note on myeloarchitectonics. *Journal of comparative Neurology,* 118(2), 141-156.

Brealy, J. (2015). *The relationship between variation in genes, GABA, structure and gamma oscillations in the visual and auditory system of healthy individuals and psychiatric disorder* (Doctoral dissertation, Cardiff University).

Bressler, S. L., & Menon, V. (2010). Large-scale brain networks in cognition: emerging methods and principles. *Trends in cognitive sciences*, *14*(6), 277-290.

Brodmann, K. (1908). *Beiträge zur histologischen Lokalisation der Großhirnrinde*.

Brookes, M. J., Tewarie, P. K., Hunt, B. A., Robson, S. E., Gascoyne, L. E., Liddle,E. B., ... & Morris, P. G. (2016). A multi-layer network approach to MEGconnectivity analysis. *NeuroImage*, *132*, 425-438.

Buffalo, E. A., Fries, P., Landman, R., Buschman, T. J., & Desimone, R. (2011).

Laminar differences in gamma and alpha coherence in the ventral stream. *Proceedings of the National Academy of Sciences*, *108*(27), 11262-11267.

Buzsáki, G., & Wang, X. J. (2012). Mechanisms of gamma oscillations. *Annual review of neuroscience*, *35*, 203-225.

Calhoun, V. D., & Sui, J. (2016). Multimodal fusion of brain imaging data: A key to finding the missing link (s) in complex mental illness. *Biological Psychiatry: Cognitive Neuroscience and Neuroimaging*, *1*(3), 230-24

Castelo-Branco, M., Neuenschwander, S., & Singer, W. (1998). Synchronization of visual responses between the cortex, lateral geniculate nucleus, and retina in the anesthetized cat. *Journal of neuroscience*, *18*(16), 6395-6410.

Cohen, D. (1968). Magnetoencephalography: evidence of magnetic fields produced by alpha-rhythm currents. *Science*, *161*(3843), 784-786.

Cohen-Adad, J. (2014). What can we learn from T 2* maps of thecortex? *NeuroImage*, *93*, 189-200.

Colclough, G. L., Brookes, M. J., Smith, S. M., & Woolrich, M. W. (2015). A symmetric multivariate leakage correction for MEG connectomes. *Neuroimage*, *117*,439-448.

Colclough, G. L., Woolrich, M. W., Tewarie, P. K., Brookes, M. J., Quinn, A. J., & Smith, S. M. (2016). How reliable are MEG resting-state connectivity metrics?. *Neuroimage*, *138*, 284-293.

Cornew, L., Roberts, T. P., Blaskey, L., & Edgar, J. C. (2012). Resting-stateoscillatory activity in autism spectrum disorders. *Journal of autism and developmental disorders*, *42*(9), 1884-1894.

Cousijn, H., Haegens, S., Wallis, G., Near, J., Stokes, M. G., Harrison, P. J., & Nobre, A. C. (2014). Resting GABA and glutamate concentrations do not predict visual gamma frequency or amplitude. *Proceedings of the National Academy of Sciences*, *111*(25), 9301-9306.

Dale, A. M., Fischl, B., & Sereno, M. I. (1999). Cortical surface-based analysis: I. Segmentation and surface reconstruction. *Neuroimage*, *9*(2), 179-194.

da Rocha, J. L. D., Schneider, P., Benner, J., Santoro, R., Atanasova, T., Van De Ville, D., & Golestani, N. (2020). tASH: toolbox for the Automated Segmentation ofHeschl's gyrus. *Scientific reports*, *10*(1), 1-15.

da Silva, F. L. (2013). EEG and MEG: relevance to neuroscience. *Neuron*, *80*(5), 1112-1128.

Dassios, G., & Fokas, A. S. (2013). The definite non-uniqueness results fordeterministic EEG and MEG data. *Inverse Problems*, *29*(6), 065012.

David, O., Kiebel, S. J., Harrison, L. M., Mattout, J., Kilner, J. M., & Friston, K. J.(2006). Dynamic causal modeling of evoked responses in EEG and MEG. *NeuroImage*, *30*(4), 1255-1272.

de Beeck, H. O., & Nakatani, C. (2019). *Introduction to human neuroimaging*. Cambridge University Press.

DeFelipe, J., & Fariñas, I. (1992). The pyramidal neuron of the cerebral cortex: morphological and chemical characteristics of the synaptic inputs. *Progress in neurobiology*, *39*(6), 563-607.

Delorme, A., & Makeig, S. (2004). EEGLAB: an open source toolbox for analysis of single-trial EEG dynamics including independent component analysis. *Journal of neuroscience methods*, *134*(1), 9-21.

De Martino, F., Moerel, M., Xu, J., van de Moortele, P. F., Ugurbil, K., Goebel, R.,... & Formisano, E. (2015). High-resolution mapping of myeloarchitecture in vivo:localization of auditory areas in the human brain. *Cerebral Cortex*, *25*(10), 3394- 3405.

Deistung, A., Schäfer, A., Schweser, F., Biedermann, U., Turner, R., & Reichenbach, J. R. (2013). Toward in vivo histology: a comparison of quantitative susceptibility mapping (QSM) with magnitude-, phase-, and R 2∗-imaging at ultra-high magnetic field strength. *Neuroimage*, *65*, 299-314.

Desikan, R. S., Ségonne, F., Fischl, B., Quinn, B. T., Dickerson, B. C., Blacker, D.,... & Killiany, R. J. (2006). An automated labeling system for subdividing the humancerebral cortex on MRI scans into gyral based regions of interest. *Neuroimage*, *31*(3), 968-980.

De Stefano, L. A., Schmitt, L. M., White, S. P., Mosconi, M. W., Sweeney, J. A., & Ethridge, L. E. (2019). Developmental effects on auditory neural oscillatory synchronization abnormalities in autism spectrum disorder. *Frontiers in integrative neuroscience*, *13*, 34.

Devlin, J. T., & Poldrack, R. A. (2007). In praise of tedious anatomy. *Neuroimage*, *37*(4), 1033-1041.

Dick, F., Tierney, A. T., Lutti, A., Josephs, O., Sereno, M. I., & Weiskopf, N.(2012). In vivo functional and myeloarchitectonic mapping of human primaryauditory areas. *Journal of Neuroscience*, *32*(46), 16095-16105.

Dinse, J., Härtwich, N., Waehnert, M. D., Tardif, C. L., Schäfer, A., Geyer, S., ... & Bazin, P. L. (2015). A cytoarchitecture-driven myelin model reveals area-specific signatures in human primary and secondary areas using ultra-high resolution in-vivobrain MRI. *Neuroimage*, *114*, 71-87.

Duyn, J. H. (2017). Studying brain microstructure with magnetic susceptibilitycontrast at high-field. *NeuroImage*.

Edgar, J. C., Chen, Y. H., Lanza, M., Howell, B., Chow, V. Y., Heiken, K., ... & Cañive, J. M. (2014). Cortical thickness as a contributor to abnormal oscillations in schizophrenia?. *NeuroImage: Clinical*, *4*, 122-129.

Edwards, L. J., Kirilina, E., Mohammadi, S., & Weiskopf, N. (2018).Microstructural imaging of human neocortex in vivo. *NeuroImage*.

Efron, B. (1979). Bootstrap Methods: Another Look at the Jackknife. *Ann. Statist. 7(1),* 1-26. doi:10.1214/aos/1176344552

Eggenschwiler, F., Kober, T., Magill, A. W., Gruetter, R., & Marques, J. P. (2012). SA2RAGE: A new sequence for fast $B1^{+}$+-mapping. *Magnetic resonance in medicine*, *67*(6), 1609-1619.

Engel, A. K., & Fries, P. (2010). Beta-band oscillations—signalling the status quo?. *Current opinion in neurobiology*, *20*(2), 156-165.

Engels, M. M. A., van Der Flier, W. M., Stam, C. J., Hillebrand, A., Scheltens, P., &van Straaten, E. C. W. (2017). Alzheimer's disease: the state of the art in resting- state magnetoencephalography. *Clinical Neurophysiology*, *128*(8), 1426-1437.

Ethridge, L. E., White, S. P., Mosconi, M. W., Wang, J., Pedapati, E. V., Erickson, C. A., ... & Sweeney, J. A. (2017). Neural synchronization deficits linked to corticalhyper-excitability and auditory hypersensitivity in fragile X syndrome. *Molecular autism*, *8*(1), 22.

Farahani, E. D., Wouters, J., & van Wieringen, A. (2020). Brain mapping of auditory steady-state responses: A broad view of cortical and subcortical sources. *Human Brain Mapping*.

Fields, R. D. (2014). Myelin—more than insulation. *Science*, *344*(6181), 264-266.

Fischl, B. (2012). FreeSurfer. *Neuroimage*, *62*(2), 774-781.

Friston, K. J., Harrison, L., & Penny, W. (2003). Dynamic causalmodelling. *Neuroimage*, *19*(4), 1273-1302.

Fukunaga, M., Li, T. Q., van Gelderen, P., de Zwart, J. A., Shmueli, K., Yao, B., ... & Duyn, J. H. (2010). Layer-specific variation of iron content in cerebral cortex as asource of MRI contrast. *Proceedings of the National Academy of Sciences*, *107*(8), 3834-3839.

Freund, P., Friston, K., Thompson, A. J., Stephan, K. E., Ashburner, J., Bach, D. R.,... & Schwab, M. E. (2016). Embodied neurology: an integrative framework forneurological disorders. *Brain*, *139*(6), 1855.

Galambos, R., Makeig, S., & Talmachoff, P. J. (1981). A 40- Hz auditory potential recorded from the human scalp. *Proceedings of the national academy of sciences*, *78*(4), 2643-2647.

Geyer, S., Weiss, M., Reimann, K., Lohmann, G., & Turner, R. (2011). Microstructural parcellation of the human cerebral cortex–from Brodmann's post-mortem map to in vivo mapping with high-field magnetic resonance imaging. *Frontiers in human neuroscience*, *5*, 19.

Ghaffarian, N., Mesgari, M., Cerina, M., Göbel, K., Budde, T., Speckmann, E. J., ...& Gorji, A. (2016). Thalamocortical-auditory network alterations following cuprizone-induced demyelination. *Journal of neuroinflammation*, *13*(1), 1-11.

Gibson, E. M., Purger, D., Mount, C. W., Goldstein, A. K., Lin, G. L., Wood, L. S.,... & Barres, B. A. (2014). Neuronal activity promotes oligodendrogenesis andadaptive myelination in the mammalian brain. *Science*, *344*(6183), 1252304.

Gilbert, C. D. (1983). Microcircuitry of the visual cortex. *Annual review ofneuroscience*, *6*(1), 217-247.

Glasser, M. F., Coalson, T. S., Robinson, E. C., Hacker, C. D., Harwell, J., Yacoub,E., ... & Van Essen, D. C. (2016). A multi-modal parcellation of human cerebral cortex. Nature, 536(7615), 171-178.

Glasser, M. F., & Van Essen, D. C. (2011). Mapping human cortical areas in vivo based on myelin content as revealed by T1-and T2-weighted MRI. *Journal of Neuroscience*, *31*(32), 11597-11616.

Gregory, S., Fusca, M., Rees, G., Schwarzkopf, D. S., & Barnes, G. (2016). Gamma Frequency and the Spatial Tuning of Primary Visual Cortex. *PloS one*, *11*(6), e0157374.

Griskova, I., Morup, M., Parnas, J., Ruksenas, O., & Arnfred, S. M. (2007). The amplitude and phase precision of 40 Hz auditory steady-state response depend on the level of arousal. *Experimental brain research*, *183*(1), 133-138.

Grydeland H., Walhovd K. B., Tamnes C. K., Westlye L. T., Fjell A. M. (2013). Intracortical myelin links with performance variability across the human lifespan:results from T1- and T2-weighted MRI myelin mapping and diffusion tensor imaging. J. Neurosci. 33, 18618– 18630

Grydeland, H., Westlye, L. T., Walhovd, K. B., & Fjell, A. M. (2015). Intracortical posterior cingulate myelin content relates to error processing: results from T1-and T2 weighted MRI myelin mapping and electrophysiology in healthy adults. *CerebralCortex*, bhv065.

Grydeland H., Vértes P. E., Váša F., Romero-Garcia R., Whitaker K., Alexander- Bloch A. F., et al. . (2019). Waves of maturation and senescence in microstructuralMRI markers of human cortical myelination over the lifespan. Cereb. Cortex 29, 1369–1381. 10.1093/cercor/bhy330

Haast, R. A., Ivanov, D., Formisano, E., & Uludağ, K. (2016). Reproducibility and reliability of quantitative and weighted T1 and T2 mapping for myelin-based cortical parcellation at 7 Tesla. *Frontiers in neuroanatomy*, *10*, 112.

Haast, R. A., Ivanov, D., & Uludağ, K. (2018). The impact of correction on MP2RAGE cortical T 1 and apparent cortical thickness at 7 T. *Human brainmapping*, *39*(6), 24122425.

Hall, E. L., Robson, S. E., Morris, P. G., & Brookes, M. J. (2014). The relationship between MEG and fMRI. *Neuroimage*, *102*, 80-91.

Hämäläinen, M., & Hari, R. (2002). Magnetoencephalographic (MEG) characterization of dynamic brain activation. *Brain mapping: the methods, Ed*, *2*, 227-254.

Hämäläinen, M., Hari, R., Ilmoniemi, R. J., Knuutila, J., & Lounasmaa, O. V. (1993). Magnetoencephalography—theory, instrumentation, and applications to noninvasive studies of the working human brain. *Reviews of modern Physics*, *65*(2), 413.

Hämäläinen, M. S., Lin, F. H., & Mosher, J. C. (2010). Anatomically and functionally constrained minimum-norm estimates. *MEG: an introduction tomethods (Hansen P, Kringelbach M, Salmelin R, eds)*, 186-215.

Hamm, J. P., Gilmore, C. S., Picchetti, N. A., Sponheim, S. R., & Clementz, B. A. (2011). Abnormalities of neuronal oscillations and temporal integration to low-and high-frequency auditory stimulation in schizophrenia. *Biological psychiatry*, *69*(10),989-996.

Hari, R., Parkkonen, L., & Nangini, C. (2010). The brain in time: insights from neuromagnetic recordings. *Annals of the New York Academy of Sciences*, *1191*(1), 89.

Hari, R., & Salmelin, R. (2012). Magnetoencephalography: From SQUIDs to neuroscience: Neuroimage 20th anniversary special edition. *Neuroimage*, *61*(2), 386-396.

Heinrich, S. P., & Bach, M. (2004). High-frequency oscillations in human visual cortex do not mirror retinal frequencies. *Neuroscience letters*, *369*(1), 55-58.

Helbling, S., Teki, S., Callaghan, M. F., Sedley, W., Mohammadi, S., Griffiths, T. D., ... & Barnes, G. R. (2015). Structure predicts function: combining non-invasive electrophysiology with in-vivo histology.Neuroimage, 108, 377-385.

Hellwig, B. (1993). How the myelin picture of the human cerebral cortex can becomputed from cytoarchitectural data. A bridge between von Economo and Vogt. *Journal für Hirnforschung*, *34*(3), 387.

Herculano-Houzel, S. (2009). The human brain in numbers: a linearly scaled-up primate brain. *Frontiers in human neuroscience*, *3*, 31.

Herdman, A. T., Lins, O., Van Roon, P., Stapells, D. R., Scherg, M., & Picton, T. W. (2002). Intracerebral sources of human auditory steady-state responses. *Brain topography*, *15*(2), 69-86.

Hillebrand, A., & Barnes, G. R. (2002). A quantitative assessment of the sensitivity of whole-head MEG to activity in the adult human cortex. *Neuroimage*, *16*(3), 638-650.

Hillebrand, A., Barnes, G. R., Bosboom, J. L., Berendse, H. W., & Stam, C. J. (2012). Frequency-dependent functional connectivity within resting-state networks:an atlas-based MEG beamformer solution. *Neuroimage*, *59*(4), 3909-3921.

Hillebrand, A., Singh, K. D., Holliday, I. E., Furlong, P. L., & Barnes, G. R. (2005).A new approach to neuroimaging with magnetoencephalography. *Human brain mapping*, *25*(2), 199-211.

Hinds, O. P., Rajendran, N., Polimeni, J. R., Augustinack, J. C., Wiggins, G., Wald,L. L., ... & Fischl, B. (2008). Accurate prediction of V1 location from cortical foldsin a surface coordinate system. *Neuroimage*, *39*(4), 1585-1599.

Hinkley, L. B., Vinogradov, S., Guggisberg, A. G., Fisher, M., Findlay, A. M., & Nagarajan, S. S. (2011). Clinical symptoms and alpha band resting-state functional connectivity imaging in patients with schizophrenia: implications for novel approaches to treatment. *Biological psychiatry*, *70*(12), 1134-1142.

Honey, C. J., Sporns, O., Cammoun, L., Gigandet, X., Thiran, J. P., Meuli, R., & Hagmann, P. (2009). Predicting human resting-state functional connectivity from structural connectivity. *Proceedings of the National Academy of Sciences*, *106*(6),2035-2040.

Hunt, B. A., Tewarie, P. K., Mougin, O. E., Geades, N., Jones, D. K., Singh, K. D.,... & Brookes, M. J. (2016). Relationships between cortical myeloarchitecture and electrophysiological networks. Proceedings of the National Academy of Sciences,113(47), 13510-13515.

Huntenburg, J. M., Bazin, P. L., Goulas, A., Tardif, C. L., Villringer, A., & Margulies, D. S. (2017). A Systematic Relationship Between Functional Connectivity and Intracortical Myelin in the Human Cerebral Cortex. *CerebralCortex*, *27*(2), 981-997.

Hurley, A. C., Al-Radaideh, A., Bai, L., Aickelin, U., Coxon, R., Glover, P., & Gowland, P. A. (2010). Tailored RF pulse for magnetization inversion at ultrahigh field. *Magnetic Resonance in Medicine: An Official Journal of the International Society for Magnetic Resonance in Medicine*, *63*(1), 51-58.

Iaccarino, H. F., Singer, A. C., Martorell, A. J., Rudenko, A., Gao, F., Gillingham, T.Z., ... & Tsai, L. H. (2016). Gamma frequency entrainment attenuates amyloid load and modifies microglia. *Nature*, *540*(7632), 230-235.

Isomura, S., Onitsuka, T., Tsuchimoto, R., Nakamura, I., Hirano, S., Oda, Y., ... & Kanba, S. (2016). Differentiation between major depressive disorder and bipolar disorder by auditory steady-state responses. *Journal of affective disorders*, *190*, 800-806.

Iivanainen, J., Zetter, R., & Parkkonen, L. (2020). Potential of on-scalp MEG:Robust detection of human visual gamma-band responses. *Human brain mapping*, *41*(1), 150-161.

Johns, P. (2014). Chapter 3 - Functional neuroanatomy. In Johns, P (Eds) *Clinical Neuroscience,* pp.27-47, Churchill Livingstone. https://doi.org/10.1016/B978-0-443-10321-6.00003-5.

Kapfhammer, Josef, and Martin E. Schwab. "Inverse patterns of myelination and GAP-43 expression in the adult CNS: neurite growth inhibitors as regulators of neuronal plasticity?." *Journal of Comparative Neurology* 340.2 (1994): 194-206.

Kim, S., Jang, S. K., Kim, D. W., Shim, M., Kim, Y. W., Im, C. H., & Lee, S. H. (2019). Cortical volume and 40-Hz auditory-steady-state responses in patients with schizophrenia and healthy controls. *NeuroImage: Clinical*, *22*, 101732.

Kim, S. G., & Knösche, T. R. (2016). Intracortical myelination in musicians with absolute pitch: Quantitative morphometry using 7-T MRI. *Human brain mapping*,*37*(10), 3486-3501.

Koelewijn, L., Lancaster, T. M., Linden, D., Dima, D. C., Routley, B. C., Magazzini,L., ... & Bompas, A. (2019). Oscillatory hyperactivity and hyperconnectivity in young APOE-ε4 carriers and hypoconnectivity in Alzheimer's disease. *Elife*, *8*, e36011.

Koenig, S. H. (1991). Cholesterol of myelin is the determinant of gray-white contrast in MRI of brain. *Magnetic resonance in medicine*, *20*(2), 285-291.

Lachaux, J. P., Rodriguez, E., Martinerie, J., & Varela, F. J. (1999). Measuring phase synchrony in brain signals. *Human brain mapping*, *8*(4), 194-208.

Lauterbur, P. C. (1973). Image formation by induced local interactions: examples employing nuclear magnetic resonance. *nature*, *242*(5394), 190-191.

Lazari, A., & Lipp, I. (2020). Can MRI measure myelin? Systematic review, qualitative assessment, and meta-analysis of studies validating microstructuralimaging with myelin histology. *bioRxiv*.

Lebenberg, J., Mangin, J. F., Thirion, B., Poupon, C., Hertz-Pannier, L., Leroy, F., ... & Dubois, J. (2019). Mapping the asynchrony of cortical maturation in the infant brain: a MRI multi-parametric clustering approach. *Neuroimage*, *185*, 641-653.

Lee, C. C. (2013). Thalamic and cortical pathways supporting auditoryprocessing. *Brain and language*, *126*(1), 22-28.

Lins, O. G., Picton, P. E., Picton, T. W., Champagne, S. C., & Durieux-Smith, A.(1995). Auditory steady-state responses to tones amplitude-modulated at 80–110 Hz. *The Journal of the Acoustical Society of America*, *97*(5), 3051-3063.

Lipp, I., Jones, D. K., Bells, S., Sgarlata, E., Foster, C., Stickland, R., ... & Tomassini, V. (2019). Comparing MRI metrics to quantify white matter microstructural damage in multiple sclerosis. Human brain mapping, 40(10), 2917-2932.

Lozano, A. M., Schmidt, M., & Roach, A. (1995). A convenient in vitro assay for the inhibition of neurite outgrowth by adult mammalian CNS myelin using immortalized neuronal cells. *Journal of neuroscience methods*, *63*(1-2), 23-28.

Luders, E., Narr, K. L., Thompson, P. M., Rex, D. E., Jancke, L., & Toga, A. W. (2006). Hemispheric asymmetries in cortical thickness. *Cerebral Cortex*, *16*(8), 1232-1238.

Lutti, A., Dick, F., Sereno, M. I., & Weiskopf, N. (2014). Using high-resolution quantitative mapping of R1 as an index of cortical myelination.*Neuroimage*, *93*, 176-188

Lutti, A., Stadler, J., Josephs, O., Windischberger, C., Speck, O., Bernarding, J., ... & Weiskopf, N. (2012). Robust and fast whole brain mapping of the RF transmit field B1 at 7T. *PLoS One*, *7*(3), e32379.

Magazzini, L., Muthukumaraswamy, S. D., Campbell, A. E., Hamandi, K., Lingford-Hughes, A., Myers, J. F., ... & Singh, K. D. (2016). Significant reductions in human visual gamma frequency by the gaba reuptake inhibitor tiagabine revealed by robust peak frequency estimation. *Human brain mapping*, *37*(11), 3882-3896.

Mancini, M., Karakuzu, A., Nichols, T., Cohen-Adad, J., Cercignani, M., & Stikov,N. (2020). The quest for measuring myelin with MRI-An interactive meta-analysis of quantitative comparisons with histology. *BioRxiv*.

Mansfield, P., & Maudsley, A. A. (1977). Medical imaging by NMR. *The British journal of radiology*, *50*(591), 188-194.

Marie, D., Jobard, G., Crivello, F., Perchey, G., Petit, L., Mellet, E., ... & Tzourio-Mazoyer, N. (2015). Descriptive anatomy of Heschl's gyri in 430 healthy volunteers, including 198 left-handers. *Brain Structure and Function*, *220*(2), 729-743.

Marques, J. P., Kober, T., Krueger, G., van der Zwaag, W., Van de Moortele, P. F., & Gruetter, R. (2010). MP2RAGE, a self bias-field corrected sequence for improved segmentation and T 1-mapping at high field. *Neuroimage*, *49*(2), 1271-1281.

Marques, J. P., & Gruetter, R. (2013). New Developments and Applications of the MP2RAGE Sequence-Focusing the Contrast and High Spatial Resolution R 1 Mapping. PloS one, 8(7), e69294.

Marques, J. P., Khabipova, D., & Gruetter, R. (2017). Studying cyto and myeloarchitecture of the human cortex at ultra-high field with quantitative imaging:R 1, R 2* and magnetic susceptibility. NeuroImage, 147, 152-163.

Marques, J. P., & Norris, D. G. (2018). How to choose the right MR sequence foryour research question at 7 T and above?. *NeuroImage*, *168*, 119-140.

Mathalon, D. H., & Sohal, V. S. (2015). Neural oscillations and synchrony in brain dysfunction and neuropsychiatric disorders: it's about time. *JAMA psychiatry*, *72*(8),840-844.

McDermott, B., Porter, E., Hughes, D., McGinley, B., Lang, M., O'Halloran, M., &Jones, M. (2018). Gamma band neural stimulation in humans and the promise of a new modality to prevent and treat Alzheimer's disease. Journal of Alzheimer's Disease, 65(2), 363-392.

McFadden, K. L., Steinmetz, S. E., Carroll, A. M., Simon, S. T., Wallace, A., & Rojas, D. C. (2014). Test-retest reliability of the 40 Hz EEG auditory steady-stateresponse. *PLoS One*, *9*(1), e85748.

Messaritaki, E., Foley, S., Schiavi, S., Magazzini, L., Routley, B., Jones, D. K., &Singh, K. D. (2020). Predicting MEG resting-state functional connectivity using microstructural information. *bioRxiv*.

Michalareas, G., Vezoli, J., Van Pelt, S., Schoffelen, J. M., Kennedy, H., & Fries, P. (2016). Alpha-beta and gamma rhythms subserve feedback and feedforward influences among human visual cortical areas. *Neuron*, *89*(2), 384-397.

Micheva, K. D., Chang, E. F., Nana, A. L., Seeley, W. W., Ting, J. T., & Cobbs, C. (2018). Distinctive structural and molecular features of myelinated inhibitory axons in human neocortex. *Eneuro*, *5*(5).

Micheva, K. D., Wolman, D., Mensh, B. D., Pax, E., Buchanan, J., Smith, S. J., & Bock, D. D. (2016). A large fraction of neocortical myelin ensheathes axons of localinhibitory neurons. *elife*, *5*, e15784.

Mišić, B., & Sporns, O. (2016). From regions to connections and networks: newbridges between brain and behavior. *Current opinion in neurobiology*, *40*, 1-7.

Mitew, S., Gobius, I., Fenlon, L. R., McDougall, S. J., Hawkes, D., Xing, Y. L., ... & Merson, T. D. (2018). Pharmacogenetic stimulation of neuronal activity increases myelination in an axon-specific manner. *Nature communications*, *9*(1), 306.

Molyneaux, B. J., Arlotta, P., Menezes, J. R., & Macklis, J. D. (2007). Neuronal subtype specification in the cerebral cortex. *Nature reviews neuroscience*, *8*(6), 427-437.

Moran, R. J., Stephan, K. E., Dolan, R. J., & Friston, K. J. (2011). Consistentspectral predictors for dynamic causal models of steady-state responses. *Neuroimage*, *55*(4), 1694-1708.

Moran, R. J., Symmonds, M., Stephan, K. E., Friston, K. J., & Dolan, R. J. (2011).An in vivo assay of synaptic function mediating human cognition. *Current Biology*, *21*(15), 1320-1325.

Moran, R. J., Stephan, K. E., Seidenbecher, T., Pape, H. C., Dolan, R. J., & Friston, K. J. (2009). Dynamic causal models of steady-state responses. *Neuroimage*, *44*(3),796-811.

Murakami, S., & Okada, Y. (2006). Contributions of principal neocortical neurons to magnetoencephalography and electroencephalography signals. *The Journal of physiology*, *575*(3), 925-936.

Muthukumaraswamy, S. D., Edden, R. A., Jones, D. K., Swettenham, J. B., & Singh, K. D. (2009). Resting GABA concentration predicts peak gamma frequency and fMRI amplitude in response to visual stimulation in humans. *Proceedings of the National Academy of Sciences*, *106*(20), 8356-8361.

Muthukumaraswamy, S. D., Singh, K. D., Swettenham, J. B., & Jones, D. K. (2010). Visual gamma oscillations and evoked responses: variability, repeatability and structural MRI correlates. *Neuroimage*, *49*(4), 3349-3357.

Muthukumaraswamy, SD and Singh, KD (2011) A Cautionary note on the interpretation of phase-locking estimates with concurrent changes in power. ClinicalNeurophysiology, 122(11): 2324-2325.

Muthukumaraswamy, Suresh D., et al. (2015): "Evidence that subanesthetic doses of ketamine cause sustained disruptions of NMDA and AMPA-mediated frontoparietal connectivity in humans." *Journal of Neuroscience* 35.33.11694-11706.

Muthukumaraswamy, S. D., & Singh, K. D. (2013). Visual gamma oscillations: theeffects of stimulus type, visual field coverage and stimulus motion on MEG and EEG recordings. *Neuroimage*, *69*, 223-230.

Nieuwenhuys, R. (2013). The myeloarchitectonic studies on the human cerebralcortex of the Vogt–Vogt school, and their significance for the interpretation of functional neuroimaging data. *Brain Structure and Function*, *218*(2), 303-352.

Oda, Y., Onitsuka, T., Tsuchimoto, R., Hirano, S., Oribe, N., Ueno, T., Hirano, Y., Nakamura, I., Miura, T. & Kanba, S. (2012). Gamma band neural synchronization deficits for auditory steady state responses in bipolar disorder patients. PLoS One 7,e39955

O'Donnell, B. F., Vohs, J. L., Krishnan, G. P., Rass, O., Hetrick, W. P., & Morzorati,

S. L. (2013). The auditory steady-state response (ASSR): a translational biomarkerfor schizophrenia. In *Supplements to Clinical neurophysiology* (Vol. 62, pp. 101- 112). Elsevier.

Okada, Y. C., Lahteenmäki, A., & Xu, C. (1999). Experimental analysis of distortion of magnetoencephalography signals by the skull. *Clinical neurophysiology*, *110*(2), 230-238.

Oke, O. O., Magony, A., Anver, H., Ward, P. D., Jiruska, P., Jefferys, J. G., & Vreugdenhil, M. (2010). High-frequency gamma oscillations coexist with low-frequency gamma oscillations in the rat visual cortex in vitro. *European Journal of Neuroscience*, *31*(8), 1435-1445.

Oostenveld, R., Fries, P., Maris, E., & Schoffelen, J. M. (2011). FieldTrip: open source software for advanced analysis of MEG, EEG, and invasive electrophysiological data. *Computational intelligence and neuroscience*, *2011*.

Pajevic, S., Basser, P. J., & Fields, R. D. (2014). Role of myelin plasticity inoscillations and synchrony of neuronal activity. *Neuroscience*, *276*, 135-147.

Palomero-Gallagher, N., & Zilles, K. (2019). Cortical layers: Cyto-, myelo-, receptor-and synaptic architecture in human cortical areas. *Neuroimage*, *197*, 716-741.

Paquola, C., Bethlehem, R. A., Seidlitz, J., Wagstyl, K., Romero-Garcia, R., Whitaker, K. J., ... & Bernhardt, B. (2019). Shifts in myeloarchitecture characteriseadolescent development of cortical gradients. eLife, 8.

Perry, G., Hamandi, K., Brindley, L. M., Muthukumaraswamy, S. D., & Singh, K. D. (2013). The properties of induced gamma oscillations in human visual cortex show individual variability in their dependence on stimulus size. *Neuroimage*, *68*, 83-92.

Picton, T. W., John, M. S., Dimitrijevic, A., & Purcell, D. (2003). Human auditorysteady-state responses: Respuestas auditivas de estado estable en humanos. *International journal of audiology*, *42*(4), 177-219.

Pinotsis, D. A., Perry, G., Litvak, V., Singh, K. D., & Friston, K. J. (2016). Intersubject variability and induced gamma in the visual cortex: DCM with empiricalBayes and neural fields. *Human brain mapping*, *37*(12), 4597-4614.

Pirko, I., & Noseworthy, J. H. (2007). Demyelinating disorders of the central nervous system. *Textbook of Clinical Neurology*, 1103.

Prantner, A. M., Bretthorst, G. L., Neil, J. J., Garbow, J. R., & Ackerman, J. J.(2008). Magnetization transfer induced biexponential longitudinal relaxation. *Magnetic resonance in medicine*, *60*(3), 555-563.

Rauschecker, J. P. (2015). Auditory and visual cortex of primates: a comparison oftwo sensory systems. *European Journal of Neuroscience*, *41*(5), 579-585.

Ray, S., & Maunsell, J. H. (2011). Different origins of gamma rhythm and high-gamma activity in macaque visual cortex. *PLoS Biol*, *9*(4), e1000610.

Reis, C., Sharott, A., Magill, P. J., van Wijk, B. C., Parr, T., Zeidman, P., ... & Cagnan, H. (2019). Thalamocortical dynamics underlying spontaneous transitions inbeta power in Parkinsonism. *Neuroimage*, *193*, 103-114.

Ribary, U., Ioannides, A. A., Singh, K. D., Hasson, R., Bolton, J. P., Lado, F., ... &Llinas, R. (1991). Magnetic field tomography of coherent thalamocortical 40- Hz oscillations in humans. *Proceedings of the National Academy of Sciences*, *88*(24), 11037-11041.

Rioux, J. A., Levesque, I. R., & Rutt, B. K. (2016). Biexponential longitudinal relaxation in white matter: characterization and impact on T1 mapping with IR-FSEand MP2RAGE. *Magnetic resonance in medicine*, *75*(6), 2265-2277.

Roß, B., Borgmann, C., Draganova, R., Roberts, L. E., & Pantev, C. (2000). A high-precision magnetoencephalographic study of human auditory steady-state responses to amplitude-modulated tones. *The Journal of the Acoustical Society of America*, *108*(2), 679-691.

Ross, B., Herdman, A. T. & Pantev, C. (2005). Right hemispheric laterality ofhuman 40 Hz auditory steady-state responses. Cereb Cortex 15, 2029-39.

Rowley, C. D., Bazin, P. L., Tardif, C. L., Sehmbi, M., Hashim, E., Zaharieva, N., ... & Bock, N. A. (2015). Assessing intracortical myelin in the living human brain using myelinated cortical thickness. *Frontiers in neuroscience*, *9*.

Sarvas, J. (1987). Basic mathematical and electromagnetic concepts of the biomagnetic inverse problem. *Physics in Medicine & Biology*, *32*(1), 11.

Scheeringa, R., & Fries, P. (2017). Cortical layers, rhythms and BOLD signals. *NeuroImage*. *197*, 689-698.

Schoonhoven, D. N., Fraschini, M., Tewarie, P., Uitdehaag, B. M., Eijlers, A. J.,Geurts, J. J., ... & Strijbis, E. M. (2018). Resting-state MEG measurement of functional activation as a biomarker for cognitive decline in MS. *Multiple SclerosisJournal*, 1352458518810260.

Schmierer, K., Wheeler-Kingshott, C. A., Tozer, D. J., Boulby, P. A., Parkes, H. G., Yousry, T. A., ... & Miller, D. H. (2008). Quantitative magnetic resonance of postmortem multiple sclerosis brain before and after fixation. *Magnetic Resonance in Medicine: An Official Journal of the International Society for Magnetic Resonance in Medicine*, *59*(2), 268-277.

Schnitzler, A., & Gross, J. (2005). Normal and pathological oscillatory communication in the brain. *Nature reviews neuroscience*, *6*(4), 285-296.

Schwarzkopf, D. S., Robertson, D. J., Song, C., Barnes, G. R., & Rees, G. (2012). The frequency of visually induced gamma-band oscillations depends on the size of early human visual cortex. *Journal of Neuroscience*, *32*(4), 1507-1512.

Schweser, F., Deistung, A., Lehr, B. W., Sommer, K., & Reichenbach, J. R. (2011,May). SEMI-TWInS: simultaneous extraction of myelin and iron using a T2*- weighted imaging sequence. In *Proc Intl Soc Mag Reson Med* (Vol. 19, p. 120).

Sederberg, P. B., Schulze-Bonhage, A., Madsen, J. R., Bromfield, E. B., McCarthy, D. C., Brandt, A., ... & Kahana, M. J. (2007). Hippocampal and neocortical gamma oscillations predict memory formation in humans. *Cerebral Cortex*, *17*(5), 1190-1196.

Sereno, M. I., Lutti, A., Weiskopf, N., & Dick, F. (2013). Mapping the humancortical surface by combining quantitative T 1 with retinotopy. *Cerebral cortex*, *23*(9), 2261-2268.

Seymour, R. A., Rippon, G., Gooding-Williams, G., Schoffelen, J. M., & Kessler, K. (2019). Dysregulated oscillatory connectivity in the visual system in autism spectrum disorder. *Brain*, *142*(10), 3294-3305.

Seymour, R. A., Rippon, G., Gooding-Williams, G., Sowman, P. F., & Kessler, K.(2020). Reduced auditory steady state responses in autism spectrum disorder. *Molecular autism*, *11*(1), 1-13.

Siegel, M., Donner, T. H., & Engel, A. K. (2012). Spectral fingerprints of large-scale neuronal interactions. *Nature Reviews Neuroscience*, *13*(2), 121-134.

Simon, D. M., & Wallace, M. T. (2016). Dysfunction of sensory oscillations in Autism Spectrum Disorder. *Neuroscience & Biobehavioral Reviews*, *68*, 848-861.

Singh, K. (2006). “Magnetoencephalography”. In: Methods in Mind. Cambridge:MIT Press, pp. 291–326.

Singh, K. D. (2012). Which “neural activity” do you mean? fMRI, MEG, oscillationsand neurotransmitters. *Neuroimage*, *62*(2), 1121-1130.

Shaw, A. D., Knight, L., Freeman, T. C., Williams, G. M., Moran, R. J., Friston, K. J., ... & Singh, K. D. (2020). Oscillatory, Computational, and Behavioral Evidence for Impaired GABAergic Inhibition in Schizophrenia. *Schizophrenia Bulletin*, *46*(2),345-353.

Shaw, A. D., Moran, R. J., Muthukumaraswamy, S. D., Brealy, J., Linden, D. E., Friston, K. J., & Singh, K. D. (2017). Neurophysiologically-informed markers of individual variability and pharmacological manipulation of human cortical gamma.*NeuroImage*, *161*, 19-31.

Sacolick, L. I., Wiesinger, F., Hancu, I., & Vogel, M. W. (2010). B1 mapping by Bloch-Siegert shift. *Magnetic resonance in medicine*, *63*(5), 1315-1322.

Spencer, K. M., Salisbury, D. F., Shenton, M. E., & McCarley, R. W. (2008a). γ-Band auditory steady-state responses are impaired in first episodepsychosis. *Biological psychiatry*, *64*(5), 369-375.

Spencer, K. M., Niznikiewicz, M. A., Shenton, M. E., & McCarley, R. W. (2008b). Sensory-evoked gamma oscillations in chronic schizophrenia. *Biological psychiatry*, *63*(8), 744-747.

Sporns, O. (2013). Structure and function of complex brain networks. *Dialogues in Clinical Neuroscience*, *15*(3), 247.

Sprooten, E., O'Halloran, R., Dinse, J., Lee, W. H., Moser, D. A., Doucet, G. E., ... & Leibu, E. (2019). Depth-dependent intracortical myelin organization in the livinghuman brain determined by in vivo ultra-high field magnetic resonance imaging. *NeuroImage*, *185*, 27-34.

Steen, R. G., Gronemeyer, S. A., Kingsley, P. B., Reddick, W. E., Langston, J. S., & Taylor, J. S. (1994). Precise and accurate measurement of proton T1 in human brain in vivo: validation and preliminary clinical application. *Journal of Magnetic Resonance Imaging*, *4*(5), 681-691.

Stephan, K. E., Tittgemeyer, M., Knösche, T. R., Moran, R. J., & Friston, K. J. (2009). Tractography-based priors for dynamic causal models. *Neuroimage*, *47*(4),1628-1638.

Stikov, N., Boudreau, M., Levesque, I. R., Tardif, C. L., Barral, J. K., & Pike, G. B. (2015). On the accuracy of T1 mapping: searching for common ground. *Magnetic resonance in medicine*, *73*(2), 514-522.

Stollberger, R., & Wach, P. (1996). Imaging of the active B1 field in vivo. *Magnetic resonance in medicine*, *35*(2), 246-251.

Stüber, C., Morawski, M., Schäfer, A., Labadie, C., Wähnert, M., Leuze, C., ... & Spemann, D. (2014). Myelin and iron concentration in the human brain: a quantitative study of MRI contrast. *Neuroimage*, *93*, 95-106.

Sui, J., Huster, R., Yu, Q., Segall, J. M., & Calhoun, V. D. (2014). Function– structure associations of the brain: evidence from multimodal connectivity andcovariance studies. *Neuroimage*, *102*, 11-23.

Sumner, R. L., McMilllan, R. L., Shaw, A. D., Singh, K. D., Sundram, F., & Muthukumaraswamy, S. D. (2018). Peak gamma frequency and cortical laminarprocessing are modified across the healthy menstrual cycle. *bioRxiv*, 219196.

Sweet, R. A., Pierri, J. N., Auh, S., Sampson, A. R., & Lewis, D. A. (2003). Reduced pyramidal cell somal volume in auditory association cortex of subjects with schizophrenia. *Neuropsychopharmacology*, *28*(3), 599-609.

Swettenham, J. B., Muthukumaraswamy, S. D., & Singh, K. D. (2009). Spectral properties of induced and evoked gamma oscillations in human early visual cortex tomoving and stationary stimuli. *Journal of neurophysiology*, *102*(2), 1241-1253.

Tadel, F., Baillet, S., Mosher, J. C., Pantazis, D., & Leahy, R. M. (2011). Brainstorm: a user-friendly application for MEG/EEG analysis. *Computational intelligence and neuroscience*, *2011*.

Tan, H. R., Gross, J., & Uhlhaas, P. J. (2015). MEG—measured auditory steady-state oscillations show high test–retest reliability: A sensor and source-space analysis. *Neuroimage*, *122*, 417-426.

Tan, H. R., Gross, J., & Uhlhaas, P. J. (2016). MEG sensor and source measures of visually induced gamma-band oscillations are highly reliable. *NeuroImage*, *137*, 34-44

Tardif, C. L., Gauthier, C. J., Steele, C. J., Bazin, P. L., Schäfer, A., Schaefer, A., ...& Villringer, A. (2016). Advanced MRI techniques to improve our understanding of experience-induced neuroplasticity. *Neuroimage*, *131*, 55-72.

Tewarie, P., Steenwijk, M. D., Tijms, B. M., Daams, M., Balk, L. J., Stam, C. J., ...& Pouwels, P. J. (2014). Disruption of structural and functional networks in long- standing multiple sclerosis. *Human brain mapping*, *35*(12), 5946-5961.

Thallmair, M., Metz, G. A., Z'Graggen, W. J., Raineteau, O., Kartje, G. L., & Schwab, M. E. (1998). Neurite growth inhibitors restrict plasticity and functional recovery following corticospinal tract lesions. *Nature neuroscience*, *1*(2), 124-131.

Thuné, H., Recasens, M., & Uhlhaas, P. J. (2016). The 40- Hz auditory steady-stateresponse in patients with schizophrenia: a meta-analysis. *JAMA psychiatry*, *73*(11),1145-1153.

Tofts PS, Steens SCA, van Buchem MA. MT: magnetization transfer. In: Tofts PS,editor. Quantitative MRI of the brain: measuring changes caused by disease.Chichester, West Sussex: Wiley; 2003. p 257–298.

Tomassy, G. S., Berger, D. R., Chen, H. H., Kasthuri, N., Hayworth, K. J., Vercelli, A., ... & Arlotta, P. (2014). Distinct profiles of myelin distribution along single axons of pyramidal neurons in the neocortex. *Science*, *344*(6181), 319-324.

Tong, F. (2003). Primary visual cortex and visual awareness. *Nature reviewsneuroscience*, *4*(3), 219-229.

Tustison, N. J., Avants, B. B., Cook, P. A., Zheng, Y., Egan, A., Yushkevich, P. A., & Gee, J. C. (2010). N4ITK: improved N3 bias correction. *IEEE transactions on medical imaging*, *29*(6), 1310-1320.

Turner, R. (2019). Myelin and modeling: Bootstrapping corticalmicrocircuits. *Frontiers in neural circuits*, *13*, 34.

Turner, R., Oros-Peusquens, A. M., Romanzetti, S., Zilles, K., & Shah, N. J. (2008). Optimised in vivo visualisation of cortical structures in the human brain at 3 T using IR-TSE. *Magnetic resonance imaging*, *26*(7), 935-942.

Trampel, R., Bazin, P. L., Pine, K., & Weiskopf, N. (2019). In-vivo magnetic resonance imaging (MRI) of laminae in the human cortex. *Neuroimage*, *197*, 707-715.

Tzourio-Mazoyer, N., Landeau, B., Papathanassiou, D., Crivello, F., Etard, O., Delcroix, N., ... & Joliot, M. (2002). Automated anatomical labeling of activations inSPM using a macroscopic anatomical parcellation of the MNI MRI single-subject brain. *Neuroimage*, *15*(1), 273-289.

Uhlhaas, P. J., Roux, F., Singer, W., Haenschel, C., Sireteanu, R., & Rodriguez, E.(2009). The development of neural synchrony reflects late maturation and restructuring of functional networks in humans. *Proceedings of the National Academy of Sciences*, *106*(24), 9866-9871.

Uhlhaas, P. J., Roux, F., Rodriguez, E., Rotarska-Jagiela, A., & Singer, W. (2010).Neural synchrony and the development of cortical networks. *Trends in cognitive sciences*, *14*(2), 7280.

Uhlhaas, P. J., & Singer, W. (2010). Abnormal neural oscillations and synchrony in schizophrenia. *Nature reviews neuroscience*, *11*(2), 100-113.

Uhlhaas, P. J., Roux, F., Rodriguez, E., Rotarska-Jagiela, A., & Singer, W. (2010).Neural synchrony and the development of cortical networks. *Trends in cognitive sciences*, *14*(2), 7280

van der Weijden, C. W., García, D. V., Borra, R. J., Thurner, P., Meilof, J. F., vanLaar, P. J., ... & de Vries, E. F. (2020). Myelin quantification with MRI: A systematic review of accuracy and reproducibility. *NeuroImage*, 117561.

van Diepen, R. M., & Mazaheri, A. (2018). The caveats of observing inter-trial phase-coherence in cognitive neuroscience. *Scientific reports*, *8*(1), 1-9.

van Pelt, S., Boomsma, D. I., & Fries, P. (2012). Magnetoencephalography in twinsreveals a strong genetic determination of the peak frequency of visually induced gamma-band synchronization. *Journal of Neuroscience*, *32*(10), 3388-3392

van Pelt, S., Shumskaya, E., & Fries, P. (2018). Cortical volume and sex influencevisual gamma. *Neuroimage*, *178*, 702-712.

Vrba, J., & Robinson, S. E. (2001). Signal processing in magnetoencephalography. *Methods*, *25*(2), 249-271.

Vogt, O., & Vogt, C. (1903). Zur anatomischen Gliederung des Cortex cerebri. *J Psychol Neurol*, *2*(4), 160-180.

Waehnert, M. D., Dinse, J., Weiss, M., Streicher, M. N., Waehnert, P., Geyer, S., ...& Bazin, P. L. (2014). Anatomically motivated modeling of cortical laminae. *Neuroimage*, *93*, 210-220.

Wansapura, J. P., Holland, S. K., Dunn, R. S., & Ball Jr, W. S. (1999). NMR relaxation times in the human brain at 3.0 tesla. *Journal of Magnetic Resonance Imaging: An Official Journal of the International Society for Magnetic Resonance in Medicine*, *9*(4), 531-538.

Waehnert, M. D., Dinse, J., Schäfer, A., Geyer, S., Bazin, P. L., Turner, R., & Tardif, C. L. (2016). A subject-specific framework for in vivo myeloarchitectonic analysisusing high resolution quantitative MRI.*Neuroimage*, *125*, 94-107.

Weiskopf, N., Mohammadi, S., Lutti, A., & Callaghan, M. F. (2015). Advances in MRI-based computational neuroanatomy: from morphometry to in-vivo histology. *Current opinion in neurology*, *28*(4), 313-322.

Westbrook, C., & Talbot, J. (2018). *MRI in Practice*. John Wiley & Sons.

Westlye, L. T., Walhovd, K. B., Bjørnerud, A., Due-Tønnessen, P., & Fjell, A. M. (2008). Error-related negativity is mediated by fractional anisotropy in the posteriorcingulate gyrus—a study combining diffusion tensor imaging and electrophysiologyin healthy adults. *Cerebral Cortex*, *19*(2), 293-304.

Whitaker, K. J., Vértes, P. E., Romero-Garcia, R., Váša, F., Moutoussis, M., Prabhu,G., ... & Tait, R. (2016). Adolescence is associated with genomically patterned consolidation of the hubs of the human brain connectome. *Proceedings of the National Academy of Sciences*, *113*(32), 9105-9110

Zilles, K., & Palomero-Gallagher, N. (2017). Multiple transmitter receptors in regions and layers of the human cerebral cortex. *Frontiers in neuroanatomy*, *11*, 78.

Zimmerman, J. E., Thiene, P., & Harding, J. T. (1970). Design and operation of stable rf-biased superconducting point-contact quantum devices, and a note on the properties of perfectly clean metal contacts. *Journal of Applied Physics*, *41*(4), 1572-1580.

Xing, D., Yeh, C. I., Burns, S., & Shapley, R. M. (2012). Laminar analysis of visually evoked activity in the primary visual cortex. *Proceedings of the NationalAcademy of Sciences*, 109(34), 13871-13876. .